
# Final Annual Report

**"Functional Studies on Glutathione S-Transferases (GSTs) from *Anopheles dirus* a Thai Malaria Vector" TRF BRG/47/80021**

Associate Professor Albert J. Ketterman Ph.D. et al.

August 2007

TRF BRG/47/80021

# Final Annual Report

## "Functional Studies on Glutathione S-Transferases (GSTs) from *Anopheles dirus* a Thai Malaria Vector"


| | |
|---|---|
| 1. Assoc. Prof. Albert J. Ketterman | Institute of Molecular Biology and Genetics (IMBG), Mahidol University, Salaya Campus |
| 2. Dr. Rungrutai Udomsinprasert | IMBG, Mahidol University |
| 3. Dr. Ardcharaporn Vararattanavech | IMBG, Mahidol University |
| 4. Dr. Jantana Wongsantichon | IMBG, Mahidol University |
| 5. Pakorn Winayanuwattikun | IMBG, Mahidol University |
| 6. Gulsiri Charoensilp | IMBG, Mahidol University |
| 7. Chonticha Saisawang | IMBG, Mahidol University |
| 8. Juthamart Piromjitpong | IMBG, Mahidol University |
| 9. Mashamon Mitprasat | IMBG, Mahidol University |
| 10.Piya Temviriyanukul | IMBG, Mahidol University |
| 11.Tassanee Lerksuthirat | IMBG, Mahidol University |



**Funded by the Thailand Research Fund (TRF)**

## Acknowledgements

The progress achieved for the last three years on this project was possible because of the efforts and contributions from the following people:

**Institute of Molecular Biology and Genetics, Mahidol University**

*Research Assistants:*
Juthamart Piromjitpong
Suthasinee Somyong

*Post-doctoral Researchers:*
Dr. Rungrutai Udomsinprasert
Dr. Ardcharaporn Vararattanavech
Dr. Jantana Wongsantichon

**Ph.D. Students**:
Rungrutai Udomsinprasert (now completed; funded by the Royal Golden Jubilee).
Pakorn Winayanuwattikun (now completed; funded by the Royal Golden Jubilee).
Ardcharaporn Vararattanavech (now completed; funded by the Royal Golden Jubilee).
Jantana Wongsantichon (now completed; funded by the Royal Golden Jubilee).
Gulsiri Charoensilp (now completed; funded by the Royal Golden Jubilee).
Chonticha Saisawang (funded by the Royal Golden Jubilee).

**M.Sc. Students**:
Juthamart Piromjitpong (now completed)
Mashamon Mitprasat (now completed)
Piya Temviriyanukul (now completed)
Tassanee Lerksuthirat

**Dept of Biochem/Center Excell Protein Structure and Function, Mahidol University**
Dr. J.Yuvaniyama

**Maejo University**
Dr. S. Pongjareankit

**Chiang Mai University**
Dr. L. Prapanthadara
Dr. J. Wongtrakul.

**University of Western Australia, Australia**
Dr. M.A. Bogoyevitch

**Australian National University**
Dr. A.J. Oakley

## Abstracts

The aim of this project is to characterize functional relationships for the amino acids that can affect substrate specificity as well as protein-protein interactions in glutathione S-transferases. We have published fourteen papers in the last three years for a total Impact Factor of 43.633 (2005 Impact Factors). Reprints of these fourteen papers are included in the appendix. For the sake of simplicity we only present the three Biochemical Journal (2005 Impact Factor 4.224) papers published in 2007. Therefore this Final Annual Report consists of three papers that have been published and the format is of separate studies, one from each paper. These studies involve characterization of structural amino acid residues that also appear to modulate enzymatic properties such as substrate and inhibitor specificity. Each study utilizes one of the enzymes and its crystal structure obtained from the research previously funded by the TRF. This report therefore describes on-going structure function studies.



## บทคัดย่อ

งานวิจัยนี้มุ่งศึกษาความสำคัญของกรดอะมิโนที่มีต่อหน้าที่ของเอนไซม์กลูตาไธโอน เอส-ทรานสเฟอเรส โดยศึกษาผลกระทบต่อความจำเพาะเจาะจงกับสารตั้งต้น รวมทั้งการมีปฏิสัมพันธ์กับโปรตีนอื่นๆ ในช่วงสามปีที่ผ่านมา ได้มีผลงานตีพิมพ์ทั้งสิ้น 14 บทความด้วยค่า Impact Factor รวม 43.633 (ค่า Impact Factor ปี 2548) เพื่อความเรียบง่ายของรายงานประจำปีฉบับนี้ จึงได้นำเสนอในรูปแบบของบทความ 3 เรื่อง จาก 3 การศึกษาวิจัยที่แตกต่างกันซึ่งได้ตีพิมพ์ในปี 2550 การศึกษานี้ได้จำแนกกรดอะมิโนที่มีผลต่อโครงสร้างของเอนไซม์ และพบว่ากรดอะมิโนเหล่านี้มีส่วนในการควบคุมคุณสมบัติทางจลนศาสตร์ อันได้แก่ความจำเพาะเจาะจงกับสารตั้งต้นและกับตัวยับยั้งปฏิกิริยาด้วย แต่ละการศึกษาใช้เอนไซม์และโครงร่างผลึกของเอนไซม์ที่ได้จากการวิจัยก่อนหน้านี้ ซึ่งได้รับการสนับสนุนจาก สกว. รายงานฉบับนี้จึงเป็นความก้าวหน้าของการศึกษาดังกล่าว

# Executive Summary

We have published fourteen papers in the last three years for a total 2005 impact factor of 43.633. For the sake of simplicity we only present the three Biochemical Journal (2005 Impact Factor 4.224) papers published this year (2007) in this Final Annual Report. Therefore this Final Annual Report consists of three papers that have been published and the format is of separate studies, one from each paper.

The present study characterized conserved residues in a GST (glutathione S-transferase) in the active-site region that interacts with glutathione. This region of the active site is near the glycine moiety of glutathione and consists of a hydrogen bond network. In the GSTD (Delta class GST) studied, adGSTD4-4, the network consisted of His38, Met39, Asn47, Gln49, His50 and Cys51. In addition to contributing to glutathione binding, this region also had major effects on enzyme catalysis, as shown by changes in kinetic parameters and substrate specific activity. The results also suggest that the electron distribution of this network plays a role in stabilization of the ionized thiol of glutathione as well as impacting on the catalytic rate-limiting step. This area constitutes a second glutathione active site network involved in glutathione ionization distinct from a network previously observed interacting with the glutamyl end of glutathione. This second network also appears to be functionally conserved inGSTs. In the present study, His50 is the key basic residue stabilized by this network as shown by up to a 300-fold decrease in *k*cat and 5200-fold decrease in *k*cat/*K*m for glutathione. Although these network residues have a minor role in structural integrity, the replaced residues induced changes in active site topography as well as generating positive co-operativity towards glutathione. Moreover, this network at the glycinemoiety ofGSH (glutathione) also contributed to the 'base-assisted deprotonationmodel' forGSHionization. Taken together, the results indicate a critical role for the functionally conserved basic residue His50 and this hydrogen bond network in the active site.

In *Anopheles dirus* glutathione transferaseD3-3, position 64 is occupied by a functionally conserved glutamate residue, which interacts directly with the $\gamma$ -glutamate moiety of GSH (glutathione) as part of an electron-sharing network present in all soluble GSTs (glutathione transferases). Primary sequence alignment of all GST classes suggests that Glu64 is one of a few residues that is functionally conserved in the GST superfamily. Available crystal structures as well as consideration of the property of the equivalent residue at position 64, acidic or polar, suggest that the GST electron-sharing motif can be divided into two types. Electrostatic interaction between the GSH glutamyl and carboxylic Glu64, as well as with Arg66 and Asp100, was observed to extend the electron-sharing motif identified previously. Glu64 contributes to the catalytic function of this motif and the 'base-assisted deprotonation' that are essential for GSH ionization during catalysis. Moreover, this residue also appears to affect multiple steps in the enzyme catalytic strategy, including binding of GSH, nucleophilic attack by thiolate at the electrophilic centre and product formation, probably through active-site packing effects. Replacement with non-functionally-conserved amino acids alters initial packing or folding by favouring aggregation during heterologous expression. Thermodynamic and reactivation *in vitro* analysis indicated that Glu64 also contributes to the initial folding pathway and overall structural stability. Therefore Glu64 also appears to impact upon catalysis through roles in both initial folding and structural maintenance.

GSTs (glutathione transferases) are multifunctional widespread enzymes. Currently there are 13 identified classes within this family. Previously most structural characterization has been

reported for mammalian Alpha, Mu and Pi class GSTs. In the present study we characterize two enzymes from the insect-specific Delta class, adGSTD3-3 and adGSTD4-4. These two proteins are alternatively spliced products from the same gene and have very similar tertiary structures. Several major contributions to the dimer interface area can be separated into three regions: conserved electrostatic interactions in region 1, hydrophobic interactions in region 2 and an ionic network in region 3. The four amino acid side chains studied in region 1 interact with each other as a planar rectangle. These interactions are highly conserved among theGST classes, Delta, Sigma and Theta. The hydrophobic residues in region 2 are not only subunit interface residues but also active site residues. Overall these three regions provide important contributions to stabilization and folding of the protein. In addition, decreases in yield aswell as catalytic activity changes, suggest that the mutations in these regions can disrupt the active site conformation which decreases binding affinity, alters kinetic constants and alters substrate specificity. Several of these residues have only a slight effect on the initial folding of each subunit but have more influence on the dimerization process as well as impacting upon appropriate active site conformation. The results also suggest that even splicing products from the same gene may have specific features in the subunit interface area that would preclude heterodimerization.

Keywords: *Anopheles dirus*, glutathione transferase (GST), subunit interface, conserved active-site residue, enzyme catalysis, electron sharing network, structural integrity.

## Objectives:

The aim of this project is to characterize functional relationships for the amino acids that can affect substrate specificity as well as protein-protein interactions in glutathione S-transferases from the Thai malaria vector *Anopheles dirus*. We will obtain new GSTs from different classes as well as enzyme sequence variants generated by site-directed mutagenesis for kinetic characterization studies. The available crystal structures in my laboratory and these new protein forms will yield data that will increase our understanding of the mechanism of GSTs in their role in resistance to insecticides. We will also continue studying the protein-protein interactions of the GSTs and the Jun N-terminal kinase (JNK) pathway proteins. This will provide information on other physiological functions of GSTs and will increase our understanding of the interaction and regulation of proteins *in vivo*. This GST-JNK interaction is important as the JNK pathway has been shown to be involved in cell growth, cell differentiation, the cell stress response and apoptosis or cell death.

To achieve this goal the project entails continuing several aspects of the research previously funded by the Thailand Research Fund. These aspects include the following:

1. To continue to obtain new recombinant GST enzymes for kinetic characterization studies including enzyme sequence variants generated by site-directed mutagenesis.
2. To continue to obtain more GST crystal structures and to use the now available *An. dirus* GST crystal structures to provide a basis for understanding the mechanism of GSTs in their role in resistance to insecticides.
3. To continue studying the protein-protein interactions of the GSTs and the JNK kinase pathway proteins.

---

We have published fourteen papers in the last three years for a total 2005 impact factor of 43.633. For the sake of simplicity we only present the three Biochemical Journal (2005 Impact Factor 4.224) papers published this year (2007) in this Final Annual Report. Therefore this Final Annual Report consists of three papers that have been published and the format is of separate studies, one from each paper.

# A functionally conserved basic residue in glutathione S-transferases interacts with the glycine moiety of glutathione and is pivotal for enzyme catalysis

Ardcharaporn VARARATTANAVECH and Albert J. KETTERMAN[1]

Institute of Molecular Biology and Genetics, Mahidol University, Salaya Campus, 25/25 Putthamonthol Road 4, Salaya, Nakon Pathom 73170, Thailand

The present study characterized conserved residues in a GST (glutathione S-transferase) in the active-site region that interacts with glutathione. This region of the active site is near the glycine moiety of glutathione and consists of a hydrogen bond network. In the GSTD (Delta class GST) studied, adGSTD4-4, the network consisted of $His^{38}$, $Met^{39}$, $Asn^{47}$, $Gln^{49}$, $His^{50}$ and $Cys^{51}$. In addition to contributing to glutathione binding, this region also had major effects on enzyme catalysis, as shown by changes in kinetic parameters and substrate specific activity. The results also suggest that the electron distribution of this network plays a role in stabilization of the ionized thiol of glutathione as well as impacting on the catalytic rate-limiting step. This area constitutes a second glutathione active site network involved in glutathione ionization distinct from a network previously observed interacting with the glutamyl end of glutathione. This second network also appears to be functionally conserved in GSTs. In the present study, $His^{50}$ is the key basic residue stabilized by this network as shown by up to a 300-fold decrease in $k_{cat}$ and 5200-fold decrease in $k_{cat}/K_m$ for glutathione. Although these network residues have a minor role in structural integrity, the replaced residues induced changes in active site topography as well as generating positive co-operativity towards glutathione. Moreover, this network at the glycine moiety of GSH (glutathione) also contributed to the 'base-assisted deprotonation model' for GSH ionization. Taken together, the results indicate a critical role for the functionally conserved basic residue $His^{50}$ and this hydrogen bond network in the active site.

Key words: base-assisted deprotonation model, conserved active-site residue, Delta class GST, enzyme catalysis, glutathione S-transferase (GST), glycine moiety of glutathione (GSH).

## INTRODUCTION

GSTs (glutathione S-transferases; EC 2.5.1.18) are intracellular proteins, which are widely distributed in nature, being found in most aerobic eukaryotes and prokaryotes [1,2]. GSTs are polymorphic with most organisms possessing a genetic capacity to encode multiple isoforms of various classes [3,4]. The enzymes are an integral part of the phase II detoxification mechanism being involved in xenobiotic metabolism as well as protection against peroxide damage. GSTs catalyse reactions with a very broad range of structurally diverse electrophilic substrates (e.g. alkylhalides, arylhalides, lactones, epoxides, quinones, esters and activated alkenes) [4–6]. This enzyme family therefore displays a wide range of catalytic functions while retaining a high specificity towards the thiol substrate glutathione (GSH). The GSH conjugation by GST increases the solubility of the target molecule, thus facilitating the excretion of the molecule from the organism.

All cytosolic GSTs have very similar three-dimensional structures and the active site pocket is very similar in the G-site (GSH-binding site) [7–9]. The N-terminal domain of GST adopts a $\beta\alpha\beta\alpha\beta\beta\alpha$ topology that contributes most of the contacts to GSH and is called the G-site. The crystal structures of GSTs show that most of the active site residues involved in the binding and activation of GSH are found within the N-terminus; hence this region of the protein is therefore highly conserved between GSTs [7,8,10]. The C-terminal domain is all $\alpha$-helical providing some of the contacts to the hydrophobic binding site that lies adjacent to the G-site.

Substrate conjugation of electrophilic xenobiotics involves its nucleophilic attack at the ionized thiol of GSH in the active site. A conserved tyrosine (for Alpha, Mu and Pi classes) or serine (for Theta and Delta classes) residue within hydrogen-bonding distance of the thiol of GSH has been shown to be of primary importance in facilitating GSH deprotonation as well as stabilization of the ionized GSH by hydrogen-bonding [10–14]. In addition, conserved residues that interact directly with the glutamyl moiety of GSH, for example $Ser^{65}$, $Arg^{66}$ and $Ile^{52}$ in GSTD (Delta class GST) have also been implicated in critical roles in the catalytic mechanism, involvement in GSH binding, GSH thiol ionization, as well as structural integrity [15–17]. Therefore the residues interacting with the other end of GSH, the glycine moiety ($His^{38}$, $Met^{39}$, $Asn^{47}$, $Gln^{49}$, $His^{50}$ and $Cys^{51}$) were of interest (Figure 1) [18]. $His^{38}$ and $His^{50}$ interact directly with the glycine carboxylic group of GSH [19]. Both histidines appear to be assisted or stabilized by dipole–dipole interaction with $Met^{39}$. Moreover, a hydrogen bond network in the G-site near the glycine moiety of GSH, involving several residues ($His^{50}$, $Asn^{47}$, $Gln^{49}$ and $Cys^{51}$) and GSH, is proposed to be essential to electron distribution for enzyme catalysis. To investigate the roles of these residues, mutagenesis studies were performed and the engineered enzymes characterized by kinetic constants, substrate specific activity, $pK_a$ determination and rate-limiting step determination in addition to physical properties.

Abbreviations used: CDNB, 1-chloro-2,4-dinitrobenzene; DCNB, 1,2-dichloro-4-nitrobenzene; EA, ethacrynic acid; FDNB, 1-fluoro-2,4-dinitrobenzene; G-site, GSH (glutathione)-binding site; GST, glutathione S-transferase; GSTD, Delta class GST; hGSTP1-1, human GSTP1-1; PNBC, *p*-nitrobenzyl chloride; PNPBr, *p*-nitrophenethyl bromide; ZmGST1, *Zea mays* (maize) GST1.

[1] To whom correspondence should be addressed (email albertketterman@yahoo.com).

COLOUR

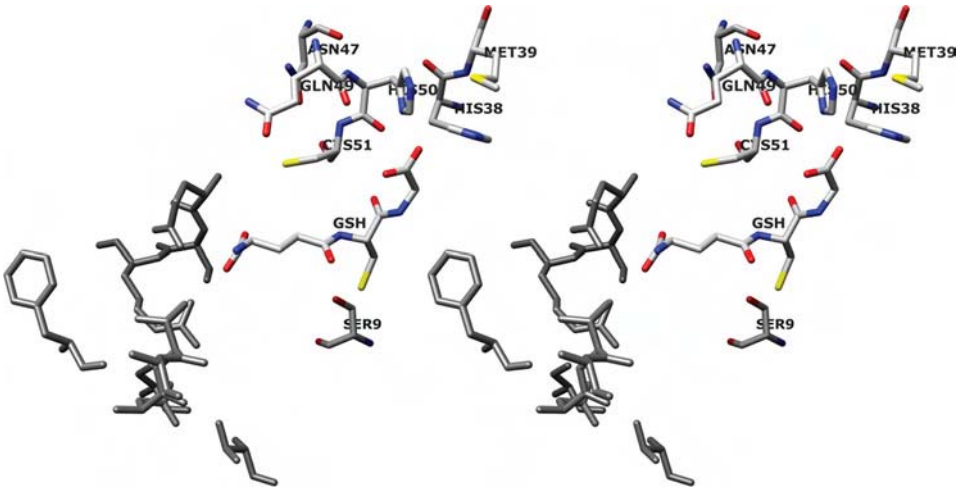


**Figure 1 Stereoview of conserved G-site residues that directly interact with the glycine moiety of GSH and generate a hydrogen bond network**

His[38] and His[50] interact directly with the glycine carboxylic group of GSH and are assisted or stabilized by dipole–dipole interaction with Met[39]. A hydrogen bond network in the G-site is formed by several residues (His[50], Asn[47], Gln[49] and Cys[51]) and GSH. The previously identified electron-sharing network at the glutamyl end of GSH is shown in grey [16]. The image was produced using the UCSF Chimera package from the Resource for Biocomputing, Visualization, and Informatics at the University of California, San Francisco, CA, U.S.A. (http://www.cgl.ucsf.edu/chimera) (supported by National Institutes of Health grant P41 RR-01081) [18].

## MATERIALS AND METHODS

### Site directed mutagenesis

The engineered enzymes were generated using Stratagene's QuikChange® site-directed mutagenesis protocol. The primers used were designed based on the sequence of the *adGSTD4* wild-type gene (GenBank® accession number AF273040). Full-length DNA sequencing in both directions was performed to confirm the engineered clones.

### Protein expression and purification

After transformation of the engineered plasmids into *Escherichia coli* BL21(DE3)pLysS, protein expression was performed. The recombinant adGSTD4-4 engineered enzymes and wild-type were purified either by glutathione affinity chromatography according to the manufacturer's instructions (Amersham Biosciences) or by cation exchanger (SP-XL) followed by hydrophobic interaction chromatography (phenyl-Sepharose) as described previously [19]. The purified enzymes (in 50 mM potassium phosphate, pH 6.5) were stored in 50 % (v/v) glycerol at −20 °C until used. The concentrations of the proteins were determined by Bio-Rad protein reagent (Bio-Rad) by using BSA as the standard protein and the purity of the proteins was observed by SDS/PAGE.

### Kinetic parameters determination

Kinetic experiments were performed as previously described [20]. Kinetic constants were determined by varying the CDNB (1-chloro-2,4-dinitrobenzene) concentration (0.031–3.0 mM) while GSH was held constant at a saturating concentration and by varying GSH concentrations (0.25–20 mM) at a saturating concentration of CDNB. The standard GST assay was performed using 3 mM CDNB and 10 mM GSH for adGSTD4-4 wild-type. The rate of conjugation between GSH and CDNB was monitored by continuously measuring change in absorbance at 340 nm for 1 min using a SpectraMax 250 at 25–27 °C. A molar absorption coefficient ($\varepsilon$) of 9.6 $mM^{-1} \cdot cm^{-1}$ was used to convert the absorbance to moles [21]. Steady-state kinetics followed Michaelis–Menten kinetics except where stated. With evidence of co-operativity upon GSH binding, demonstrated by a sigmoidal curve instead of a hyperbolic curve on a Michaelis–Menten plot, a Hill equation (eqn 1) was used to fit the experimental kinetic data on the plot. $K_{0.5}$ is the substrate concentration that gives the rate of reaction at half of $V_{max}$, similar to the $K_m$ value for non-co-operative binding ($h = 1$).

$$Y = V/V_{max} = [S]^h/(K_{0.5} + [S]^h) \quad (1)$$

$$\log[Y/(1-Y)] = h \log[S] - \log K_{0.5} \quad (2)$$

A sigmoidal Hill equation was practically transformed into a linear rate equation (eqn 2), where $Y$ is the fractional saturation; $h$ is the Hill coefficient; and $K_{0.5}$ is an averaged binding constant at $Y = 0.5$. A Hill plot, a plot between $\log[Y/(1–Y)]$ and $\log[S]$, was employed to determine the degree of co-operativity by the slope of the plot that yields the Hill coefficient ($h$) [22]. Catalytic constant ($k_{cat}$) and the catalytic efficiency ($k_{cat}/K_m$) were calculated on an active site basis using the subunit molecular mass of each enzyme. Maximal velocity ($V_{max}$) and Michaelis constant ($K_m$) were determined by nonlinear regression software analysis (GraphPad Prism version 5.00 for Windows; GraphPad Software, San Diego, CA, U.S.A.; http://www.graphpad.com). One-way ANOVA with Dunnett's multiple comparison post test was performed with wild-type as control using GraphPad Prism 5.

### Specific activity determination

The specific activities towards several GST substrates were determined as previously described [23]. All measurements were performed at 25–27 °C in 0.1 M potassium phosphate buffer (pH 6.5 or 7.5). The GST activities were measured with glutathione and five hydrophobic substrates: CDNB, DCNB (1,2-dichloro-4-nitrobenzene), EA (ethacrynic acid), PNPBr (*p*-nitrophenethyl bromide) and PNBC (*p*-nitrobenzyl chloride). Specific activities were calculated according to the molar absorption coefficient for each substrate [21].

### pH dependence of kinetic parameters

The pH dependence of $k_{cat}/K_m^{CDNB}$ was obtained by performing kinetic measurements in the following buffers: 0.1 M sodium

**Table 1 Steady-state kinetic constants using GSH and CDNB as GST substrates**

The units of $V_{max}$, $k_{cat}$, $K_m$ and $k_{cat}/K_m$ are $\mu$mol · min$^{-1}$ · mg of protein$^{-1}$, s$^{-1}$, mM and s$^{-1}$ · mM$^{-1}$ respectively. *These engineered GSTs showed positive co-operativity upon GSH binding with Hill coefficient ($h$) shown. The value shown is $K_{0.5}$, obtained from the Hill equation, which is the substrate concentration that gives the rate of reaction at half of $V_{max}$ [22]. [a]Some of these values have been previously reported and are shown for purposes of comparison [19,20]. One-way ANOVA with Dunnett's multiple comparison test was performed with wild-type as control; statistical significance is shown by † for $P < 0.05$, ‡ for $P < 0.01$ and § for $P < 0.001$.

| | | | CDNB | | GSH | | |
|---|---|---|---|---|---|---|---|
| Enzyme | $V_{max}$ | $k_{cat}$ | $K_m$ | $k_{cat}/K_m$ | $K_m$ | $k_{cat}/K_m$ | $h$ |
| Wild-type[a] | 62.45 ± 1.24 | 26.13 | 0.50 ± 0.02 | 51.84 | 0.50 ± 0.10 | 52.06 | 0.91 ± 0.02 |
| H38A[a] | 36.4 ± 1.12§ | 15.26 | 1.25 ± 0.12§ | 12.21 | 15.8 ± 1.19§ | 0.97 | – |
| H38E[a] | 14.91 ± 0.44§ | 6.23 | 0.92 ± 0.11§ | 6.76 | 8.32 ± 0.22*§ | 0.74 | 1.83 ± 0.01§ |
| H38F[a] | 9.71 ± 0.43§ | 4.06 | 0.98 ± 0.09§ | 4.14 | 35.26 ± 0.86§ | 0.12 | – |
| H38D | 4.61 ± 0.12§ | 1.93 | 0.71 ± 0.01† | 2.71 | 15.90 ± 0.21§ | 0.12 | – |
| H38K | 5.54 ± 0.12§ | 2.32 | 0.71 ± 0.08† | 3.27 | 23.50 ± 1.21§ | 0.10 | – |
| M39A | 25.56 ± 0.96§ | 10.70 | 0.79 ± 0.06§ | 13.50 | 6.32 ± 0.34*§ | 1.69 | 1.72 ± 0.12§ |
| M39F | 38.56 ± 1.72§ | 16.14 | 0.50 ± 0.02 | 32.22 | 2.18 ± 0.09† | 5.75 | – |
| N47A | 0.225 ± 0.003§ | 0.09 | 0.67 ± 0.06 | 0.13 | 11.50 ± 0.51§ | 0.01 | – |
| Q49A | 43.28 ± 0.96§ | 18.11 | 0.74 ± 0.06‡ | 24.47 | 5.58 ± 0.46*§ | 3.24 | 1.64 ± 0.04§ |
| Q49E | 49.75 ± 1.36§ | 20.82 | 0.49 ± 0.05 | 42.49 | 2.87 ± 0.09*§ | 7.26 | 1.51 ± 0.03§ |
| H50A[a] | 6.46 ± 0.26§ | 2.70 | 1.10 ± 0.15§ | 2.45 | 7.34 ± 0.21§ | 0.37 | – |
| H50E[a] | 0.21 ± 0.01§ | 0.09 | 0.81 ± 0.04§ | 0.11 | 12.34 ± 0.36§ | 0.01 | – |
| H50Y[a] | 0.87 ± 0.02§ | 0.36 | 0.83 ± 0.06§ | 0.43 | 12.57 ± 0.73§ | 0.03 | – |
| H50K | 8.14 ± 0.03§ | 3.40 | 0.69 ± 0.06† | 4.95 | 6.77 ± 0.27*§ | 0.45 | 1.54 ± 0.06§ |
| H50F | 1.44 ± 0.03§ | 0.60 | 0.76 ± 0.01‡ | 0.79 | 6.43 ± 0.38§ | 0.09 | – |
| C51A | 19.64 ± 0.65§ | 8.22 | 0.82 ± 0.04§ | 10.01 | 6.40 ± 0.12*§ | 1.28 | 1.57 ± 0.08§ |
| C51D | 2.16 ± 0.07§ | 0.91 | 1.30 ± 0.08§ | 0.7 | 16.94 ± 0.69*§ | 0.05 | 1.40 ± 0.03§ |

acetate buffers (from pH 5.0 to 5.5) and 0.1 M potassium phosphate buffer (from pH 6.0 to 8.5). Increments of pH were 0.5 and control experiments showed no discontinuities from buffer types. The p$K_a$ values of bound GSH were obtained by fitting the data to the equation $y = y^{lim}/(1 + 10^{pKa-pH})$ as previously described [13]. The program GraphPad Prism 5 was used for nonlinear fit of the data to the sigmoidal dose–response (variable slope) equation.

### Fluoride/chloride leaving group substitution

A diagnostic test in evaluating the rate-limiting step in nucleophilic aromatic substitution reactions is the effect of different leaving groups on kinetic parameters [13]. The second order kinetic constants at pH 6.5 for the spontaneous reaction of GSH with CDNB and FDNB (1-fluoro-2,4-dinitrobenzene) were determined by kinetic measurement by using CDNB or FDNB as co-substrate as previously described [24]. The ratios of the catalytic constants ($k_{cat}^{FDNB}/k_{cat}^{CDNB}$) were determined.

### Effect of viscosity on the kinetic parameters

The dependence of the steady-state kinetic parameters on relative viscosity was observed by performing kinetics measurements in the presence of varying glycerol concentrations. The range of relative viscosities ($\eta/\eta^0$) was between 1.53 and 4.43. The slope of the plots for relative catalytic constant ($k_{cat}^0/k_{cat}$) versus relative viscosity ($\eta/\eta^0$) was determined. Viscosity values ($\eta$) at 25 °C were calculated as described previously [25].

### Thermal stability assay

The enzymes at 0.1 mg/ml in 0.1 M phosphate buffer (pH 6.5) containing 1 mM EDTA and 5 mM dithiothreitol were incubated at 45 °C for various times and then activity was measured in the standard GST assay. The data were plotted as log percentage of remaining activity versus pre-incubation time. The half-life ($t_{½}$) of the enzyme at 45 °C was calculated from the slope of the plot using the equations: Slope = $k$/2.3, $k = 0.693/t_{½}$.

### Intrinsic fluorescence measurement

There are two tryptophan residues in each monomer of adGSTD4-4: Trp$^{64}$ and Trp$^{191}$. The intrinsic fluorescence from Trp$^{64}$, which is exposed to solvent at the base of the G-site, can be used to monitor the active site conformation indirectly. The intrinsic fluorescence of adGSTD4-4 was measured in a single-photon counting spectrofluorimeter. Excitation was at 295 nm and emission was scanned from 300 to 450 nm. In these experiments, a number of samples containing 0.1 mg/ml GST in 0.1 M potassium phosphate buffer (pH 6.5) were prepared similarly for the wild-type and engineered enzymes. The wavelength that gives the maximum fluorescence intensity ($\lambda_{max}$) and fluorescence intensity at $\lambda_{max}$ were observed. The experimental data was corrected both for dilution and for inner filter effects.

## RESULTS

### Enzymatic characterization

Michaelis–Menten analysis was performed using nonlinear regression to determine steady-state kinetic constants (Table 1). The kinetic constants showed the residue changes of His$^{38}$, His$^{50}$, Met$^{39}$, Asn$^{47}$, Cys$^{51}$ and Gln$^{49}$ impacted upon catalysis. The engineered G-site residue enzymes showed only small changes in $K_m^{CDNB}$, whereas remarkably lower affinities towards GSH were shown (greater $K_m^{GSH}$) compared with wild-type. Positive co-operativity for GSH binding was observed for several engineered enzymes that displayed deviation of steady-state kinetics from a Michaelis–Menten hyperbolic to a sigmoidal curve response. The extent of positive co-operativity is shown by Hill coefficients ($h$) ranging from 1 (no co-operativity) to 2 (full co-operativity) for a dimeric enzyme with two active sites. Positive co-operativity was observed for H38E, M39A, H50K, C51A, C51D, Q49A and GA49E as determined by Hill coefficients ranging from 1.40 to 1.83, suggesting that the changed residues altered the movement of $\alpha$2-helix and its flanking region to influence the induced-fit mechanism.

**Table 2 Substrate-specific activity of the engineered enzymes compared to the wild-type**

The substrates used were 3 mM CDNB, 1 mM DCNB, 0.1 mM PNPBr, 0.1 mM PNBC and 0.2 mM EA. The reactions were performed at a constant GSH concentration (appropriate for each enzyme). [a]Some of these values have been previously reported and are shown for purposes of comparison [19,20]. One-way ANOVA with Dunnett's multiple comparison test was performed with wild-type as control; statistical significance is shown by † for $P < 0.05$, ‡ for $P < 0.01$ and § for $P < 0.001$.

| | Specific activity ($\mu$mol · min$^{-1}$ · mg$^{-1}$) | | | | |
|---|---|---|---|---|---|
| Enzyme | CDNB | DCNB | EA | PNPBr | PNBC |
| Wild-type[a] | 52.50 ± 0.52 | 0.035 ± 0.006 | 0.286 ± 0.062 | 0.074 ± 0.012 | 0.064 ± 0.002 |
| H38A[a] | 21.70 ± 0.20§ | 0.037 ± 0.001 | 0.146 ± 0.016§ | 0.040 ± 0.004§ | 0.013 ± 0.002§ |
| H38E[a] | 11.21 ± 0.24§ | < 0.001 | 0.191 ± 0.026§ | < 0.008 | < 0.005 |
| H38F[a] | 3.76 ± 0.09§ | < 0.001 | 0.230 ± 0.019† | < 0.005 | < 0.003 |
| H38D | 2.33 ± 0.07§ | < 0.001 | 0.111 ± 0.011§ | < 0.001 | < 0.003 |
| H38K | 2.02 ± 0.07§ | < 0.001 | 0.165 ± 0.007§ | < 0.003 | < 0.002 |
| M39A | 18.84 ± 0.66§ | 0.012 ± 0.001§ | 0.183 ± 0.011§ | < 0.005 | < 0.003 |
| M39F | 28.67 ± 0.71§ | 0.043 ± 0.002† | 0.166 ± 0.010§ | 0.029 ± 0.008§ | 0.065 ± 0.009 |
| N47A | 0.13 ± 0.01§ | < 0.001 | 0.079 ± 0.001§ | < 0.001 | < 0.001 |
| Q49A | 33.36 ± 0.92§ | 0.023 ± 0.002‡ | 0.244 ± 0.012 | 0.050 ± 0.002§ | 0.044 ± 0.001‡ |
| Q49E | 41.76 ± 0.60§ | 0.032 ± 0.001 | 0.244 ± 0.020 | 0.020 ± 0.001§ | 0.048 ± 0.003‡ |
| H50A[a] | 3.80 ± 0.10§ | 0.015 ± 0.007§ | 0.146 ± 0.050§ | 0.012 ± 0.002§ | 0.016 ± 0.007§ |
| H50E[a] | 0.15 ± 0.01§ | < 0.001 | 0.026 ± 0.004§ | < 0.005 | < 0.005 |
| H50Y[a] | 0.47 ± 0.01§ | < 0.001 | 0.064 ± 0.008§ | < 0.008 | < 0.005 |
| H50K | 6.28 ± 0.04§ | 0.007 ± 0.001§ | 0.053 ± 0.020§ | < 0.007 | < 0.004 |
| H50F | 0.93 ± 0.03§ | < 0.001 | 0.077 ± 0.005§ | < 0.001 | < 0.001 |
| C51A | 15.44 ± 0.58§ | 0.009 ± 0.001§ | 0.046 ± 0.001§ | 0.019 ± 0.001§ | < 0.001 |
| C51D | 1.24 ± 0.03§ | < 0.001 | 0.080 ± 0.004§ | < 0.002 | < 0.001 |

Although Met[39] interacts directly with GSH interacting residues, His[38] and His[50], the contribution to catalytic function is through the effect on GSH binding. The results suggest that the effect is mostly through a packing rearrangement that includes any perturbation of the orientation of His[38] or His[50]. Rearrangement of active site residues is elicited by M39A to accommodate the decreased volume as well as the lack of dipole–dipole interaction with the histidines. This condition also appears to engender flexibility to this region, which is shown by positive co-operativity for GSH binding with a Hill coefficient of 1.72 ± 0.12 (Table 1).

The GSH interaction was decreased for all His[38] engineered enzymes as shown by an increase in $K_m^{GSH}$ of 17–71-fold. In addition, positive co-operativity for GSH was observed for H38E with a Hill coefficient ($h$) of 1.83 ± 0.01.

There is a hydrogen bond network in the GST active site that is adjacent to the GSH glycine moiety. This network is formed by several residues, Asn[47], Gln[49] and Cys[51], as well as His[50], with the latter directly interacting with GSH. His[50] replacements not only decreased binding affinity to GSH (ranging from 13- to 25-fold) but also impacted upon catalytic rates as shown by $k_{cat}$ values that decreased from 13 to 0.3 % of the wild-type enzyme $k_{cat}$ values. The N47A change displayed several large effects on the enzyme, one on enzyme catalysis with the enzyme having only 0.3 % $k_{cat}$ of the wild-type, and another on GSH binding with a 23-fold increase in $K_m^{GSH}$. Gln[49] and Cys[51] interaction is through their main-chain nitrogens and oxygens. Changes in these residues showed intermediate effects on catalysis except for C51D, which had a $k_{cat}$ only 3.5 % of wild-type. However, the changes in these residues all showed a major impact on GSH binding with increased $K_m^{GSH}$ values from 6- to 34-fold. The results suggest that a packing rearrangement occurred. This rearrangement also enabled subunit–subunit communication as shown by the observed positive co-operativity upon GSH binding (Table 1).

Substrate specific activity was affected for all the engineered enzymes to varying degrees (Table 2). For example, most of the enzymes exhibited less effect on activity for EA. This suggests that the binding mode and the orientation of this substrate are different from the other substrates. Both GSH and hydrophobic substrate-binding sites are located in the same active site pocket of GSTs, therefore it is not surprising that changes in the G-site residues can perturb the hydrophobic substrate site.

It has been proposed that many steps occur in the GST catalytic mechanism including GSH ionization through thiol deprotonation, substrate conjugation by nucleophilic attack of the thiolate at the electrophilic centre, product formation and product release from the active site [13,26–28]. The overall velocity of the enzyme-catalysed reaction is affected by most of the engineered residues, although to different extents. Therefore several steps in the catalytic pathway were studied to determine the roles of the engineered residues.

### pH dependence of kinetic constants

The p$K_a$ values of ionized GSH (enzyme-bound GSH) were calculated from plots of $k_{cat}/K_m^{CDNB}$ versus pH for the wild-type and engineered enzymes (Table 3; Figure 2). The apparent p$K_a$ for wild-type is approx. 6.0. The p$K_a$ values of ionized GSH in the engineered enzymes varied, with the greatest effect shown by H50A which increased it by almost 1 pH unit. GSH ionization is considered to be an important step in the catalytic mechanism of GST that generates the thiolate anion (intermediate deprotonated form of GSH) for conjugation with the electrophilic substrate. This kinetically relevant ionization of GSH has been shown to be reflected in pH dependence for $k_{cat}/K_m^{CDNB}$ [13]. Several reports have shown that residues located near the cysteine thiol and glutamyl $\alpha$-carboxylate of GSH contribute to promoting and stabilizing the anionic glutathione thiol group [13,27–31]. However, this is the first report of involvement of the GSH glycine moiety in GSH ionization.

### Meisenheimer complex formation

Meisenheimer complex or $\sigma$-complex intermediate, is generated during a nucleophilic aromatic substitution reaction. Leaving group effects on enzyme catalysis can be used to determine

**Table 3 The p$K_a$ value of ionized GSH in the active site of wild-type and engineered enzymes**

The effect of pH on $k_{cat}/k_m^{CDNB}$ was obtained by measuring kinetic constants using various pH buffers of 0.1 M sodium acetate buffers (from pH 5.0 to 5.5) and 0.1 M potassium phosphate buffer (from pH 6.0 to 8.5). The p$K_a$ values of ionized GSH (GSH-bound enzyme) were determined. n.d., Not determined (low activity precluded measurement). One-way ANOVA with Dunnett's multiple comparison test was performed with wild-type as control; statistical significance is shown by § for $P < 0.001$. See Figure 2 for a plot of the experimental data.

| Enzyme | p$K_a$ (ionized GSH) |
|---|---|
| Wild-type | 6.00 ± 0.05 |
| H38A | 6.10 ± 0.02 |
| M39A | 6.52 ± 0.05§ |
| N47A | n.d. |
| Q49A | 6.23 ± 0.05§ |
| H50A | 6.92 ± 0.06§ |
| C51A | 6.22 ± 0.03§ |
| C51D | 6.42 ± 0.03§ |

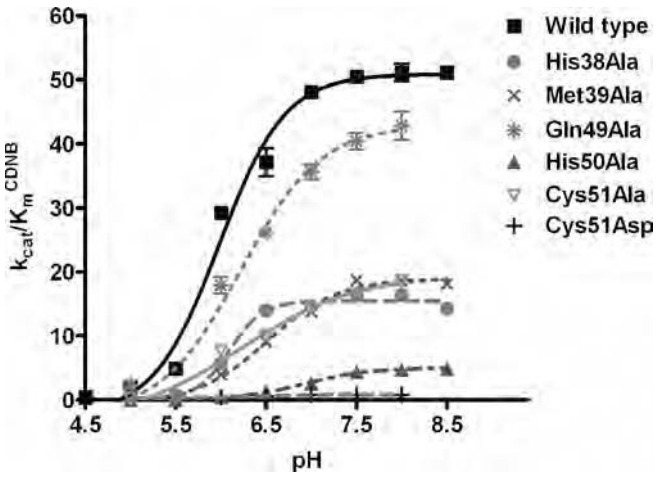


**Figure 2 Plot of the data to determine the p$K_a$ value of ionized GSH in the active site of wild-type and engineered enzymes**

The effect of pH on $k_{cat}/k_m^{CDNB}$ was obtained by measuring kinetic constants using various pH buffers of 0.1 M sodium acetate buffers (from pH 5.0 to 5.5) and 0.1 M potassium phosphate buffer (from pH 6.0 to 8.5). The p$K_a$ values of ionized GSH (GSH-bound enzyme) were determined (see Table 3). The results are presented as means ± S.D. from at least three independent experiments.

whether the rate-limiting step of the reaction is $\sigma$-complex formation. The substitution of a more electronegative leaving group concomitant with an increase in the rate constant of the spontaneous reaction with glutathione is a signal that the $\sigma$-complex formation is a rate-limiting step [13]. Therefore the influence on the catalytic constant of the chlorine leaving group of CDNB replaced with fluorine was examined (Table 4).

Although the wild-type enzyme was insensitive, several of the engineered enzymes demonstrated sensitivity to the halogen leaving group, particularly H50A, C51D and D47A, with increased ratio values of 19-, 27- and 18-fold respectively. The catalytic efficiency ($k_{cat}/K_m$) of the engineered enzymes showed a different sensitivity to the nature of the leaving group, suggesting that an alteration of the relative catalytic-centre activity is a consequence of changes in the rate of $\sigma$-complex formation rather than changes in binding affinity towards the different substrate

**Table 4 Effect of fluoride/chloride leaving group substitution on the rate of catalysis**

The ratio of catalytic rates for the conjugation reaction catalysed by wild-type and engineered GSTs using GSH and CDNB or FDNB as co-substrates. One-way ANOVA with Dunnett's multiple comparison test was performed with wild-type as control; statistical significance is shown by † for $P < 0.05$, ‡ for $P < 0.01$ and § for $P < 0.001$.

| | Leaving group effect | |
|---|---|---|
| Enzyme | $k_{cat}^{FDNB}/k_{cat}^{CDNB}$ | $(k_{cat}/K_m)^{FDNB}/(k_{cat}/K_m)^{CDNB}$ |
| Wild-type | 1.76 ± 0.01 | 20.59 ± 1.02 |
| H38A | 3.11 ± 0.21 | 14.12 ± 0.84† |
| M39A | 8.29 ± 0.95§ | 32.45 ± 3.72§ |
| N47A | 18.09 ± 0.90§ | 29.65 ± 1.32‡ |
| Q49A | 2.63 ± 0.08 | 26.29 ± 1.77† |
| Q49E | 1.50 ± 0.08 | 24.95 ± 1.21 |
| H50A | 18.57 ± 0.41§ | 16.55 ± 1.59 |
| C51A | 2.93 ± 0.05 | 30.31 ± 2.85§ |
| C51D | 26.75 ± 0.99§ | 44.71 ± 4.15§ |

**Table 5 Viscosity effect on kinetic constants and free energy changes of wild-type and engineered enzymes**

The effect of viscosity on kinetic constants was assayed by using 0.1 M potassium phosphate buffer (pH 6.5) with various glycerol concentrations. The slope of a reciprocal plot of the relative catalytic constant ($k_{cat}^0/k_{cat}$) versus relative viscosity ($\eta/\eta^0$) was determined. n.d., Not determined (low activity precluded measurement); $\Delta\Delta G$ (the difference in the free energy changes for the formation of the transition states in the wild-type and engineered enzymes) is calculated from the equation: $\Delta\Delta G = -RT \ln(k_{cat}/K_m^{CDNB})_{engineered}/(k_{cat}/K_m^{CDNB})_{wild-type}$. One-way ANOVA with Dunnett's multiple comparison test was performed with wild-type as control; statistical significance is shown by § for $P < 0.001$.

| Enzyme | Slope | $\Delta\Delta G$ (kJ/mol) |
|---|---|---|
| Wild-type | 0.959 ± 0.036 | – |
| H38A | 0.485 ± 0.019§ | 3.58 ± 0.033 |
| M39A | 0.430 ± 0.031§ | 3.33 ± 0.132 |
| N47A | n.d. | 14.8 ± 0.222 |
| Q49A | 0.797 ± 0.036§ | 1.86 ± 0.105 |
| H50A | 0.005 ± 0.001§ | 7.56 ± 0.095 |
| C51A | 1.11 ± 0.010§ | 4.08 ± 0.125 |
| C51D | 0.051 ± 0.007§ | 10.7 ± 0.201 |

leaving groups. The results suggest that the process of $\sigma$-complex intermediate formation is affected by the disruption of the hydrogen bond network to GSH which affected the overall velocity of the enzyme-catalysed reaction. It is possible that the residue changes caused incorrect orientation of the GSH thiol or of the $His^{50}$ side chain, which then disturbs the conjugation process of the thiolate anion with the electrophilic substrate. Additionally, the results strongly support that the hydrogen bond network contributes to both the GSH ionization process and $\sigma$-complex intermediate formation. This contribution appears to stabilize the $His^{50}$ residue as shown by the changes in p$K_a$ and the greater effect of the leaving group on the catalytic constants of C51D but not C51D.

### Viscosity effect on kinetic constants

The viscosity effect was studied to determine if the rate-limiting step of the reaction is physical or chemical. The slope of the reciprocal plot of inverse relative catalytic constant ($k_{cat}^0/k_{cat}$) versus relative medium viscosity ($\eta/\eta^0$) was determined (Table 5). A slope near unity gives a proportional decrease in rate constant with increasing viscosity of the solution and shows a physical

**Table 6 Thermal stability of wild-type and engineered adGSTD4-4 at 45 °C**

The remaining GST activity was measured after incubating the enzyme at various time points at 45 °C. n.d., Not determined (low activity precluded measurement). [a]Some of these values have been previously reported and are shown for purposes of comparison [19,20]. One-way ANOVA with Dunnett's multiple comparison test was performed with wild-type as control; statistical significance is shown by ‡ for $P < 0.01$ and § for $P < 0.001$.

| Enzyme | Half-life at 45 °C (min) |
|---|---|
| Wild-type[a] | 15.32 ± 0.31 |
| H38A[a] | 15.33 ± 0.88§ |
| H38E[a] | 40.17 ± 1.26§ |
| H38F[a] | 19.33 ± 0.59§ |
| H38D | 15.18 ± 1.67 |
| H38K | 14.07 ± 0.73 |
| M39A | 4.71 ± 0.16§ |
| M39F | 4.72 ± 0.23§ |
| N47A | n.d. |
| Q49A | 15.19 ± 1.06§ |
| Q49E | 25.19 ± 1.37§ |
| H50A[a] | 25.81 ± 1.99§ |
| H50E[a] | 15.31 ± 0.54 |
| H50Y[a] | 20.79 ± 0.34§ |
| H50K | 11.99 ± 0.51§ |
| H50F | 27.07 ± 0.82§ |
| C51A | 14.86 ± 0.64 |
| C51D | 18.18 ± 1.01‡ |

step is rate-determining, whereas a slope of zero indicates that a chemical reaction step is rate limiting [32,33].

Wild-type enzyme displayed a linear dependence with a slope of approx. 1.0 suggesting that a physical step of the reaction that includes product release and/or structural transition is rate limiting. The engineered enzymes exhibited viscosity effects on $k_{cat}$ to different degrees. H50A and C51D were viscosity-independent with a slope approaching zero. These engineered enzymes changed the rate-limiting step of the reaction to a chemical step that includes GSH ionization step and $\sigma$-complex formation as described above, whereas partial dependence on a diffusion barrier and other viscosity-dependent motions were observed for the remaining enzymes that displayed viscosity effects with intermediate values ($0 < \text{slope} < 1$).

Also displayed in Table 5 is $\Delta\Delta G$, which is shown to illustrate the differences in the free energy changes for the formation of the transition states in the wild-type and engineered enzymes, as calculated at 25 °C from the equation below [34]:

$$\Delta\Delta G = -RT \ln \left(k_{cat}/K_m^{CDNB}\right)_{mutant} / \left(k_{cat}/K_m^{CDNB}\right)_{wild\text{-}type}.$$

H50A, D47A and C51D have a greater $\Delta\Delta G$ (7.562, 14.842 and 10.671 kJ/mol respectively) compared with other engineered enzymes (ranging from 1.860 to 4.075 kJ/mol) indicating that upon disruption of the hydrogen bond network, the enzymes require more energy than the wild-type enzyme to form and stabilize the transition state.

### Characterization of physical properties

The stability of the proteins was determined in comparison with the adGSTD4-4 wild-type (Table 6). In general, the engineered His[38], His[50], Asn[47], Cys[51] and Gln[49] proteins exhibited comparable stabilities to the wild-type, indicating a minor role of these residues in structural maintenance. However, H38E increased stability of the enzyme 2.6-fold, suggesting that a conformational change occurred which also is supported by the observed positive co-operativity. Met[39] appears to play a role in structural integrity as shown by 3-fold decreased enzyme stability for both the alanine and phenylalanine changes. However, the initial folding processes of the enzymes were observed to yield comparable refolding rates to the wild-type (results not shown). These results suggest that the Met[39] dipole–dipole interaction and positioning of His[38] and His[50] in a suitable conformation impact not only the kinetic properties but also enzyme stability.

The intrinsic fluorescence of tryptophan was used as an indicator of changes in tertiary structure (Figure 3). The $\lambda_{max}$ of tryptophan fluorescence in the engineered enzymes was slightly different from wild-type with a red shift in the range of 1–4 nm indicating a different polarity in tryptophan environments. In addition, differences in fluorescence intensity between wild-type and engineered enzymes were observed. This result suggests that there are minor conformational disturbances in the active site topography, which affect orientations of tryptophan and/or its neighbouring residues thereby modulating the quenching and tryptophan exposure to the electrophilic environment. For example, the active site topology changes that generated the positive co-operativity in H50K also yielded the lowest fluorescence intensity among the His[50] engineered enzymes (~44 % of wild-type). Moreover, the conformational change induced by glutamic acid residue replacement of His[38] also gave a 2-fold increase in enzyme stability, increased intrinsic fluorescence intensity to 197 % of wild-type, modulated GSH binding and enzyme catalysis as well as yielding the observed positive co-operativity towards GSH.

## DISCUSSION

The G-site residues interacting directly with cysteine and glutamyl moieties of GSH have been shown in several studies to contribute to GST catalytic mechanisms including GSH binding, catalysis, GSH ionization as well as rate-limiting step determination [10–14]. In the present study, we have examined the significant contributions of GST residues that interact with the GSH glycine moiety as well as identification of a hydrogen bond network. The network consists of His[38], Met[39], Asn[47], Gln[49], His[50] and Cys[51] and contributes to catalysis through multiple processes including GSH ionization, nucleophilic substitution, product formation and product dissociation.

The kinetic studies demonstrated that the engineered residues greatly impacted the enzyme's ability to interact with GSH. Moreover, the engineered enzymes of His[38], Met[39], His[50], Cys[51] and Gln[49] have shown strong positive co-operativity upon binding of GSH. However, the positive co-operativity was not observed for the engineered enzymes of residues interacting with the other moieties of GSH [11–13,15]. Therefore it can be suggested that the residues interacting with the GSH glycine moiety are not only involved in GSH interaction but also control the motion of a flexible region of GST. Upon binding of GSH in the active site, these GST residues induce an active site conformational change for the induced-fit mechanism. These residues are on the loops on either side of $\alpha$2-helix which connects the helix to $\beta$2-sheet and $\beta$3-sheet. These loops would serve as hinges for the movement of $\alpha$2-helix.

In the present study, changes of the active-site residues generated positive co-operativity between two subunits, a finding similar to that obtained in previous studies in which the subunit interface had been changed or where changes in highly flexible regions, for example Gly[41], Cys[47] and Lys[54] of hGSTP1-1 (human GSTP1-1) [33,35] or Asn[49] and Gln[53] of maize GST1 [36,37],

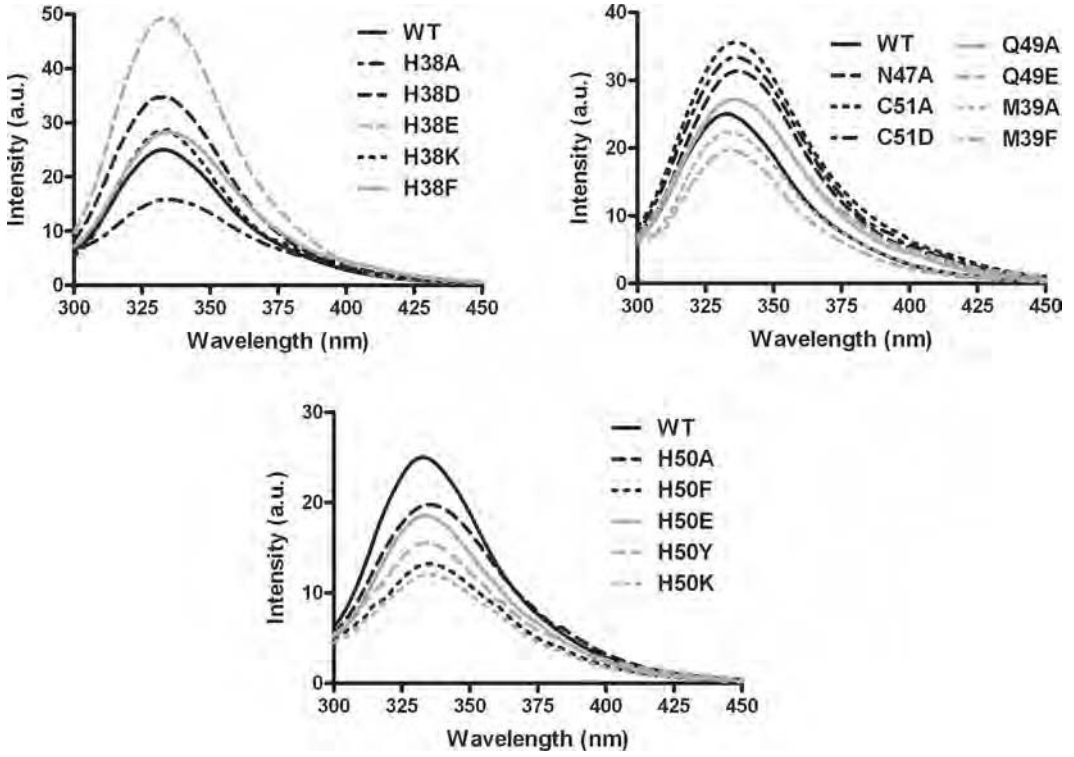


**Figure 3 The maximum emission wavelength ($\lambda_{max}$) and intrinsic fluorescence intensity at $\lambda_{max}$ of tryptophan fluorescence of wild-type and the engineered enzymes**

Excitation was at 295 nm and emission was scanned from 300 to 450 nm. Samples ($n = 3$) contained 0.1 mg/ml protein in 0.1 M potassium phosphate buffer (pH 6.5). Percent intensity change compared with wild-type enzyme was measured at fluorescence $\lambda_{max}$ averaged over three scans corrected for dilution and inner filter effects.

had been made. It has been proposed that the conformational transitions generate two different binding modes upon GSH binding: low-affinity and high-affinity conformations, which are related to positive co-operativity observed [5,38,39]. The binding of GSH to the first active site stabilizes the low-affinity conformation of the enzyme which then becomes the high-affinity conformational state. Positive co-operativity upon GSH binding observed in $His^{38}$, $Met^{39}$, $His^{50}$, $Cys^{51}$ and $Gln^{49}$ engineered enzymes may be relevant to this conformational transition concept. These residues are located in a highly flexible region; therefore the residue changes would alter the flexibility of the $\alpha$2-helix to fit GSH in the active site, which may then generate two different conformational transition states upon GSH binding.

Both $His^{38}$ and $His^{50}$ interact directly with the glycine carboxylate of GSH. The functional groups at positions 38 and 50 are significant in size, volume and polarity for GSH binding and enzyme catalysis. However, $His^{50}$ contributes more to the GSH activation process and enzyme catalysis in which the full function is achieved by the synergistic action with the hydrogen bond network residues ($Asn^{47}$, $Gln^{49}$ and $Cys^{51}$). The disruption of the hydrogen bond network, for the engineered enzymes of $His^{50}$, $Asn^{47}$ and $Cys^{51}$, showed progressively decreased $k_{cat}$ values to more than 90 %. Moreover, several aspects of the GST catalytic mechanism were altered by H50A. H50A decreased the enzyme's ability to lower the p$K_a$ of the GSH thiol group up to 1 pH unit; this large an effect has been observed for mutations of the conserved serine/tyrosine residue interacting with the GSH thiol group [13,40–42]. Additionally, the rate-limiting step of the H50A is fully switched from a physical step to a chemical step as determined by fluoride/chloride leaving group and viscosity effect on the kinetic constants. As the important $His^{50}$ is still present, lesser effects were observed for the engineered enzymes of $Gln^{49}$ and $Cys^{51}$ for minor disruptions of the stabilizing hydrogen bond network.

The results strongly support that $His^{50}$ is a key residue in the hydrogen bond network which functions as a proton acceptor as well as controls the electron distribution in the active site to promote ionization and stabilization of the GSH thiolate anion. The $His^{50}$ residue contributes to precise residue and substrate orientations, GSH ionization, $\sigma$-complex intermediate formation and the release of product from the active site. The regulation of the electrostatic field in the active site by positively charged residues has also been reported in several studies [15,43,44].

The changes in catalytic efficiency are also related to differences in free energy changes for the formation of transition states in the engineered and wild-type enzymes as determined by $\Delta\Delta G$ [34]. The greater value of $\Delta\Delta G$ refers to a decrease in the stabilization of transition state compared with wild-type in which the enzyme utilizes more energy to stabilize its transition state. Moreover, the stabilization of transition state contributes to multiple mechanisms in enzyme-catalysed reactions. $\Delta\Delta G$ values are increased up to 7.562, 14.84 and 10.666 kJ/mol for H50A, D47A and C51D respectively in which the hydrogen bond network is strongly disrupted, indicative of the incomplete pre-organized environment for enhancing catalysis along the reaction pathway of the engineered enzymes [45]. Therefore it can be noted that the network of hydrogen bonds is also required for the organization inside the enzyme molecule to provide stabilization of the transition state.

The positively charged residue position 50 appears to be highly conserved or functionally conserved across GST classes by histidine, lysine or arginine located at the equivalent structural

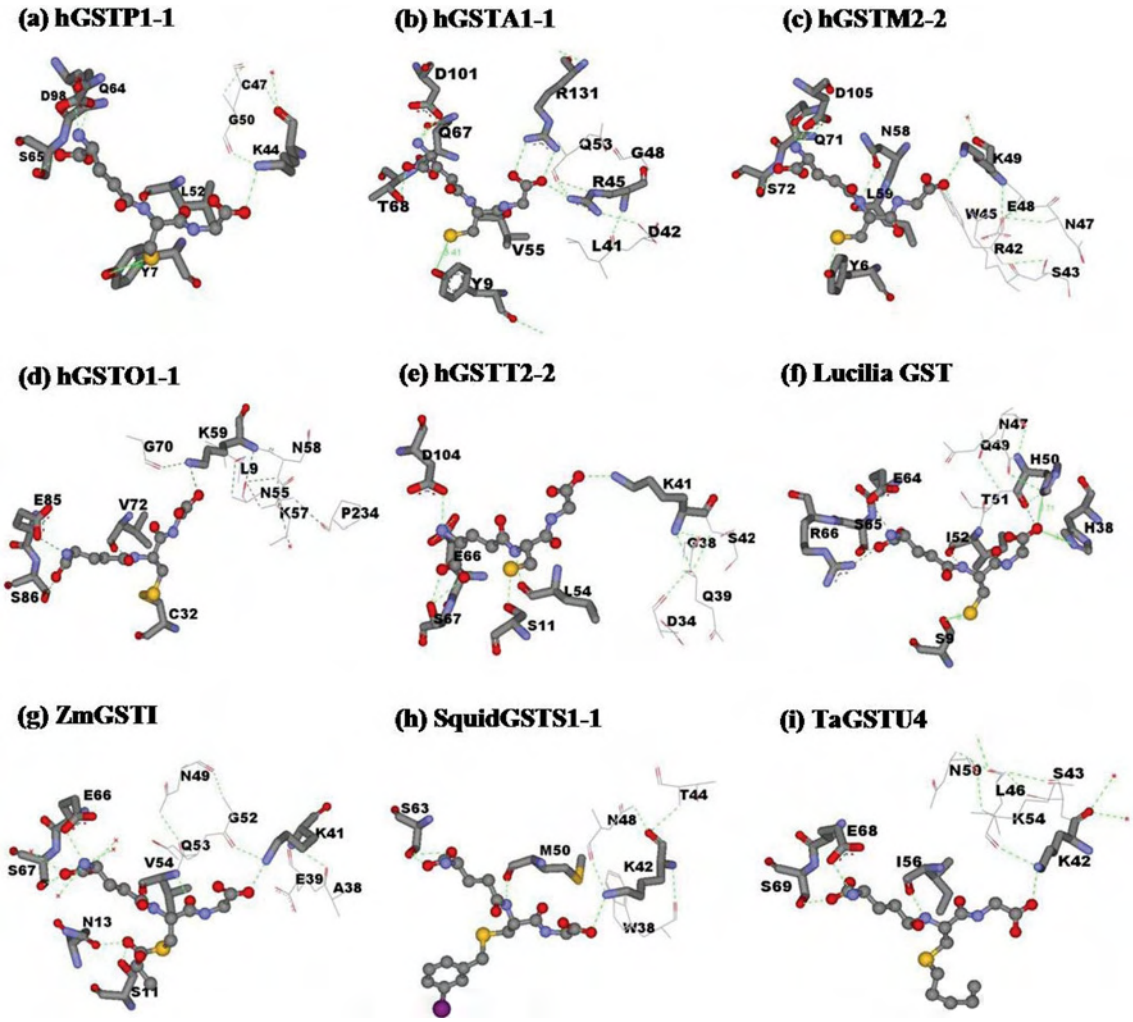


COLOUR

**Figure 4 Conserved G-site residues that directly interact with the glycine moiety of GSH and generate a hydrogen bond network in several GST classes**

The conserved G-site residues are shown by stick models, while line models represent the hydrogen bond network residues at the glycine moiety of GSH. GSH or GSH analogues are illustrated in ball-and-stick; GSH (**a**, **b**, **c**, **d**, **e**, **f**), lactoylglutathione (**g**), iodobenzylglutathione (**h**) and *S*-hexyl-GSH (**i**). Green dotted lines represent hydrogen-bond interactions. PDB code numbers: hGSTP1-1 (PDB id 8GSS), hGSTA1-1 (PDB id 1PKW), hGSTM2-2 (PDB id 1XW5), hGSTO1-1 (PDB id 1EEM), hGSTT2-2 (PDB id 1LJR), Lucilia GST [7], ZmGST1 (PDB id 1AXD), squid GSTS1-1 (PDB id 2GSQ) and TaGSTU4 [*Triticum aestivum* (wheat) GSTU4; PDB id 1GWC]. The Figure was created with Accelrys DS ViewerPro 5.0.

position. This conserved residue is in hydrogen bonding distance to the glycine carboxylate moiety of GSH which is stabilized by a hydrogen bond network of surrounding residues (Figure 4) for example Lys[40] in PtGSTU1 [*Pinus tabulaeformis* (Chinese hard pine) GSTU1], Lys[41] in ZmGST1 [*Zea mays* (maize) GST1], Lys[44] in hGSTP1-1, Lys[41] in hGSTT2-2, Lys[59] in hGSTO1-1, Lys[49] in hGSTM2-2, Lys[42] in squid GSTS1-1, Lys[45] in Sj26GST [26 kDa GST from *Schistosoma japonicum* (oriental blood-fluke)] and Arg[45] in hGSTA1-1. However, the feature of two positively charged histidines, His[38] and His[50], interacting with the glycine carboxylate moiety of GSH is a unique trait for insect GSTDs. His[38] is responsible for GSH binding, whereas His[50] contributes to several steps of the enzyme-catalysed reaction from GSH interaction to the release of product from the active site.

For the GSH activation mechanism of Alpha, Mu and Pi GST isoenzymes, it has been described that the thiol proton is quantitatively released into solution after the thiolate anion is formed [46,47]. In contrast with GSTD, which behaves differently, the thiol proton is captured by at least an internal base residue at high pH value [46,47]. The present study shows that His[50] is also a candidate for the thiol proton acceptor in addition to the residues at the $\gamma$-glutamyl portion of GSH reported previously [15,31]. Moreover, the overall velocity of His[50] engineered enzymes is progressively restricted; therefore it can be assumed that the thiol proton released must be accepted first by the active site residues, e.g. His[50], before a new cycle of the reaction can initiate.

The 'base-assisted deprotonation model' is an alternative model that describes the mechanism of GST enzymes in GSH ionization process. This model has been implicated in several studies of the glutamyl $\alpha$-carboxylate of GSH acting as a catalytic base, involved in the thiol proton acceptance from the GSH thiol group [15,16,31,46]. In the present study, we addressed the contribution of the glycine moiety of GSH for GSH ionization in which this end of GSH is involved in proton acceptance by providing a counter ion from the charged His[50] which is stabilized by the hydrogen bond network.

In conclusion, the present study revealed a critical role for residues located at the glycine moiety of GSH in catalytic rate determination. This area constitutes a second G-site network involved in GSH ionization distinct from the network previously

reported interacting with the glutamyl end of GSH [16,17]. This second network also appears to be functionally conserved in GSTs (Figure 4). In the present study, we showed that $His^{50}$ is a central residue in the hydrogen bond network to GSH with the protonated imidazole ring of $His^{50}$ being stabilized by the network. $His^{50}$ plays important roles in several processes of the enzyme mechanism. Moreover, this network at the glycine moiety of GSH also contributed to the 'base-assisted deprotonation model' for GSH ionization.

This work was funded by the TRF (Thailand Research Fund). A.V. was supported by a Royal Golden Jubilee Ph.D. Scholarship.

## REFERENCES


1 Sheehan, D., Meade, G., Foley, V. M. and Dowd, C. A. (2001) Structure, function and evolution of glutathione transferases: implications for classification of non-mammalian members of an ancient enzyme superfamily. Biochem. J. **360**, 1–16

2 Ketterer, B. (2001) A bird's eye view of the glutathione transferase field. Chem. Biol. Interact. **138**, 27–42

3 Mannervik, B., Awasthi, Y. C., Board, P. G., Hayes, J. D., Di Ilio, C., Ketterer, B., Listowsky, I., Morgenstern, R., Muramatsu, M., Pearson, W. R. et al. (1992) Nomenclature for human glutathione transferases. Biochem. J. **282**, 305–306

4 Hayes, J. D., Flanagan, J. U. and Jowsey, I. R. (2005) Glutathione transferases. Annu. Rev. Pharmacol. Toxicol. **45**, 51–88

5 Mannervik, B. and Danielson, U. H. (1988) Glutathione transferases – structure and catalytic activity. CRC Crit. Rev. Biochem. **23**, 283–337

6 Armstrong, R. N. (1997) Structure, catalytic mechanism, and evolution of the glutathione transferases. Chem. Res. Toxicol. **10**, 2–18

7 Wilce, M. C. J., Board, P. G., Feil, S. C. and Parker, M. W. (1995) Crystal structure of a theta-class glutathione transferase. EMBO J. **14**, 2133–2143

8 Dirr, H., Reinemer, P. and Huber, R. (1994) X-ray crystal structures of cytosolic glutathione S-transferases. Implications for protein architecture, substrate recognition and catalytic function. Eur. J. Biochem. **220**, 645–661

9 Rossjohn, J., Feil, S. C., Wilce, M. C. J., Sexton, J., Spithill, T. W. and Parker, M. W. (1997) Crystallization, structural determination and analysis of a novel parasite vaccine candidate: *Fasciola hepatica* glutathione S-transferase. J. Mol. Biol. **273**, 857–872

10 Stenberg, G., Board, P. G., Carlberg, I. and Mannervik, B. (1991) Effects of directed mutagenesis on conserved arginine residues in a human class Alpha glutathione transferase. Biochem. J. **274**, 549–555

11 Liu, S., Zhang, P., Ji, X., Johnson, W. W., Gilliland, G. L. and Armstrong, R. N. (1992) Contribution of tyrosine 6 to the catalytic mechanism of isoenzyme 3-3 of glutathione S-transferase. J. Biol. Chem. **267**, 4296–4299

12 Kolm, R. H., Sroga, G. E. and Mannervik, B. (1992) Participation of the phenolic hydroxyl group of Tyr-8 in the catalytic mechanism of human glutathione transferase P1-1. Biochem. J. **285**, 537–540

13 Caccuri, A. M., Antonini, G., Nicotra, M., Battistoni, A., Lo Bello, M., Board, P. G., Parker, M. W. and Ricci, G. (1997) Catalytic mechanism and role of hydroxyl residues in the active site of theta class glutathione S-transferases. Investigation of Ser-9 and Tyr-113 in a glutathione S-transferase from the Australian sheep blowfly, *Lucilia cuprina*. J. Biol. Chem. **272**, 29681–29686

14 Tan, K.-L., Chelvanayagam, G., Parker, M. W. and Board, P. G. (1996) Mutagenesis of the active site of the human Theta-class glutathione transferase GSTT2-2: catalysis with different substrates involves different residues. Biochem. J. **319**, 315–321

15 Winayanuwattikun, P. and Ketterman, A. J. (2004) Catalytic and structural contributions for glutathione binding residues in a Delta class glutathione S-transferase. Biochem. J. **382**, 751–757

16 Winayanuwattikun, P. and Ketterman, A. J. (2005) An electron-sharing network involved in the catalytic mechanism is functionally conserved in different glutathione transferase classes. J. Biol. Chem. **280**, 31776–31782

17 Winayanuwattikun, P. and Ketterman, A. J. (2007) Glutamate 64, a newly identified residue of the functionally conserved electron-sharing network contributes to catalysis and structural integrity of glutathione transferases. Biochem. J. **402**, 339–348

18 Pettersen, E. F., Goddard, T. D., Huang, C. C., Couch, G. S., Greenblatt, D. M., Meng, E. C. and Ferrin, T. E. (2004) UCSF chimera – a visualization system for exploratory research and analysis. J. Comput. Chem. **25**, 1605–1612

19 Vararattanavech, A. and Ketterman, A. (2003) Multiple roles of glutathione binding-site residues of glutathione S-transferase. Protein Peptide Lett. **10**, 441–448

20 Vararattanavech, A., Prommeenate, P. and Ketterman, A. J. (2006) The structural roles of a conserved small hydrophobic core in the active site and an ionic bridge in domain I of Delta class glutathione S-transferase. Biochem. J. **393**, 89–95

21 Habig, W. H., Pabst, M. J. and Jakoby, W. B. (1974) Glutathione S-transferases. The first enzymatic step in mercapturic acid formation. J. Biol. Chem. **249**, 7130–7139

22 Segel, I. H. (1993) Enzyme Kinetics, Behavior and Analysis of Rapid Equilibrium and Steady-state Enzyme Systems, John Wiley and Sons, New York

23 Jirajaroenrat, K., Pongjaroenkit, S., Krittanai, C., Prapanthadara, L. and Ketterman, A. J. (2001) Heterologous expression and characterization of alternatively spliced glutathione *S*-transferases from a single *Anopheles* gene. Insect Biochem. Mol. Biol. **31**, 867–875

24 Caccuri, A. M., Ascenzi, P., Lo Bello, M., Federici, G., Battistoni, A., Mazzetti, P. and Ricci, G. (1994) Are the steady state kinetics of glutathione transferase always dependent on the deprotonation of the bound glutathione? New insights in the kinetic mechanism of GST P1-1. Biochem. Biophys. Res. Commun. **200**, 1428–1434

25 Wolf, A. V., Brown, M. G. and Prentiss, P. G. (1985) Handbook of Chemistry and Physics, CRC Press, Boca Raton, FL

26 Armstrong, R. N., Rife, C. and Wang, Z. (2001) Structure, mechanism and evolution of thiol transferases. Chem. Biol. Interact. **133**, 167–169

27 Caccuri, A. M., Ascenzi, P., Antonini, G., Parker, M. W., Oakley, A. J., Chiessi, E., Nuccetelli, M., Battistoni, A., Bellizia, A. and Ricci, G. (1996) Structural flexibility modulates the activity of human glutathione transferase P1-1. Influence of a poor co-substrate on dynamics and kinetics of human glutathione transferase. J. Biol. Chem. **271**, 16193–16198

28 Caccuri, A. M., Lo Bello, M., Nuccetelli, M., Rossi, P., Antonini, G., Federici, G. and Ricci, G. (1998) Proton release upon glutathione binding to glutathione transferase P1-1: kinetic analysis of a multistep glutathione binding process. Biochemistry **37**, 3028–3034

29 Armstrong, R. N. (1997) Structure, catalytic mechanism, and evolution of the glutathione transferases. Chem. Res. Toxicol. **10**, 2–18

30 Gustafsson, A., Pettersson, P. L., Grehn, L., Jemth, P. and Mannervik, B. (2001) Role of the glutamyl $\alpha$-carboxylate of the substrate glutathione in the catalytic mechanism of human glutathione transferase A1-1. Biochemistry **40**, 15835–15845

31 Widersten, M., Björnestedt, R. and Mannervik, B. (1996) Involvement of the carboxyl groups of glutathione in the catalytic mechanism of human glutathione transferase A1-1. Biochemistry **35**, 7731–7742

32 Johnson, W. W., Liu, S., Ji, X., Gilliland, G. L. and Armstrong, R. N. (1993) Tyrosine 115 participates both in chemical and physical steps of the catalytic mechanism of a glutathione S-transferase. J. Biol. Chem. **268**, 11508–11511

33 Ricci, G., Caccuri, A. M., Lo Bello, M., Rosato, N., Mei, G., Nicotra, M., Chiessi, E., Mazzetti, A. P. and Federici, G. (1996) Structural flexibility modulates the activity of human glutathione transferase P1-1. Role of helix 2 flexibility in the catalytic mechanism. J. Biol. Chem. **271**, 16187–16192

34 Dirr, H. W., Little, T., Kuhnert, D. C. and Sayed, Y. (2005) A conserved N-capping motif contributes significantly to the stabilization and dynamics of the C-terminal region of class alpha glutathione transferases. J. Biol. Chem. **280**, 19480–19487

35 Lo Bello, M., Nuccetelli, M., Chiessi, E., Lahm, A., Mazzetti, A. P., Parker, M. W., Tramontano, A., Federici, G. and Ricci, G. (1998) Mutations of Gly to Ala in human glutathione transferase P1-1 affect helix 2 (G-site) and induce positive cooperativity in the binding of glutathione. J. Mol. Biol. **284**, 1717–1725

36 Labrou, N. E., Mello, L. V. and Clonis, Y. D. (2001) Functional and structural roles of the glutathione-binding residues in maize (*Zea mays*) glutathione S-transferase I. Biochem. J. **358**, 101–110

37 Labrou, N. E., Mello, L. V. and Clonis, Y. D. (2001) The conserved Asn49 of maize glutathione *S*-transferase I modulates substrate binding, catalysis and intersubunit communication. Eur. J. Biochem. **268**, 3950–3957

38 Principato, G. B., Danielson, U. H. and Mannervik, B. (1988) Relaxed thiol substrate specificity of glutathione transferase effected by a non-substrate glutathione derivative. FEBS Lett. **231**, 155–158

39 Jemth, P. and Mannervik, B. (1999) Fast product formation and slow product release are important features in a hysteretic reaction mechanism of glutathione transferase T2-2. Biochemistry **38**, 9982–9991

40 Wang, J., Barycki, J. J. and Colman, R. F. (1996) Tyrosine 8 contributes to catalysis but is not required for activity of rat liver glutathione S-transferase, 1-1. Protein Sci. **5**, 1032–1042

41 Gustafsson, A., Etahadieh, M., Jemth, P. and Mannervik, B. (1999) The C-terminal region of human glutathione transferase A1-1 affects the rate of glutathione binding and the ionization of the active-site Tyr9. Biochemistry **38**, 16268–16275

42 Labrou, N. E., Rigden, D. J. and Clonis, Y. D. (2003) Engineering the pH-dependence of kinetic parameters of maize glutathione *S*-transferase I by site-directed mutagenesis. Biomol. Eng. **21**, 61–66

43 Patskovsky, Y. V., Patskovska, L. N. and Listowsky, I. (2000) The enhanced affinity for thiolate anion and activation of enzyme-bound glutathione is governed by an arginine residue of human Mu class glutathione S-transferases. J. Biol. Chem. **275**, 3296–3304
44 Björnestedt, R., Tardioli, S. and Mannervik, B. (1995) The high activity of rat glutathione transferase 8-8 with alkene substrates is dependent on a glycine residue in the active site. J. Biol. Chem. **270**, 29705–29709
45 Garcia-Viloca, M., Gao, J., Karplus, M. and Truhlar, D. G. (2004) How enzymes work: analysis by modern rate theory and computer simulations. Science **303**, 186–195
46 Caccuri, A. M., Antonini, G., Board, P. G., Parker, M. W., Nicotra, M., Lo Bello, M., Federici, G. and Ricci, G. (1999) Proton release on binding of glutathione to Alpha, Mu and Delta class glutathione transferases. Biochem. J. **344**, 419–425
47 Caccuri, A. M., Antonini, G., Board, P. G., Flanagan, J., Parker, M. W., Paolesse, R., Turella, P., Federici, G., Lo Bello, M. and Ricci, G. (2001) Human glutathione transferase T2-2 discloses some evolutionary strategies for optimization of substrate binding to the active site of glutathione transferases. J. Biol. Chem. **276**, 5427–5431

Received 27 March 2007/22 May 2007; accepted 24 May 2007
Published as BJ Immediate Publication 24 May 2007, doi:10.1042/BJ20070422

BJ www.biochemj.org

BJ Structure

Biochem. J. (2007) **402**, 339–348 (Printed in Great Britain) doi:10.1042/BJ20061253



# Glutamate-64, a newly identified residue of the functionally conserved electron-sharing network contributes to catalysis and structural integrity of glutathione transferases

Pakorn WINAYANUWATTIKUN and Albert J. KETTERMAN[1]

Institute of Molecular Biology and Genetics, Mahidol University, Salaya Campus, Nakhon Pathom 73170, Thailand

In *Anopheles dirus* glutathione transferase D3-3, position 64 is occupied by a functionally conserved glutamate residue, which interacts directly with the $\gamma$-glutamate moiety of GSH (glutathione) as part of an electron-sharing network present in all soluble GSTs (glutathione transferases). Primary sequence alignment of all GST classes suggests that $Glu^{64}$ is one of a few residues that is functionally conserved in the GST superfamily. Available crystal structures as well as consideration of the property of the equivalent residue at position 64, acidic or polar, suggest that the GST electron-sharing motif can be divided into two types. Electrostatic interaction between the GSH glutamyl and carboxylic $Glu^{64}$, as well as with $Arg^{66}$ and $Asp^{100}$, was observed to extend the electron-sharing motif identified previously. $Glu^{64}$ contributes to the catalytic function of this motif and the 'base-assisted deprotonation' that are essential for GSH ionization during catalysis. Moreover, this residue also appears to affect multiple steps in the enzyme catalytic strategy, including binding of GSH, nucleophilic attack by thiolate at the electrophilic centre and product formation, probably through active-site packing effects. Replacement with non-functionally-conserved amino acids alters initial packing or folding by favouring aggregation during heterologous expression. Thermodynamic and reactivation *in vitro* analysis indicated that $Glu^{64}$ also contributes to the initial folding pathway and overall structural stability. Therefore $Glu^{64}$ also appears to impact upon catalysis through roles in both initial folding and structural maintenance.

Key words: active-site residue, *Anopheles dirus*, catalytic mechanism, electron sharing network, glutathione transferase, structural integrity.

## INTRODUCTION

GSTs (glutathione transferases; EC 2.5.1.18) are a superfamily of enzymes that contribute towards diverse cellular processes ranging from detoxification to control of gene expression [1–4]. The enzymes generally catalyse nucleophilic attack of the GSH (glutathione) sulfhydryl group to an electrophilic centre of a number of endogenous and xenobiotic compounds [1,5,6]. Conjugation of GSH to such organic molecules enhances solubility, thus facilitating their eventual elimination [5–7]. This reaction is an early step along the mercapturic acid pathway in which hydrophobic compounds are inactivated and eliminated from an organism [8]. Based on amino acid identity, substrate specificities and immunological cross-reactivity, cytosolic GSTs are currently divided into at least 12 distinct evolutionary classes, namely Alpha, Mu, Pi, Theta, Sigma, Zeta, Omega, Phi, Tau, Delta, Epsilon and Beta [6,9–15]. In addition, the number of members identified in this enzyme superfamily is increasing due to the massive growth of genomic information, which includes a number of unclassified GSTs [16].

All cytosolic GSTs adopt the same highly conserved tertiary structure [17]. GSTs are dimeric proteins (with a molecular mass of about 50 kDa) assembled from identical or structurally related subunits. Each subunit is characterized by two distinct domains and an active site. However, each active site is only fully functional when amino acid residues from both subunits are present in the final dimeric structure. The active-site of GSTs consists of two adjacent regions. The first region is the G-site (GSH binding site), formed mostly by the N-terminal domain (domain I), which adopts an $\alpha/\beta$ topology that binds GSH as the thiol substrate [7]. The second region is the non-polar H-site (hydrophobic substrate binding site), generated primarily by the C-terminal domain (domain II), which is an all-helical structure that provides structural elements for recognition of a wide range of hydrophobic co-substrates [7]. Although GSTs possess a high specificity for GSH as the nucleophile, the enzymes exhibit broad specificity with regard to structurally diverse hydrophobic substrates [17]. The catalytic strategy of GSTs for the nucleophilic substitution reaction can be divided into several steps: binding of substrates to the enzyme active site, activation of GSH by thiol deprotonation, nucleophilic attack by thiolate at the electrophilic centre, product formation and product release [18–20].

The roles of several active-site residues and functional groups of GSH have been studied intensively and a potential model has been proposed to describe deprotonation of the GSH thiol group which enhances the nucleophilicity of the reaction [20–24]. The hydroxyl group of the conserved tyrosine/serine residue at the G-site of GSTs (i.e. $Tyr^{8}$ for Pi, $Tyr^{9}$ for Alpha, $Tyr^{6}$ for Mu and $Ser^{9}$ for Delta classes) is within hydrogen-bonding distance of the thiol group of the bound GSH, and is required for correct orientation and stabilization of the deprotonated thiol anion. The deprotonated anionic GSH results from subtraction of a thiol proton by the glutamyl $\alpha$-carboxylate of GSH, which acts as a catalytic base in the base-assisted deprotonation model with assistance from an electron-sharing network. The functionally conserved electron-sharing network is characterized by an ionic

Abbreviations used: adGSTD3-3, *Anopheles dirus* glutathione transferase Delta class homodimer of subunit 3; CDNB, 1-chloro-2,4-dinitrobenzene; DTT, dithiothreitol; FDNB, 1-fluoro-2,4-dinitrobenzene; GdmCl, guanidinium chloride; GSH, glutathione; G-site, GSH binding site; GST, glutathione transferase; PtGSTU1-1, plant Tau class GST.

[1] To whom correspondence should be addressed (email frakt@mahidol.ac.th).

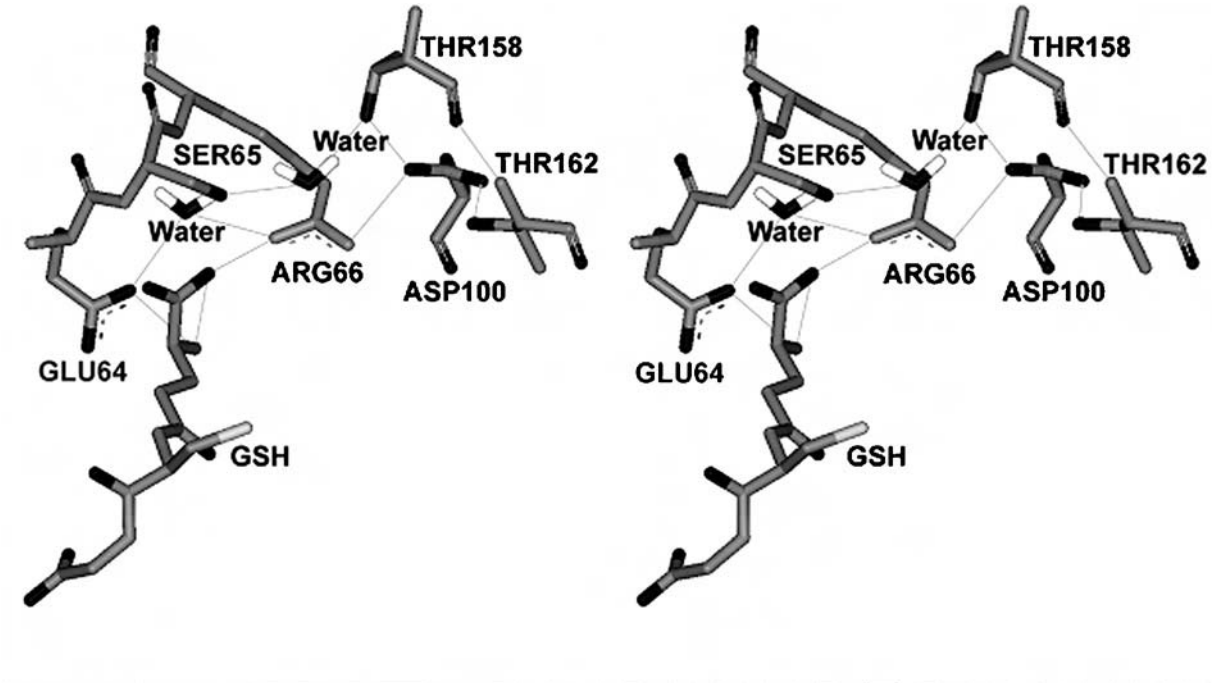


| NCBI Seq ID | GST class | Source | Isoform | | | | | | | | | | | | | | | | | | | | | | | | | | | |
|---|---|---|---|---|---|---|---|---|---|---|---|---|---|---|---|---|---|---|---|---|---|---|---|---|---|---|---|---|---|---|
| AAG38505 | Delta | *A.dirus* | 3 | 52 | I | P | T | L | V | D | N | - | G | F | A | L | W | E | S | R | A | I | C | T | Y | L | A | E | K | Y | G |
| NP_000844.1 | Theta | *H.sapiens* | 1 | 54 | V | P | A | L | K | D | G | - | D | F | T | L | T | E | S | V | A | I | L | L | Y | L | T | R | K | Y | K |
| AH004172.1 | Omega | *H.sapiens* | 1 | 72 | V | P | V | L | E | N | S | Q | G | Q | L | I | Y | E | S | A | I | T | C | E | Y | L | D | E | A | Y | P |
| CAC94005.1 | Tau | *T.aestivum* | 1 | 59 | V | P | V | L | I | H | N | - | G | R | P | V | C | E | S | L | L | I | L | E | Y | L | D | D | A | V | G |
| CAD29575.1 | Phi | *T.aestivum* | 1 | 55 | I | P | A | F | Q | D | G | - | D | L | L | L | F | E | S | R | A | I | A | R | Y | V | L | R | K | Y | K |
| P15214 | Beta | *P.mirabilis* | 1 | 52 | V | P | V | L | Q | L | D | N | G | D | I | L | T | E | G | V | A | I | V | Q | Y | L | A | D | L | K | P |
| NP_611323.1 | Epsilon | *D.melanogaster* | 1 | 57 | V | P | M | L | D | D | N | - | G | T | F | I | W | D | S | H | A | I | A | A | Y | L | V | D | K | Y | A |
| A37378 | Pi | *H.sapiens* | 1 | 53 | L | P | K | F | Q | D | G | - | D | L | T | L | Y | Q | S | N | T | I | L | R | H | L | G | R | T | L | G |
| NP_665683.1 | Alpha | *H.sapiens* | 1 | 55 | V | P | M | V | E | I | D | - | G | M | K | L | V | Q | T | R | A | I | L | N | Y | I | A | S | K | Y | N |
| P46088 | Sigma | *O.sloani* | 1 | 51 | M | P | V | L | D | I | D | - | G | T | K | M | S | Q | S | M | C | I | A | R | H | L | A | R | E | F | G |
| NP_000552 | Mu | *H.sapiens* | 1 | 60 | L | P | Y | L | I | D | G | - | A | H | K | I | T | Q | S | N | A | I | L | C | Y | I | A | R | K | H | N |
| O43708 | Zeta | *H.sapiens* | 1 | 59 | V | P | T | L | K | I | D | - | G | I | T | I | H | Q | S | L | A | I | I | E | Y | L | E | E | T | R | P |

**Figure 1 Newly identified extension of an electron-sharing network in adGSTD3-3**

The electron-sharing network is an ionic interaction between negatively charged and positively charged residues stabilized by a network of hydrogen-bonds. The stereo view of corresponding three-dimensional structure of the electron-sharing network is shown in the upper panel. The lines show the putative electron movement pathway with distances between 2.5 and 3.0 Å. The lower panel shows the sequence alignment of amino acid residues in Delta, Theta, Omega, Tau, Phi, Beta, Epsilon, Pi, Alpha, Sigma, Mu and Zeta class GSTs. The newly identified functionally conserved glutamate, aspartate and glutamine in the electron-sharing network are identified by an arrow.

bridge interaction between the negatively charged glutamyl $\alpha$-carboxylate of GSH, a positively charged residue and a negatively charged residue, forming a resonance motif stabilized by a network of hydrogen-bonds with surrounding residues. The network is distributed among multiple interacting amino acids that collectively provide a network function. This conserved motif's contribution to the base-assisted deprotonation is essential for the GSH ionization step of catalysis.

The functionally conserved glutamate residue, $Glu^{64}$ in adGSTD3-3 (*Anopheles dirus* GST Delta class homodimer of subunit 3) is located in the same region as the electron-sharing network (Figure 1). Initial characterization of the electron-sharing network has provided further insight into this motif [25]. The carboxylic group of $Glu^{64}$ interacts directly with the glutamyl $\alpha$-amino group of GSH. Moreover, by observing the configuration of the GSH glutamyl $\alpha$-carboxylate, the GSH glutamyl $\alpha$-amino, $Glu^{64}$ and the electron-sharing network, it is now possible to extend this conserved motif, which is maintained in all GSTs. The aim of the present paper was to ascertain the validity of $Glu^{64}$ function in the electron-sharing network. We have observed previously [25] that alanine replacement of $Glu^{64}$ caused the enzyme to be expressed in an insoluble form. This suggested that $Glu^{64}$ is a critical residue involved in tertiary structure or initial folding of the enzyme. Therefore the contribution of this residue to structural maintenance and initial folding was also examined. The results of the present paper indicate that $Glu^{64}$ is a part of the functionally conserved electron-sharing network and has roles both in catalysis as well as structural folding and maintenance.

## MATERIALS AND METHODS

### Site-directed mutagenesis

The plasmid pET3a-adgstD3, described previously [26], was used as the template to generate the single point mutations via PCR-based site-directed mutagenesis. The functionally conserved active-site residue $Glu^{64}$ was replaced by an alanine, leucine, valine, lysine, glutamine, asparagine or aspartate residue by using

PCR primers based on the wild-type *adgstD3* gene sequence (Genbank accession number AF273039). Mutants were screened randomly by restriction enzyme digestion analysis. Mutant plasmids could be distinguished from the wild-type template by digestion with restriction enzymes corresponding to the restriction recognition site introduced by the mutagenic primers. The full-length GST coding sequence carrying E64A, E64L, E64V, E64K, E64Q, E64D and E64N mutations were verified by the dideoxy chain termination method.

#### Heterologous expression and purification

The proteins were expressed from the pET3a-adgstD3 vector in *Escherichia coli* BL21 (DE3) pLysS cells. The cells were grown to $D_{600} = 0.5$ and expression was induced by addition of 0.1 mM isopropyl $\beta$-D-thiogalactoside. Following a 3 h induction, cells were collected by centrifugation at 10000 ***g*** for 20 min at 4 °C and lysed by sonication using an Ultrasonic processor XL (Misonix) at power level 3 for 10 s, paused for 1 min and repeated three times at 4 °C. The soluble recombinant GST proteins were purified by GSTrap™ affinity chromatography (Amersham Biosciences) or *S*-hexylglutathione agarose (Sigma–Aldrich) affinity chromatography. The protein concentration was determined by the Bradford method [27] using BSA as a standard.

#### Steady-state kinetics

Steady-state kinetics were studied for wild-type and mutant enzymes at varying concentrations of CDNB (1-chloro-2,4-dinitrobenzene) and GSH in 0.1 M phosphate buffer pH 6.5. The reaction was monitored at 340 nm, $\varepsilon$ 9600 $M^{-1}cm^{-1}$. Apparent kinetic constants, $k_{cat}$, $K_m$ and $k_{cat}/K_m$ were determined by fitting the collected data to a Michaelis–Menten equation by non-linear regression analysis using GraphPad Prism (GraphPad software).

#### pH dependence of kinetic constants

The pH dependence of $k_{cat}/K_m^{CDNB}$ was obtained as stated above by recording the enzymatic reaction in the following buffers: 0.1 M sodium acetate buffers (from pH 5.0 to 5.5) and 0.1 M potassium phosphate buffer (from pH 6.0 to 8.5). The pH was altered in increments of 0.5, and control experiments showed no discontinuities from buffer types. p$K_a$ values were obtained by fitting the data to eqn (1) [20]:

$$y = y_{lim}/(1 + 10^{pKa-pH}) \quad (1)$$

#### Fluoride/chloride leaving group replacement

The second order kinetic constants at pH 6.5 for the spontaneous reaction of GSH with CDNB and FDNB (1-fluoro-2,4-dinitrobenzene) and the catalytic-centre activities at pH 6.5 for adGSTD3-3 with CDNB and FDNB as co-substrates were obtained as described previously [28].

#### Viscosity effect on the kinetic parameters

The effect of viscosity on kinetic parameters was obtained by using 0.1 M potassium phosphate buffer pH 6.5 with various glycerol concentrations. Viscosity values ($\eta$) at 25 °C were calculated as described previously [29].

#### Structural studies

A Jasco J-714 spectropolarimeter was used for CD measurements in the far-UV region from 190–260 nm. Spectra were recorded using 0.3 mg/ml of protein in 2-mm path length cuvettes. Intrinsic fluorescence emission spectra were measured with a Jasco FP-6300 spectrofluorimeter. The excitation wavelength was 295 nm and the $\lambda_{max}$ and the fluorescence intensity of emission spectra were analysed at a protein concentration of 0.2 mg/ml.

#### Kinetics of thermal denaturation

Heat inactivation of the wild-type and Glu[64] mutant enzymes was monitored at different temperatures. Enzymes (40 $\mu$M) were incubated in 0.1 mM potassium phosphate buffer pH 6.5, 1 mM EDTA and 5 mM DTT (dithiothreitol). The inactivation time-courses were determined by withdrawing suitable aliquots at different time points to assay the remaining activity using the first time point as 100 % native protein. An equation describing a single exponential decay with a rate constant of thermal unfolding $k_u$ was fitted to the data according to eqn (2) [30]:

$$-\ln(\%\text{native}/100\%) = k_u t \quad (2)$$

The free-energy of activation of thermal unfolding ($\Delta G_u$) was calculated according to Eyring theory as eqn (3) [30]:

$$\ln k_u = \ln\frac{K k_b T}{h} - \frac{\Delta G_u}{RT} \quad (3)$$

where $k_b$ is the Boltzmann constant; T, absolute temperature Kelvin; h, Plank's constant; R, the gas constant; and $K$ is the transmission factor, which was set to unity. The difference of free-energy of activation of the thermal denaturation between wild-type (wt) and each mutant (mut) protein ($\Delta\Delta G_u$) was calculated according to eqn (4) [30]:

$$\Delta\Delta G_u = \Delta G_u^{wt} - \Delta G_u^{mut} = -RT \times \ln\left(k_u^{wt}/k_u^{mut}\right) \quad (4)$$

Substitution of Equation 5:

$$\Delta G_u = \Delta H_u - T\Delta S_u \quad (5)$$

into eqn (3) yields eqn (6):

$$\ln\frac{k_u}{T} = \ln\frac{K \times k_b}{h} - \frac{\Delta H_u}{R} \times \frac{1}{T} + \frac{\Delta S_u}{R} \quad (6)$$

Both activation enthalpy $\Delta H_u$ and entropy $\Delta S_u$ were determined from the temperature dependence of $k_u$.

#### Temperature dependence of refolding *in vitro*

The *in vitro* refolding of the wild-type and Glu[64] mutant enzymes were monitored at different temperatures. Enzyme (20 $\mu$M) was first denatured in 4 M GdmCl (guanidinium chloride) in renaturation buffer (0.2 M potassium phosphate buffer, 1 mM EDTA and 5 mM DTT, pH 7.0) at room temperature (25 °C) for 30 min and then rapidly diluted (defining time 0) 1:40 (v/v) into renaturation buffer at 18, 25 and 33 °C. The final GdmCl concentration was 0.1 M during refolding. All refolding experiments were carried out by rapid addition of the denatured enzyme to renaturation buffer. The recovery of activity of the proteins was monitored as a function of time by withdrawal of appropriate aliquots of the renaturation mixture and immediately assaying for activity at 25 °C. Refolding rate constants were determined by nonlinear regression analysis of the experimental data by using SigmaPlot 2001 for Windows version 7.0 (SPSS). The refolding rates of all variants were independent, in the range 10 to 30 $\mu$M, of the protein concentration. At greater enzyme concentrations all

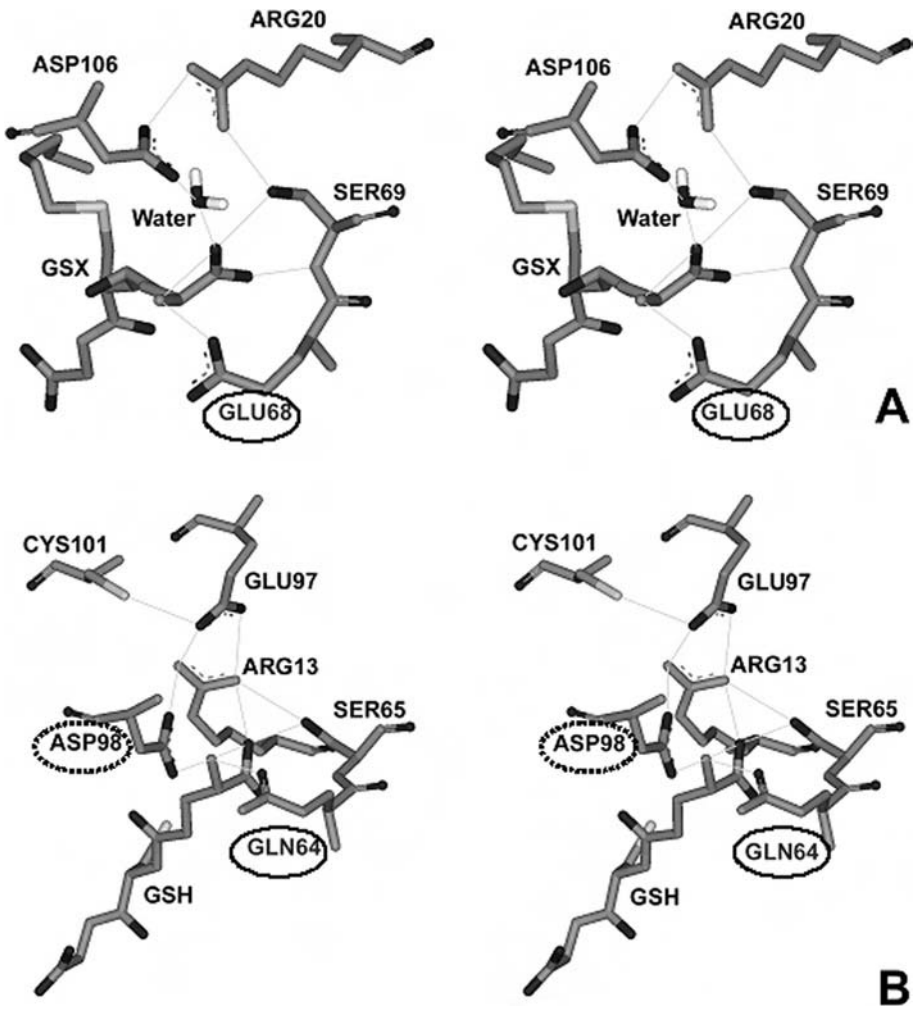


**Figure 2 Stereo views of examples of electron-sharing networks for type I (A) and type II (B) of GSTs**

Categorization is based on properties of the equivalent amino acid at position 64 and configuration of the electron-sharing network. (**A**) Electron-sharing network type I is composed of only one conserved acidic amino acid (circled), which forms an ionic interaction. Wheat Tau GSTI (PDB accession number 1GWC). (**B**) Electron-sharing network type II contains two strictly conserved polar and acidic residues (circled by solid and dotted lines respectively), which participate in an ionic bridge interaction. Human Pi hGSTP1-1 (PDB accession number 1PKW).

variants were characterized by reduced refolding yield. The values reported represent the means for three different experimental data sets. Under these conditions, an equation describing a single exponential reaction can be fitted to the data:

$$F(\mathrm{t}) = A[1 - \exp(-k_{\mathrm{ref}})] + B \quad (7)$$

where $F(\mathrm{t})$ is the activity at time t; $A$, the amplitude; $k_{\mathrm{ref}}$, the rate constant; and $B$, the reactivation value at time 0 [31]. The effect of mutation on the energy of the transition state of folding can be calculated using transition-state theory in a similar manner to that reported by Jackson et al. [32]. The stability of the transition state of a mutant protein relative to that of the wild-type is calculated from:

$$\Delta\Delta G_{\mathrm{ref}} = -RT \times \ln\left(k_{\mathrm{ref}}{}^{\mathrm{wt}} / k_{\mathrm{ref}}{}^{\mathrm{mut}}\right) \quad (8)$$

where $\Delta\Delta G_{\mathrm{ref}}$ is the difference in energy of the transition state of folding relative to the unfolded state between wild-type (wt) and mutant (mut) proteins and $k_{\mathrm{ref}}$, the rate constants of refolding [32].

## RESULTS AND DISCUSSION

A functionally conserved electron-sharing network can be observed in the same region for all GSTs, but with slightly different residue positions [22]. However, a primary sequence alignment of the known GST classes suggests that $Glu^{64}$ is one of a few residues that is functionally conserved in the GST superfamily. Observation of available crystal structures; adGSTD3-3, hGSTP1-1 (human Pi GST1), hGSTA1-1 (human Alpha GST1), rGSTM1-1 (rat Mu GST1), hGSTO1-1 (human Omega GST1), hGSTT2-2 (human Theta GST2), squid Sigma GST and wheat Tau GST, as well as consideration of the property of the equivalent residue at position 64, acidic or polar, suggests that the GST electron-sharing motif can be divided into two types (Figure 2). Electron-sharing network type I, consisting of GSTs from Delta, Theta, Omega, Pi and Tau classes, contain an acidic amino acid (glutamate or aspartate) at this position. The equivalent residue is the only amino acid in an acceptable distance range to form an ionic interaction between its own negatively charged side chain and the positively charged GSH glutamyl $\alpha$-amino (Figure 2A). On the other hand, electron-sharing network type II GSTs from the Alpha, Mu, Pi and Sigma classes have a polar amino acid (glutamine) side-chain

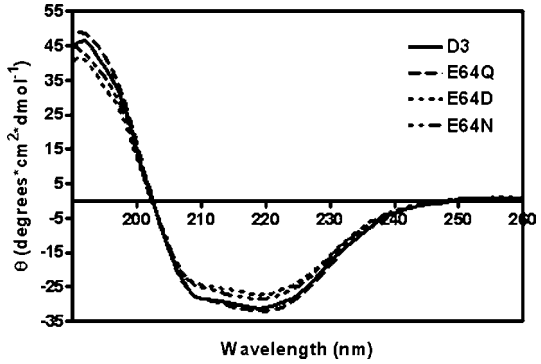


**Figure 3 Far-UV CD spectra of adGSTD3-3 and mutants**

CD spectra were measured in far-UV region from 190–260 nm. Spectra were recorded at a protein concentration of 0.3 mg/ml with cuvettes with a 2-$\mu$m path-length. D3, wild-type adGSTD3-3.

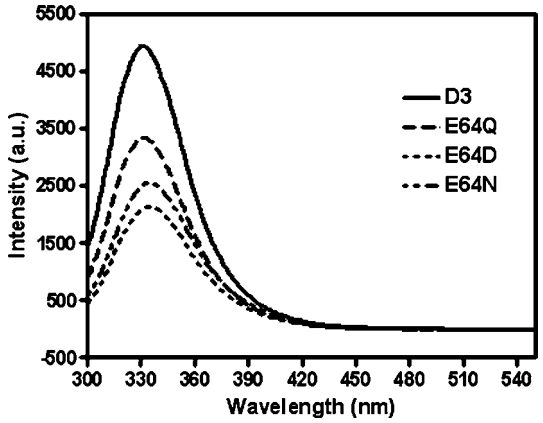


**Figure 4 Intrinsic fluorescence spectra of wild-type and mutant adGSTD3-3**

Intrinsic fluorescence emission spectra were measured with the excitation wavelength 295 nm. The $\lambda_{max}$ and the fluorescence intensity of emission spectra were analysed at a protein concentration of 0.2 mg/ml. The $\lambda_{max}$ are 331 nm for wild-type (D3), 332 nm for E64Q, 335 nm for E64D and 334 nm for E64N. The intensity is shown in arbitrary units. The results are means $\pm$ S.D. for experiments performed in triplicate.

that interacts directly with the GSH glutamyl $\alpha$-amino. In addition, type II networks have a strictly conserved acidic amino acid (Asp[98] in the Pi class, Asp[101] in the Alpha class, Asp[105] in the Mu class and Asp[97] in the Sigma class) that participates in an ionic interaction (Figure 2B). In the Pi class GSTs, replacement of this acidic residue (Asp[98] with asparagine) was shown to increase the p$K_a$ for GSH by approx. 0.5 pH unit [33]. These results suggest the importance of a negative charge involvement with the positively charged GSH glutamyl $\alpha$-amino to fulfil the function of the electron-sharing network in the ionization process [33]. Dividing the electron-sharing network into two types is supported by studies of binding, activation and ionization of GSH, including the fate of the thiol proton in Pi, Alpha, Mu and Delta class GSTs [23]. It has been reported that GST classes Pi, Alpha and Mu, which are classified as electron-sharing network type II GSTs, display similarities in the multi-step mechanism for binding of the substrate and also yield a similar fate for the thiol proton. The Delta class GST, which we propose belongs to electron-sharing network type I, shows a difference in proton extrusion that implies a different activation mechanism for GSH. Moreover, the modality of proton output is also preserved in Pi, Alpha and Mu class enzymes. This mechanistic difference suggests that Delta GST is distantly related to Pi, Alpha and Mu GSTs in evolutionary terms.

To investigate the role of the functionally conserved Glu[64] residue in adGSTD3-3, this residue was replaced with seven amino acids; alanine, leucine, valine, lysine, glutamine, aspartate or asparagine. Evidence suggested that the replacements were temperature-sensitive therefore protein expression was performed at 18, 25 and 37 °C. The E64A, E64L, E64V and E64K mutants were expressed as insoluble proteins at all temperatures. Attempts at refolding these four proteins were unsuccessful. The yields of the E64Q, E64D and E64N mutants were less than wild-type and clearly decreased with increasing temperature (results not shown). This probably reflects the fact that the E64Q, E64D and E64N molecules fail to achieve the native folding at near physiological temperatures. Therefore, proteins expressed at the more permissive temperature of 18 °C were utilized in this study.

In the present study, a structural role for Glu[64] for stability and folding was examined. The similarity of the far-UV CD spectra of all the Glu[64] mutants indicated that the secondary structure content of the proteins are essentially unaffected by the mutations (Figure 3). The intrinsic fluorescence spectra show differences between the wild-type and all of the Glu[64] mutants (Figure 4). The spectra of the Glu[64] mutants were slightly red-shifted compared with the wild-type protein ($\lambda_{max}$ at 331 nm) to give a $\lambda_{max}$ at 332 nm for E64Q, 335 nm for E64D and 334 nm for E64N. The normalized intensities of the fluorescence of the mutants were slightly less than that of the wild-type. Changes in amino acid side-chains around Trp[63] resulted in an alteration in fluorescence intensity, and a red-shifted spectrum is observed as the protein unfolds to random coil [34]. Consequently, the differences in both $\lambda_{max}$ and fluorescence intensity suggest that the mutation of Glu[64] causes the tryptophan residue to be more exposed to the solvent. Heat inactivation of wild-type and Glu[64] mutants was performed at different temperatures (Figure 5). Furthermore, the E64Q and E64N mutants were much more unstable than the wild-type or E64D mutant. It is important to note that the single Glu[64] replacement with polar residues (glutamine and asparagine) became unstable at a lower temperature than the negatively charged residues (wild-type and E64D) and their inactivation generated the formation of protein aggregates under the experimental conditions used. Thermal denaturation of all variants was irreversible, showing that inactivation kinetics could not be used to determine thermodynamic parameters at equilibrium. However, making use of the temperature dependence of the unfolding rate, the application of Eyring formalism provides the thermodynamic parameters of the activation barrier of the thermal denaturation [30]. The heat inactivation of all variants is described by straight lines in an Eyring plot. This indicates that the temperature dependence of both the unfolding activation enthalpy ($\Delta H$) and activation entropy ($\Delta S$) is negligible. The temperature dependence of $\Delta G$ is reflected in the slope of the linear fit, dependent on $\Delta H$. Table 1 summarizes the kinetic and thermodynamic constants for the activation barrier of thermal denaturation for the wild-type and Glu[64] mutant enzymes. The large energy changes of Glu[64] mutants compared with the wild-type ($\Delta\Delta H$) are almost completely compensated for by an accompanying reduction in $\Delta S$ (that is, $\Delta\Delta S$). At 42 °C, this corresponds to lower values of the unfolding free-energy for all the Glu[64] mutant enzymes ($\Delta\Delta G$). The Glu[64] mutants were remarkably more destabilized than the wild-type enzyme, especially for the polar amino acids glutamine and asparagine (Table 1). This corresponds to an unfolding free-energy difference ($\Delta\Delta G$) for the polar amino acid replacements compared with the wild-type, being greater

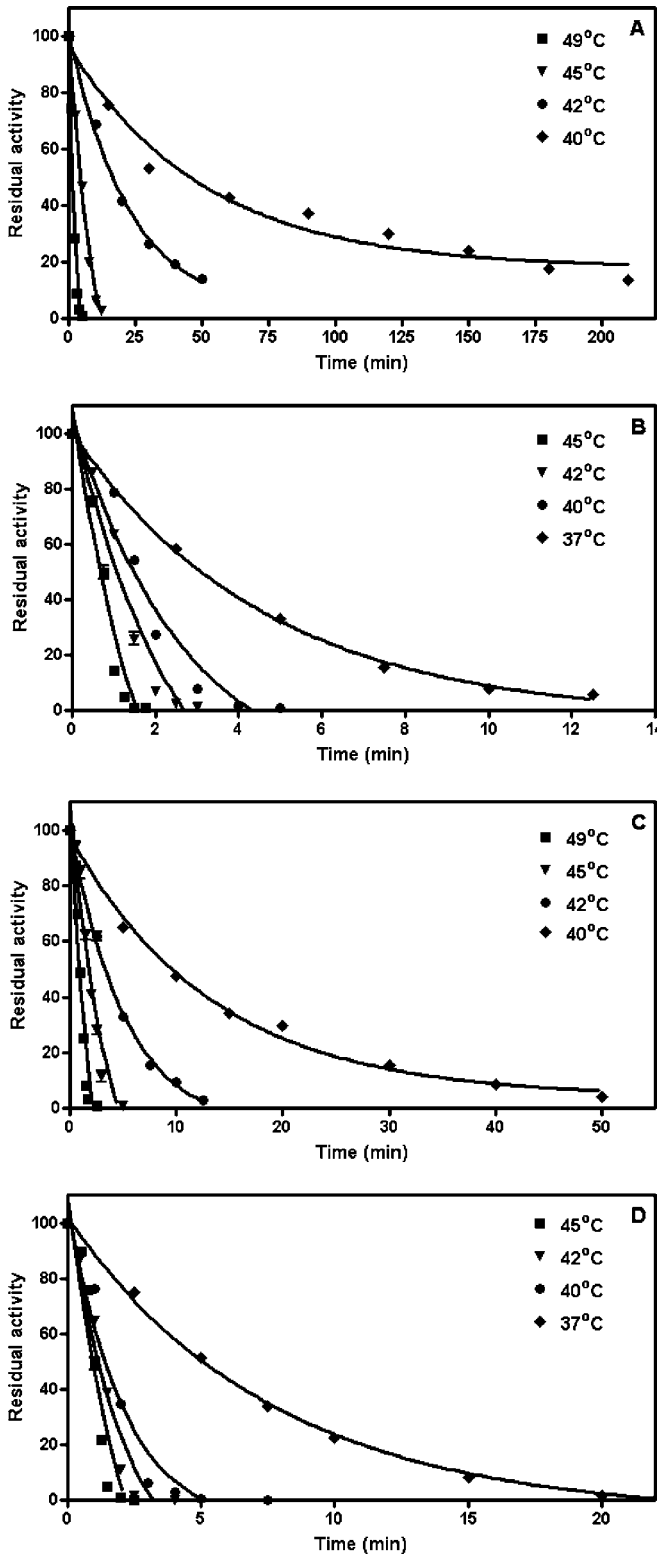


**Figure 5 Thermal stability of wild-type adGSTD3-3 (A), E64Q (B), E64D (C) and E64N (D) mutants at different temperatures**

Each enzyme (40 $\mu$M) was incubated at various temperatures in 0.1 M potassium phosphate buffer, pH 6.5, 1 mM EDTA and 5 mM DTT. Appropriate aliquots from an incubation mixture were assayed at 25 °C to monitor residual activity. The lines represent fits according to eqn (2), as described in the Materials and methods section.

than with the acidic residue aspartate. The Gibbs free-energy for the unfolding process of wild-type and Glu$^{64}$ mutants were comparable, with general estimations of Gibbs free-energy for small globular proteins based on the summation of increments of the different stabilizing forces that give values in the range 42–84 kJ/mol [35]. Due to the large decrease in activation enthalpy ($\Delta\Delta H$, 131–220 kJ/mol), the destabilizing effects of the Glu$^{64}$ mutants were clearly significant to the structural properties of the enzymes. In addition the magnitude of $T\Delta\Delta S$ at 42 °C, which is the energy difference from decreases in the entropy of the thermal unfolding pathway (198.4, 126.0 and 211.0 kJ/mol for E64Q, E64D and E64N respectively), indicates that major changes in the conformational freedom characterizes the denaturation of the wild-type protein compared with those occurring during the thermal inactivation of the Glu$^{64}$ mutants [36]. This means that the wild-type adGSTD3-3, because it is more rigid than the Glu$^{64}$ mutants, tolerates larger perturbations of its structure before the unfolding transition state is reached. The replacement of polar amino acids, both glutamine and asparagine, give greater values of all thermodynamic constants than for the acidic amino acids glutamate and aspartate. This data suggests that the negatively charged residue forming an ionic bridge interaction in this position plays an essential role for the overall stability of the protein. Recent studies proposed that Glu$^{64}$ is a critical residue involved in the determination of the direction of the polypeptide chain during folding [25]. One consequence of replacing Glu$^{64}$ with other amino acid residues results in a completely impaired folding property (for E64A, E64L, E64V and E64K) or temperature-sensitive folding (for E64Q, E64D and E64N). To test this hypothesis, reactivation yields of adGSTD3-3 and its mutants at different temperatures were determined. The denaturant 4 M GdmCl was sufficient to completely unfold 20 $\mu$M enzyme, as shown by CD spectrum (results not shown). The reactivation yields of the Glu$^{64}$ mutants were very different from the wild-type protein at increasing temperatures of refolding (Table 2 and Figure 6). The reactivation yield of the wild-type enzyme was unaffected by temperatures from 18–33 °C, whereas the yield of the mutants, although to different extents, decreased markedly with increasing temperature. All data sets were fit to a single exponential equation for the refolding kinetics (Figure 6). At each temperature, as shown in Table 2, the temperature-dependent refolding rates show a similar tendency in the wild-type and Glu$^{64}$ mutants that was expected, that is, the enzymes refold at higher temperature more rapidly than at lower temperature. The refolding rates of both E64Q and E64D mutants were slightly different from the wild-type at all temperatures. These differences in refolding rates reflect changes in free-energy of activation of folding for a mutation. Estimated free-energy values ($\Delta\Delta G_{ref}$) at 18 °C that were significantly different from zero indicate that interactions of the residue at position 64 toward neighbouring residues are present in the transition state of the reactivation process. The *in vitro* refolding experiments suggest that the thermal stability of the final structure of the mutants reflects differences in the conformational properties of a productive folding intermediate. Reactivation *in vitro* of all Glu$^{64}$ mutants was thermosensitive, and so the refolding yields of the Glu$^{64}$ mutants, although to different extents, decreased markedly with increasing temperature. The analysis of the reactivation at 18 °C indicates that amino acid replacement of Glu$^{64}$ destabilizes the transition of folding. It should be noted that a single exponential equation could be fitted to refolding data for all adGSTD3-3 variants indicating that no significant amount of intermediate is accumulated during the reactivation of wild-type and variants, and that none of the mutations had a major change on the refolding pathway. Upon

**Table 1 Kinetic and thermodynamic parameters for the activation barrier of thermal denaturation for wild-type and Glu$^{64}$ mutants of adGSTD3-3**

| Enzyme | $k_u$ (min$^{-1}$) | $k_u/k_{u,wt}$* | $\Delta G_u$* (kJ/mol) | $\Delta\Delta G_u$ (kJ/mol) | $\Delta H_u$† (kJ/mol) | $\Delta\Delta H_u$† (kJ/mol) | $\Delta S_u$† (kJ/mol · K) | $\Delta\Delta S_u$† (kJ/mol · K) |
|---|---|---|---|---|---|---|---|---|
| Wild-type | 0.040 ± 0.001 | 1 | 85.69 ± 0.09 | 0 | 439.00 ± 4.90 | 0 | 1.120 ± 0.015 | 0 |
| E64Q | 1.583 ± 0.028 | 39.58 | 76.08 ± 0.05 | 9.63 | 231.38 ± 13.02 | 207.62 | 0.490 ± 0.041 | 0.630 |
| E64D | 0.256 ± 0.008 | 6.40 | 80.85 ± 0.08 | 4.86 | 307.51 ± 1.28 | 131.49 | 0.720 ± 0.004 | 0.400 |
| E64N | 1.590 ± 0.045 | 39.75 | 76.07 ± 0.08 | 9.64 | 218.52 ± 10.92 | 220.48 | 0.450 ± 0.035 | 0.670 |

* From denaturation kinetics at 42 °C according to eqns 2 and 4.
† From temperature dependence of thermal unfolding (Eyring plot) according to eqn 6.

**Table 2 Kinetics of the reactivation and percentage recovery of wild-type adGSTD3-3 and Glu$^{64}$ mutants during refolding at different temperatures and changes in free energy of the transition state of folding at 18 °C**

Statistics performed using one-way ANOVA and Tukey–Kramer multiple comparisons test. Values significantly different from wild-type are shown by * $P < 0.001$. Nd, not determined, low enzymatic activity precluded performing this experiment.

| | 18 °C | | 25 °C | | 37 °C | | |
|---|---|---|---|---|---|---|---|
| Enzyme | $k_{ref}$ (min$^{-1}$) | % recovery | $k_{ref}$ (min$^{-1}$) | % recovery | $k_{ref}$ (min$^{-1}$) | % recovery | $\Delta\Delta G_{ref}$ at 18 °C (kJ/mol) |
| Wild-type | 0.169 ± 0.020 | 60.9 ± 0.4 | 0.518 ± 0.053 | 35.1 ± 3.4 | 0.957 ± 0.027 | 35.1 ± 0.6 | 0 |
| E64Q | 0.074 ± 0.003 | 63.8 ± 0.7 | 0.289 ± 0.004 | 40.0 ± 0.3 | 1.073 ± 0.124 | 10.6 ± 0.3 | −1.987 ± 0.371* |
| E64D | 0.059 ± 0.005 | 93.0 ± 6.5 | 0.242 ± 0.024 | 57.7 ± 1.1 | 0.981 ± 0.030 | 34.5 ± 1.3 | −2.521 ± 0.129* |
| E64N | Nd | Nd | Nd | Nd | Nd | Nd | Nd |

mutation of adGSTD3-3, rate constants decreased for all mutants (Table 2). This is because the removal of the negative charge or size decrease of the side-chain at this position destabilized the transition state and thereby increased the activation energy for folding. In particular, the $\Delta\Delta G_{ref}$ value for E64D is greater than E64Q, suggesting that the functional group size is important for the Glu$^{64}$ position, which contributes to stabilizing the transition state. Previous investigations of the equivalent residue, Glu$^{66}$, in PtGSTU1-1 (plant Tau class GST) demonstrated that alanine replacement made the enzyme unstable at 50 °C, retaining only about 15 % of its activity compared with 95 % for the wild-type enzyme [37]. In contrast, the reactivation yield of E66A was 2-fold greater than the wild-type. The effect of the mutation at this equivalent residue in PtGSTU1-1 was less than found in adGSTD3-3, an insect Delta class GST. This result might be explained by data for Glu$^{64}$ in adGSTD4-4, an alternatively spliced product derived from the same gene as adGSTD3-3. Glu$^{64}$ is not only located at the dimeric interface of the enzyme, but has also been identified as a 'lock' residue in the Delta class specific 'lock-and-key clasp' motif, which is not found in plant Tau class GST [38]. The lock-and-key motif, including the Delta class specific lock-and-key clasp motif, is located at the intersubunit interface and plays a crucial role in the structural stability of dimeric GSTs [39,40]. These data therefore confirm a critical structural role for the functionally conserved Glu$^{64}$ residue for both overall protein stability and initial folding process.

Steady-state kinetic constants were obtained with various concentrations of GSH and CDNB substrate. Michaelis–Menten kinetic analysis was performed using non-linear regression (Table 3). All of the mutations showed significantly increased $K_m$ values for GSH. Individually, the mutants; E64Q, E64D and E64N had values 26-, 34- and 29-fold greater than wild-type. Conversely, no significant changes were found in the $K_m$ values for CDNB substrate when compared with the wild-type enzyme. The differences in $k_{cat}$ values with CDNB observed for E64D and E64N decreased approximately 1.5- and 25-fold respectively. The kinetic studies of soluble Glu$^{64}$ mutant enzymes demonstrated that replacement with a glutamine residue, a similar size and property functional group, preserved the catalytic activity, whereas replacement with the slightly smaller amino acids aspartate and asparagine reduced $k_{cat}$, especially the arparagine replacement, which nearly abolished enzyme activity. This suggests that the volume of the amino acid at this position affects packing of the active-site, which directly impacts upon enzyme catalysis. However, all the mutants showed a substantially lower affinity (greater $K_m$) towards GSH indicating that the Glu$^{64}$ position impacts upon the binding of GSH possibly through active-site rearrangement. Catalytic efficiency can be related to the difference in free-energy change for formation of transition states in the mutant and wild-type enzymes ($\Delta\Delta G$), as calculated from eqn (9) [41]:

$$\Delta\Delta G = -RT \times \ln\left(k_{cat}/K_m^{GSH}\right)_{mut}/\left(k_{cat}/K_m^{GSH}\right)_{wt} \quad (9)$$

These calculated values are 8.03 kJ/mol for E64Q, 9.94 kJ/mol for E64D and 16.33 kJ/mol for E64N at 25 °C, indicative of a decreased stabilization of the transition state for the Glu$^{64}$ mutations. Stabilization of the transition state may occur through a pre-organized active-site contributing to catalysis through multiple mechanisms: binding interaction with GSH, activation of GSH by thiol deprotonation or nucleophilic attack at the electrophilic centre ($\sigma$-bond formation) by the thiolate. Deficiency in the pre-organized environment (the changes that occur along the reaction pathway from reactants to the transition state) would decrease the rate of catalysis by incompletely providing a stabilization of the transition state [42]. Therefore, the effect on the rate-limiting step in the catalytic mechanism was examined. The pH dependence of $k_{cat}/K_m^{CDNB}$ reflects a kinetically relevant ionization of the GST–GSH complex. Therefore, an apparent p$K_a$ value of 6.36 was determined for the wild-type adGSTD3-3. To differentiate the influence of the functional group of Glu$^{64}$ on the GSH thiol ionization, the p$K_a$ values for Glu$^{64}$ mutants were measured by this kinetic approach (Table 3). An increased p$K_a$ for bound GSH of approx. 0.6 and 1 pH unit greater than that found for wild-type were observed for the E64Q and E64N mutants. It has been shown previously that a crucial function of the electron-sharing

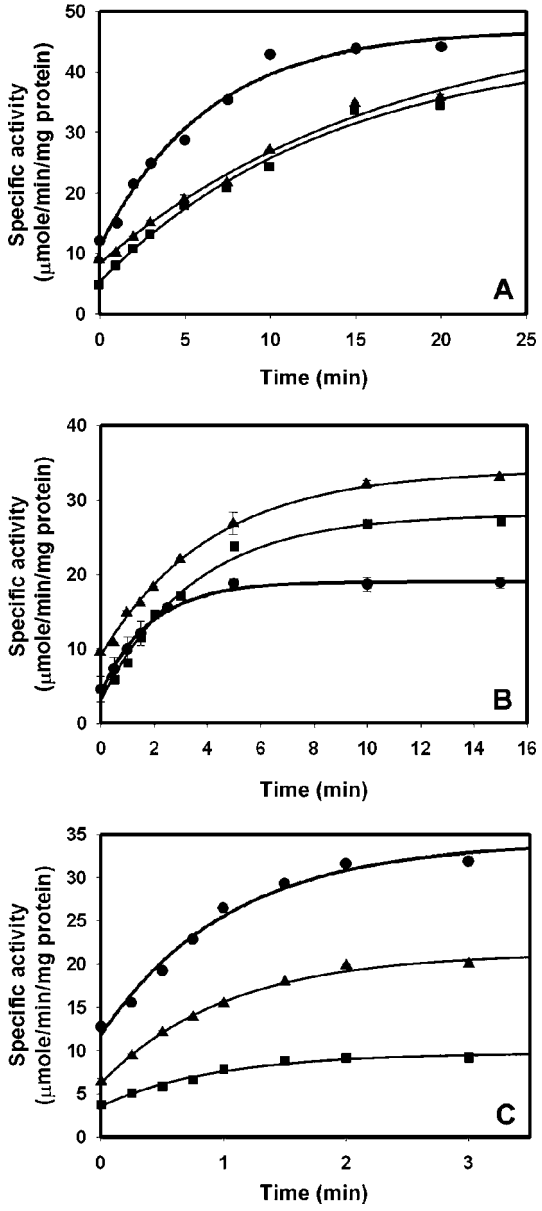


**Figure 6 Kinetics of reactivation of wild-type adGSTD3-3 (●), E64Q (■) and E64D (▲) during refolding at different temperatures: 18 °C (A), 25 °C (B) and 33 °C (C)**

Purified enzyme (20 $\mu$M), heterologously expressed at 18 °C, was first denatured in 4 M GdmCl for 30 min. This denaturant concentration was sufficient to completely unfold the proteins, as indicated by the loss of secondary structure shown by CD. Successive aliquots of unfolded enzyme were diluted (defining time 0) 1:40 into renaturation buffer at the different temperatures. The final GdmCl concentration was 0.1 M during the refolding. Appropriate aliquots from this incubation mixture were immediately assayed for catalytic activity at 25 °C.

network is to lower the p$K_a$ of the thiol group of the bound GSH [22]. Our results show that Glu$^{64}$ replacement with the polar amino acids glutamine and asparagine increased the p$K_a$ values by about 0.5–1.0 pH unit. This consequence appears to be due to the deletion of the negative charge, resulting in loss of ionic interaction within the electron-sharing network. This is supported by the replacement of the critical glutamate residue with the negatively charged aspartate, which has no affect on the ionization process. Therefore, an acidic amino acid in this position is essential to form an ionic interaction to fulfil the function of the electron-sharing network in the ionization process. However, the formation of a $\sigma$-complex intermediate in the enzyme-catalysed reaction was affected by the replacement with glutamine and aspartate. It is well established that the bimolecular nucleophilic substitution reactions proceed through a $\sigma$-complex intermediate [43]. Thus, the rate-limiting formation of a spontaneous $\sigma$-complex intermediate can be increased by replacement of chlorine in the CDNB molecule with the more electronegative fluorine. The ratio of the catalytic rate of GSH with FDNB and CDNB was comparable to the ratio of the second-order rate constants for a spontaneous uncatalysed reaction. That is, $k_{cat}^{FDNB}/k_{cat}^{CDNB} = 40$ is similar to $k_c^{FDNB}/k_c^{CDNB} = 47$, which indicates that the $\sigma$-complex formation is the rate-limiting step. Although the $k_{cat}^{FDNB}/k_{cat}^{CDNB}$ of all Glu$^{64}$ mutants reflected varying insensitivity to the nature of the leaving group, there were two mutants E64Q and E64D that exhibited significant differences in the catalytic efficiency ($k_{cat}/K_m$) (Table 4). For the E64N mutant, it appears that an alteration of the relative turn-over number is a consequence of changes in binding affinity towards different substrate leaving groups rather than a reflection of the rate of $\sigma$-complex formation. Differences in relative catalytic efficiency ($k_{cat}/K_m$) for the fluoride/chloride leaving group replacement may not strongly support the idea that the rate-determining step to $\sigma$-complex formation for E64Q and E64D was changed. Although it appears that transition state stability of the enzyme–intermediate complex, influenced by electron density and distribution in the $\sigma$-complex, was partially altered by these two amino acid replacements [43,44].

**Table 3 Steady-state kinetic constants and p$K_a$ values for the thiol group of GSH of wild-type and mutants of adGSTD3-3 for the CDNB conjugation reaction at pH 6.5 and 25 °C**

The enzyme activities were measured at various concentrations of CDNB and GSH in 0.1 M phosphate buffer pH 6.5. The p$K_a$ was obtained by using 0.1 M sodium acetate buffers (from pH 5.0 to 5.5) and 0.1 M potassium phosphate buffer (from pH 6.0 to 8.5).The reaction was monitored at 340 nm, $\varepsilon$ 9600 $M^{-1}cm^{-1}$. Statistics were performed using one-way ANOVA and Tukey–Kramer multiple comparisons test. Values significantly different from wild-type are shown by * $P < 0.001$. The wild-type values have been reported previously [25].

| Enzyme | $k_{cat}$ ($s^{-1}$) | $K_m^{GSH}$ (mM) | $K_m^{CDNB}$ (mM) | $k_{cat}/K_m^{GSH}$ ($s^{-1}$/mM) | $k_{cat}/K_m^{CDNB}$ ($s^{-1}$/mM) | p$K_a$ |
|---|---|---|---|---|---|---|
| Wild-type | 35.4 | 0.27 ± 0.05 | 0.14 ± 0.01 | 131 | 246 | 6.36 ± 0.11 |
| E64Q | 36.3 | 7.10 ± 0.28* | 0.43 ± 0.03 | 5.11 | 83.6 | 6.97 ± 0.14* |
| E64D | 21.6 | 9.12 ± 0.20* | 0.28 ± 0.01 | 2.37 | 75.8 | 6.42 ± 0.12 |
| E64N | 1.4 | 7.89 ± 0.19* | 0.33 ± 0.01 | 0.18 | 4.4 | 7.37 ± 0.07* |

**Table 4 Effect of fluoride/chloride leaving group substitution on the rate of catalysis**

The ratios of kinetic constants for the conjugation reaction catalyzed by adGSTD3-3 enzymes for GSH with CDNB or FDNB as co-substrates were calculated at pH 6.5. Statistics performed using one-way ANOVA and Tukey–Kramer multiple comparisons test. Values significantly different from wild-type are shown by * $P < 0.001$. The wild-type values have been reported previously [25].

| Enzyme | $k_{cat}^{FDNB}/k_{cat}^{CDNB}$ | $(k_{cat}/K_m)^{FDNB}/(k_{cat}/K_m)^{CDNB}$ |
|---|---|---|
| Wild-type | 2.40 ± 0.08 | 6.72 ± 0.34 |
| E64Q | 6.97 ± 0.24* | 14.36 ± 1.22* |
| E64D | 8.40 ± 0.08* | 10.31 ± 0.38* |
| E64N | 5.92 ± 0.05* | 6.58 ± 0.05 |

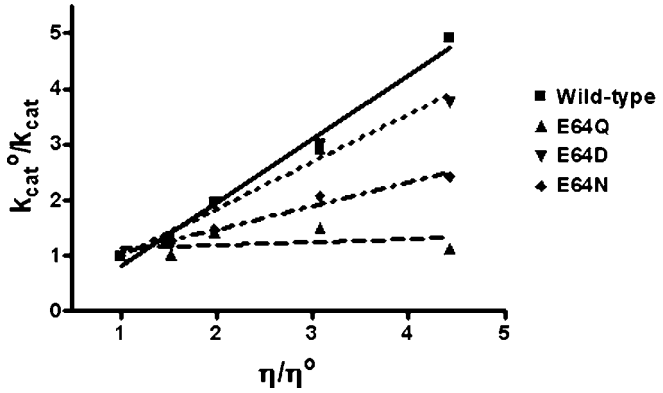


**Figure 7 Viscosity effect on kinetic parameters of wild-type adGSTD3-3 and mutant enzymes**

The effect of viscosity on kinetic constants was assayed by using 0.1 M potassium phosphate buffer, pH 6.5, with various glycerol concentrations. Dependence of the reciprocal of the relative turn-over number ($k_{cat}^{o}/k_{cat}$) on the relative viscosity ($\eta/\eta^{o}$) for CDNB as a co-substrate. The experiment was performed in triplicate and the lines were calculated by linear regression analysis. The slopes of the linear regression lines are $1.14 \pm 0.01$ for wild-type, $0.05 \pm 0.01$ for E64Q, $0.85 \pm 0.01$ for E64D and $0.42 \pm 0.02$ for E64N.

The effect of viscosity on kinetic parameters was examined to elucidate the rate-limiting step in the catalytic reaction. A decrease in the rate constant with increasing medium viscosity should reflect the weight of diffusion events on catalysis [45]. It would indicate that the rate-limiting step is related to diffusion-controlled motions of the protein or the dissociation of the product. A plot of the reciprocal of the relative catalytic constant ($k_{cat}^{o}/k_{cat}$) against the relative viscosity ($\eta/\eta^{o}$) should be linear. The slope should be equal to unity when the product release or structural transition is limited by a strictly diffusional barrier. If the slope approaches zero either the chemistry or another non-diffusion barrier is rate-limiting. For wild-type adGSTD3-3, a plot of the inverse relative rate constant ($k_{cat}^{o}/k_{cat}$) versus the relative viscosity ($\eta/\eta_{o}$) gives a linear dependence with a slope ($1.14 \pm 0.01$) very close to unity (Figure 7). In contrast the E64Q mutant enzyme yields plots that are fully viscosity independent, with a slope approaching zero ($0.05 \pm 0.01$). The other mutants, E64D and E64N, exhibited $k_{cat}$ values with different degrees of viscosity dependence compared with the wild-type enzyme. The viscosity experiment showed that the rate-limiting step catalysed by adGSTD3-3 is a non-physical step (Figure 7). However, structural alterations in the Glu[64] mutants decreased the viscosity effects on the enzyme to intermediate values ($0 < \text{slope} < 1$), especially for the replacement with the polar residues glutamine and asparagine. This indicates that the rate-limiting step is not strictly dependent on a diffusion barrier or other viscosity-dependent motions and that conformational changes of the engineered proteins contribute to the rate-limiting step [45]. This suggests that the structural flexibility of functionally important regions of the engineered enzymes have been altered. Previously, we have observed [22] that changing the residues in the electron-sharing network can influence the topology of the active-site, which affects both the catalytic mechanism as well as the structural maintenance of the enzyme. The results of the present study demonstrate that the functionally conserved Glu[64], which is now identified as being part of the electron-sharing network, impacts upon enzyme catalysis not only through its negative charge but also through structural effects.

In conclusion, the results of the present paper, as well as the high level of functional conservation of the residue at position 64 among all classes of GSTs supports the hypothesis that Glu[64] is part of a functionally conserved electron-sharing network. The present paper now extends the network identified previously to include three critical residues that form ionic bridge interactions. These are between a negatively charged/polar active site residue (glutamate, aspartate or glutamine), a positively charged GSH glutamyl $\alpha$-amino, a negatively charged GSH glutamyl $\alpha$-carboxylate, a positively charged active-site residue (primarily arginine) and a negatively charged active-site residue (glutamate or aspartate) stabilized by hydrogen-bonding networks with surrounding residues (serine, threonine and/or water mediated contact). Glu[64] in the electron-sharing network contributes to the function of this motif and the base-assisted deprotonation model which are essential for the GSH ionization process in the catalytic mechanism. However, this residue also appears to affect additional steps in the enzyme catalytic strategy including binding of GSH to the enzyme active site, nucleophilic attack by thiolate at the electrophilic centre and product formation. Therefore, the Glu[64] position also appears to impact upon catalysis through roles in both initial folding and structural maintenance.

This work was supported by the Thailand Research Fund. P.W. was supported by a Royal Golden Jubilee Scholarship and a scholarship from the Senior Research Fellowship of Professor Emeritus Sakol Panyim.

## REFERENCES

1 Sheehan, D., Meade, G., Foley, V. M. and Dowd, C. A. (2001) Structure, function and evolution of glutathione transferases: implications for classification of non-mammalian members of an ancient enzyme superfamily. Biochem. J. **360**, 1–16
2 Cho, S.-G., Lee, Y. H., Park, H.-S., Ryoo, K., Kang, K. W., Park, J., Eom, S.-J., Kim, M. J., Chang, T.-S., Choi, S.-Y. et al. (2001) Glutathione *S*-transferase Mu modulates the stress-activated signals by suppressing apoptosis signal-regulating kinase 1. J. Biol. Chem. **276**, 12749–12755
3 Gate, L., Majumdar, R. S., Lunk, A. and Tew, K. D. (2004) Increased myeloproliferation in glutathione *S*-transferase $\pi$ deficient mice is associated with a deregulation of JNK and janus kinase/STAT. J. Biol. Chem. **279**, 8608–8616
4 Ronai, Z. (2001) Coordinated regulation of stress kinases by GSTp. Chem. Biol. Interact. **133**, 285–286
5 Hayes, J. D. and Pulford, D. J. (1995) The glutathione S-transferase supergene family: regulation of GST and the contribution of the isoenzymes to cancer chemoprotection and drug resistance. CRC Crit. Rev. Biochem. Mol. Biol. **30**, 445–600
6 Mannervik, B. and Danielson, U. H. (1988) Glutathione transferases: structure and catalytic activity. CRC Crit. Rev. Biochem. **23**, 283–337
7 Armstrong, R. N. (1997) Structure, catalytic mechanism, and evolution of the glutathione transferases. Chem. Res. Toxicol. **10**, 2–18
8 Habig, W. H., Pabst, M. J. and Jakoby, W. B. (1974) Glutathione *S*-transferases. The first enzymatic step in mercapturic acid formation. J. Biol. Chem. **249**, 7130–7139
9 Ahmad, H., Wilson, D. E., Fritz, R. R., Singh, S. V., Medh, R. D., Nagle, G. T., Awasthi, Y. C. and Kurosky, A. (1990) Primary and secondary structural analyses of glutathione S-transferase $\pi$ from human placenta. Arch. Biochem. Biophys. **278**, 398–408
10 Board, P., Baker, R. T., Chelvanayagam, G. and Jermiin, L. S. (1997) Zeta, a novel class of glutathione transferases in a range of species from plants to humans. Biochem. J. **328**, 929–935
11 Mannervik, B., Ålin, P., Guthenberg, C., Jensson, H., Tahir, M. K., Warholm, M. and Jörnvall, H. (1985) Identification of three classes of cytosolic glutathione transferase common to several mammalian species: correlation between structural data and enzymatic properties. Proc. Natl. Acad. Sci. U.S.A. **82**, 7202–7206
12 Mannervik, B., Awasthi, Y. C., Board, P. G., Hayes, J. D., Di Ilio, C., Ketterer, B., Listowsky, I., Morgenstern, R., Muramatsu, M., Pearson, W. R. et al. (1992) Nomenclature for human glutathione transferases. Biochem. J. **282**, 305–306
13 Meyer, D. J., Coles, B., Pemble, S. E., Gilmore, K. S., Fraser, G. M. and Ketterer, B. (1991) Theta, a new class of glutathione transferases purified from rat and man. Biochem. J. **274**, 409–414
14 Motoyama, N. and Dauterman, W. C. (1978) Molecular weight, subunits, and multiple forms of glutathione S-transferase from the house fly. Insect Biochem. **8**, 337–348

15 Pemble, S. E. and Taylor, J. B. (1992) An evolutionary perspective on glutathione transferases inferred from class-Theta glutathione transferase cDNA sequences. Biochem. J. **287**, 957–963
16 Ding, Y., Ortelli, F., Rossiter, L. C., Hemingway, J. and Ranson, H. (2003) The *Anopheles gambiae* glutathione transferase supergene family: annotation, phylogeny and expression profiles. BMC Genomics **4**, 35–50
17 Wilce, M. C. J. and Parker, M. W. (1994) Structure and function of glutathione S-transferases. Biochim. Biophys. Acta **1205**, 1–18
18 Armstrong, R. N., Rife, C. and Wang, Z. (2001) Structure, mechanism and evolution of thiol transferases. Chem. Biol. Interact. **133**, 167–169
19 Caccuri, A. M., Ascenzi, P., Antonini, G., Parker, M. W., Oakley, A. J., Chiessi, E., Nuccetelli, M., Battistoni, A., Bellizia, A. and Ricci, G. (1996) Structural flexibility modulates the activity of human glutathione transferase P1-1. Influence of a poor co-substrate on dynamics and kinetics of human glutathione transferase. J. Biol. Chem. **271**, 16193–16198
20 Caccuri, A. M., Antonini, G., Nicotra, M., Battistoni, A., Lo Bello, M., Board, P. G., Parker, M. W. and Ricci, G. (1997) Catalytic mechanism and role of hydroxyl residues in the active site of theta class glutathione S-transferases. Investigation of Ser-9 and Tyr-113 in a glutathione S-transferase from the Australian sheep blowfly, *Lucilia cuprina*. J. Biol. Chem. **272**, 29681–29686
21 Gustafsson, A., Pettersson, P. L., Grehn, L., Jemth, P. and Mannervik, B. (2001) Role of the glutamyl $\alpha$-carboxylate of the substrate glutathione in the catalytic mechanism of human glutathione transferase A1-1. Biochemistry **40**, 15835–15845
22 Winayanuwattikun, P. and Ketterman, A. J. (2005) An electron-sharing network involved in the catalytic mechanism is functionally conserved in different glutathione transferase classes. J. Biol. Chem. **280**, 31776–31782
23 Caccuri, A. M., Antonini, G., Board, P. G., Parker, M. W., Nicotra, M., Lo Bello, M., Federici, G. and Ricci, G. (1999) Proton release on binding of glutathione to Alpha, Mu and Delta class glutathione transferases. Biochem. J. **344**, 419–425
24 Tan, K.-L., Chelvanayagam, G., Parker, M. W. and Board, P. G. (1996) Mutagenesis of the active site of the human Theta-class glutathione transferase GSTT2-2: catalysis with different substrates involves different residues. Biochem. J. **319**, 315–321
25 Winayanuwattikun, P. and Ketterman, A. J. (2004) Catalytic and structural contributions for glutathione binding residues in a delta class glutathione S-transferase. Biochem. J. **382**, 751–757
26 Jirajaroenrat, K., Pongjaroenkit, S., Krittanai, C., Prapanthadara, L. and Ketterman, A. J. (2001) Heterologous expression and characterization of alternatively spliced glutathione *S*-transferases from a single *Anopheles* gene. Insect Biochem. Mol. Biol. **31**, 867–875
27 Bradford, M. M. (1976) A rapid and sensitive method for the quantitation of microgram quantities of protein utilizing the principle of protein-dye binding. Anal. Biochem. **72**, 248–254
28 Caccuri, A. M., Ascenzi, P., Lo Bello, M., Federici, G., Battistoni, A., Mazzetti, P. and Ricci, G. (1994) Are the steady state kinetics of glutathione transferase always dependent on the deprotonation of the bound glutathione? New insights in the kinetic mechanism of GST P1-1. Biochem. Biophys. Res. Commun. **200**, 1428–1434
29 Wolf, A. V., Brown, M. G. and Prentiss, P. G. (1985) Handbook of Chemistry and Physics, CRC Press, Boca Raton
30 Kong, G. K. W., Polekhina, G., McKinstry, W. J., Parker, M. W., Dragani, B., Aceto, A., Paludi, D., Principe, D. R., Mannervik, B. and Stenberg, G. (2003) Contribution of glycine 146 to a conserved folding module affecting stability and refolding of human glutathione transferase P1-1. J. Biol. Chem. **278**, 1291–1302
31 Stenberg, G., Dragani, B., Cocco, R., Principe, D. R., Mannervik, B. and Aceto, A. (2001) A conserved 'hydrophobic staple motif' plays a crucial role in the refolding of human glutathione transferase P1-P1. Chem. Biol. Interact. **133**, 49–50
32 Jackson, S. E., el Masry, N. and Fersht, A. R. (1993) Structure of the hydrophobic core in the transition state for folding of chymotrypsin inhibitor 2: a critical test of the protein engineering method of analysis. Biochemistry **32**, 11270–11278
33 Widersten, M., Kolm, R. H., Björnestedt, R. and Mannervik, B. (1992) Contribution of five amino acid residues in the glutathione binding site to the function of human glutathione transferase P1-1. Biochem. J. **285**, 377–381
34 Dirr, H. W. and Wallace, L. A. (1999) Role of the C-terminal helix 9 in the stability and ligandin function of class a glutathione transferase A1-1. Biochemistry **38**, 15631–15640
35 Jones, M. N. (1979) In Biochemical Thermodynamics (Studies in Modern Thermodynamics). (Jones, M. N., ed.), pp. 75–115, Elsevier, Oxford
36 Haynie, D. T. (2001) Statistical thermodynamics. In Biological thermodynamics, pp. 185–222, Cambridge University Press, Cambridge
37 Zeng, Q.-Y. and Wang, X.-R. (2005) Catalytic properties of glutathione-binding residues in a $\tau$ class glutathione transferase (PtGSTU1) from *Pinus tabulaeformis*. FEBS Lett. **579**, 2657–2662
38 Wongsantichon, J. and Ketterman, A. J. (2006) An intersubunit lock-and-key 'clasp' motif in the dimer interface of delta class glutathione transferase. Biochem. J. **394**, 135–144
39 Sayed, Y., Wallace, L. A. and Dirr, H. W. (2000) The hydrophobic lock-and-key intersubunit motif of glutathione transferase A1-1: implications for catalysis, ligandin function and stability. FEBS Lett. **465**, 169–172
40 Stenberg, G., Abdalla, A.-M. and Mannervik, B. (2000) Tyrosine 50 at the subunit interface of dimeric human glutathione transferase P1-1 is a structural key residue for modulating protein stability and catalytic function. Biochem. Biophys. Res. Commun. **271**, 59–63
41 Dirr, H. W., Little, T., Kuhnert, D. C. and Sayed, Y. (2005) A conserved N-capping motif contributes significantly to the stabilisation and dynamics of the C-terminal region of class alpha glutathione transferases. J. Biol. Chem. **280**, 19480–19487
42 Garcia-Viloca, M., Gao, J., Karplus, M. and Truhlar, D. G. (2004) How enzymes work: analysis by modern rate theory and computer simulations. Science **303**, 186–195
43 Chen, W.-J., Graminski, G. F. and Armstrong, R. N. (1988) Dissection of the catalytic mechanism of isozyme 4–4 of glutathione S-transferase with alternative substrates. Biochemistry **27**, 647–654
44 Graminski, G. F., Zhang, P., Sesay, M. A., Ammon, H. L. and Armstrong, R. N. (1989) Formation of the 1-(*S*-glutathionyl)-2,4,6-trinitrocyclohexadienate anion at the active site of glutathione *S*-transferase: evidence for enzymic stabilization of $\sigma$-complex intermediates in nucleophilic aromatic substitution reactions. Biochemistry **28**, 6252–6258
45 Johnson, W. W., Liu, S., Ji, X., Gilliland, G. L. and Armstrong, R. N. (1993) Tyrosine 115 participates both in chemical and physical steps of the catalytic mechanism of a glutathione S-transferase. J. Biol. Chem. **268**, 11508–11511

Received 16 August 2006/19 October 2006; accepted 14 November 2006
Published as BJ Immediate Publication 14 November 2006, doi:10.1042/BJ20061253

BJ www.biochemj.org

BJ Structure

Biochem. J. (2007) **401**, 635–644 (Printed in Great Britain) doi:10.1042/BJ20060603



# Differences in the subunit interface residues of alternatively spliced glutathione transferases affects catalytic and structural functions

Juthamart PIROMJITPONG, Jantana WONGSANTICHON and Albert J. KETTERMAN[1]

Institute of Molecular Biology and Genetics, Mahidol University, Salaya Campus, Nakhon Pathom 73170, Thailand

GSTs (glutathione transferases) are multifunctional widespread enzymes. Currently there are 13 identified classes within this family. Previously most structural characterization has been reported for mammalian Alpha, Mu and Pi class GSTs. In the present study we characterize two enzymes from the insect-specific Delta class, adGSTD3-3 and adGSTD4-4. These two proteins are alternatively spliced products from the same gene and have very similar tertiary structures. Several major contributions to the dimer interface area can be separated into three regions: conserved electrostatic interactions in region 1, hydrophobic interactions in region 2 and an ionic network in region 3. The four amino acid side chains studied in region 1 interact with each other as a planar rectangle. These interactions are highly conserved among the GST classes, Delta, Sigma and Theta. The hydrophobic residues in region 2 are not only subunit interface residues but also active site residues. Overall these three regions provide important contributions to stabilization and folding of the protein. In addition, decreases in yield as well as catalytic activity changes, suggest that the mutations in these regions can disrupt the active site conformation which decreases binding affinity, alters kinetic constants and alters substrate specificity. Several of these residues have only a slight effect on the initial folding of each subunit but have more influence on the dimerization process as well as impacting upon appropriate active site conformation. The results also suggest that even splicing products from the same gene may have specific features in the subunit interface area that would preclude heterodimerization.

Key words: *Anopheles dirus*, glutathione transferase (GST), hydrophobic interaction, subunit interface.

## INTRODUCTION

GSTs (glutathione transferases; EC 2.5.1.18) are a supergene family of multifunctional enzymes which are widely distributed in nature and found in most aerobic eukaryotes and prokaryotes. The dimeric cytosolic GSTs catalyse reactions with a broad range of substrates and play an essential role in detoxification of endogenous and xenobiotic compounds [1,2]. The dimerization of the GSTs not only contributes to stabilization of the subunit tertiary structure, but also allows for the construction of a fully functional active site [3]. Although tertiary structures of all classes of GSTs are similar, dimerization is highly specific and is thought to occur only between subunits within the same class [4,5].

The structural features at the dimer interface of the GSTs suggest at least two major subunit interaction areas [6]. The first area is the predominantly hydrophobic interaction at the outer ends of the interface called a hydrophobic 'lock-and-key' (also referred to as a 'ball-and-socket') motif which is formed by the insertion of an aromatic residue from domain I of one subunit into a 'lock' of five residues of domain II in the other subunit [6–9]. The second major subunit interaction area is the symmetry axis interactions at the 2-fold axis of the protein which show highly conserved electrostatic interactions at one edge of the subunit interface and a variety of interactions along the interface depending on the GST class. The *Anopheles dirus* mosquito is an important malaria vector in South East Asia. From an *A. dirus* genomic library, a 7.5 kb fragment containing the adgst1AS1 gene (*A. dirus* alternatively spliced GST gene) was identified [10]. This gene contains six exons that encode four Delta class GSTs, adGSTD1-1, 2-2, 3-3 and 4-4, which possess 61–77 % amino acid identity compared among themselves. Previously these proteins had been named adGST1-1, 1-2, 1-3 and 1-4, according to insect GST nomenclature in use (that is, insect class 1-protein 1, 2, 3 and 4 respectively). However, to be in alignment with a proposed universal GST nomenclature, the proteins were renamed adGSTD1-1, adGSTD2-2, adGSTD3-3 and adGSTD4-4 respectively [11,12]. The subunit number remains the same, since subunits were enumerated as they were initially discovered, 'D' refers to GST Delta class and '4-4' refers to the homodimeric isoenzyme. These four GSTs share an untranslated exon 1 and a translated exon 2 coding for 45 amino acids at the N-terminus but vary between four different exon 3 sequences (exons 3A–3D). The arrangement of each exon is similar to the aggst1$\alpha$ gene from *A. gambiae,* the major malaria vector in Africa, with approx. 79 % nucleotide identity for the two genes [13]. In *A. dirus*, although four splice products are encoded from the same gene, the enzymes possess distinct enzyme kinetic properties for substrates, inhibitors, including insecticides, as well as physical properties such as stability [14,15]. Although two splice products, adgstD3-3 (PDB accession number: 1JLV) and adgstD4-4 (PDB accession number: 1JLW), have very similar tertiary structures when aligned, the amino acid identity is only 68 % [16].

When compared with human Alpha, Mu and Pi classes, the dimer interfaces of both Delta class isoenzymes are more extensively hydrophilic. Although lacking the previously identified hydrophobic 'lock-and-key' motif (a conserved motif in human Alpha, Mu and Pi classes), the Delta class does possess a 'Clasp' motif with a similar function [17]. In addition to this motif, there are nine amino acids making major contributions to the interactions within this interface area, which can be separated into three regions: conserved electrostatic interactions in region

Abbreviations used: ANS, 8-anilino-1-naphthalene sulfonate; CDNB, 1-chloro-2,4-dinitrobenzene; DCNB, 1,2-dichloro-4-nitrobenzene; EA, ethacrynic acid; GST, glutathione transferase; PNBC, p-nitrobenzyl chloride; PNPB, p-nitrophenethyl bromide.

[1] To whom correspondence should be addressed (email albertketterman@yahoo.com).

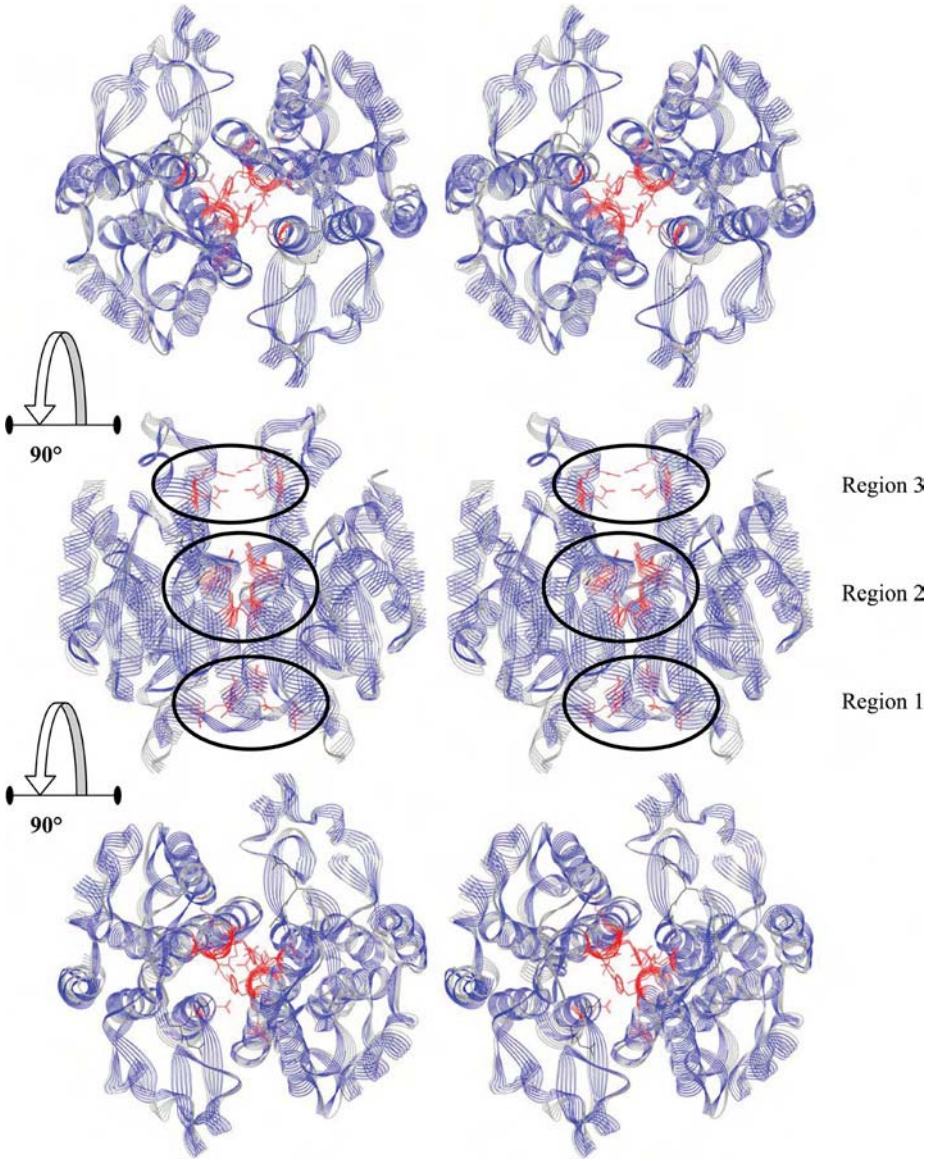


**Figure 1 The three regions of the interface characterized in the present study**

The two GST proteins are carbon backbone aligned with the adGSTD3-3 secondary structure wire ribbon shown in blue and the adGSTD4-4 secondary structure ribbon shown in grey. The GSH in the two active sites is shown as a black stick; the residues engineered in the present study are shown in red. The top panel is a stereo view looking at the 2-fold axis from the side opposite to the active sites. The middle panel shows the proteins rotated 90°, to show the position of the studied interface residues down the length of $\alpha$-helices 3 and 4. The bottom panel shows the proteins rotated a further 90° and looking down upon the 2-fold axis on to the active sites. The Figure was created using Accelrys DS ViewerPro 5.0.

1, hydrophobic interactions in region 2 and an ionic network in region 3 (Figure 1).

The conserved electrostatic interactions in region 1 of the subunit interface are formed by two amino acid residues from one subunit (a glutamate residue in $\alpha$-helix 3 and an arginine residue in $\alpha$-helix 4) interacting with the same two amino acids from the other subunit. These interactions are of interest because the four amino acid side chains interact with each other as a planar rectangle with distances of 3.83–4.26 Å (1Å = 0.1 nm). These interactions are highly conserved among the GST classes, Delta, Sigma and Theta, however at present there are no reports of these interactions for any of the three GST classes. In adGSTD4-4, each arginine residue not only interacts with both of the negatively charged Glu$^{75}$ residues in both subunits, but also forms cation–$\pi$ interactions with the aromatic ring of Tyr$^{89}$ and an ionic interaction with the carboxy group of Pro$^{90}$. In adGSTD3-3, the equivalent residues to Glu$^{75}$ and Arg$^{96}$ of adGSTD4-4 are Glu$^{74}$ and Arg$^{90}$. These residues also form the same planar rectangle arrangement within adGSTD3-3 and are stabilized in a similar manner by interactions with Tyr$^{83}$ and Pro$^{84}$ (Tyr$^{89}$ and Pro$^{90}$ in adGSTD4-4). Therefore as the motif appears to be highly conserved in both proteins it was only studied in adGSTD4-4. In addition, these interactions appear to be highly conserved among the insect GST classes. Therefore the aim of the present study was to determine whether the inter- and intra-subunit electrostatic interactions of these residues are important contributions that help to maintain tertiary and quaternary structures.

Region 2 at the subunit interface shows the most variation in amino acid residues at equivalent positions between the two isoenzymes, Tyr$^{98}$, Met$^{101}$ and Gly$^{102}$ of adGSTD3-3 and Phe$^{104}$,

Val[107] and Ala[108] of adGSTD4-4 respectively. These residues are of interest because they are not only subunit interface residues but also active site residues with several of them involved in both active sites of the dimeric enzyme. Therefore the amino acids at the equivalent positions of the two isoenzymes were studied by switching the amino acids of the two proteins; Y98F, M101V, G102A and Y98F/M101V/G102A of adGSTD3-3 and F104Y, V107M, A108G and F104Y/V107M/A108G of adGSTD4-4.

The last region is the hydrophilic area in region 3 of the subunit interface, Asp[110] of adGSTD3-3 and Glu[116] of adGSTD4-4. Not only are these subunit interface residues, but these two equivalent positions also are involved in the active site as part of the H-site (hydrophobic substrate-binding site). For adGSTD4-4, Glu[116] forms hydrogen bonds with Arg[134] in both inter- and intra-subunit interactions; however, these interactions do not appear in adGSTD3-3. For adGSTD3-3, there are hydrogen bonds only in the same subunit between Asp[110] and the highly conserved residue Glu[106]. To study the influence of the ionic network in region 3 of the subunit interface and whether it impacts upon the catalytic activity and stability of the enzymes, mutations at the equivalent positions of these two isoenzymes were generated, that is, D110A of adGSTD3-3 and E116A of adGSTD4-4.

## MATERIALS AND METHODS

### Site-directed mutagenesis and protein purification

The adGSTD3-3 and adGSTD4-4 plasmid DNA templates were prepared from previous constructs [14]. The construction of the mutants was based on the Stratagene QuikChange® site-directed mutagenesis kit using *pfu* DNA polymerase. The expression constructs of recombinant plasmid that were obtained were sequenced at least twice and transformed into *Escherichia coli* BL21DE3plysS. The soluble recombinant GSTs were purified by GSTrap affinity chromatography (Amersham Phamacia) as previously described [14]. After purification, proteins were homogeneous as judged by SDS/PAGE, and the protein concentration was determined using the Bradford protein reagent with bovine serum albumin as a standard [18].

### Catalytic activity and kinetic studies

Steady-state kinetics were studied at various concentrations of CDNB (1-chloro-2,4-dinitrobenzene) and GSH in 0.1 M phosphate buffer (pH 6.5). The reaction was monitored at 340 nm, $\varepsilon = 9600\ M^{-1} \cdot cm^{-1}$. Apparent kinetic parameters, $k_{cat}$, $K_m$ and $k_{cat}/K_m$ were determined by fitting the collected data to a Michaelis–Menten equation by non-linear regression analysis using GraphPad Prism version 4 (GraphPad software; www.graphpad.com) [19,20]. Specific activities of the enzymes were determined with five different substrates; CDNB, DCNB (1,2-dichloro-4-nitrobenzene), EA (ethacrynic acid), PNPB (p-nitrophenethyl bromide) and PNBC (p-nitrobenzyl chloride) as previously described [21]. Specific activities reported are the means ± S.D. from at least three independent experiments. One-way ANOVA with Dunnett's post test was performed using GraphPad InStat version 3.06 for Windows (GraphPad software; www.graphpad.com).

### Structural studies

Enzymes at 0.1 mg/ml final concentration were incubated at 45 °C. Inactivation time courses were determined by withdrawing suitable aliquots at different time points for an assay of remaining activity to calculate the half-life of the enzyme [22]. Data are the means ± S.D. from at least three independent experiments.

Spectroscopic properties of wild-type and mutant proteins were measured for evidence of conformational changes. Intrinsic fluorescence emission spectra were measured at an excitation wavelength of 295 nm and $\lambda_{max}$ and fluorescence intensity of emission spectra were analysed at a protein concentration of 0.2 mg/ml [23].

A refolding experiment was performed with enzymes first being denatured in 4 M guanidinium chloride in renaturation buffer [0.2 M phosphate, 1 mM EDTA and 5 mM dithiothreitol (pH 7.0)] at room temperature (25 °C) for 1 h and then rapidly diluted (defining time zero) 1:40 into renaturation buffer. Therefore the final guanidinium chloride concentration was 0.1 M during refolding. Recovered activity was monitored as a function of time by withdrawal of appropriate aliquots of renaturation mixture and immediately assaying for activity. Refolding rate constants were determined by non-linear regression analysis using a single exponential equation [23].

The ANS (8-anilino-1-naphthalenesulfonate) binding assay was monitored using a PerkinElmer Luminescence spectrometer LS50B. ANS [200 $\mu$M in 0.1 M sodium phosphate buffer (pH 6.5)] was added to a final concentration of 2 $\mu$M enzyme in a 400 $\mu$l reaction mixture [24]. The spectrum of ANS in phosphate buffer (pH 6.5) was subtracted from the spectrum of protein-binding ANS. A total of three scans each for blank and sample were recorded and averaged for each enzyme. Reported spectra are the means from at least three independent experiments. Enzyme activity measurements in the presence of ANS were assessed immediately after adding ANS by using the standard reaction assay.

## RESULTS AND DISCUSSION

The investigations of GST dimerization performed in mammalian GSTs indicated that the subunit interactions are a significant source of stabilization not only for the association of subunits but also for tertiary structures of the individual subunits [9,25,26]. In the present study, most mutations gave similar purification yields as the wild-type with the exception of the E75A and R96A mutants of adGSTD4-4, which had yields approx. 2 and 0.4 % of the wild-type respectively. As the proteins were expressed in similar amounts, it appears that the alteration of these residues disrupts the intra-subunit interaction between helix 3 and helix 4 which impacts upon the active site architecture thereby affecting binding to the affinity matrix.

Both adGSTD3-3 and adGSTD4-4 have two tryptophan residues in each subunit that are located in $\beta$-sheet 4 in domain I and $\alpha$-helix 7 in domain II. The tryptophan residue located in $\beta$-sheet 4 in domain I (Trp[63]) is in close proximity to the active site, with an involvement in sequestering the substrate glutathione, as well as being in the subunit interface. This makes it a sensitive fluorescence probe to monitor conformational changes at/near the active site. The normalized fluorescence spectra of adGSTD3-3 and adGSTD4-4 wild-type compared with the mutants were obtained to study the effect of mutations on the enzyme tertiary structure (Figure 2). The results showed that although every mutant had the same $\lambda_{max}$ as the wild-type, several mutants presented differences in the normalized intensities of fluorescence, implying that the mutations caused significant conformational changes in the environment of the tryptophan residues located near the subunit interface and the mutation site. The mutants also had different intensities from their wild-type especially R96A, with the intensity of fluorescence decreased by approx. 66 %. This finding suggests that there are significant conformational changes in the tryptophan residue neighbourhood that distinguish the final structure of the mutant from that of the wild-type. This decrease

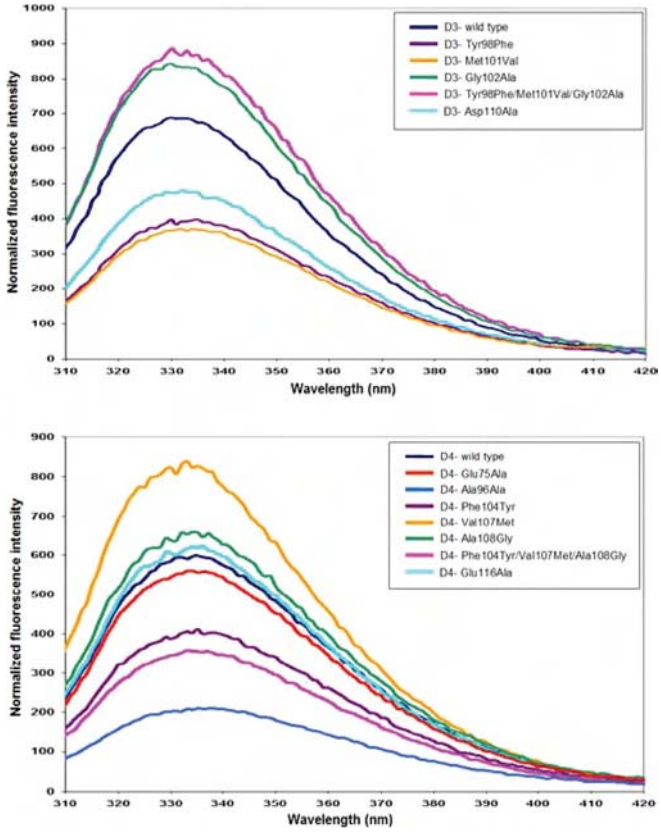


**Figure 2 Normalized intrinsic tryptophan residue fluorescence spectra of the adGSTD3-3 and adGSTD4-4 (wild-type) and the recombinant mutant GSTs**

The same colour represents the equivalent position. The data are means of three independent experiments.

demonstrates that movements have occurred in the tryptophan residues or in the surrounding fluorescence quenching groups.

The half-life of the enzymes corresponds to the time of incubation when there is 50 % remaining activity (Table 1). The conserved cation–$\pi$ interaction residue, Arg[96], and the conserved electrostatic interaction residue, Glu[75], have important roles in stabilizing enzyme structure as shown by a much decreased stability for R96A and E75A of approx. 15- and 7.4-fold respectively. For region 2, several mutants possessed similar stability as the wild-type enzymes. However, there were three mutants which had very different thermal stabilities. Two of the mutations were at an equivalent position, adGSTD3-3 Gly[102] and adGSTD4-4 Ala[108]. Replacement of a glycine residue by an alanine residue in adGSTD3-3 at this position caused decreases of about 8-fold in half-life, whereas a glycine residue substitution of adGSTD4-4 showed an increase in half-life of about 4.7-fold. The other mutant that showed stability changes was the V104M protein which decreased the half-life by approx. 3-fold. For region 3, the half-life of D110A of adGSTD3-3 was similar to the wild-type. However, the equivalent adGSTD4-4 mutation E116A disrupted the charge–charge network and showed a 64 % decreased stability for the enzyme. The results showed that the positively charged residue at the edge of the subunit interface of adGSTD4-4 participates in stabilizing the enzyme structure while the equivalent residue of adGSTD3-3 appeared to have only a minor contribution.

Three mutations in adGSTD4-4, E75A, R96A and V107M, did not recover activity after being unfolded by 4 M guanidinium chloride (Table 1). This implies that these residues play a critical role in the folding process of the enzymes. For the remaining mutants, the refolding rate constants were similar. The activity recovered illustrates the ability of the enzymes to recover their appropriate active site conformation for catalytic activity. After unfolding, the enzymes were able to recover activity ranging from 19 % to 94 %. To study the influence of mutations on protein folding and to assess whether the changes affected tertiary folding of each subunit or dimerization of the two subunits, intrinsic tryptophan residue fluorescence spectroscopy was performed. The fluorescence spectra of native, unfolded and refolded enzymes were monitored to compare the tertiary structure of the proteins in each state (Figures 3 and 4). The $\lambda_{max}$ values of the native (335 nm) and the unfolded form (355 nm) of the protein were observed for every enzyme. The data showed that the enzymes were refolded in a similar manner as the native form, as shown by similar $\lambda_{max}$ values, including the E75A, R96A and V107M mutants, although

**Table 1 Half-life, refolding rate constants, activity recovered (%) and the effect of ANS on CDNB specific activity of the adGSTD3-3 and adGSTD4-4 (wild-type) and the recombinant engineered GSTs**

The data are means ± S.D. for at least three independent experiments. One-way ANOVA with Dunnett's post test was performed to show statistical significance with $*P < 0.05$ and $\dagger P < 0.01$. D3 and D4 indicate adGSTD3-3 and adGSTD4-4 respectively. Inside parentheses the numbers indicate the subunit interface region: 1 is region 1, 2 is region 2 and 3 is region 3; and the same lowercase letter indicates an equivalent residue position for the two GST isoenzymes. nd, not detectable.

| Enzymes | Half-life (min) | Refolding rate constant ($min^{-1}$) | Activity recovered (%) | Inhibition by ANS (%) |
|---|---|---|---|---|
| D3-wild-type | 2.71 ± 0.35 | 0.87 ± 0.09 | 56.9 ± 0.23 | 24.6 ± 1.41 |
| D3-Y98F (2/a) | 3.12 ± 0.33 | 0.58 ± 0.05† | 66.1 ± 2.83* | 13.1 ± 0.54† |
| D3-M101V (2/b) | 2.77 ± 0.43 | 0.42 ± 0.05† | 40.5 ± 1.93† | 11.9 ± 0.80† |
| D3-G102A (2/c) | 0.34 ± 0.03† | 0.38 ± 0.07† | 94.4 ± 5.77† | 13.7 ± 2.66† |
| D3-Y98F/M101V/G102A (2/d) | 1.88 ± 0.01* | 0.31 ± 0.03† | 85.8 ± 4.39† | 18.4 ± 0.65† |
| D3-D110A (3/e) | 2.21 ± 0.24 | 0.58 ± 0.11† | 80.5 ± 3.48† | 23.4 ± 1.83 |
| D4-wild-type | 14.0 ± 1.70 | 0.59 ± 0.03 | 19.7 ± 0.70 | 18.4 ± 1.20 |
| D4-G75A(1) | 1.89 ± 0.13† | nd | 0.00 | 22.5 ± 0.82 |
| D4-R96A(1) | 0.91 ± 0.07† | nd | 0.00 | 18.8 ± 3.89 |
| D4-F104Y (2/a) | 17.1 ± 1.76* | 0.28 ± 0.02† | 23.5 ± 0.51 | 31.9 ± 1.96† |
| D4-V107M (2/b) | 4.76 ± 0.15† | nd | 0.00 | 25.4 ± 1.41† |
| D4-A108G (2/c) | 65.4 ± 1.45† | 0.32 ± 0.04† | 69.6 ± 7.55† | 32.8 ± 1.03† |
| D4-F104Y/V107M/A108G (2/d) | 16.7 ± 1.23 | 0.60 ± 0.10 | 25.0 ± 0.18 | 21.1 ± 1.83 |
| D4-E116A (3/e) | 5.16 ± 0.93† | 0.68 ± 0.11 | 9.93 ± 0.68* | 17.3 ± 2.05 |

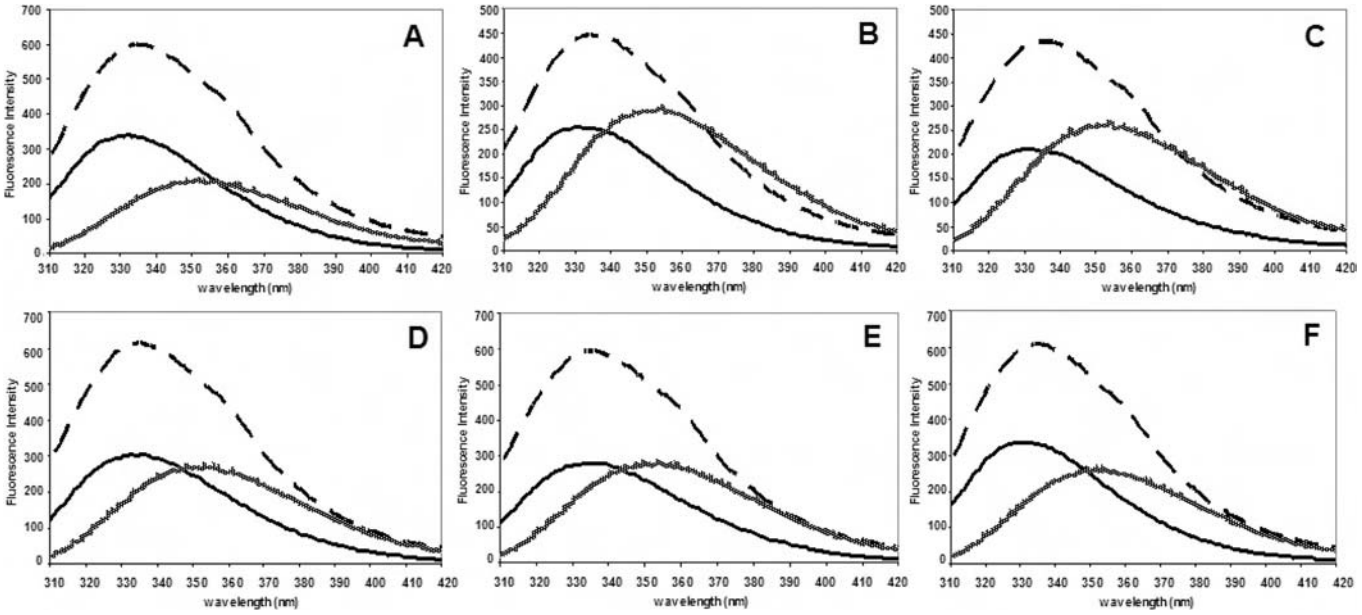


**Figure 3 Normalized intrinsic tryptophan residue fluorescence spectra compared with the native, refolded and unfolded forms of the adGSTD3-3 (wild-type) and the recombinant mutant GSTs**

(**A**) Wild-type, (**B**) Y98F, (**C**) M101V, (**D**) G102A, (**E**) Y98F/M101V/G102A and (**F**) D110A. The data are means for at least three independent experiments. Solid line, native form; dashed line, refolded form; and hashed line, unfolded form of the enzyme.

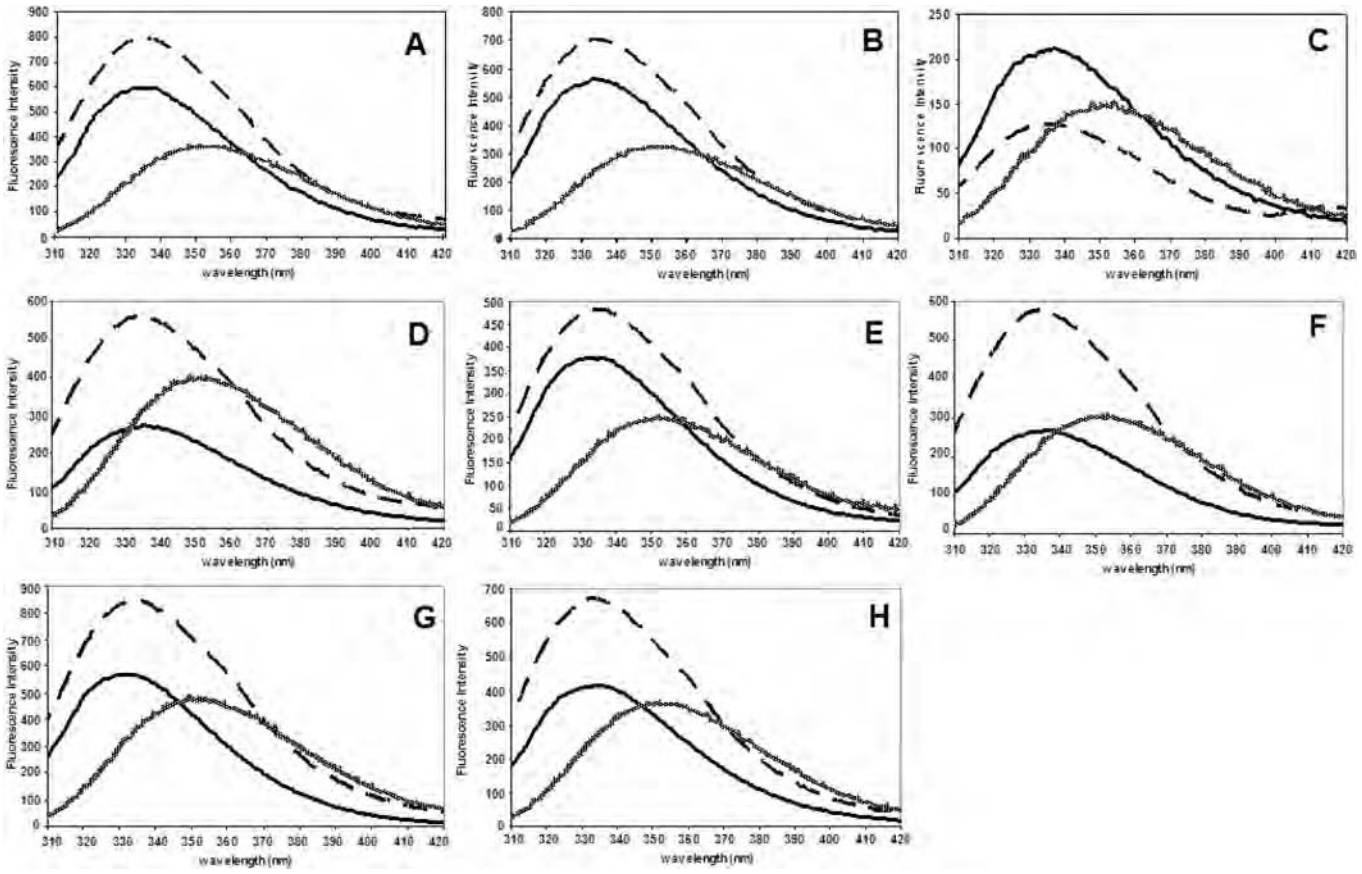


**Figure 4 Normalized intrinsic tryptophan residue fluorescence spectra compared with the native, refolded and unfolded forms of the adGSTD4-4 (wild-type) and the recombinant mutant GSTs**

(**A**) Wild-type, (**B**) G75A, (**C**) R96A, (**D**) F104Y, (**E**) V107M, (**F**) A108G, (**G**) F104Y/V107M/A108G and (**H**) E116A. The data are means for at least three independent experiments. Solid line, native form; dashed line, refolded form; and hashed line, unfolded form of the enzyme.

these enzymes could not recover catalytic activity. As shown by the similar patterns of the adGSTD3-3 mutant spectra, the mutations did not affect the tertiary folding of each subunit but influenced the dimerization process, which is necessary to achieve an appropriate active site conformation. Therefore both catalytic and structural data suggest that the single mutation of $Gly^{102}$ and the triple mutation had significant effects on the dimerization of the enzymes by increasing the activity recovered from 56.9 % for wild-type to approx. 94.4 % and 85.8 % for the two proteins respectively (Table 1). In both catalytic and structural experiments, the refolding data showed that loss of the conserved electrostatic interactions, E75A and R96A, and the hydrophobic residue, V107M, had a dramatic effect on the dimerization process, which is critical to formation of the complete active site pocket. The results for the $Arg^{96}$ position indicated that not only does this residue have a critical role in the dimerization process, but it is also important for the protein folding pathway of each monomeric subunit.

The anionic dye ANS has been shown to bind in the solvent-exposed cleft in the subunit interface of class Alpha and Pi enzymes [27–29]. Therefore ANS was utilized as a probe to monitor the appearance/disappearance of hydrophobic patches or surfaces on the proteins that were undergoing structural changes. When ANS was bound to the proteins the fluorescence was enhanced, accompanied by a blue shift in its emission maximum from 514 nm (free ANS in buffer) to 498 nm for adGSTD3-3 and 482 nm for wild-type adGSTD4-4, indicating that the polarity of the binding site had become more hydrophobic, with decreasing polarity the greater the blue shift.

When compared with the wild-type proteins, there was no change in the emission maximum wavelength of ANS bound to all mutants (Figure 5). For the ANS fluorescence intensity, which reflects the degree of solvent quenching of ANS bound to the protein, the adGSTD4-4 mutants showed variations in the amount of ANS bound, except E75A, which showed a similar intensity to the wild-type. However, there was no relative intensity change for the adGSTD3-3 mutants. The results showed that the residue substitutions of adGSTD4-4 with the adGSTD3-3 amino acids had a dramatic effect at the subunit interface, much more than for adGSTD3-3.

To study the impact of ANS on the enzyme conformation, the enzyme activity in the presence and absence of ANS was measured using the standard reaction assay. The results showed that for the mutants, ANS molecules can bind and alter the active site architecture in a manner similar to the wild-type (Table 1). It implied that differences in ANS spectra intensities in Figure 5 occurred only from an alteration of a hydrophobic patch at the subunit-binding site.

In general, the engineered enzyme reactions followed Michaelis–Menten kinetics as did the wild-type except for E75A, F104Y and E116A of adGSTD4-4 which showed positive co-operativity upon substrate binding. Positive co-operativity is shown by a sigmoidal velocity curve which reflects the substrate binding in the first active site, that then facilitates a second substrate molecule binding in the second active site by increasing the binding affinity of the vacant binding site [30]. For CDNB, two of the enzymes had significantly different Hill coefficients (shown by one-way ANOVA with Dunnett's post test) compared with wild-type enzyme [Hill coefficients for wild-type $1.08 \pm 0.08$ versus E75A $1.79 \pm 0.03$ ($P < 0.01$) and E116A $1.40 \pm 0.20$ ($P < 0.05$)]. For GSH only F104Y had a significantly different Hill coefficient (shown by one-way ANOVA with Dunnett's post test) compared with wild-type enzyme [Hill coefficients for wild-type $1.06 \pm 0.14$ versus F104Y $2.01 \pm 0.09$ ($P < 0.01$)]. These data show that two of the mutant enzymes, E75A and F104Y, had very strong positive co-operativity, with the Hill coefficients approaching the number of substrate-binding sites. In addition, comparison of the kinetic constants of the mutants with the wild-type values showed that the residue changes affected additional enzymatic properties (Table 2). These effects on the active site were also reflected in changes in substrate specificity with changes in the equivalent residue position showing different effects on the two isoforms (Table 3). For example, D110A activity was significantly decreased with CDNB and DCNB in adGSTD3-3 but E116A activity was significantly increased with CDNB and showed no significant activity with DCNB in adGSTD4-4. For another position, M101V in adGSTD3-3 equivalent to V107M in adGSTD4-4, both enzymes showed significant decreases in activity with CDNB. However, the adGSTD4-4 enzyme showed significant increases in activity with DCNB and EA, whereas the adGSTD3-3 enzyme showed a significant decrease with DCNB and no significant change with EA.

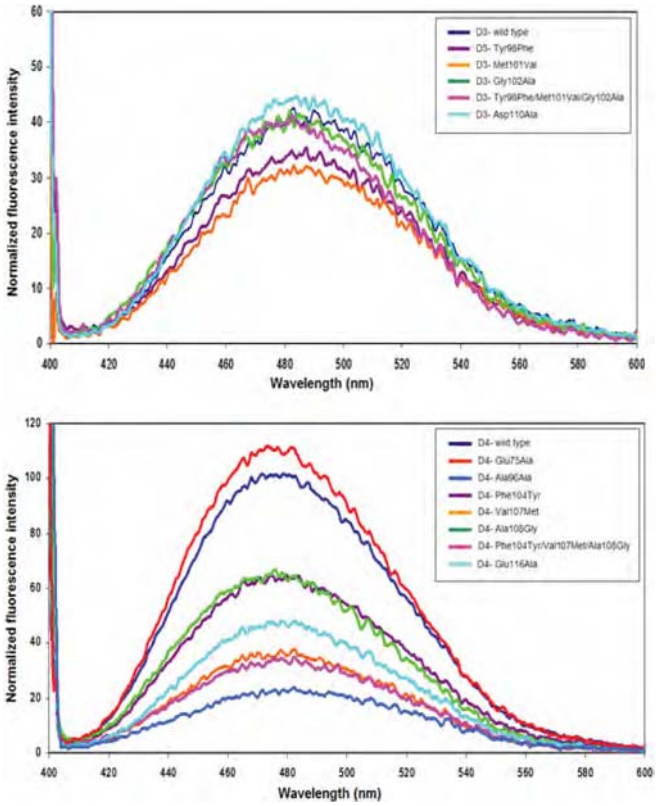


**Figure 5 ANS binding spectra of the adGSTD3-3 and adGSTD4-4 (wild-type) and the recombinant mutant GSTs**

The same colour represents the equivalent position. The spectra were measured immediately after addition of ANS. As ANS fluorescence is quenched by water, alteration of the fluorescence intensity of protein-bound ANS is highly dependent upon its accessibility to water. The data are means for at least three independent experiments.

The insect GST class Delta has a conserved planar rectangular electrostatic motif formed by four amino acid residues from different helices of both subunits ($Glu^{75}$ in $\alpha$-helix 3 and $Arg^{96}$ in $\alpha$-helix 4) (Figure 6). These interactions are highly conserved among GST classes Delta, Sigma and Theta. This is the first report of these interactions for any of these three classes. To study the function of this motif two mutants were generated, E75A and R96A, which break the conserved electrostatic interactions and ionic network at the dimer interface of adGSTD4-4. The results showed that the motif provides an important contribution

**Table 2 Yield of purification and kinetic parameters of the adGSTD3-3 and adGSTD4-4 (wild-type) and the recombinant engineered GSTs**

The data are means ± S.D. for at least three independent experiments. One-way ANOVA with Dunnett's post test was performed to show statistical significance with $*P < 0.05$ and $\dagger P < 0.01$. D3 and D4 indicate adGSTD3-3 and adGSTD4-4 respectively. Inside parentheses the numbers indicate the subunit interface region: 1 is region 1, 2 is region 2 and 3 is region 3; and the same lowercase letter indicates an equivalent residue position for the two GST isoenzymes.

| Enzymes | CDNB $k_{cat}$ ($s^{-1}$) | CDNB $K_m$ (mM) | CDNB $k_{cat}/K_m$ ($mM^{-1}•s^{-1}$) | GSH $K_m$ (mM) | GSH $k_{cat}/K_m$ ($mM^{-1}•s^{-1}$) | Purification yield (%) |
|---|---|---|---|---|---|---|
| D3-wild-type | 39.2 | 0.15 ± 0.01 | 258 | 0.29 ± 0.04 | 114 | 53.7 |
| D3-Y98F (2/a) | 24.9† | 0.12 ± 0.01 | 213 | 0.47 ± 0.05 | 53.1 | 49.2 |
| D3-M101V (2/b) | 26.0† | 0.72 ± 0.06† | 36.3 | 1.04 ± 0.06† | 25.0 | 60.0 |
| D3-G102A (2/c) | 23.5† | 0.37 ± 0.02† | 63.3 | 2.94 ± 0.38† | 7.99 | 47.6 |
| D3-Y98F/M101V/G102A (2/d) | 40.7 | 0.28 ± 0.03† | 147 | 1.12 ± 0.07† | 36.7 | 58.3 |
| D3-D110A (3/e) | 51.7† | 0.49 ± 0.07† | 106 | 0.54 ± 0.04 | 95.8 | 34.3 |
| D4-wild-type | 22.5 | 0.63 ± 0.09 | 35.7 | 0.67 ± 0.05 | 33.6 | 61.3 |
| D4-G75A (1) | 23.3 | 8.26 ± 2.63† | 2.82 | 0.54 ± 0.06 | 43 | 5.5 |
| D4-R96A (1) | 16.2† | 0.80 ± 0.06 | 22.0 | 1.08 ± 0.02 | 15.0 | 1.4 |
| D4-F104Y (2/a) | 15.5† | 0.52 ± 0.03 | 29.8 | 24.01 ± 2.94† | 0.65 | 42.2 |
| D4-V107M (2/b) | 13.7† | 1.6 ± 0.08 | 8.56 | 0.76 ± 0.11 | 18.0 | 60.0 |
| D4-A108G (2/c) | 26.8 | 0.87 ± 0.07 | 26.8 | 0.73 ± 0.12 | 36.7 | 59.2 |
| D4-F104Y/V107M/A108G (2/d) | 32.5† | 0.72 ± 0.04 | 45.2 | 0.25 ± 0.02 | 130 | 59.2 |
| D4- E116A (3/e) | 46.1† | 1.55 ± 0.01 | 29.7 | 1.24 ± 0.06 | 37.1 | 37.1 |

**Table 3 Specific activities of the adGSTD3-3 and adGSTD4-4 (wild-type) and the recombinant engineered GSTs**

The data are means ± S.D. for at least three independent experiments. One-way ANOVA with Dunnett's post test was performed to show statistical significance with $*P < 0.05$ and $\dagger P < 0.01$. The substrate concentrations used were 1 mM CDNB for adGSTD3 and 3 mM CDNB for adGSTD4, 1 mM DCNB, 0.1 mM PNBC, 0.1 mM PNPB and 0.2 mM EA. D3 and D4 indicate adGSTD3-3 and adGSTD4-4 respectively. Inside parentheses the numbers indicate the subunit interface region: 1 is region 1, 2 is region 2 and 3 is region 3; and the same lowercase letter indicates an equivalent residue position for the two GST isoenzymes. nd is not detectable.

| Enzymes | Specific Activity ($\mu$mol/min/mg) CDNB | DCNB | EA | PNPB | PNBC |
|---|---|---|---|---|---|
| D3-wild-type | 85.3 ± 3.23 | 0.25 ± 0.01 | 0.10 ± 0.05 | nd | 0.13 ± 0.01 |
| D3-Y98F (2/a) | 46.9 ± 6.38† | 0.23 ± 0.03 | 0.03 ± 0.01* | nd | 0.05 ± 0.00† |
| D3-M101V (2/b) | 41.1 ± 0.81† | 0.05 ± 0.01† | 0.08 ± 0.02 | nd | 0.09 ± 0.00† |
| D3-G102A (2/c) | 46.8 ± 0.25† | 0.08 ± 0.01† | nd | nd | 0.05 ± 0.00† |
| D3-Y98F/M101V/G102A (2/d) | 84.8 ± 5.47 | 0.21 ± 0.01* | 0.15 ± 0.01 | nd | 0.08 ± 0.00† |
| D3-D110A (3/e) | 71.6 ± 2.69† | 0.16 ± 0.01† | 0.01 ± 0.01† | 0.03 ± 0.01 | 0.07 ± 0.01† |
| D4-wild-type | 48.0 ± 1.98 | 0.03 ± 0.00 | 0.27 ± 0.00 | 0.06 ± 0.01 | 0.03 ± 0.01 |
| D4-E75A (1) | 36.6 ± 5.03† | 0.06 ± 0.01 | 0.12 ± 0.01 | 0.02 ± 0.01 | 0.06 ± 0.00 |
| D4-R96A (1) | 26.0 ± 0.13† | 0.27 ± 0.04† | 0.18 ± 0.01 | 0.23 ± 0.02 | nd |
| D4-F104Y (2/a) | 28.5 ± 2.24† | 0.06 ± 0.01 | 0.14 ± 0.01 | 0.05 ± 0.01 | 0.11 ± 0.05 |
| D4-V107M (2/b) | 22.0 ± 2.29† | 0.08 ± 0.004* | 2.06 ± 0.29† | 0.31 ± 0.08 | nd |
| D4-A108G (2/c) | 55.3 ± 2.07 | 0.06 ± 0.02 | 0.32 ± 0.01 | nd | 0.08 ± 0.02 |
| D4-F104Y/V107M/A108G (2/d) | 53.8 ± 1.43 | 0.05 ± 0.01 | 0.02 ± 0.00* | nd | 0.04 ± 0.01 |
| D4- E116A (3/e) | 56.3 ± 6.83* | 0.06 ± 0.01 | 0.01 ± 0.01* | 0.04 ± 0.01 | 0.04 ± 0.01 |

to the stabilization and folding of the protein. The mutants were expressed in both inclusion and soluble forms, with the R96A mutant mostly being expressed as an inclusion body. This evidence and the results from the refolding assay (Table 1; Figures 3 and 4) indicated that the folding process was altered by the mutations. In addition, decreases in yield as well as catalytic activity changes (Table 2), suggest that the mutations disrupt the active site conformation which decreases binding affinity, alters kinetic constants and substrate specificities.

Although both $Glu^{75}$ and $Arg^{96}$ are located in the same area, in the present study region 1 of the subunit interface, there is a conserved amino acid sequence around $Arg^{96}$ which forms a pocket around the arginine residue. $Arg^{96}$ is stabilized by several highly conserved residues in a cation–$\pi$ interaction with $Tyr^{89}$ and $Pro^{90}$, whereas $Glu^{75}$ does not have amino acids surrounding it, except $Arg^{96}$, as it is located within a hole in the subunit interface edge (Figure 6). Therefore substitution of an alanine residue for $Arg^{96}$ appears to have more impact on the tertiary and quaternary structure of the protein compared with $Glu^{75}$, as shown by decreases in the fluorescence intensities of both intrinsic tryptophan spectroscopy (Figure 2) and the ANS binding assay (Figure 5). This also suggests that there are significant conformational changes in amino acid side chains near the subunit interface and the mutation site. However, disappearance of the salt bridges with the loss of either $Glu^{75}$ or $Arg^{96}$ affected both initial protein folding, as shown in the refolding experiment, and the protein stability as shown by decreased half-life. Although $Arg^{96}$ is not located in the active site pocket, structural changes that occurred due to this mutation also affected the active site conformation, probably through packing effects (Tables 2 and 3).

Region 2 of the subunit interface, which shows the most variation in amino acid residues at the equivalent positions between adGSTD3-3 and adGSTD4-4, is of interest because the residues are not only in the interface but also in the active site,

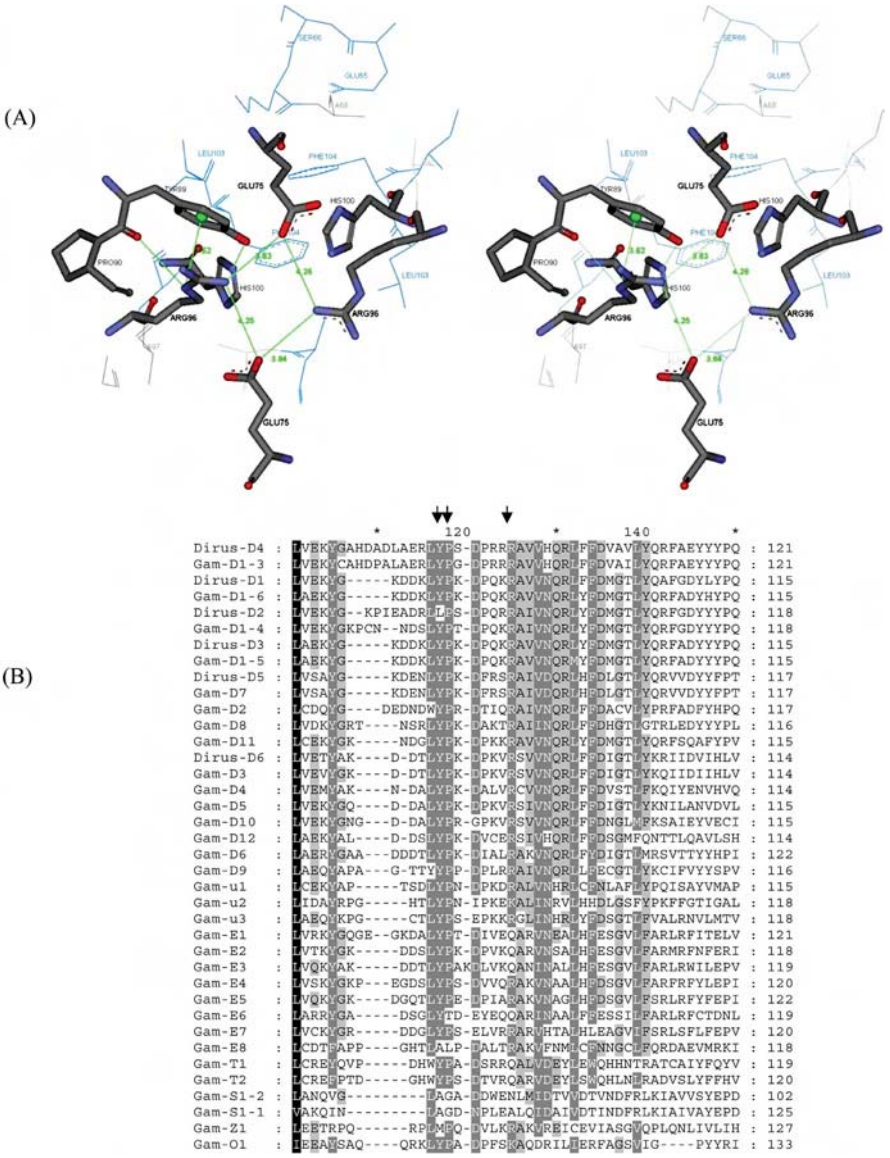


**Figure 6 Conserved electrostatic interaction in region 1 of the subunit interface**

(**A**) The planar rectangle electrostatic interaction of Glu$^{75}$ and Arg$^{96}$ from both subunits. Distances between the charged atoms are shown in Å. Also shown are the conserved anion–cation–$\pi$ interactions between Tyr$^{89}$, Pro$^{90}$ and Arg$^{96}$. (**B**) Amino acid alignment of insect GST classes. Dirus is *A. dirus* and Gam is *A. gambiae*. The arrows point to the highly conserved tyrosine, proline and arginine residues. D is Delta, u is unclassified, E is Epsilon, T is Theta, S is Sigma, Z is Zeta and O is Omega GST class. GenBank® accession numbers: adGSTD1 (AF273041), adGSTD2 (AF273038), adGSTD3 (AF273039), adGSTD4 (AF273040), adGSTD5 (AF251478), adGSTD6 (AY014406), agGSTD1-3 (Protein ID AAC79992), agGSTD1-4 (Protein ID AAC79994), agGSTD1-5 (Protein ID AAC79993), agGSTD1-6 (Protein ID AAC79995), agGSTD2 (Z71480), agGSTD3 (AF513638), agGSTD4 (AF513635), agGSTD5 (AF513634), agGSTD6 (AF513636), agGSTD7 (AF071161), agGSTD8 (AF316637), agGSTD9 (AY255857), agGSTD10 (AF515527), agGSTD11 (AF513637), agGSTD12 (AF316638), agGSTu1 (AF515521), agGSTu2 (AF515523), agGSTu3 (AF515524), agGSTE1 (AF316635), agGSTE2 (AF316636), agGSTE3 (AY070234), agGSTE4 (AY070254), agGSTE5 (AY070255), agGSTE6 (AY070256), agGSTE7 (AF491816), agGSTE8 (AY070257), agGSTT1 (AF515526), agGSTT2 (AF515525), agGSTS1-1 (L07880), agGSTS1-2 (AF513639), agGSTZ1 (AF515522), agGSTO1 (AY255856). agGSTD6 and agGSTD9 were suggested to be pseudogenes [33]. The Figure in (**A**) was created using Accelrys DS ViewerPro 5.0.

with several residues involved in both active sites of the dimer. The effects of the different hydrophobic amino acids at the equivalent positions of the two isoenzymes were studied by switching the equivalent amino acids with the amino acid from the other protein; that is, Y98F, M101V, G102A and Y98F/M101V/G102A for adGSTD3-3 and F104Y, V107M, A108G and F104Y/V107M/A108G for adGSTD4-4. The refolding experiments demonstrated that every enzyme could be refolded, although the activity recovered varied (Table 1). This indicates that the mutations have only a slight effect on the initial folding of each subunit but have more influence on the dimerization process through subunit interface conformation, as well as other structural aspects which impact upon appropriate active site conformation. When comparing the two isoforms adGSTD3-3 and adGSTD4-4, in terms of changes in catalytic activity, the mutations affected the proteins in different ways for the equivalent residues, as shown in Table 2. The crystal structures show that all selected equivalent positions are located in the active site pocket suggesting that the whole electrostatic field in the active site pocket was disturbed by the mutations, which thereby altered catalytic parameters of the enzymes. Moreover, these residues are also located at the interface of the two active

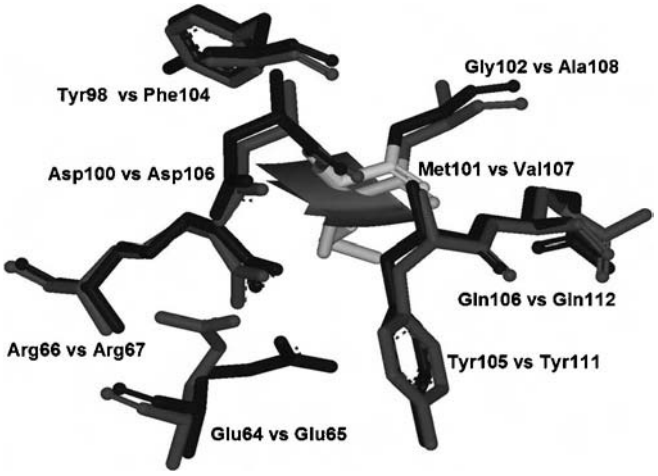


**Figure 7 In region 2 the amino acid milieu of adGSTD3-Met[101] and adGSTD4-Val[107]**

The dark grey represents adGSTD3-3 and medium grey is adGSTD4-4. The Figure was created using Accelrys DS ViewerPro 5.0.

site areas which provide different substrate-binding sites for GSH and the hydrophobic substrate. Therefore these positions would allow the residues to influence binding of both substrates as shown by the $K_m$ values.

The first sphere milieu of the equivalent positions, Met[101] of adGSTD3-3 and Val[107] of adGSTD4-4, consists of seven amino acids of which only two residues are different between the two isoforms, adGSTD3-3 Tyr[98] compared with adGSTD4-4 Phe[104] and adGSTD3-3 Gly[102] compared with adGSTD4-4 Ala[108] (Figure 7). However, the triple mutations which changed all three amino acids at these equivalent positions to the amino acid of the other isoform, showed that they had only a slight effect on the half-life. Steric interactions and van der Waals forces are important interactions for the stability of proteins [31,32]. The side chain size of the three amino acids at these equivalent positions had a major impact on subunit interface packing, with differences between the two splice forms, especially Met[101] and Gly[102] of adGSTD3-3 and Val[107] and Ala[108] of adGSTD4-4. Although the amino acids possess similar properties, the packing effects were great enough to alter the protein and enzyme properties.

From the conserved electrostatic interactions in region 1 to the hydrophobic area in region 2 of the subunit interface, every residue appears to contribute to either maintaining structure or subunit binding. The last area to be examined was the hydrophilic area in region 3 of the subunit interface, Asp[110] of adGSTD3-3 and Glu[116] of adGSTD4-4. Both mutations, D110A of adGSTD3-3 and G116A of adGSTD4-4, affected catalysis as shown by changes in both specific activity and kinetic constants. The equivalent residue in the human Alpha class A1-1 is Glu[104] whereas in the human Pi class GST it is a polar Ser[105]. In insects, the acidic residue appears to be conserved within the Delta class, however in the Epsilon class it is generally an aromatic amino acid and in the other insect classes, such as Sigma, Theta and Zeta, the residue is hydrophobic. This residue therefore appears to be conserved within a class and would contribute to class specific dimerization motifs. Additionally, in adGSTD4-4 the Glu[116] interacts with Arg[134] in a similar fashion to Glu[75] and Arg[96] in region 1 (Figure 8). That is, electrostatic interactions occur between the two residues within the same subunit as well as with the identical residues from the other subunit. So in adGSTD4-4 but not in adGSTD3-3 similar intra- and inter-subunit electrostatic interactions occur in both regions 1 and 3 of the subunit interface. In adGSTD3-3 the equivalent residue to Arg[134] is Asn[126] and so, because of the shorter side chains of the Asp[110] and the Asn[126], the distances preclude electrostatic interaction across the subunits.

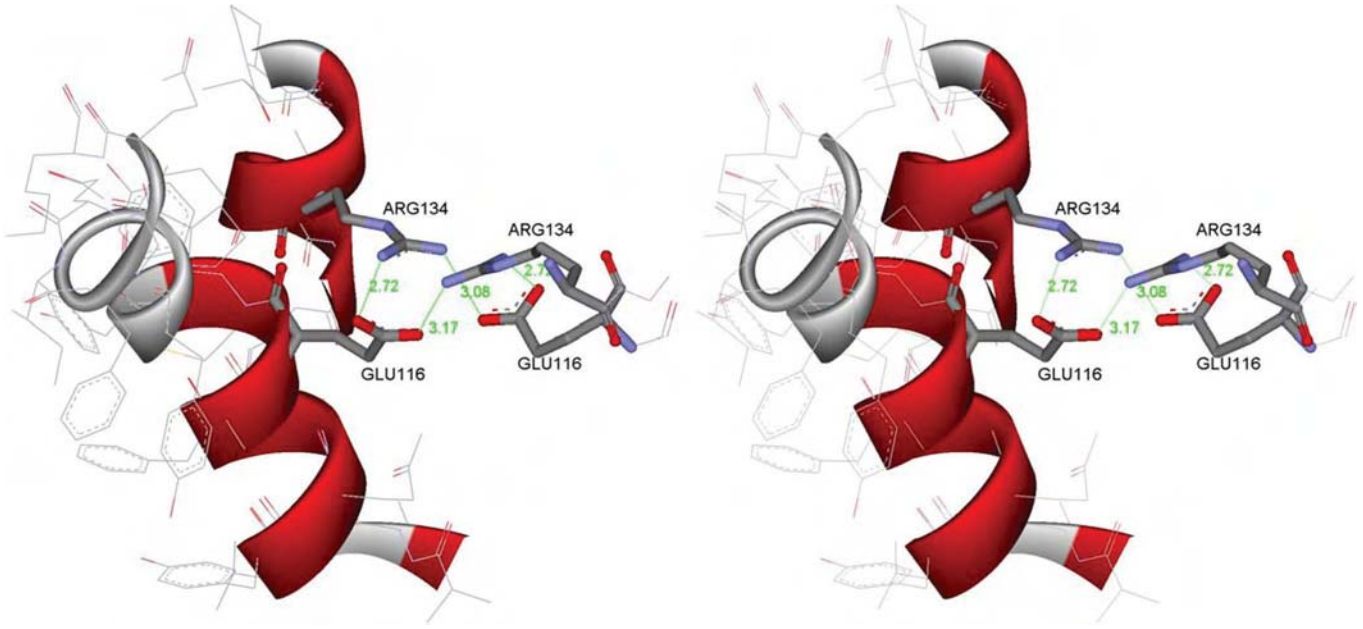


**Figure 8 The electrostatic interaction in region 3 of Glu[116] and Arg[134] in adGSTD4-4**

The two residues from each subunit are in proximity to interact electrostatically with each other as well as with the same residues from the other subunit. For the first subunit parts of $\alpha$-helices 4 and 5, containing Glu[116] and Arg[134] respectively, are shown. For clarity only Glu[116] and Arg[134] from the second subunit are shown. Distances between the charged atoms are shown in Å. The Figure was created using Accelrys DS ViewerPro 5.0.

In conclusion, the conserved electrostatic interactions between the charged residues from $\alpha$-helix 3 and $\alpha$-helix 4 show important roles for protein folding, stabilization and dimerization of the alternatively spliced enzymes. However, the subunit interface region with the most variation in amino acid residues at equivalent positions between adGSTD3-3 and adGSTD4-4 showed that although the mutations did not alter the overall protein folding, the enzyme properties were changed, especially the catalytic activity, thermal stability and subunit interface. Even highly conservative amino acid replacements changed the protein properties. The results suggest that even splicing products from the same gene may have specific features in the subunit interface area that would preclude heterodimerization.

This work was funded by the TRF (Thailand Research Fund). J. P. held a DPST (Development and Promotion of Science and Technology Talent) scholarship. J. W. was supported by a Royal Golden Jubilee scholarship.

## REFERENCES


1 Ketterer, B. (2001) A bird's eye view of the glutathione transferase field. Chem.-Biol. Interact. **138**, 27–42
2 Hayes, J. D., Flanagan, J. U. and Jowsey, I. R. (2005) Glutathione transferases. Annu. Rev. Pharmacol. Toxicol. **45**, 51–88
3 Luo, J.-K., Hornby, J. A. T., Wallace, L. A., Chen, J., Armstrong, R. N. and Dirr, H. W. (2002) Impact of domain interchange on conformational stability and equilibrium folding of chimeric class $\mu$ glutathione transferases. Protein Sci. **11**, 2208–2217
4 Hornby, J. A. T., Luo, J.-K., Stevens, J. M., Wallace, L. A., Kaplan, W., Armstrong, R. N. and Dirr, H. W. (2000) Equilibrium folding of dimeric class $\mu$ glutathione transferases involves a stable monomeric intermediate. Biochemistry **39**, 12336–12344
5 Luo, J.-K., Hornby, J. A. T., Armstrong, R. N. and Dirr, H. W. (2001) Equilibrium unfolding and enzyme kinetics of chimeric Mu class glutathione transferases. Chem.-Biol. Interact. **133**, 58–59
6 Sinning, I., Kleywegt, G. J., Cowan, S. W., Reinemer, P., Dirr, H. W., Huber, R., Gilliland, G. L., Armstrong, R. N., Ji, X., Board, P. G. et al. (1993) Structure determination and refinement of human Alpha class glutathione transferase A1-1, and a comparison with the Mu and Pi class enzymes. J. Mol. Biol. **232**, 192–212
7 Ji, X., Zhang, P., Armstrong, R. N. and Gilliland, G. L. (1992) The three-dimensional structure of a glutathione S-transferase from the Mu gene class: structural analysis of the binary complex of isoenzyme 3-3 and glutathione at 2.2 Å resolution. Biochemistry **31**, 10169–10184
8 Reinemer, P., Dirr, H. W., Ladenstein, R., Huber, R., Lo Bello, M., Federici, G. and Parker, M. W. (1992) Three-dimensional structure of class $\pi$ glutathione S-transferase from human placenta in complex with S-hexylglutathione at 2.8 Å resolution. J. Mol. Biol. **227**, 214–226
9 Hornby, J. A. T., Codreanu, S. G., Armstrong, R. N. and Dirr, H. W. (2002) Molecular recognition at the dimer interface of a class Mu glutathione transferase: role of a hydrophobic interaction motif in dimer stability and protein function. Biochemistry **41**, 14238–14247
10 Pongjaroenkit, S., Jirajaroenrat, K., Boonchauy, C., Chanama, U., Leetachewa, S., Prapanthadara, L. and Ketterman, A. J. (2001) Genomic organization and putative promotors of highly conserved glutathione S-transferases originating by alternative splicing in *Anopheles dirus*. Insect Biochem. Mol. Biol. **31**, 75–85
11 Chelvanayagam, G., Parker, M. W. and Board, P. G. (2001) Fly fishing for GSTs: a unified nomenclature for mammalian and insect glutathione transferases. Chem.-Biol. Interact. **133**, 256–260
12 Wongsantichon, J., Harnnoi, T. and Ketterman, A. J. (2003) A sensitive core region in the structure of glutathione S-transferases. Biochem. J. **373**, 759–765
13 Ranson, H., Collins, F. and Hemingway, J. (1998) The role of alternative mRNA splicing in generating heterogeneity within the *Anopheles gambiae* class I glutathione S-transferase family. Proc. Natl. Acad. Sci. U.S.A. **95**, 14284–14289
14 Jirajaroenrat, K., Pongjaroenkit, S., Krittanai, C., Prapanthadara, L. and Ketterman, A. J. (2001) Heterologous expression and characterization of alternatively spliced glutathione S-transferases from a single *Anopheles* gene. Insect Biochem. Mol. Biol. **31**, 867–875
15 Ketterman, A. J., Prommeenate, P., Boonchauy, C., Chanama, U., Leetachewa, S., Promtet, N. and Prapanthadara, L. (2001) Single amino acid changes outside the active site significantly affect activity of glutathione S-transferases. Insect Biochem. Mol. Biol. **31**, 65–74
16 Oakley, A. J., Harnnoi, T., Udomsinprasert, R., Jirajaroenrat, K., Ketterman, A. J. and Wilce, M. C. J. (2001) The crystal structures of glutathione S-transferases isozymes 1-3 and 1-4 from *Anopheles dirus* species B. Protein Sci. **10**, 2176–2185
17 Wongsantichon, J. and Ketterman, A. J. (2006) An intersubunit lock-and-key 'Clasp' motif in the dimer interface of Delta class glutathione transferase. Biochem. J. **394**, 135–144
18 Bradford, M. M. (1976) A rapid and sensitive method for the quantitation of microgram quantities of protein utilizing the principle of protein–dye binding. Anal. Biochem. **72**, 248–254
19 Prapanthadara, L., Koottathep, S., Promtet, N., Hemingway, J. and Ketterman, A. J. (1996) Purification and characterization of a major glutathione S-transferase from the mosquito *Anopheles dirus* (species B). Insect Biochem. Mol. Biol. **26**, 277–285
20 Udomsinprasert, R. and Ketterman, A. J. (2002) Expression and characterization of a novel class of glutathione S-transferase from *Anopheles dirus*. Insect Biochem. Mol. Biol. **32**, 425–433
21 Habig, W. H., Pabst, M. J. and Jakoby, W. B. (1974) Glutathione S-transferases: the first enzymatic step in mercapturic acid formation. J. Biol. Chem. **249**, 7130–7139
22 Vararattanavech, A. and Ketterman, A. (2003) Multiple roles of glutathione binding-site residues of glutathione S-transferase. Protein Pept. Lett. **10**, 441–448
23 Stenberg, G., Dragani, B., Cocco, R., Mannervik, B. and Aceto, A. (2000) A conserved 'hydrophobic staple motif' plays a crucial role in the refolding of human glutathione transferase P1-1. J. Biol. Chem. **275**, 10421–10428
24 Stevens, J. M., Hornby, J. A. T., Armstrong, R. N. and Dirr, H. W. (1998) Class Sigma glutathione transferase unfolds via a dimeric and a monomeric intermediate: impact of subunit interface on conformational stability in the superfamily. Biochemistry **37**, 15534–15541
25 Dirr, H. (2001) Folding and assembly of glutathione transferases. Chem.-Biol. Interact. **133**, 19–23
26 Sayed, Y., Wallace, L. A. and Dirr, H. W. (2000) The hydrophobic lock-and-key intersubunit motif of glutathione transferase A1-1: implications for catalysis, ligandin function and stability. FEBS Lett. **465**, 169–172
27 Sluis-Cremer, N., Naidoo, N. and Dirr, H. (1996) Class-Pi glutathione S-transferase is unable to regain its native conformation after oxidative inactivation by hydrogen peroxide. Eur. J. Biochem. **242**, 301–307
28 Sayed, Y., Hornby, J. A. T., Lopez, M. and Dirr, H. (2002) Thermodynamics of the ligandin function of human class Alpha glutathione transferase A1-1: energetics of organic anion ligand binding. Biochem. J. **363**, 341–346
29 Sluis-Cremer, N., Naidoo, N. N., Kaplan, K. H., Manoharan, T. H., Fahl, W. E. and Dirr, H. W. (1996) Determination of a binding site for a nonsubstrate ligand in mammalian cytosolic glutathione S-transferases by means of fluorescence-resonance energy transfer. Eur. J. Biochem. **241**, 484–488
30 Segel, I. H. (1993) Enzyme kinetics, Behavior and Analysis of Rapid Equilibrium and Steady State Enzyme Systems. John Wiley & Sons, New York
31 Otzen, D. E., Rheinnecker, M. and Fersht, A. R. (1995) Structural factors contributing to the hydrophobic effect: the partly exposed hydrophobic minicore in chymotrypsin inhibitor 2. Biochemistry **34**, 13051–13058
32 Xu, J., Baase, W. A., Baldwin, E. and Matthews, B. W. (1998) The response of T4 lysozyme to large-to-small substitutions within the core and its relation to the hydrophobic effect. Protein Sci. **7**, 158–177
33 Ding, Y., Ortelli, F., Rossiter, L. C., Hemingway, J. and Ranson, H. (2003) The *Anopheles gambiae* glutathione transferase supergene family: annotation, phylogeny and expression profiles. BMC Genomics **4**, 35–50


Received 24 April 2006/21 August 2006; accepted 29 August 2006
Published as BJ Immediate Publication 29 August 2006, doi:10.1042/BJ20060603

**Future Plans**

We will continue to perform structure function studies to increase our understanding of which amino acid residues affect enzyme specificity. We are also interested in determining the mechanism of how the elucidated amino acids contribute to the observed specificity.

**Publications**

We have published fourteen papers in the last three years for a total 2005 impact factor of 43.633. For the sake of simplicity we only present the three Biochemical Journal (2005 Impact Factor 4.224) papers published this year (2007; publications 1-3 in the list below) in this Final Annual Report. The complete reprints of all fourteen papers are included in the appendix.


1. Vararattanavech, A. and **Ketterman**, A.J. (2007) A functionally conserved basic residue in glutathione transferases interacts with the glycine moiety of glutathione and is pivotal for enzyme catalysis. *Biochem. J.* Immediate Publication **DOI (Digital Object Identifier): 10.1042/BJ20070422,** In press. (2005 Impact Factor 4.224)
2. Winayanuwattikun, P. and **Ketterman**, A.J. (2007) Glutamate 64, a newly identified residue of the functionally conserved electron-sharing network contributes to catalysis and structural integrity of glutathione transferases. *Biochem. J.* **402**, 339-348. (2005 Impact Factor 4.224)
3. Piromjitpong, J., Wongsantichon, J. and **Ketterman**, A.J. (2007) Differences in the subunit interface residues of alternatively spliced glutathione transferases affects catalytic and structural functions. *Biochem. J.* **401,** 635-644. (2005 Impact Factor 4.224)
4. Wongsantichon, J., Yuvaniyama, J. and **Ketterman**, A.J. (2006) Crystallization and preliminary X-ray crystallographic analysis of a highly stable mutant V107A of glutathione transferase from *Anopheles dirus* in complex with glutathione. *Acta Crys. F* **62**, 310-312. (No impact factor)
5. Laohavechvanich, P., Kangsadalampai, K., Tirawanchai, N. and **Ketterman**, A.J. (2006) Effect of different Thai traditional processing of various hot chili peppers on urethane-induced somatic mutation and recombination in *Drosophila melanogaster*: assessment of the role of glutathione transferase activity. *Food Chem. Toxicol.* **44**, 1348-1354. (2005 Impact Factor 2.047)
6. Charoensilp, G., Vararattanavech, A., Leelapat, P., Prapanthadara, L. and **Ketterman**, A.J. (2006) Characterization of *Anopheles dirus* glutathione transferase Epsilon 4. *ScienceAsia* **32**, 159-165. (No impact factor)
7. Wongsantichon, J. and **Ketterman**, A.J. (2006) An Intersubunit Lock-and-Key 'Clasp' Motif in the Dimer Interface of Delta Class Glutathione Transferase. *Biochem. J.* **394,** 135-144. (2005 Impact Factor 4.224)
8. Vararattanavech, A., Prommeenate, P. and **Ketterman**, A.J. (2006) The structural roles of a conserved small hydrophobic core in the active site and an ionic bridge in domain I of delta class glutathione transferase. *Biochem. J.* **393,** 89-95. (2005 Impact Factor 4.224)
9. Bogoyevitch, M.A., Barr, R.K., **Ketterman**, A.J. (2005) Peptide inhibitors of protein kinases – discovery, characterisation and use. *Biochim. Biophys. Acta - Proteins & Proteomics* **1754**, 79-99. (2005 Impact Factor 2.980)
10. Winayanuwattikun, P. and **Ketterman**, A.J. (2005) An electron-sharing network involved in the catalytic mechanism is functionally conserved in different glutathione transferase classes. *J. Biol. Chem.* **280**, 31776-31782. (2005 Impact Factor 5.854)
11. Wongsantichon, J. and **Ketterman**, A.J. (2005) [6] Alternative Splicing Of Glutathione S-Transferases. Edited by Helmut Sies and Lester Packer. **In** *Methods in Enzymology,* "Phase II: Conjugation Enzymes, Glutathione Transferases and Transport Systems". Vol. **401**, 100-116. Elsevier Inc., San Diego. (2005 Impact Factor 1.695)
12. Udomsinprasert, R., Pongjaroenkit, S., Wongsantichon, J., Oakley, A.J., Prapanthadara, L., Wilce, M.C.J. and **Ketterman**, A.J. (2005) Identification, characterization and structure of a new delta class glutathione transferase isoenzyme. *Biochem. J.* **388**, 763-771. (2005 Impact Factor 4.224)
13. Wongtrakul, J., Sramala, I., Prapanthadara, L. and **Ketterman**, A.J. (2005) Intra-subunit residue interactions from the protein surface to the active site of glutathione S-transferase AdGSTD3-3 impact on structure and enzyme properties. *Insect Biochem. Molec. Biol.* **35,** 197-205**.** (2005 Impact Factor 2.733)
14. Bogoyevitch, M.A., Boehm, I., Oakley, A., **Ketterman**, A.J. and Barr, R.K. (2004) Targeting the JNK MAPK cascade for inhibition: basic science and therapeutic potential. *Biochim. Biophys Acta* **1697**, 89-101. (2005 Impact Factor 2.980)

**Professional Invitations**
Within the last 3 years, I have been invited to join the Panel of Editorial Advisers for the *Biochemical Journal* (http://www.biochemj.org/bj/bjedavpanel.htm). I have also been a co-author on the top downloaded paper of BBA Proteins and Proteomics in 2005 (**Publications** Paper 14). I have been an invited speaker at the 17th FAOBMB Symposium/2nd IUBMB Special Meeting/7th S-IMBN Conference on "Genomics and Health in the 21st Century". 22-26 November 2004, Bangkok, Thailand. Session R: Protein Expression, Structure and Function. IL-C11 Structural studies on glutathione S-transferases from *Anopheles dirus*.

**Collaborations Domestic and International**
I have several working collaborations. One collaboration is with Dr. L. Prapanthadara at the Research Institute for Health Sciences, Chiangmai University. Dr. Prapanthadara is involved with the enzyme characterization studies and also in supplying my laboratory with *An. dirus* mosquitoes. I have two collaborations with my former PhD students who have now completed, Dr. Saengtong Pongjareankit and Dr. Jeerang Wongtrakul. Both have now returned to their universities, Maejo and Chiangmai University. Another collaboration within Thailand is with Dr. Jirundon Yuvaniyama at the Department of Biochemistry and Center for Excellence in Protein Structure and Function, Faculty of Science, Mahidol University. Dr. Yuvaniyama has been involved in helping us to obtain new GST structures. An overseas collaboration is with Dr. Marie A. Bogoyevitch in the Cell Signalling Laboratory, Department of Biochemistry, University of Western Australia. The collaboration with Dr. Bogoyevitch is investigating the GST interactions with the MAP kinase pathways. The second overseas collaboration is with Dr. Aaron J. Oakley in the Biological Chemistry Section of the Research School of Chemistry at the Australian National University. Dr. Oakley is a crystallographer and is currently crystallizing and elucidating the tertiary structure of the *An. dirus* recombinant GSTs that we are studying. We have also now formed a new collaboration with Assoc. Prof. Robert Robinson at the Institute of Molecular and Cell Biology, Proteos, Singapore. Dr. Robinson is also a crystallographer and is helping us to obtain new GST structures.

**Collaborations within Institute**
We have formed a scientific support network consisting of the following four ajarns and their respective groups (at this time this includes 30 people): Drs. G. Katzenmeier, C. Angsuthanasombat, A. Ketterman, and C. Krittanai.

**Problems**
There are no unusual problems.

**Comments and Suggestions**
It would be helpful to receive the next funding budget quickly.

# Appendix

Reprints of the fourteen papers published in the last three years.

# A functionally conserved basic residue in glutathione S-transferases interacts with the glycine moiety of glutathione and is pivotal for enzyme catalysis

Ardcharaporn VARARATTANAVECH and Albert J. KETTERMAN[1]

Institute of Molecular Biology and Genetics, Mahidol University, Salaya Campus, 25/25 Putthamonthol Road 4, Salaya, Nakon Pathom 73170, Thailand

The present study characterized conserved residues in a GST (glutathione S-transferase) in the active-site region that interacts with glutathione. This region of the active site is near the glycine moiety of glutathione and consists of a hydrogen bond network. In the GSTD (Delta class GST) studied, adGSTD4-4, the network consisted of $His^{38}$, $Met^{39}$, $Asn^{47}$, $Gln^{49}$, $His^{50}$ and $Cys^{51}$. In addition to contributing to glutathione binding, this region also had major effects on enzyme catalysis, as shown by changes in kinetic parameters and substrate specific activity. The results also suggest that the electron distribution of this network plays a role in stabilization of the ionized thiol of glutathione as well as impacting on the catalytic rate-limiting step. This area constitutes a second glutathione active site network involved in glutathione ionization distinct from a network previously observed interacting with the glutamyl end of glutathione. This second network also appears to be functionally conserved in GSTs. In the present study, $His^{50}$ is the key basic residue stabilized by this network as shown by up to a 300-fold decrease in $k_{cat}$ and 5200-fold decrease in $k_{cat}/K_m$ for glutathione. Although these network residues have a minor role in structural integrity, the replaced residues induced changes in active site topography as well as generating positive co-operativity towards glutathione. Moreover, this network at the glycine moiety of GSH (glutathione) also contributed to the 'base-assisted deprotonation model' for GSH ionization. Taken together, the results indicate a critical role for the functionally conserved basic residue $His^{50}$ and this hydrogen bond network in the active site.

Key words: base-assisted deprotonation model, conserved active-site residue, Delta class GST, enzyme catalysis, glutathione S-transferase (GST), glycine moiety of glutathione (GSH).

## INTRODUCTION

GSTs (glutathione S-transferases; EC 2.5.1.18) are intracellular proteins, which are widely distributed in nature, being found in most aerobic eukaryotes and prokaryotes [1,2]. GSTs are polymorphic with most organisms possessing a genetic capacity to encode multiple isoforms of various classes [3,4]. The enzymes are an integral part of the phase II detoxification mechanism being involved in xenobiotic metabolism as well as protection against peroxide damage. GSTs catalyse reactions with a very broad range of structurally diverse electrophilic substrates (e.g. alkylhalides, arylhalides, lactones, epoxides, quinones, esters and activated alkenes) [4–6]. This enzyme family therefore displays a wide range of catalytic functions while retaining a high specificity towards the thiol substrate glutathione (GSH). The GSH conjugation by GST increases the solubility of the target molecule, thus facilitating the excretion of the molecule from the organism.

All cytosolic GSTs have very similar three-dimensional structures and the active site pocket is very similar in the G-site (GSH-binding site) [7–9]. The N-terminal domain of GST adopts a $\beta\alpha\beta\alpha\beta\beta\alpha$ topology that contributes most of the contacts to GSH and is called the G-site. The crystal structures of GSTs show that most of the active site residues involved in the binding and activation of GSH are found within the N-terminus; hence this region of the protein is therefore highly conserved between GSTs [7,8,10]. The C-terminal domain is all $\alpha$-helical providing some of the contacts to the hydrophobic binding site that lies adjacent to the G-site.

Substrate conjugation of electrophilic xenobiotics involves its nucleophilic attack at the ionized thiol of GSH in the active site. A conserved tyrosine (for Alpha, Mu and Pi classes) or serine (for Theta and Delta classes) residue within hydrogen-bonding distance of the thiol of GSH has been shown to be of primary importance in facilitating GSH deprotonation as well as stabilization of the ionized GSH by hydrogen-bonding [10–14]. In addition, conserved residues that interact directly with the glutamyl moiety of GSH, for example $Ser^{65}$, $Arg^{66}$ and $Ile^{52}$ in GSTD (Delta class GST) have also been implicated in critical roles in the catalytic mechanism, involvement in GSH binding, GSH thiol ionization, as well as structural integrity [15–17]. Therefore the residues interacting with the other end of GSH, the glycine moiety ($His^{38}$, $Met^{39}$, $Asn^{47}$, $Gln^{49}$, $His^{50}$ and $Cys^{51}$) were of interest (Figure 1) [18]. $His^{38}$ and $His^{50}$ interact directly with the glycine carboxylic group of GSH [19]. Both histidines appear to be assisted or stabilized by dipole–dipole interaction with $Met^{39}$. Moreover, a hydrogen bond network in the G-site near the glycine moiety of GSH, involving several residues ($His^{50}$, $Asn^{47}$, $Gln^{49}$ and $Cys^{51}$) and GSH, is proposed to be essential to electron distribution for enzyme catalysis. To investigate the roles of these residues, mutagenesis studies were performed and the engineered enzymes characterized by kinetic constants, substrate specific activity, $pK_a$ determination and rate-limiting step determination in addition to physical properties.

Abbreviations used: CDNB, 1-chloro-2,4-dinitrobenzene; DCNB, 1,2-dichloro-4-nitrobenzene; EA, ethacrynic acid; FDNB, 1-fluoro-2,4-dinitrobenzene; G-site, GSH (glutathione)-binding site; GST, glutathione S-transferase; GSTD, Delta class GST; hGSTP1-1, human GSTP1-1; PNBC, *p*-nitrobenzyl chloride; PNPBr, *p*-nitrophenethyl bromide; ZmGST1, *Zea mays* (maize) GST1.

[1] To whom correspondence should be addressed (email albertketterman@yahoo.com).

COLOUR

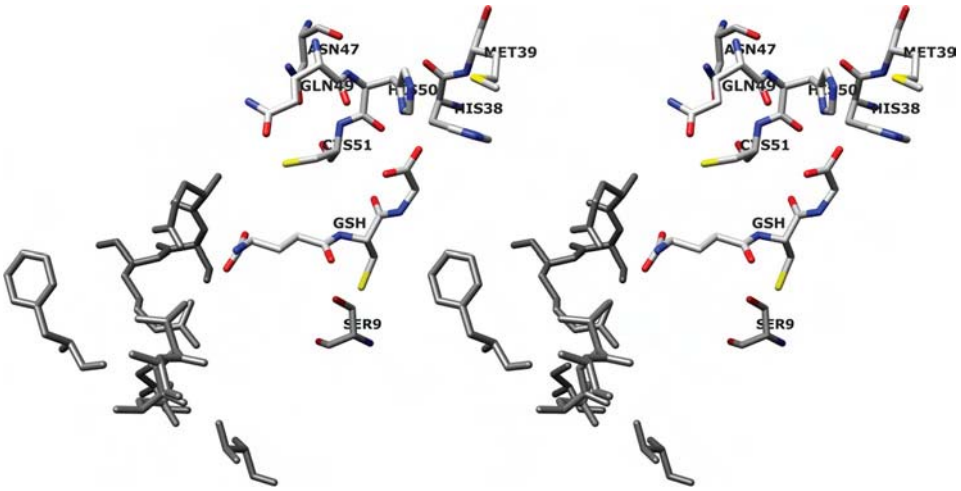


**Figure 1 Stereoview of conserved G-site residues that directly interact with the glycine moiety of GSH and generate a hydrogen bond network**

His[38] and His[50] interact directly with the glycine carboxylic group of GSH and are assisted or stabilized by dipole–dipole interaction with Met[39]. A hydrogen bond network in the G-site is formed by several residues (His[50], Asn[47], Gln[49] and Cys[51]) and GSH. The previously identified electron-sharing network at the glutamyl end of GSH is shown in grey [16]. The image was produced using the UCSF Chimera package from the Resource for Biocomputing, Visualization, and Informatics at the University of California, San Francisco, CA, U.S.A. (http://www.cgl.ucsf.edu/chimera) (supported by National Institutes of Health grant P41 RR-01081) [18].

## MATERIALS AND METHODS

### Site directed mutagenesis

The engineered enzymes were generated using Stratagene's QuikChange® site-directed mutagenesis protocol. The primers used were designed based on the sequence of the *adGSTD4* wild-type gene (GenBank® accession number AF273040). Full-length DNA sequencing in both directions was performed to confirm the engineered clones.

### Protein expression and purification

After transformation of the engineered plasmids into *Escherichia coli* BL21(DE3)pLysS, protein expression was performed. The recombinant adGSTD4-4 engineered enzymes and wild-type were purified either by glutathione affinity chromatography according to the manufacturer's instructions (Amersham Biosciences) or by cation exchanger (SP-XL) followed by hydrophobic interaction chromatography (phenyl-Sepharose) as described previously [19]. The purified enzymes (in 50 mM potassium phosphate, pH 6.5) were stored in 50 % (v/v) glycerol at −20 °C until used. The concentrations of the proteins were determined by Bio-Rad protein reagent (Bio-Rad) by using BSA as the standard protein and the purity of the proteins was observed by SDS/PAGE.

### Kinetic parameters determination

Kinetic experiments were performed as previously described [20]. Kinetic constants were determined by varying the CDNB (1-chloro-2,4-dinitrobenzene) concentration (0.031–3.0 mM) while GSH was held constant at a saturating concentration and by varying GSH concentrations (0.25–20 mM) at a saturating concentration of CDNB. The standard GST assay was performed using 3 mM CDNB and 10 mM GSH for adGSTD4-4 wild-type. The rate of conjugation between GSH and CDNB was monitored by continuously measuring change in absorbance at 340 nm for 1 min using a SpectraMax 250 at 25–27 °C. A molar absorption coefficient ($\varepsilon$) of 9.6 $mM^{-1} \cdot cm^{-1}$ was used to convert the absorbance to moles [21]. Steady-state kinetics followed Michaelis–Menten kinetics except where stated. With evidence of co-operativity upon GSH binding, demonstrated by a sigmoidal curve instead of a hyperbolic curve on a Michaelis–Menten plot, a Hill equation (eqn 1) was used to fit the experimental kinetic data on the plot. $K_{0.5}$ is the substrate concentration that gives the rate of reaction at half of $V_{max}$, similar to the $K_m$ value for non-co-operative binding ($h = 1$).

$$Y = V/V_{max} = [S]^h/(K_{0.5} + [S]^h) \quad (1)$$

$$\log[Y/(1-Y)] = h \log[S] - \log K_{0.5} \quad (2)$$

A sigmoidal Hill equation was practically transformed into a linear rate equation (eqn 2), where $Y$ is the fractional saturation; $h$ is the Hill coefficient; and $K_{0.5}$ is an averaged binding constant at $Y = 0.5$. A Hill plot, a plot between $\log[Y/(1–Y)]$ and $\log[S]$, was employed to determine the degree of co-operativity by the slope of the plot that yields the Hill coefficient ($h$) [22]. Catalytic constant ($k_{cat}$) and the catalytic efficiency ($k_{cat}/K_m$) were calculated on an active site basis using the subunit molecular mass of each enzyme. Maximal velocity ($V_{max}$) and Michaelis constant ($K_m$) were determined by nonlinear regression software analysis (GraphPad Prism version 5.00 for Windows; GraphPad Software, San Diego, CA, U.S.A.; http://www.graphpad.com). One-way ANOVA with Dunnett's multiple comparison post test was performed with wild-type as control using GraphPad Prism 5.

### Specific activity determination

The specific activities towards several GST substrates were determined as previously described [23]. All measurements were performed at 25–27 °C in 0.1 M potassium phosphate buffer (pH 6.5 or 7.5). The GST activities were measured with glutathione and five hydrophobic substrates: CDNB, DCNB (1,2-dichloro-4-nitrobenzene), EA (ethacrynic acid), PNPBr (*p*-nitrophenethyl bromide) and PNBC (*p*-nitrobenzyl chloride). Specific activities were calculated according to the molar absorption coefficient for each substrate [21].

### pH dependence of kinetic parameters

The pH dependence of $k_{cat}/K_m^{CDNB}$ was obtained by performing kinetic measurements in the following buffers: 0.1 M sodium

**Table 1 Steady-state kinetic constants using GSH and CDNB as GST substrates**

The units of $V_{max}$, $k_{cat}$, $K_m$ and $k_{cat}/K_m$ are $\mu$mol · min$^{-1}$ · mg of protein$^{-1}$, s$^{-1}$, mM and s$^{-1}$ · mM$^{-1}$ respectively. *These engineered GSTs showed positive co-operativity upon GSH binding with Hill coefficient ($h$) shown. The value shown is $K_{0.5}$, obtained from the Hill equation, which is the substrate concentration that gives the rate of reaction at half of $V_{max}$ [22]. [a]Some of these values have been previously reported and are shown for purposes of comparison [19,20]. One-way ANOVA with Dunnett's multiple comparison test was performed with wild-type as control; statistical significance is shown by † for $P < 0.05$, ‡ for $P < 0.01$ and § for $P < 0.001$.

| | | | CDNB | | GSH | | |
|---|---|---|---|---|---|---|---|
| Enzyme | $V_{max}$ | $k_{cat}$ | $K_m$ | $k_{cat}/K_m$ | $K_m$ | $k_{cat}/K_m$ | $h$ |
| Wild-type[a] | 62.45 ± 1.24 | 26.13 | 0.50 ± 0.02 | 51.84 | 0.50 ± 0.10 | 52.06 | 0.91 ± 0.02 |
| H38A[a] | 36.4 ± 1.12§ | 15.26 | 1.25 ± 0.12§ | 12.21 | 15.8 ± 1.19§ | 0.97 | – |
| H38E[a] | 14.91 ± 0.44§ | 6.23 | 0.92 ± 0.11§ | 6.76 | 8.32 ± 0.22*§ | 0.74 | 1.83 ± 0.01§ |
| H38F[a] | 9.71 ± 0.43§ | 4.06 | 0.98 ± 0.09§ | 4.14 | 35.26 ± 0.86§ | 0.12 | – |
| H38D | 4.61 ± 0.12§ | 1.93 | 0.71 ± 0.01† | 2.71 | 15.90 ± 0.21§ | 0.12 | – |
| H38K | 5.54 ± 0.12§ | 2.32 | 0.71 ± 0.08† | 3.27 | 23.50 ± 1.21§ | 0.10 | – |
| M39A | 25.56 ± 0.96§ | 10.70 | 0.79 ± 0.06§ | 13.50 | 6.32 ± 0.34*§ | 1.69 | 1.72 ± 0.12§ |
| M39F | 38.56 ± 1.72§ | 16.14 | 0.50 ± 0.02 | 32.22 | 2.18 ± 0.09† | 5.75 | – |
| N47A | 0.225 ± 0.003§ | 0.09 | 0.67 ± 0.06 | 0.13 | 11.50 ± 0.51§ | 0.01 | – |
| Q49A | 43.28 ± 0.96§ | 18.11 | 0.74 ± 0.06‡ | 24.47 | 5.58 ± 0.46*§ | 3.24 | 1.64 ± 0.04§ |
| Q49E | 49.75 ± 1.36§ | 20.82 | 0.49 ± 0.05 | 42.49 | 2.87 ± 0.09*§ | 7.26 | 1.51 ± 0.03§ |
| H50A[a] | 6.46 ± 0.26§ | 2.70 | 1.10 ± 0.15§ | 2.45 | 7.34 ± 0.21§ | 0.37 | – |
| H50E[a] | 0.21 ± 0.01§ | 0.09 | 0.81 ± 0.04§ | 0.11 | 12.34 ± 0.36§ | 0.01 | – |
| H50Y[a] | 0.87 ± 0.02§ | 0.36 | 0.83 ± 0.06§ | 0.43 | 12.57 ± 0.73§ | 0.03 | – |
| H50K | 8.14 ± 0.03§ | 3.40 | 0.69 ± 0.06† | 4.95 | 6.77 ± 0.27*§ | 0.45 | 1.54 ± 0.06§ |
| H50F | 1.44 ± 0.03§ | 0.60 | 0.76 ± 0.01‡ | 0.79 | 6.43 ± 0.38§ | 0.09 | – |
| C51A | 19.64 ± 0.65§ | 8.22 | 0.82 ± 0.04§ | 10.01 | 6.40 ± 0.12*§ | 1.28 | 1.57 ± 0.08§ |
| C51D | 2.16 ± 0.07§ | 0.91 | 1.30 ± 0.08§ | 0.7 | 16.94 ± 0.69*§ | 0.05 | 1.40 ± 0.03§ |

acetate buffers (from pH 5.0 to 5.5) and 0.1 M potassium phosphate buffer (from pH 6.0 to 8.5). Increments of pH were 0.5 and control experiments showed no discontinuities from buffer types. The p$K_a$ values of bound GSH were obtained by fitting the data to the equation $y = y^{lim}/(1 + 10^{pKa-pH})$ as previously described [13]. The program GraphPad Prism 5 was used for nonlinear fit of the data to the sigmoidal dose–response (variable slope) equation.

### Fluoride/chloride leaving group substitution

A diagnostic test in evaluating the rate-limiting step in nucleophilic aromatic substitution reactions is the effect of different leaving groups on kinetic parameters [13]. The second order kinetic constants at pH 6.5 for the spontaneous reaction of GSH with CDNB and FDNB (1-fluoro-2,4-dinitrobenzene) were determined by kinetic measurement by using CDNB or FDNB as co-substrate as previously described [24]. The ratios of the catalytic constants ($k_{cat}^{FDNB}/k_{cat}^{CDNB}$) were determined.

### Effect of viscosity on the kinetic parameters

The dependence of the steady-state kinetic parameters on relative viscosity was observed by performing kinetics measurements in the presence of varying glycerol concentrations. The range of relative viscosities ($\eta/\eta^0$) was between 1.53 and 4.43. The slope of the plots for relative catalytic constant ($k_{cat}^0/k_{cat}$) versus relative viscosity ($\eta/\eta^0$) was determined. Viscosity values ($\eta$) at 25 °C were calculated as described previously [25].

### Thermal stability assay

The enzymes at 0.1 mg/ml in 0.1 M phosphate buffer (pH 6.5) containing 1 mM EDTA and 5 mM dithiothreitol were incubated at 45 °C for various times and then activity was measured in the standard GST assay. The data were plotted as log percentage of remaining activity versus pre-incubation time. The half-life ($t_{½}$) of the enzyme at 45 °C was calculated from the slope of the plot using the equations: Slope $= k/2.3$, $k = 0.693/t_{½}$.

### Intrinsic fluorescence measurement

There are two tryptophan residues in each monomer of adGSTD4-4: Trp$^{64}$ and Trp$^{191}$. The intrinsic fluorescence from Trp$^{64}$, which is exposed to solvent at the base of the G-site, can be used to monitor the active site conformation indirectly. The intrinsic fluorescence of adGSTD4-4 was measured in a single-photon counting spectrofluorimeter. Excitation was at 295 nm and emission was scanned from 300 to 450 nm. In these experiments, a number of samples containing 0.1 mg/ml GST in 0.1 M potassium phosphate buffer (pH 6.5) were prepared similarly for the wild-type and engineered enzymes. The wavelength that gives the maximum fluorescence intensity ($\lambda_{max}$) and fluorescence intensity at $\lambda_{max}$ were observed. The experimental data was corrected both for dilution and for inner filter effects.

## RESULTS

### Enzymatic characterization

Michaelis–Menten analysis was performed using nonlinear regression to determine steady-state kinetic constants (Table 1). The kinetic constants showed the residue changes of His$^{38}$, His$^{50}$, Met$^{39}$, Asn$^{47}$, Cys$^{51}$ and Gln$^{49}$ impacted upon catalysis. The engineered G-site residue enzymes showed only small changes in $K_m^{CDNB}$, whereas remarkably lower affinities towards GSH were shown (greater $K_m^{GSH}$) compared with wild-type. Positive co-operativity for GSH binding was observed for several engineered enzymes that displayed deviation of steady-state kinetics from a Michaelis–Menten hyperbolic to a sigmoidal curve response. The extent of positive co-operativity is shown by Hill coefficients ($h$) ranging from 1 (no co-operativity) to 2 (full co-operativity) for a dimeric enzyme with two active sites. Positive co-operativity was observed for H38E, M39A, H50K, C51A, C51D, Q49A and GA49E as determined by Hill coefficients ranging from 1.40 to 1.83, suggesting that the changed residues altered the movement of $\alpha$2-helix and its flanking region to influence the induced-fit mechanism.

**Table 2 Substrate-specific activity of the engineered enzymes compared to the wild-type**

The substrates used were 3 mM CDNB, 1 mM DCNB, 0.1 mM PNPBr, 0.1 mM PNBC and 0.2 mM EA. The reactions were performed at a constant GSH concentration (appropriate for each enzyme). [a]Some of these values have been previously reported and are shown for purposes of comparison [19,20]. One-way ANOVA with Dunnett's multiple comparison test was performed with wild-type as control; statistical significance is shown by † for $P < 0.05$, ‡ for $P < 0.01$ and § for $P < 0.001$.

| | Specific activity ($\mu$mol · min$^{-1}$ · mg$^{-1}$) | | | | |
|---|---|---|---|---|---|
| Enzyme | CDNB | DCNB | EA | PNPBr | PNBC |
| Wild-type[a] | 52.50 ± 0.52 | 0.035 ± 0.006 | 0.286 ± 0.062 | 0.074 ± 0.012 | 0.064 ± 0.002 |
| H38A[a] | 21.70 ± 0.20§ | 0.037 ± 0.001 | 0.146 ± 0.016§ | 0.040 ± 0.004§ | 0.013 ± 0.002§ |
| H38E[a] | 11.21 ± 0.24§ | < 0.001 | 0.191 ± 0.026§ | < 0.008 | < 0.005 |
| H38F[a] | 3.76 ± 0.09§ | < 0.001 | 0.230 ± 0.019† | < 0.005 | < 0.003 |
| H38D | 2.33 ± 0.07§ | < 0.001 | 0.111 ± 0.011§ | < 0.001 | < 0.003 |
| H38K | 2.02 ± 0.07§ | < 0.001 | 0.165 ± 0.007§ | < 0.003 | < 0.002 |
| M39A | 18.84 ± 0.66§ | 0.012 ± 0.001§ | 0.183 ± 0.011§ | < 0.005 | < 0.003 |
| M39F | 28.67 ± 0.71§ | 0.043 ± 0.002† | 0.166 ± 0.010§ | 0.029 ± 0.008§ | 0.065 ± 0.009 |
| N47A | 0.13 ± 0.01§ | < 0.001 | 0.079 ± 0.001§ | < 0.001 | < 0.001 |
| Q49A | 33.36 ± 0.92§ | 0.023 ± 0.002‡ | 0.244 ± 0.012 | 0.050 ± 0.002§ | 0.044 ± 0.001‡ |
| Q49E | 41.76 ± 0.60§ | 0.032 ± 0.001 | 0.244 ± 0.020 | 0.020 ± 0.001§ | 0.048 ± 0.003‡ |
| H50A[a] | 3.80 ± 0.10§ | 0.015 ± 0.007§ | 0.146 ± 0.050§ | 0.012 ± 0.002§ | 0.016 ± 0.007§ |
| H50E[a] | 0.15 ± 0.01§ | < 0.001 | 0.026 ± 0.004§ | < 0.005 | < 0.005 |
| H50Y[a] | 0.47 ± 0.01§ | < 0.001 | 0.064 ± 0.008§ | < 0.008 | < 0.005 |
| H50K | 6.28 ± 0.04§ | 0.007 ± 0.001§ | 0.053 ± 0.020§ | < 0.007 | < 0.004 |
| H50F | 0.93 ± 0.03§ | < 0.001 | 0.077 ± 0.005§ | < 0.001 | < 0.001 |
| C51A | 15.44 ± 0.58§ | 0.009 ± 0.001§ | 0.046 ± 0.001§ | 0.019 ± 0.001§ | < 0.001 |
| C51D | 1.24 ± 0.03§ | < 0.001 | 0.080 ± 0.004§ | < 0.002 | < 0.001 |

Although Met[39] interacts directly with GSH interacting residues, His[38] and His[50], the contribution to catalytic function is through the effect on GSH binding. The results suggest that the effect is mostly through a packing rearrangement that includes any perturbation of the orientation of His[38] or His[50]. Rearrangement of active site residues is elicited by M39A to accommodate the decreased volume as well as the lack of dipole–dipole interaction with the histidines. This condition also appears to engender flexibility to this region, which is shown by positive co-operativity for GSH binding with a Hill coefficient of 1.72 ± 0.12 (Table 1).

The GSH interaction was decreased for all His[38] engineered enzymes as shown by an increase in $K_m^{GSH}$ of 17–71-fold. In addition, positive co-operativity for GSH was observed for H38E with a Hill coefficient ($h$) of 1.83 ± 0.01.

There is a hydrogen bond network in the GST active site that is adjacent to the GSH glycine moiety. This network is formed by several residues, Asn[47], Gln[49] and Cys[51], as well as His[50], with the latter directly interacting with GSH. His[50] replacements not only decreased binding affinity to GSH (ranging from 13- to 25-fold) but also impacted upon catalytic rates as shown by $k_{cat}$ values that decreased from 13 to 0.3 % of the wild-type enzyme $k_{cat}$ values. The N47A change displayed several large effects on the enzyme, one on enzyme catalysis with the enzyme having only 0.3 % $k_{cat}$ of the wild-type, and another on GSH binding with a 23-fold increase in $K_m^{GSH}$. Gln[49] and Cys[51] interaction is through their main-chain nitrogens and oxygens. Changes in these residues showed intermediate effects on catalysis except for C51D, which had a $k_{cat}$ only 3.5 % of wild-type. However, the changes in these residues all showed a major impact on GSH binding with increased $K_m^{GSH}$ values from 6- to 34-fold. The results suggest that a packing rearrangement occurred. This rearrangement also enabled subunit–subunit communication as shown by the observed positive co-operativity upon GSH binding (Table 1).

Substrate specific activity was affected for all the engineered enzymes to varying degrees (Table 2). For example, most of the enzymes exhibited less effect on activity for EA. This suggests that the binding mode and the orientation of this substrate are different from the other substrates. Both GSH and hydrophobic substrate-binding sites are located in the same active site pocket of GSTs, therefore it is not surprising that changes in the G-site residues can perturb the hydrophobic substrate site.

It has been proposed that many steps occur in the GST catalytic mechanism including GSH ionization through thiol deprotonation, substrate conjugation by nucleophilic attack of the thiolate at the electrophilic centre, product formation and product release from the active site [13,26–28]. The overall velocity of the enzyme-catalysed reaction is affected by most of the engineered residues, although to different extents. Therefore several steps in the catalytic pathway were studied to determine the roles of the engineered residues.

### pH dependence of kinetic constants

The p$K_a$ values of ionized GSH (enzyme-bound GSH) were calculated from plots of $k_{cat}/K_m^{CDNB}$ versus pH for the wild-type and engineered enzymes (Table 3; Figure 2). The apparent p$K_a$ for wild-type is approx. 6.0. The p$K_a$ values of ionized GSH in the engineered enzymes varied, with the greatest effect shown by H50A which increased it by almost 1 pH unit. GSH ionization is considered to be an important step in the catalytic mechanism of GST that generates the thiolate anion (intermediate deprotonated form of GSH) for conjugation with the electrophilic substrate. This kinetically relevant ionization of GSH has been shown to be reflected in pH dependence for $k_{cat}/K_m^{CDNB}$ [13]. Several reports have shown that residues located near the cysteine thiol and glutamyl $\alpha$-carboxylate of GSH contribute to promoting and stabilizing the anionic glutathione thiol group [13,27–31]. However, this is the first report of involvement of the GSH glycine moiety in GSH ionization.

### Meisenheimer complex formation

Meisenheimer complex or $\sigma$-complex intermediate, is generated during a nucleophilic aromatic substitution reaction. Leaving group effects on enzyme catalysis can be used to determine

**Table 3 The p$K_a$ value of ionized GSH in the active site of wild-type and engineered enzymes**

The effect of pH on $k_{cat}/k_m^{CDNB}$ was obtained by measuring kinetic constants using various pH buffers of 0.1 M sodium acetate buffers (from pH 5.0 to 5.5) and 0.1 M potassium phosphate buffer (from pH 6.0 to 8.5). The p$K_a$ values of ionized GSH (GSH-bound enzyme) were determined. n.d., Not determined (low activity precluded measurement). One-way ANOVA with Dunnett's multiple comparison test was performed with wild-type as control; statistical significance is shown by § for $P < 0.001$. See Figure 2 for a plot of the experimental data.

| Enzyme | p$K_a$ (ionized GSH) |
|---|---|
| Wild-type | 6.00 ± 0.05 |
| H38A | 6.10 ± 0.02 |
| M39A | 6.52 ± 0.05§ |
| N47A | n.d. |
| Q49A | 6.23 ± 0.05§ |
| H50A | 6.92 ± 0.06§ |
| C51A | 6.22 ± 0.03§ |
| C51D | 6.42 ± 0.03§ |

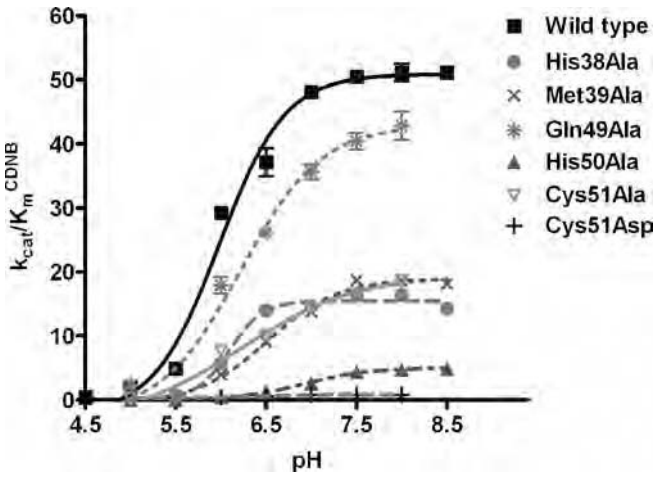


**Figure 2 Plot of the data to determine the p$K_a$ value of ionized GSH in the active site of wild-type and engineered enzymes**

The effect of pH on $k_{cat}/k_m^{CDNB}$ was obtained by measuring kinetic constants using various pH buffers of 0.1 M sodium acetate buffers (from pH 5.0 to 5.5) and 0.1 M potassium phosphate buffer (from pH 6.0 to 8.5). The p$K_a$ values of ionized GSH (GSH-bound enzyme) were determined (see Table 3). The results are presented as means ± S.D. from at least three independent experiments.

whether the rate-limiting step of the reaction is $\sigma$-complex formation. The substitution of a more electronegative leaving group concomitant with an increase in the rate constant of the spontaneous reaction with glutathione is a signal that the $\sigma$-complex formation is a rate-limiting step [13]. Therefore the influence on the catalytic constant of the chlorine leaving group of CDNB replaced with fluorine was examined (Table 4).

Although the wild-type enzyme was insensitive, several of the engineered enzymes demonstrated sensitivity to the halogen leaving group, particularly H50A, C51D and D47A, with increased ratio values of 19-, 27- and 18-fold respectively. The catalytic efficiency ($k_{cat}/K_m$) of the engineered enzymes showed a different sensitivity to the nature of the leaving group, suggesting that an alteration of the relative catalytic-centre activity is a consequence of changes in the rate of $\sigma$-complex formation rather than changes in binding affinity towards the different substrate leaving groups. The results suggest that the process of $\sigma$-complex intermediate formation is affected by the disruption of the hydrogen bond network to GSH which affected the overall velocity of the enzyme-catalysed reaction. It is possible that the residue changes caused incorrect orientation of the GSH thiol or of the His[50] side chain, which then disturbs the conjugation process of the thiolate anion with the electrophilic substrate. Additionally, the results strongly support that the hydrogen bond network contributes to both the GSH ionization process and $\sigma$-complex intermediate formation. This contribution appears to stabilize the His[50] residue as shown by the changes in p$K_a$ and the greater effect of the leaving group on the catalytic constants of C51D but not C51D.

**Table 4 Effect of fluoride/chloride leaving group substitution on the rate of catalysis**

The ratio of catalytic rates for the conjugation reaction catalysed by wild-type and engineered GSTs using GSH and CDNB or FDNB as co-substrates. One-way ANOVA with Dunnett's multiple comparison test was performed with wild-type as control; statistical significance is shown by † for $P < 0.05$, ‡ for $P < 0.01$ and § for $P < 0.001$.

| | Leaving group effect | |
|---|---|---|
| Enzyme | $k_{cat}^{FDNB}/k_{cat}^{CDNB}$ | $(k_{cat}/K_m)^{FDNB}/(k_{cat}/K_m)^{CDNB}$ |
| Wild-type | 1.76 ± 0.01 | 20.59 ± 1.02 |
| H38A | 3.11 ± 0.21 | 14.12 ± 0.84† |
| M39A | 8.29 ± 0.95§ | 32.45 ± 3.72§ |
| N47A | 18.09 ± 0.90§ | 29.65 ± 1.32‡ |
| Q49A | 2.63 ± 0.08 | 26.29 ± 1.77† |
| Q49E | 1.50 ± 0.08 | 24.95 ± 1.21 |
| H50A | 18.57 ± 0.41§ | 16.55 ± 1.59 |
| C51A | 2.93 ± 0.05 | 30.31 ± 2.85§ |
| C51D | 26.75 ± 0.99§ | 44.71 ± 4.15§ |

**Table 5 Viscosity effect on kinetic constants and free energy changes of wild-type and engineered enzymes**

The effect of viscosity on kinetic constants was assayed by using 0.1 M potassium phosphate buffer (pH 6.5) with various glycerol concentrations. The slope of a reciprocal plot of the relative catalytic constant ($k_{cat}^0/k_{cat}$) versus relative viscosity ($\eta/\eta^0$) was determined. n.d., Not determined (low activity precluded measurement); $\Delta\Delta G$ (the difference in the free energy changes for the formation of the transition states in the wild-type and engineered enzymes) is calculated from the equation: $\Delta\Delta G = -RT\ln(k_{cat}/K_m^{CDNB})_{engineered}/(k_{cat}/K_m^{CDNB})_{wild-type}$. One-way ANOVA with Dunnett's multiple comparison test was performed with wild-type as control; statistical significance is shown by § for $P < 0.001$.

| Enzyme | Slope | $\Delta\Delta G$ (kJ/mol) |
|---|---|---|
| Wild-type | 0.959 ± 0.036 | – |
| H38A | 0.485 ± 0.019§ | 3.58 ± 0.033 |
| M39A | 0.430 ± 0.031§ | 3.33 ± 0.132 |
| N47A | n.d. | 14.8 ± 0.222 |
| Q49A | 0.797 ± 0.036§ | 1.86 ± 0.105 |
| H50A | 0.005 ± 0.001§ | 7.56 ± 0.095 |
| C51A | 1.11 ± 0.010§ | 4.08 ± 0.125 |
| C51D | 0.051 ± 0.007§ | 10.7 ± 0.201 |

## Viscosity effect on kinetic constants

The viscosity effect was studied to determine if the rate-limiting step of the reaction is physical or chemical. The slope of the reciprocal plot of inverse relative catalytic constant ($k_{cat}^0/k_{cat}$) versus relative medium viscosity ($\eta/\eta^0$) was determined (Table 5). A slope near unity gives a proportional decrease in rate constant with increasing viscosity of the solution and shows a physical

**Table 6 Thermal stability of wild-type and engineered adGSTD4-4 at 45 °C**

The remaining GST activity was measured after incubating the enzyme at various time points at 45 °C. n.d., Not determined (low activity precluded measurement). [a]Some of these values have been previously reported and are shown for purposes of comparison [19,20]. One-way ANOVA with Dunnett's multiple comparison test was performed with wild-type as control; statistical significance is shown by ‡ for $P < 0.01$ and § for $P < 0.001$.

| Enzyme | Half-life at 45 °C (min) |
|---|---|
| Wild-type[a] | 15.32 ± 0.31 |
| H38A[a] | 15.33 ± 0.88§ |
| H38E[a] | 40.17 ± 1.26§ |
| H38F[a] | 19.33 ± 0.59§ |
| H38D | 15.18 ± 1.67 |
| H38K | 14.07 ± 0.73 |
| M39A | 4.71 ± 0.16§ |
| M39F | 4.72 ± 0.23§ |
| N47A | n.d. |
| Q49A | 15.19 ± 1.06§ |
| Q49E | 25.19 ± 1.37§ |
| H50A[a] | 25.81 ± 1.99§ |
| H50E[a] | 15.31 ± 0.54 |
| H50Y[a] | 20.79 ± 0.34§ |
| H50K | 11.99 ± 0.51§ |
| H50F | 27.07 ± 0.82§ |
| C51A | 14.86 ± 0.64 |
| C51D | 18.18 ± 1.01‡ |

step is rate-determining, whereas a slope of zero indicates that a chemical reaction step is rate limiting [32,33].

Wild-type enzyme displayed a linear dependence with a slope of approx. 1.0 suggesting that a physical step of the reaction that includes product release and/or structural transition is rate limiting. The engineered enzymes exhibited viscosity effects on $k_{cat}$ to different degrees. H50A and C51D were viscosity-independent with a slope approaching zero. These engineered enzymes changed the rate-limiting step of the reaction to a chemical step that includes GSH ionization step and $\sigma$-complex formation as described above, whereas partial dependence on a diffusion barrier and other viscosity-dependent motions were observed for the remaining enzymes that displayed viscosity effects with intermediate values ($0 < \text{slope} < 1$).

Also displayed in Table 5 is $\Delta\Delta G$, which is shown to illustrate the differences in the free energy changes for the formation of the transition states in the wild-type and engineered enzymes, as calculated at 25 °C from the equation below [34]:

$$\Delta\Delta G = -RT \ln \left(k_{cat}/K_m^{CDNB}\right)_{mutant} / \left(k_{cat}/K_m^{CDNB}\right)_{wild\text{-}type}.$$

H50A, D47A and C51D have a greater $\Delta\Delta G$ (7.562, 14.842 and 10.671 kJ/mol respectively) compared with other engineered enzymes (ranging from 1.860 to 4.075 kJ/mol) indicating that upon disruption of the hydrogen bond network, the enzymes require more energy than the wild-type enzyme to form and stabilize the transition state.

### Characterization of physical properties

The stability of the proteins was determined in comparison with the adGSTD4-4 wild-type (Table 6). In general, the engineered His[38], His[50], Asn[47], Cys[51] and Gln[49] proteins exhibited comparable stabilities to the wild-type, indicating a minor role of these residues in structural maintenance. However, H38E increased stability of the enzyme 2.6-fold, suggesting that a conformational change occurred which also is supported by the observed positive co-operativity. Met[39] appears to play a role in structural integrity as shown by 3-fold decreased enzyme stability for both the alanine and phenylalanine changes. However, the initial folding processes of the enzymes were observed to yield comparable refolding rates to the wild-type (results not shown). These results suggest that the Met[39] dipole–dipole interaction and positioning of His[38] and His[50] in a suitable conformation impact not only the kinetic properties but also enzyme stability.

The intrinsic fluorescence of tryptophan was used as an indicator of changes in tertiary structure (Figure 3). The $\lambda_{max}$ of tryptophan fluorescence in the engineered enzymes was slightly different from wild-type with a red shift in the range of 1–4 nm indicating a different polarity in tryptophan environments. In addition, differences in fluorescence intensity between wild-type and engineered enzymes were observed. This result suggests that there are minor conformational disturbances in the active site topography, which affect orientations of tryptophan and/or its neighbouring residues thereby modulating the quenching and tryptophan exposure to the electrophilic environment. For example, the active site topology changes that generated the positive co-operativity in H50K also yielded the lowest fluorescence intensity among the His[50] engineered enzymes (~44 % of wild-type). Moreover, the conformational change induced by glutamic acid residue replacement of His[38] also gave a 2-fold increase in enzyme stability, increased intrinsic fluorescence intensity to 197 % of wild-type, modulated GSH binding and enzyme catalysis as well as yielding the observed positive co-operativity towards GSH.

## DISCUSSION

The G-site residues interacting directly with cysteine and glutamyl moieties of GSH have been shown in several studies to contribute to GST catalytic mechanisms including GSH binding, catalysis, GSH ionization as well as rate-limiting step determination [10–14]. In the present study, we have examined the significant contributions of GST residues that interact with the GSH glycine moiety as well as identification of a hydrogen bond network. The network consists of His[38], Met[39], Asn[47], Gln[49], His[50] and Cys[51] and contributes to catalysis through multiple processes including GSH ionization, nucleophilic substitution, product formation and product dissociation.

The kinetic studies demonstrated that the engineered residues greatly impacted the enzyme's ability to interact with GSH. Moreover, the engineered enzymes of His[38], Met[39], His[50], Cys[51] and Gln[49] have shown strong positive co-operativity upon binding of GSH. However, the positive co-operativity was not observed for the engineered enzymes of residues interacting with the other moieties of GSH [11–13,15]. Therefore it can be suggested that the residues interacting with the GSH glycine moiety are not only involved in GSH interaction but also control the motion of a flexible region of GST. Upon binding of GSH in the active site, these GST residues induce an active site conformational change for the induced-fit mechanism. These residues are on the loops on either side of $\alpha$2-helix which connects the helix to $\beta$2-sheet and $\beta$3-sheet. These loops would serve as hinges for the movement of $\alpha$2-helix.

In the present study, changes of the active-site residues generated positive co-operativity between two subunits, a finding similar to that obtained in previous studies in which the subunit interface had been changed or where changes in highly flexible regions, for example Gly[41], Cys[47] and Lys[54] of hGSTP1-1 (human GSTP1-1) [33,35] or Asn[49] and Gln[53] of maize GST1 [36,37],

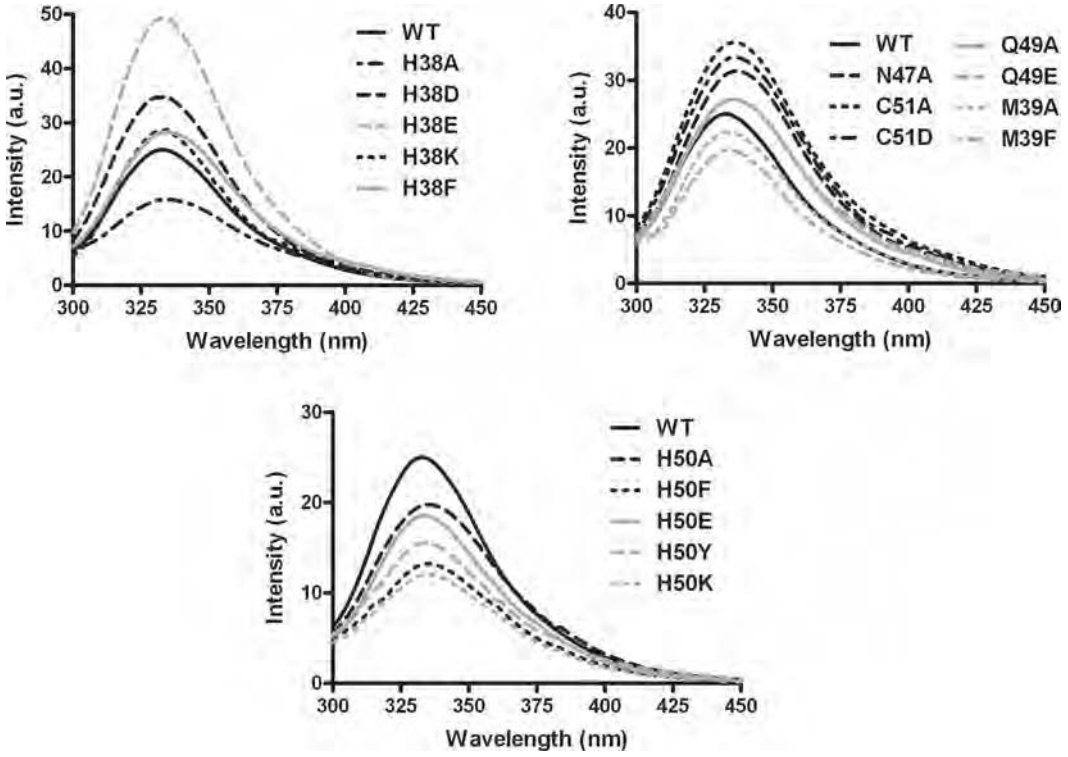


**Figure 3 The maximum emission wavelength ($\lambda_{max}$) and intrinsic fluorescence intensity at $\lambda_{max}$ of tryptophan fluorescence of wild-type and the engineered enzymes**

Excitation was at 295 nm and emission was scanned from 300 to 450 nm. Samples ($n = 3$) contained 0.1 mg/ml protein in 0.1 M potassium phosphate buffer (pH 6.5). Percent intensity change compared with wild-type enzyme was measured at fluorescence $\lambda_{max}$ averaged over three scans corrected for dilution and inner filter effects.

had been made. It has been proposed that the conformational transitions generate two different binding modes upon GSH binding: low-affinity and high-affinity conformations, which are related to positive co-operativity observed [5,38,39]. The binding of GSH to the first active site stabilizes the low-affinity conformation of the enzyme which then becomes the high-affinity conformational state. Positive co-operativity upon GSH binding observed in $His^{38}$, $Met^{39}$, $His^{50}$, $Cys^{51}$ and $Gln^{49}$ engineered enzymes may be relevant to this conformational transition concept. These residues are located in a highly flexible region; therefore the residue changes would alter the flexibility of the $\alpha$2-helix to fit GSH in the active site, which may then generate two different conformational transition states upon GSH binding.

Both $His^{38}$ and $His^{50}$ interact directly with the glycine carboxylate of GSH. The functional groups at positions 38 and 50 are significant in size, volume and polarity for GSH binding and enzyme catalysis. However, $His^{50}$ contributes more to the GSH activation process and enzyme catalysis in which the full function is achieved by the synergistic action with the hydrogen bond network residues ($Asn^{47}$, $Gln^{49}$ and $Cys^{51}$). The disruption of the hydrogen bond network, for the engineered enzymes of $His^{50}$, $Asn^{47}$ and $Cys^{51}$, showed progressively decreased $k_{cat}$ values to more than 90 %. Moreover, several aspects of the GST catalytic mechanism were altered by H50A. H50A decreased the enzyme's ability to lower the p$K_a$ of the GSH thiol group up to 1 pH unit; this large an effect has been observed for mutations of the conserved serine/tyrosine residue interacting with the GSH thiol group [13,40–42]. Additionally, the rate-limiting step of the H50A is fully switched from a physical step to a chemical step as determined by fluoride/chloride leaving group and viscosity effect on the kinetic constants. As the important $His^{50}$ is still present, lesser effects were observed for the engineered enzymes of $Gln^{49}$ and $Cys^{51}$ for minor disruptions of the stabilizing hydrogen bond network.

The results strongly support that $His^{50}$ is a key residue in the hydrogen bond network which functions as a proton acceptor as well as controls the electron distribution in the active site to promote ionization and stabilization of the GSH thiolate anion. The $His^{50}$ residue contributes to precise residue and substrate orientations, GSH ionization, $\sigma$-complex intermediate formation and the release of product from the active site. The regulation of the electrostatic field in the active site by positively charged residues has also been reported in several studies [15,43,44].

The changes in catalytic efficiency are also related to differences in free energy changes for the formation of transition states in the engineered and wild-type enzymes as determined by $\Delta\Delta G$ [34]. The greater value of $\Delta\Delta G$ refers to a decrease in the stabilization of transition state compared with wild-type in which the enzyme utilizes more energy to stabilize its transition state. Moreover, the stabilization of transition state contributes to multiple mechanisms in enzyme-catalysed reactions. $\Delta\Delta G$ values are increased up to 7.562, 14.84 and 10.666 kJ/mol for H50A, D47A and C51D respectively in which the hydrogen bond network is strongly disrupted, indicative of the incomplete pre-organized environment for enhancing catalysis along the reaction pathway of the engineered enzymes [45]. Therefore it can be noted that the network of hydrogen bonds is also required for the organization inside the enzyme molecule to provide stabilization of the transition state.

The positively charged residue position 50 appears to be highly conserved or functionally conserved across GST classes by histidine, lysine or arginine located at the equivalent structural

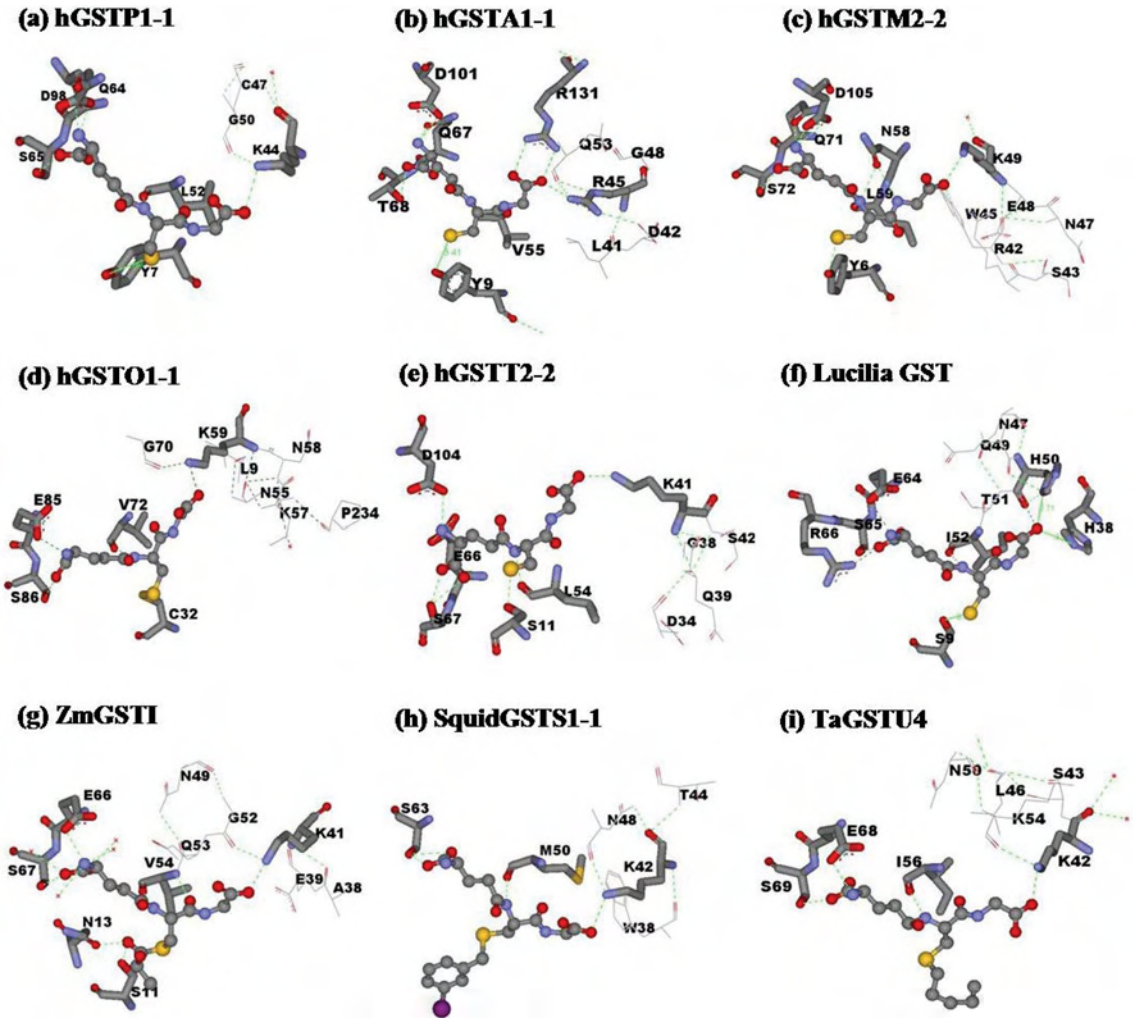


COLOUR

**Figure 4 Conserved G-site residues that directly interact with the glycine moiety of GSH and generate a hydrogen bond network in several GST classes**

The conserved G-site residues are shown by stick models, while line models represent the hydrogen bond network residues at the glycine moiety of GSH. GSH or GSH analogues are illustrated in ball-and-stick; GSH (**a**, **b**, **c**, **d**, **e**, **f**), lactoylglutathione (**g**), iodobenzylglutathione (**h**) and *S*-hexyl-GSH (**i**). Green dotted lines represent hydrogen-bond interactions. PDB code numbers: hGSTP1-1 (PDB id 8GSS), hGSTA1-1 (PDB id 1PKW), hGSTM2-2 (PDB id 1XW5), hGSTO1-1 (PDB id 1EEM), hGSTT2-2 (PDB id 1LJR), Lucilia GST [7], ZmGST1 (PDB id 1AXD), squid GSTS1-1 (PDB id 2GSQ) and TaGSTU4 [*Triticum aestivum* (wheat) GSTU4; PDB id 1GWC]. The Figure was created with Accelrys DS ViewerPro 5.0.

position. This conserved residue is in hydrogen bonding distance to the glycine carboxylate moiety of GSH which is stabilized by a hydrogen bond network of surrounding residues (Figure 4) for example Lys[40] in PtGSTU1 [*Pinus tabulaeformis* (Chinese hard pine) GSTU1], Lys[41] in ZmGST1 [*Zea mays* (maize) GST1], Lys[44] in hGSTP1-1, Lys[41] in hGSTT2-2, Lys[59] in hGSTO1-1, Lys[49] in hGSTM2-2, Lys[42] in squid GSTS1-1, Lys[45] in Sj26GST [26 kDa GST from *Schistosoma japonicum* (oriental blood-fluke)] and Arg[45] in hGSTA1-1. However, the feature of two positively charged histidines, His[38] and His[50], interacting with the glycine carboxylate moiety of GSH is a unique trait for insect GSTDs. His[38] is responsible for GSH binding, whereas His[50] contributes to several steps of the enzyme-catalysed reaction from GSH interaction to the release of product from the active site.

For the GSH activation mechanism of Alpha, Mu and Pi GST isoenzymes, it has been described that the thiol proton is quantitatively released into solution after the thiolate anion is formed [46,47]. In contrast with GSTD, which behaves differently, the thiol proton is captured by at least an internal base residue at high pH value [46,47]. The present study shows that His[50] is also a candidate for the thiol proton acceptor in addition to the residues at the $\gamma$-glutamyl portion of GSH reported previously [15,31]. Moreover, the overall velocity of His[50] engineered enzymes is progressively restricted; therefore it can be assumed that the thiol proton released must be accepted first by the active site residues, e.g. His[50], before a new cycle of the reaction can initiate.

The 'base-assisted deprotonation model' is an alternative model that describes the mechanism of GST enzymes in GSH ionization process. This model has been implicated in several studies of the glutamyl $\alpha$-carboxylate of GSH acting as a catalytic base, involved in the thiol proton acceptance from the GSH thiol group [15,16,31,46]. In the present study, we addressed the contribution of the glycine moiety of GSH for GSH ionization in which this end of GSH is involved in proton acceptance by providing a counter ion from the charged His[50] which is stabilized by the hydrogen bond network.

In conclusion, the present study revealed a critical role for residues located at the glycine moiety of GSH in catalytic rate determination. This area constitutes a second G-site network involved in GSH ionization distinct from the network previously

reported interacting with the glutamyl end of GSH [16,17]. This second network also appears to be functionally conserved in GSTs (Figure 4). In the present study, we showed that $His^{50}$ is a central residue in the hydrogen bond network to GSH with the protonated imidazole ring of $His^{50}$ being stabilized by the network. $His^{50}$ plays important roles in several processes of the enzyme mechanism. Moreover, this network at the glycine moiety of GSH also contributed to the 'base-assisted deprotonation model' for GSH ionization.

This work was funded by the TRF (Thailand Research Fund). A.V. was supported by a Royal Golden Jubilee Ph.D. Scholarship.

## REFERENCES


1 Sheehan, D., Meade, G., Foley, V. M. and Dowd, C. A. (2001) Structure, function and evolution of glutathione transferases: implications for classification of non-mammalian members of an ancient enzyme superfamily. Biochem. J. **360**, 1–16

2 Ketterer, B. (2001) A bird's eye view of the glutathione transferase field. Chem. Biol. Interact. **138**, 27–42

3 Mannervik, B., Awasthi, Y. C., Board, P. G., Hayes, J. D., Di Ilio, C., Ketterer, B., Listowsky, I., Morgenstern, R., Muramatsu, M., Pearson, W. R. et al. (1992) Nomenclature for human glutathione transferases. Biochem. J. **282**, 305–306

4 Hayes, J. D., Flanagan, J. U. and Jowsey, I. R. (2005) Glutathione transferases. Annu. Rev. Pharmacol. Toxicol. **45**, 51–88

5 Mannervik, B. and Danielson, U. H. (1988) Glutathione transferases – structure and catalytic activity. CRC Crit. Rev. Biochem. **23**, 283–337

6 Armstrong, R. N. (1997) Structure, catalytic mechanism, and evolution of the glutathione transferases. Chem. Res. Toxicol. **10**, 2–18

7 Wilce, M. C. J., Board, P. G., Feil, S. C. and Parker, M. W. (1995) Crystal structure of a theta-class glutathione transferase. EMBO J. **14**, 2133–2143

8 Dirr, H., Reinemer, P. and Huber, R. (1994) X-ray crystal structures of cytosolic glutathione S-transferases. Implications for protein architecture, substrate recognition and catalytic function. Eur. J. Biochem. **220**, 645–661

9 Rossjohn, J., Feil, S. C., Wilce, M. C. J., Sexton, J., Spithill, T. W. and Parker, M. W. (1997) Crystallization, structural determination and analysis of a novel parasite vaccine candidate: *Fasciola hepatica* glutathione S-transferase. J. Mol. Biol. **273**, 857–872

10 Stenberg, G., Board, P. G., Carlberg, I. and Mannervik, B. (1991) Effects of directed mutagenesis on conserved arginine residues in a human class Alpha glutathione transferase. Biochem. J. **274**, 549–555

11 Liu, S., Zhang, P., Ji, X., Johnson, W. W., Gilliland, G. L. and Armstrong, R. N. (1992) Contribution of tyrosine 6 to the catalytic mechanism of isoenzyme 3-3 of glutathione S-transferase. J. Biol. Chem. **267**, 4296–4299

12 Kolm, R. H., Sroga, G. E. and Mannervik, B. (1992) Participation of the phenolic hydroxyl group of Tyr-8 in the catalytic mechanism of human glutathione transferase P1-1. Biochem. J. **285**, 537–540

13 Caccuri, A. M., Antonini, G., Nicotra, M., Battistoni, A., Lo Bello, M., Board, P. G., Parker, M. W. and Ricci, G. (1997) Catalytic mechanism and role of hydroxyl residues in the active site of theta class glutathione S-transferases. Investigation of Ser-9 and Tyr-113 in a glutathione S-transferase from the Australian sheep blowfly, *Lucilia cuprina*. J. Biol. Chem. **272**, 29681–29686

14 Tan, K.-L., Chelvanayagam, G., Parker, M. W. and Board, P. G. (1996) Mutagenesis of the active site of the human Theta-class glutathione transferase GSTT2-2: catalysis with different substrates involves different residues. Biochem. J. **319**, 315–321

15 Winayanuwattikun, P. and Ketterman, A. J. (2004) Catalytic and structural contributions for glutathione binding residues in a Delta class glutathione S-transferase. Biochem. J. **382**, 751–757

16 Winayanuwattikun, P. and Ketterman, A. J. (2005) An electron-sharing network involved in the catalytic mechanism is functionally conserved in different glutathione transferase classes. J. Biol. Chem. **280**, 31776–31782

17 Winayanuwattikun, P. and Ketterman, A. J. (2007) Glutamate 64, a newly identified residue of the functionally conserved electron-sharing network contributes to catalysis and structural integrity of glutathione transferases. Biochem. J. **402**, 339–348

18 Pettersen, E. F., Goddard, T. D., Huang, C. C., Couch, G. S., Greenblatt, D. M., Meng, E. C. and Ferrin, T. E. (2004) UCSF chimera – a visualization system for exploratory research and analysis. J. Comput. Chem. **25**, 1605–1612

19 Vararattanavech, A. and Ketterman, A. (2003) Multiple roles of glutathione binding-site residues of glutathione S-transferase. Protein Peptide Lett. **10**, 441–448

20 Vararattanavech, A., Prommeenate, P. and Ketterman, A. J. (2006) The structural roles of a conserved small hydrophobic core in the active site and an ionic bridge in domain I of Delta class glutathione S-transferase. Biochem. J. **393**, 89–95

21 Habig, W. H., Pabst, M. J. and Jakoby, W. B. (1974) Glutathione S-transferases. The first enzymatic step in mercapturic acid formation. J. Biol. Chem. **249**, 7130–7139

22 Segel, I. H. (1993) Enzyme Kinetics, Behavior and Analysis of Rapid Equilibrium and Steady-state Enzyme Systems, John Wiley and Sons, New York

23 Jirajaroenrat, K., Pongjaroenkit, S., Krittanai, C., Prapanthadara, L. and Ketterman, A. J. (2001) Heterologous expression and characterization of alternatively spliced glutathione *S*-transferases from a single *Anopheles* gene. Insect Biochem. Mol. Biol. **31**, 867–875

24 Caccuri, A. M., Ascenzi, P., Lo Bello, M., Federici, G., Battistoni, A., Mazzetti, P. and Ricci, G. (1994) Are the steady state kinetics of glutathione transferase always dependent on the deprotonation of the bound glutathione? New insights in the kinetic mechanism of GST P1-1. Biochem. Biophys. Res. Commun. **200**, 1428–1434

25 Wolf, A. V., Brown, M. G. and Prentiss, P. G. (1985) Handbook of Chemistry and Physics, CRC Press, Boca Raton, FL

26 Armstrong, R. N., Rife, C. and Wang, Z. (2001) Structure, mechanism and evolution of thiol transferases. Chem. Biol. Interact. **133**, 167–169

27 Caccuri, A. M., Ascenzi, P., Antonini, G., Parker, M. W., Oakley, A. J., Chiessi, E., Nuccetelli, M., Battistoni, A., Bellizia, A. and Ricci, G. (1996) Structural flexibility modulates the activity of human glutathione transferase P1-1. Influence of a poor co-substrate on dynamics and kinetics of human glutathione transferase. J. Biol. Chem. **271**, 16193–16198

28 Caccuri, A. M., Lo Bello, M., Nuccetelli, M., Rossi, P., Antonini, G., Federici, G. and Ricci, G. (1998) Proton release upon glutathione binding to glutathione transferase P1-1: kinetic analysis of a multistep glutathione binding process. Biochemistry **37**, 3028–3034

29 Armstrong, R. N. (1997) Structure, catalytic mechanism, and evolution of the glutathione transferases. Chem. Res. Toxicol. **10**, 2–18

30 Gustafsson, A., Pettersson, P. L., Grehn, L., Jemth, P. and Mannervik, B. (2001) Role of the glutamyl $\alpha$-carboxylate of the substrate glutathione in the catalytic mechanism of human glutathione transferase A1-1. Biochemistry **40**, 15835–15845

31 Widersten, M., Björnestedt, R. and Mannervik, B. (1996) Involvement of the carboxyl groups of glutathione in the catalytic mechanism of human glutathione transferase A1-1. Biochemistry **35**, 7731–7742

32 Johnson, W. W., Liu, S., Ji, X., Gilliland, G. L. and Armstrong, R. N. (1993) Tyrosine 115 participates both in chemical and physical steps of the catalytic mechanism of a glutathione S-transferase. J. Biol. Chem. **268**, 11508–11511

33 Ricci, G., Caccuri, A. M., Lo Bello, M., Rosato, N., Mei, G., Nicotra, M., Chiessi, E., Mazzetti, A. P. and Federici, G. (1996) Structural flexibility modulates the activity of human glutathione transferase P1-1. Role of helix 2 flexibility in the catalytic mechanism. J. Biol. Chem. **271**, 16187–16192

34 Dirr, H. W., Little, T., Kuhnert, D. C. and Sayed, Y. (2005) A conserved N-capping motif contributes significantly to the stabilization and dynamics of the C-terminal region of class alpha glutathione transferases. J. Biol. Chem. **280**, 19480–19487

35 Lo Bello, M., Nuccetelli, M., Chiessi, E., Lahm, A., Mazzetti, A. P., Parker, M. W., Tramontano, A., Federici, G. and Ricci, G. (1998) Mutations of Gly to Ala in human glutathione transferase P1-1 affect helix 2 (G-site) and induce positive cooperativity in the binding of glutathione. J. Mol. Biol. **284**, 1717–1725

36 Labrou, N. E., Mello, L. V. and Clonis, Y. D. (2001) Functional and structural roles of the glutathione-binding residues in maize (*Zea mays*) glutathione S-transferase I. Biochem. J. **358**, 101–110

37 Labrou, N. E., Mello, L. V. and Clonis, Y. D. (2001) The conserved Asn49 of maize glutathione *S*-transferase I modulates substrate binding, catalysis and intersubunit communication. Eur. J. Biochem. **268**, 3950–3957

38 Principato, G. B., Danielson, U. H. and Mannervik, B. (1988) Relaxed thiol substrate specificity of glutathione transferase effected by a non-substrate glutathione derivative. FEBS Lett. **231**, 155–158

39 Jemth, P. and Mannervik, B. (1999) Fast product formation and slow product release are important features in a hysteretic reaction mechanism of glutathione transferase T2-2. Biochemistry **38**, 9982–9991

40 Wang, J., Barycki, J. J. and Colman, R. F. (1996) Tyrosine 8 contributes to catalysis but is not required for activity of rat liver glutathione S-transferase, 1-1. Protein Sci. **5**, 1032–1042

41 Gustafsson, A., Etahadieh, M., Jemth, P. and Mannervik, B. (1999) The C-terminal region of human glutathione transferase A1-1 affects the rate of glutathione binding and the ionization of the active-site Tyr9. Biochemistry **38**, 16268–16275

42 Labrou, N. E., Rigden, D. J. and Clonis, Y. D. (2003) Engineering the pH-dependence of kinetic parameters of maize glutathione *S*-transferase I by site-directed mutagenesis. Biomol. Eng. **21**, 61–66

43 Patskovsky, Y. V., Patskovska, L. N. and Listowsky, I. (2000) The enhanced affinity for thiolate anion and activation of enzyme-bound glutathione is governed by an arginine residue of human Mu class glutathione S-transferases. J. Biol. Chem. **275**, 3296–3304
44 Björnestedt, R., Tardioli, S. and Mannervik, B. (1995) The high activity of rat glutathione transferase 8-8 with alkene substrates is dependent on a glycine residue in the active site. J. Biol. Chem. **270**, 29705–29709
45 Garcia-Viloca, M., Gao, J., Karplus, M. and Truhlar, D. G. (2004) How enzymes work: analysis by modern rate theory and computer simulations. Science **303**, 186–195
46 Caccuri, A. M., Antonini, G., Board, P. G., Parker, M. W., Nicotra, M., Lo Bello, M., Federici, G. and Ricci, G. (1999) Proton release on binding of glutathione to Alpha, Mu and Delta class glutathione transferases. Biochem. J. **344**, 419–425
47 Caccuri, A. M., Antonini, G., Board, P. G., Flanagan, J., Parker, M. W., Paolesse, R., Turella, P., Federici, G., Lo Bello, M. and Ricci, G. (2001) Human glutathione transferase T2-2 discloses some evolutionary strategies for optimization of substrate binding to the active site of glutathione transferases. J. Biol. Chem. **276**, 5427–5431

Received 27 March 2007/22 May 2007; accepted 24 May 2007
Published as BJ Immediate Publication 24 May 2007, doi:10.1042/BJ20070422

BJ www.biochemj.org

BJ Structure

Biochem. J. (2007) **402**, 339–348 (Printed in Great Britain) doi:10.1042/BJ20061253

**Reprint 2** 339

# Glutamate-64, a newly identified residue of the functionally conserved electron-sharing network contributes to catalysis and structural integrity of glutathione transferases

Pakorn WINAYANUWATTIKUN and Albert J. KETTERMAN[1]

Institute of Molecular Biology and Genetics, Mahidol University, Salaya Campus, Nakhon Pathom 73170, Thailand

In *Anopheles dirus* glutathione transferase D3-3, position 64 is occupied by a functionally conserved glutamate residue, which interacts directly with the $\gamma$-glutamate moiety of GSH (glutathione) as part of an electron-sharing network present in all soluble GSTs (glutathione transferases). Primary sequence alignment of all GST classes suggests that $Glu^{64}$ is one of a few residues that is functionally conserved in the GST superfamily. Available crystal structures as well as consideration of the property of the equivalent residue at position 64, acidic or polar, suggest that the GST electron-sharing motif can be divided into two types. Electrostatic interaction between the GSH glutamyl and carboxylic $Glu^{64}$, as well as with $Arg^{66}$ and $Asp^{100}$, was observed to extend the electron-sharing motif identified previously. $Glu^{64}$ contributes to the catalytic function of this motif and the 'base-assisted deprotonation' that are essential for GSH ionization during catalysis. Moreover, this residue also appears to affect multiple steps in the enzyme catalytic strategy, including binding of GSH, nucleophilic attack by thiolate at the electrophilic centre and product formation, probably through active-site packing effects. Replacement with non-functionally-conserved amino acids alters initial packing or folding by favouring aggregation during heterologous expression. Thermodynamic and reactivation *in vitro* analysis indicated that $Glu^{64}$ also contributes to the initial folding pathway and overall structural stability. Therefore $Glu^{64}$ also appears to impact upon catalysis through roles in both initial folding and structural maintenance.

Key words: active-site residue, *Anopheles dirus*, catalytic mechanism, electron sharing network, glutathione transferase, structural integrity.

## INTRODUCTION

GSTs (glutathione transferases; EC 2.5.1.18) are a superfamily of enzymes that contribute towards diverse cellular processes ranging from detoxification to control of gene expression [1–4]. The enzymes generally catalyse nucleophilic attack of the GSH (glutathione) sulfhydryl group to an electrophilic centre of a number of endogenous and xenobiotic compounds [1,5,6]. Conjugation of GSH to such organic molecules enhances solubility, thus facilitating their eventual elimination [5–7]. This reaction is an early step along the mercapturic acid pathway in which hydrophobic compounds are inactivated and eliminated from an organism [8]. Based on amino acid identity, substrate specificities and immunological cross-reactivity, cytosolic GSTs are currently divided into at least 12 distinct evolutionary classes, namely Alpha, Mu, Pi, Theta, Sigma, Zeta, Omega, Phi, Tau, Delta, Epsilon and Beta [6,9–15]. In addition, the number of members identified in this enzyme superfamily is increasing due to the massive growth of genomic information, which includes a number of unclassified GSTs [16].

All cytosolic GSTs adopt the same highly conserved tertiary structure [17]. GSTs are dimeric proteins (with a molecular mass of about 50 kDa) assembled from identical or structurally related subunits. Each subunit is characterized by two distinct domains and an active site. However, each active site is only fully functional when amino acid residues from both subunits are present in the final dimeric structure. The active-site of GSTs consists of two adjacent regions. The first region is the G-site (GSH binding site), formed mostly by the N-terminal domain (domain I), which adopts an $\alpha/\beta$ topology that binds GSH as the thiol substrate [7]. The second region is the non-polar H-site (hydrophobic substrate binding site), generated primarily by the C-terminal domain (domain II), which is an all-helical structure that provides structural elements for recognition of a wide range of hydrophobic co-substrates [7]. Although GSTs possess a high specificity for GSH as the nucleophile, the enzymes exhibit broad specificity with regard to structurally diverse hydrophobic substrates [17]. The catalytic strategy of GSTs for the nucleophilic substitution reaction can be divided into several steps: binding of substrates to the enzyme active site, activation of GSH by thiol deprotonation, nucleophilic attack by thiolate at the electrophilic centre, product formation and product release [18–20].

The roles of several active-site residues and functional groups of GSH have been studied intensively and a potential model has been proposed to describe deprotonation of the GSH thiol group which enhances the nucleophilicity of the reaction [20–24]. The hydroxyl group of the conserved tyrosine/serine residue at the G-site of GSTs (i.e. $Tyr^{8}$ for Pi, $Tyr^{9}$ for Alpha, $Tyr^{6}$ for Mu and $Ser^{9}$ for Delta classes) is within hydrogen-bonding distance of the thiol group of the bound GSH, and is required for correct orientation and stabilization of the deprotonated thiol anion. The deprotonated anionic GSH results from subtraction of a thiol proton by the glutamyl $\alpha$-carboxylate of GSH, which acts as a catalytic base in the base-assisted deprotonation model with assistance from an electron-sharing network. The functionally conserved electron-sharing network is characterized by an ionic

Abbreviations used: adGSTD3-3, *Anopheles dirus* glutathione transferase Delta class homodimer of subunit 3; CDNB, 1-chloro-2,4-dinitrobenzene; DTT, dithiothreitol; FDNB, 1-fluoro-2,4-dinitrobenzene; GdmCl, guanidinium chloride; GSH, glutathione; G-site, GSH binding site; GST, glutathione transferase; PtGSTU1-1, plant Tau class GST.

[1] To whom correspondence should be addressed (email frakt@mahidol.ac.th).

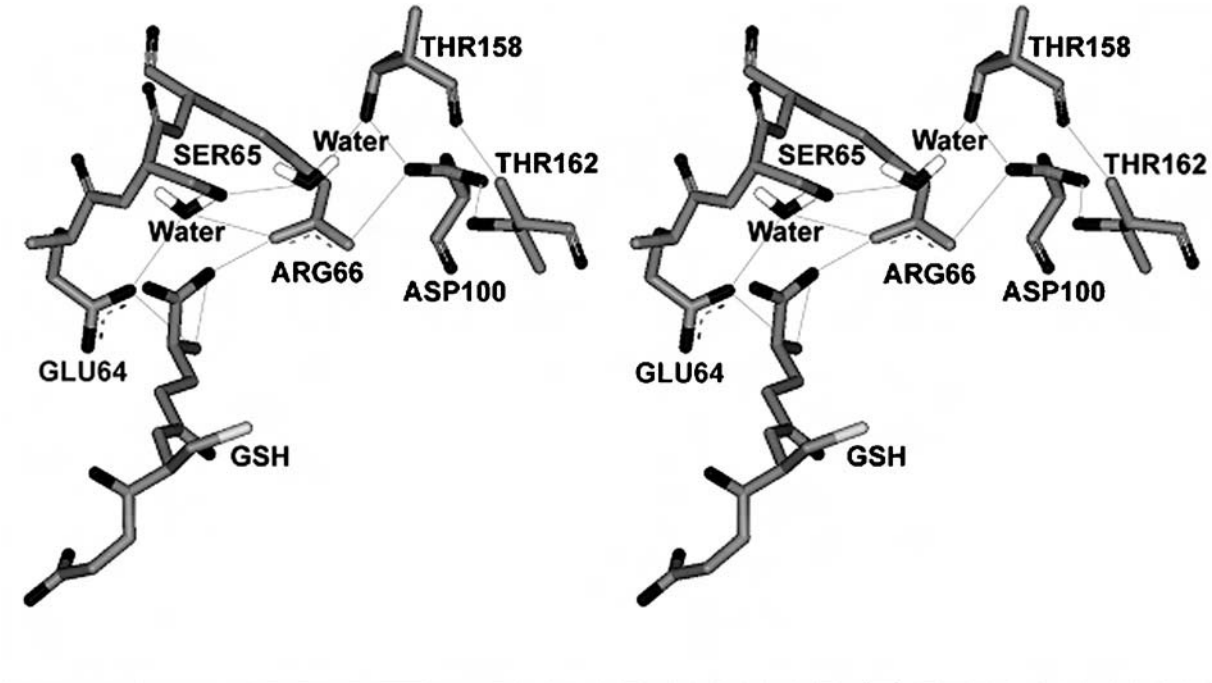


| NCBI Seq ID | GST class | Source | Isoform | | | | | | | | | | | | | | | | | | | | | | | | | | | |
|---|---|---|---|---|---|---|---|---|---|---|---|---|---|---|---|---|---|---|---|---|---|---|---|---|---|---|---|---|---|---|
| AAG38505 | Delta | *A.dirus* | 3 | 52 | I | P | T | L | V | D | N | - | G | F | A | L | W | E | S | R | A | I | C | T | Y | L | A | E | K | Y | G |
| NP_000844.1 | Theta | *H.sapiens* | 1 | 54 | V | P | A | L | K | D | G | - | D | F | T | L | T | E | S | V | A | I | L | L | Y | L | T | R | K | Y | K |
| AH004172.1 | Omega | *H.sapiens* | 1 | 72 | V | P | V | L | E | N | S | Q | G | Q | L | I | Y | E | S | A | I | T | C | E | Y | L | D | E | A | Y | P |
| CAC94005.1 | Tau | *T.aestivum* | 1 | 59 | V | P | V | L | I | H | N | - | G | R | P | V | C | E | S | L | L | I | L | E | Y | L | D | D | A | V | G |
| CAD29575.1 | Phi | *T.aestivum* | 1 | 55 | I | P | A | F | Q | D | G | - | D | L | L | L | F | E | S | R | A | I | A | R | Y | V | L | R | K | Y | K |
| P15214 | Beta | *P.mirabilis* | 1 | 52 | V | P | V | L | Q | L | D | N | G | D | I | L | T | E | G | V | A | I | V | Q | Y | L | A | D | L | K | P |
| NP_611323.1 | Epsilon | *D.melanogaster* | 1 | 57 | V | P | M | L | D | D | N | - | G | T | F | I | W | D | S | H | A | I | A | A | Y | L | V | D | K | Y | A |
| A37378 | Pi | *H.sapiens* | 1 | 53 | L | P | K | F | Q | D | G | - | D | L | T | L | Y | Q | S | N | T | I | L | R | H | L | G | R | T | L | G |
| NP_665683.1 | Alpha | *H.sapiens* | 1 | 55 | V | P | M | V | E | I | D | - | G | M | K | L | V | Q | T | R | A | I | L | N | Y | I | A | S | K | Y | N |
| P46088 | Sigma | *O.sloani* | 1 | 51 | M | P | V | L | D | I | D | - | G | T | K | M | S | Q | S | M | C | I | A | R | H | L | A | R | E | F | G |
| NP_000552 | Mu | *H.sapiens* | 1 | 60 | L | P | Y | L | I | D | G | - | A | H | K | I | T | Q | S | N | A | I | L | C | Y | I | A | R | K | H | N |
| O43708 | Zeta | *H.sapiens* | 1 | 59 | V | P | T | L | K | I | D | - | G | I | T | I | H | Q | S | L | A | I | I | E | Y | L | E | E | T | R | P |

**Figure 1 Newly identified extension of an electron-sharing network in adGSTD3-3**

The electron-sharing network is an ionic interaction between negatively charged and positively charged residues stabilized by a network of hydrogen-bonds. The stereo view of corresponding three-dimensional structure of the electron-sharing network is shown in the upper panel. The lines show the putative electron movement pathway with distances between 2.5 and 3.0 Å. The lower panel shows the sequence alignment of amino acid residues in Delta, Theta, Omega, Tau, Phi, Beta, Epsilon, Pi, Alpha, Sigma, Mu and Zeta class GSTs. The newly identified functionally conserved glutamate, aspartate and glutamine in the electron-sharing network are identified by an arrow.

bridge interaction between the negatively charged glutamyl $\alpha$-carboxylate of GSH, a positively charged residue and a negatively charged residue, forming a resonance motif stabilized by a network of hydrogen-bonds with surrounding residues. The network is distributed among multiple interacting amino acids that collectively provide a network function. This conserved motif's contribution to the base-assisted deprotonation is essential for the GSH ionization step of catalysis.

The functionally conserved glutamate residue, $Glu^{64}$ in adGSTD3-3 (*Anopheles dirus* GST Delta class homodimer of subunit 3) is located in the same region as the electron-sharing network (Figure 1). Initial characterization of the electron-sharing network has provided further insight into this motif [25]. The carboxylic group of $Glu^{64}$ interacts directly with the glutamyl $\alpha$-amino group of GSH. Moreover, by observing the configuration of the GSH glutamyl $\alpha$-carboxylate, the GSH glutamyl $\alpha$-amino, $Glu^{64}$ and the electron-sharing network, it is now possible to extend this conserved motif, which is maintained in all GSTs. The aim of the present paper was to ascertain the validity of $Glu^{64}$ function in the electron-sharing network. We have observed previously [25] that alanine replacement of $Glu^{64}$ caused the enzyme to be expressed in an insoluble form. This suggested that $Glu^{64}$ is a critical residue involved in tertiary structure or initial folding of the enzyme. Therefore the contribution of this residue to structural maintenance and initial folding was also examined. The results of the present paper indicate that $Glu^{64}$ is a part of the functionally conserved electron-sharing network and has roles both in catalysis as well as structural folding and maintenance.

## MATERIALS AND METHODS

### Site-directed mutagenesis

The plasmid pET3a-adgstD3, described previously [26], was used as the template to generate the single point mutations via PCR-based site-directed mutagenesis. The functionally conserved active-site residue $Glu^{64}$ was replaced by an alanine, leucine, valine, lysine, glutamine, asparagine or aspartate residue by using

PCR primers based on the wild-type *adgstD3* gene sequence (Genbank accession number AF273039). Mutants were screened randomly by restriction enzyme digestion analysis. Mutant plasmids could be distinguished from the wild-type template by digestion with restriction enzymes corresponding to the restriction recognition site introduced by the mutagenic primers. The full-length GST coding sequence carrying E64A, E64L, E64V, E64K, E64Q, E64D and E64N mutations were verified by the dideoxy chain termination method.

#### Heterologous expression and purification

The proteins were expressed from the pET3a-adgstD3 vector in *Escherichia coli* BL21 (DE3) pLysS cells. The cells were grown to $D_{600} = 0.5$ and expression was induced by addition of 0.1 mM isopropyl $\beta$-D-thiogalactoside. Following a 3 h induction, cells were collected by centrifugation at 10000 ***g*** for 20 min at 4 °C and lysed by sonication using an Ultrasonic processor XL (Misonix) at power level 3 for 10 s, paused for 1 min and repeated three times at 4 °C. The soluble recombinant GST proteins were purified by GSTrap™ affinity chromatography (Amersham Biosciences) or *S*-hexylglutathione agarose (Sigma–Aldrich) affinity chromatography. The protein concentration was determined by the Bradford method [27] using BSA as a standard.

#### Steady-state kinetics

Steady-state kinetics were studied for wild-type and mutant enzymes at varying concentrations of CDNB (1-chloro-2,4-dinitrobenzene) and GSH in 0.1 M phosphate buffer pH 6.5. The reaction was monitored at 340 nm, $\varepsilon$ 9600 $M^{-1}cm^{-1}$. Apparent kinetic constants, $k_{cat}$, $K_m$ and $k_{cat}/K_m$ were determined by fitting the collected data to a Michaelis–Menten equation by non-linear regression analysis using GraphPad Prism (GraphPad software).

#### pH dependence of kinetic constants

The pH dependence of $k_{cat}/K_m^{CDNB}$ was obtained as stated above by recording the enzymatic reaction in the following buffers: 0.1 M sodium acetate buffers (from pH 5.0 to 5.5) and 0.1 M potassium phosphate buffer (from pH 6.0 to 8.5). The pH was altered in increments of 0.5, and control experiments showed no discontinuities from buffer types. p$K_a$ values were obtained by fitting the data to eqn (1) [20]:

$$y = y_{lim}/(1 + 10^{pKa-pH}) \quad (1)$$

#### Fluoride/chloride leaving group replacement

The second order kinetic constants at pH 6.5 for the spontaneous reaction of GSH with CDNB and FDNB (1-fluoro-2,4-dinitrobenzene) and the catalytic-centre activities at pH 6.5 for adGSTD3-3 with CDNB and FDNB as co-substrates were obtained as described previously [28].

#### Viscosity effect on the kinetic parameters

The effect of viscosity on kinetic parameters was obtained by using 0.1 M potassium phosphate buffer pH 6.5 with various glycerol concentrations. Viscosity values ($\eta$) at 25 °C were calculated as described previously [29].

#### Structural studies

A Jasco J-714 spectropolarimeter was used for CD measurements in the far-UV region from 190–260 nm. Spectra were recorded using 0.3 mg/ml of protein in 2-mm path length cuvettes. Intrinsic fluorescence emission spectra were measured with a Jasco FP-6300 spectrofluorimeter. The excitation wavelength was 295 nm and the $\lambda_{max}$ and the fluorescence intensity of emission spectra were analysed at a protein concentration of 0.2 mg/ml.

#### Kinetics of thermal denaturation

Heat inactivation of the wild-type and Glu[64] mutant enzymes was monitored at different temperatures. Enzymes (40 $\mu$M) were incubated in 0.1 mM potassium phosphate buffer pH 6.5, 1 mM EDTA and 5 mM DTT (dithiothreitol). The inactivation time-courses were determined by withdrawing suitable aliquots at different time points to assay the remaining activity using the first time point as 100 % native protein. An equation describing a single exponential decay with a rate constant of thermal unfolding $k_u$ was fitted to the data according to eqn (2) [30]:

$$-\ln(\%\text{native}/100\%) = k_u t \quad (2)$$

The free-energy of activation of thermal unfolding ($\Delta G_u$) was calculated according to Eyring theory as eqn (3) [30]:

$$\ln k_u = \ln\frac{K k_b T}{h} - \frac{\Delta G_u}{RT} \quad (3)$$

where $k_b$ is the Boltzmann constant; T, absolute temperature Kelvin; h, Plank's constant; R, the gas constant; and $K$ is the transmission factor, which was set to unity. The difference of free-energy of activation of the thermal denaturation between wild-type (wt) and each mutant (mut) protein ($\Delta\Delta G_u$) was calculated according to eqn (4) [30]:

$$\Delta\Delta G_u = \Delta G_u^{wt} - \Delta G_u^{mut} = -RT \times \ln\left(k_u^{wt}/k_u^{mut}\right) \quad (4)$$

Substitution of Equation 5:

$$\Delta G_u = \Delta H_u - T\Delta S_u \quad (5)$$

into eqn (3) yields eqn (6):

$$\ln\frac{k_u}{T} = \ln\frac{K \times k_b}{h} - \frac{\Delta H_u}{R} \times \frac{1}{T} + \frac{\Delta S_u}{R} \quad (6)$$

Both activation enthalpy $\Delta H_u$ and entropy $\Delta S_u$ were determined from the temperature dependence of $k_u$.

#### Temperature dependence of refolding *in vitro*

The *in vitro* refolding of the wild-type and Glu[64] mutant enzymes were monitored at different temperatures. Enzyme (20 $\mu$M) was first denatured in 4 M GdmCl (guanidinium chloride) in renaturation buffer (0.2 M potassium phosphate buffer, 1 mM EDTA and 5 mM DTT, pH 7.0) at room temperature (25 °C) for 30 min and then rapidly diluted (defining time 0) 1:40 (v/v) into renaturation buffer at 18, 25 and 33 °C. The final GdmCl concentration was 0.1 M during refolding. All refolding experiments were carried out by rapid addition of the denatured enzyme to renaturation buffer. The recovery of activity of the proteins was monitored as a function of time by withdrawal of appropriate aliquots of the renaturation mixture and immediately assaying for activity at 25 °C. Refolding rate constants were determined by nonlinear regression analysis of the experimental data by using SigmaPlot 2001 for Windows version 7.0 (SPSS). The refolding rates of all variants were independent, in the range 10 to 30 $\mu$M, of the protein concentration. At greater enzyme concentrations all

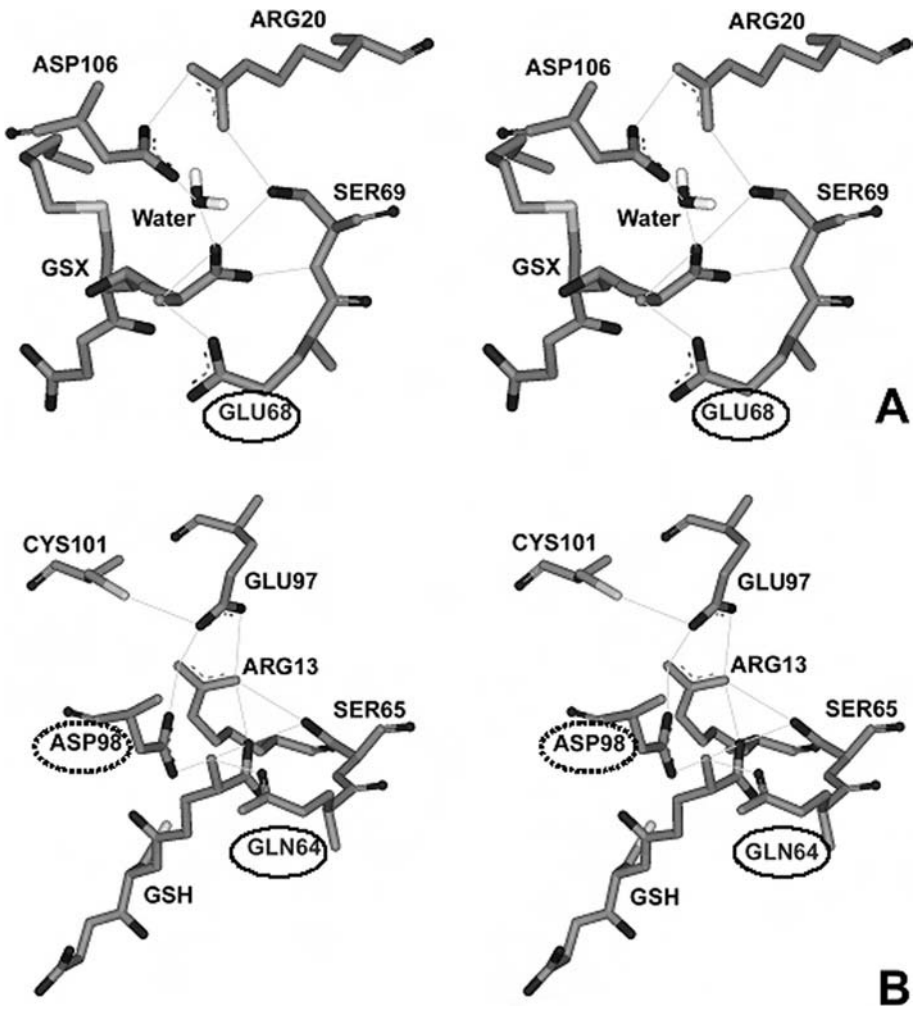


**Figure 2 Stereo views of examples of electron-sharing networks for type I (A) and type II (B) of GSTs**

Categorization is based on properties of the equivalent amino acid at position 64 and configuration of the electron-sharing network. (**A**) Electron-sharing network type I is composed of only one conserved acidic amino acid (circled), which forms an ionic interaction. Wheat Tau GSTI (PDB accession number 1GWC). (**B**) Electron-sharing network type II contains two strictly conserved polar and acidic residues (circled by solid and dotted lines respectively), which participate in an ionic bridge interaction. Human Pi hGSTP1-1 (PDB accession number 1PKW).

variants were characterized by reduced refolding yield. The values reported represent the means for three different experimental data sets. Under these conditions, an equation describing a single exponential reaction can be fitted to the data:

$$F(\mathrm{t}) = A[1 - \exp(-k_{\mathrm{ref}})] + B \quad (7)$$

where $F(\mathrm{t})$ is the activity at time t; $A$, the amplitude; $k_{\mathrm{ref}}$, the rate constant; and $B$, the reactivation value at time 0 [31]. The effect of mutation on the energy of the transition state of folding can be calculated using transition-state theory in a similar manner to that reported by Jackson et al. [32]. The stability of the transition state of a mutant protein relative to that of the wild-type is calculated from:

$$\Delta\Delta G_{\mathrm{ref}} = -RT \times \ln\left(k_{\mathrm{ref}}{}^{\mathrm{wt}} / k_{\mathrm{ref}}{}^{\mathrm{mut}}\right) \quad (8)$$

where $\Delta\Delta G_{\mathrm{ref}}$ is the difference in energy of the transition state of folding relative to the unfolded state between wild-type (wt) and mutant (mut) proteins and $k_{\mathrm{ref}}$, the rate constants of refolding [32].

## RESULTS AND DISCUSSION

A functionally conserved electron-sharing network can be observed in the same region for all GSTs, but with slightly different residue positions [22]. However, a primary sequence alignment of the known GST classes suggests that $Glu^{64}$ is one of a few residues that is functionally conserved in the GST superfamily. Observation of available crystal structures; adGSTD3-3, hGSTP1-1 (human Pi GST1), hGSTA1-1 (human Alpha GST1), rGSTM1-1 (rat Mu GST1), hGSTO1-1 (human Omega GST1), hGSTT2-2 (human Theta GST2), squid Sigma GST and wheat Tau GST, as well as consideration of the property of the equivalent residue at position 64, acidic or polar, suggests that the GST electron-sharing motif can be divided into two types (Figure 2). Electron-sharing network type I, consisting of GSTs from Delta, Theta, Omega, Pi and Tau classes, contain an acidic amino acid (glutamate or aspartate) at this position. The equivalent residue is the only amino acid in an acceptable distance range to form an ionic interaction between its own negatively charged side chain and the positively charged GSH glutamyl $\alpha$-amino (Figure 2A). On the other hand, electron-sharing network type II GSTs from the Alpha, Mu, Pi and Sigma classes have a polar amino acid (glutamine) side-chain

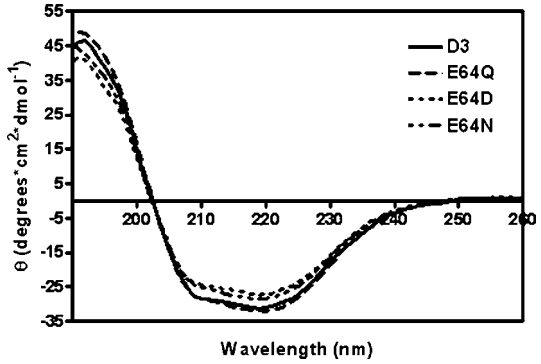


**Figure 3 Far-UV CD spectra of adGSTD3-3 and mutants**

CD spectra were measured in far-UV region from 190–260 nm. Spectra were recorded at a protein concentration of 0.3 mg/ml with cuvettes with a 2-$\mu$m path-length. D3, wild-type adGSTD3-3.

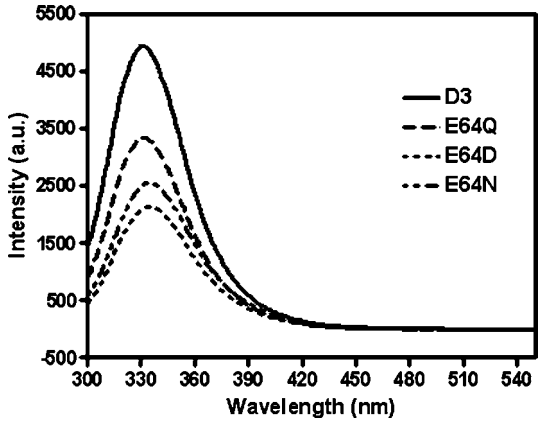


**Figure 4 Intrinsic fluorescence spectra of wild-type and mutant adGSTD3-3**

Intrinsic fluorescence emission spectra were measured with the excitation wavelength 295 nm. The $\lambda_{max}$ and the fluorescence intensity of emission spectra were analysed at a protein concentration of 0.2 mg/ml. The $\lambda_{max}$ are 331 nm for wild-type (D3), 332 nm for E64Q, 335 nm for E64D and 334 nm for E64N. The intensity is shown in arbitrary units. The results are means $\pm$ S.D. for experiments performed in triplicate.

that interacts directly with the GSH glutamyl $\alpha$-amino. In addition, type II networks have a strictly conserved acidic amino acid (Asp[98] in the Pi class, Asp[101] in the Alpha class, Asp[105] in the Mu class and Asp[97] in the Sigma class) that participates in an ionic interaction (Figure 2B). In the Pi class GSTs, replacement of this acidic residue (Asp[98] with asparagine) was shown to increase the p$K_a$ for GSH by approx. 0.5 pH unit [33]. These results suggest the importance of a negative charge involvement with the positively charged GSH glutamyl $\alpha$-amino to fulfil the function of the electron-sharing network in the ionization process [33]. Dividing the electron-sharing network into two types is supported by studies of binding, activation and ionization of GSH, including the fate of the thiol proton in Pi, Alpha, Mu and Delta class GSTs [23]. It has been reported that GST classes Pi, Alpha and Mu, which are classified as electron-sharing network type II GSTs, display similarities in the multi-step mechanism for binding of the substrate and also yield a similar fate for the thiol proton. The Delta class GST, which we propose belongs to electron-sharing network type I, shows a difference in proton extrusion that implies a different activation mechanism for GSH. Moreover, the modality of proton output is also preserved in Pi, Alpha and Mu class enzymes. This mechanistic difference suggests that Delta GST is distantly related to Pi, Alpha and Mu GSTs in evolutionary terms.

To investigate the role of the functionally conserved Glu[64] residue in adGSTD3-3, this residue was replaced with seven amino acids; alanine, leucine, valine, lysine, glutamine, aspartate or asparagine. Evidence suggested that the replacements were temperature-sensitive therefore protein expression was performed at 18, 25 and 37 °C. The E64A, E64L, E64V and E64K mutants were expressed as insoluble proteins at all temperatures. Attempts at refolding these four proteins were unsuccessful. The yields of the E64Q, E64D and E64N mutants were less than wild-type and clearly decreased with increasing temperature (results not shown). This probably reflects the fact that the E64Q, E64D and E64N molecules fail to achieve the native folding at near physiological temperatures. Therefore, proteins expressed at the more permissive temperature of 18 °C were utilized in this study.

In the present study, a structural role for Glu[64] for stability and folding was examined. The similarity of the far-UV CD spectra of all the Glu[64] mutants indicated that the secondary structure content of the proteins are essentially unaffected by the mutations (Figure 3). The intrinsic fluorescence spectra show differences between the wild-type and all of the Glu[64] mutants (Figure 4). The spectra of the Glu[64] mutants were slightly red-shifted compared with the wild-type protein ($\lambda_{max}$ at 331 nm) to give a $\lambda_{max}$ at 332 nm for E64Q, 335 nm for E64D and 334 nm for E64N. The normalized intensities of the fluorescence of the mutants were slightly less than that of the wild-type. Changes in amino acid side-chains around Trp[63] resulted in an alteration in fluorescence intensity, and a red-shifted spectrum is observed as the protein unfolds to random coil [34]. Consequently, the differences in both $\lambda_{max}$ and fluorescence intensity suggest that the mutation of Glu[64] causes the tryptophan residue to be more exposed to the solvent. Heat inactivation of wild-type and Glu[64] mutants was performed at different temperatures (Figure 5). Furthermore, the E64Q and E64N mutants were much more unstable than the wild-type or E64D mutant. It is important to note that the single Glu[64] replacement with polar residues (glutamine and asparagine) became unstable at a lower temperature than the negatively charged residues (wild-type and E64D) and their inactivation generated the formation of protein aggregates under the experimental conditions used. Thermal denaturation of all variants was irreversible, showing that inactivation kinetics could not be used to determine thermodynamic parameters at equilibrium. However, making use of the temperature dependence of the unfolding rate, the application of Eyring formalism provides the thermodynamic parameters of the activation barrier of the thermal denaturation [30]. The heat inactivation of all variants is described by straight lines in an Eyring plot. This indicates that the temperature dependence of both the unfolding activation enthalpy ($\Delta H$) and activation entropy ($\Delta S$) is negligible. The temperature dependence of $\Delta G$ is reflected in the slope of the linear fit, dependent on $\Delta H$. Table 1 summarizes the kinetic and thermodynamic constants for the activation barrier of thermal denaturation for the wild-type and Glu[64] mutant enzymes. The large energy changes of Glu[64] mutants compared with the wild-type ($\Delta\Delta H$) are almost completely compensated for by an accompanying reduction in $\Delta S$ (that is, $\Delta\Delta S$). At 42 °C, this corresponds to lower values of the unfolding free-energy for all the Glu[64] mutant enzymes ($\Delta\Delta G$). The Glu[64] mutants were remarkably more destabilized than the wild-type enzyme, especially for the polar amino acids glutamine and asparagine (Table 1). This corresponds to an unfolding free-energy difference ($\Delta\Delta G$) for the polar amino acid replacements compared with the wild-type, being greater

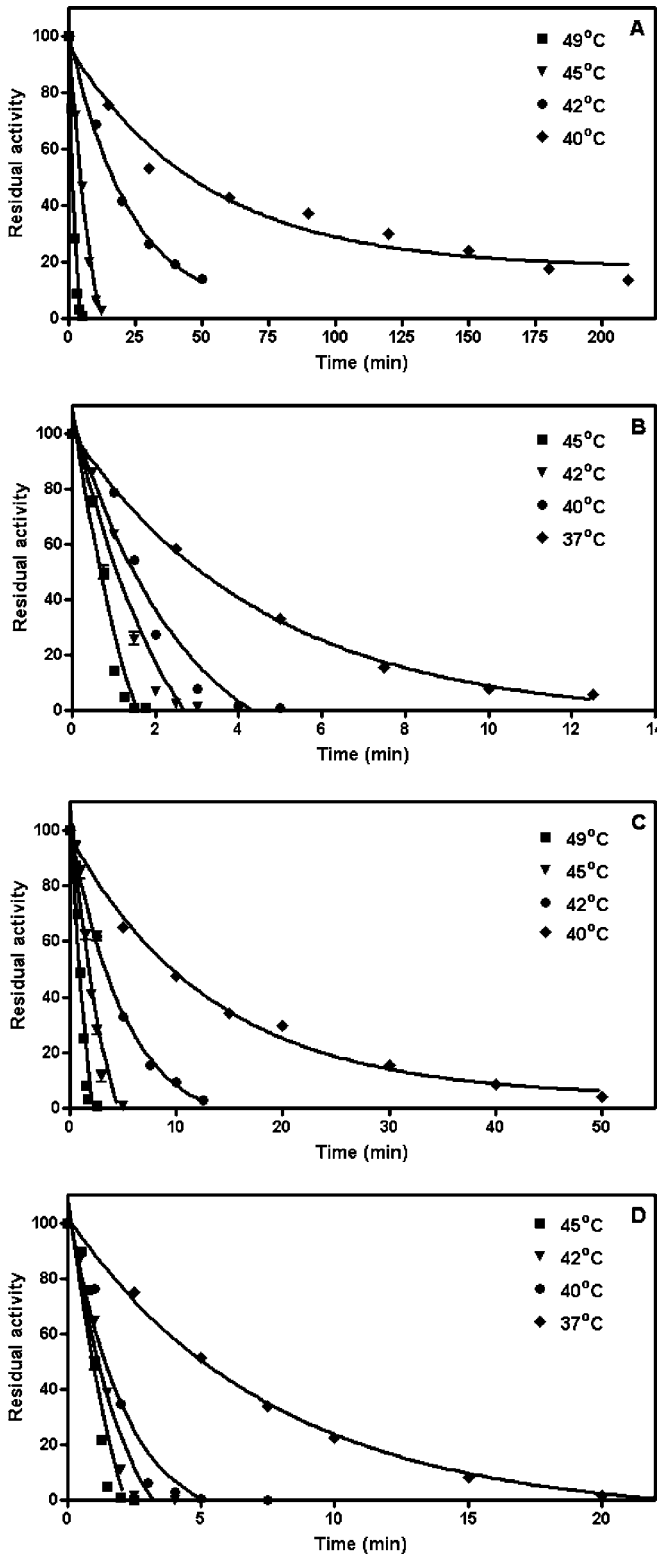


**Figure 5 Thermal stability of wild-type adGSTD3-3 (A), E64Q (B), E64D (C) and E64N (D) mutants at different temperatures**

Each enzyme (40 $\mu$M) was incubated at various temperatures in 0.1 M potassium phosphate buffer, pH 6.5, 1 mM EDTA and 5 mM DTT. Appropriate aliquots from an incubation mixture were assayed at 25 °C to monitor residual activity. The lines represent fits according to eqn (2), as described in the Materials and methods section.

than with the acidic residue aspartate. The Gibbs free-energy for the unfolding process of wild-type and Glu$^{64}$ mutants were comparable, with general estimations of Gibbs free-energy for small globular proteins based on the summation of increments of the different stabilizing forces that give values in the range 42–84 kJ/mol [35]. Due to the large decrease in activation enthalpy ($\Delta\Delta H$, 131–220 kJ/mol), the destabilizing effects of the Glu$^{64}$ mutants were clearly significant to the structural properties of the enzymes. In addition the magnitude of $T\Delta\Delta S$ at 42 °C, which is the energy difference from decreases in the entropy of the thermal unfolding pathway (198.4, 126.0 and 211.0 kJ/mol for E64Q, E64D and E64N respectively), indicates that major changes in the conformational freedom characterizes the denaturation of the wild-type protein compared with those occurring during the thermal inactivation of the Glu$^{64}$ mutants [36]. This means that the wild-type adGSTD3-3, because it is more rigid than the Glu$^{64}$ mutants, tolerates larger perturbations of its structure before the unfolding transition state is reached. The replacement of polar amino acids, both glutamine and asparagine, give greater values of all thermodynamic constants than for the acidic amino acids glutamate and aspartate. This data suggests that the negatively charged residue forming an ionic bridge interaction in this position plays an essential role for the overall stability of the protein. Recent studies proposed that Glu$^{64}$ is a critical residue involved in the determination of the direction of the polypeptide chain during folding [25]. One consequence of replacing Glu$^{64}$ with other amino acid residues results in a completely impaired folding property (for E64A, E64L, E64V and E64K) or temperature-sensitive folding (for E64Q, E64D and E64N). To test this hypothesis, reactivation yields of adGSTD3-3 and its mutants at different temperatures were determined. The denaturant 4 M GdmCl was sufficient to completely unfold 20 $\mu$M enzyme, as shown by CD spectrum (results not shown). The reactivation yields of the Glu$^{64}$ mutants were very different from the wild-type protein at increasing temperatures of refolding (Table 2 and Figure 6). The reactivation yield of the wild-type enzyme was unaffected by temperatures from 18–33 °C, whereas the yield of the mutants, although to different extents, decreased markedly with increasing temperature. All data sets were fit to a single exponential equation for the refolding kinetics (Figure 6). At each temperature, as shown in Table 2, the temperature-dependent refolding rates show a similar tendency in the wild-type and Glu$^{64}$ mutants that was expected, that is, the enzymes refold at higher temperature more rapidly than at lower temperature. The refolding rates of both E64Q and E64D mutants were slightly different from the wild-type at all temperatures. These differences in refolding rates reflect changes in free-energy of activation of folding for a mutation. Estimated free-energy values ($\Delta\Delta G_{ref}$) at 18 °C that were significantly different from zero indicate that interactions of the residue at position 64 toward neighbouring residues are present in the transition state of the reactivation process. The *in vitro* refolding experiments suggest that the thermal stability of the final structure of the mutants reflects differences in the conformational properties of a productive folding intermediate. Reactivation *in vitro* of all Glu$^{64}$ mutants was thermosensitive, and so the refolding yields of the Glu$^{64}$ mutants, although to different extents, decreased markedly with increasing temperature. The analysis of the reactivation at 18 °C indicates that amino acid replacement of Glu$^{64}$ destabilizes the transition of folding. It should be noted that a single exponential equation could be fitted to refolding data for all adGSTD3-3 variants indicating that no significant amount of intermediate is accumulated during the reactivation of wild-type and variants, and that none of the mutations had a major change on the refolding pathway. Upon

**Table 1 Kinetic and thermodynamic parameters for the activation barrier of thermal denaturation for wild-type and Glu[64] mutants of adGSTD3-3**

| Enzyme | $k_u$ (min$^{-1}$) | $k_u/k_{u,wt}$* | $\Delta G_u$* (kJ/mol) | $\Delta\Delta G_u$ (kJ/mol) | $\Delta H_u$† (kJ/mol) | $\Delta\Delta H_u$† (kJ/mol) | $\Delta S_u$† (kJ/mol · K) | $\Delta\Delta S_u$† (kJ/mol · K) |
|---|---|---|---|---|---|---|---|---|
| Wild-type | 0.040 ± 0.001 | 1 | 85.69 ± 0.09 | 0 | 439.00 ± 4.90 | 0 | 1.120 ± 0.015 | 0 |
| E64Q | 1.583 ± 0.028 | 39.58 | 76.08 ± 0.05 | 9.63 | 231.38 ± 13.02 | 207.62 | 0.490 ± 0.041 | 0.630 |
| E64D | 0.256 ± 0.008 | 6.40 | 80.85 ± 0.08 | 4.86 | 307.51 ± 1.28 | 131.49 | 0.720 ± 0.004 | 0.400 |
| E64N | 1.590 ± 0.045 | 39.75 | 76.07 ± 0.08 | 9.64 | 218.52 ± 10.92 | 220.48 | 0.450 ± 0.035 | 0.670 |

* From denaturation kinetics at 42 °C according to eqns 2 and 4.
† From temperature dependence of thermal unfolding (Eyring plot) according to eqn 6.

**Table 2 Kinetics of the reactivation and percentage recovery of wild-type adGSTD3-3 and Glu[64] mutants during refolding at different temperatures and changes in free energy of the transition state of folding at 18 °C**

Statistics performed using one-way ANOVA and Tukey–Kramer multiple comparisons test. Values significantly different from wild-type are shown by * $P < 0.001$. Nd, not determined, low enzymatic activity precluded performing this experiment.

| | 18 °C | | 25 °C | | 37 °C | | |
|---|---|---|---|---|---|---|---|
| Enzyme | $k_{ref}$ (min$^{-1}$) | % recovery | $k_{ref}$ (min$^{-1}$) | % recovery | $k_{ref}$ (min$^{-1}$) | % recovery | $\Delta\Delta G_{ref}$ at 18 °C (kJ/mol) |
| Wild-type | 0.169 ± 0.020 | 60.9 ± 0.4 | 0.518 ± 0.053 | 35.1 ± 3.4 | 0.957 ± 0.027 | 35.1 ± 0.6 | 0 |
| E64Q | 0.074 ± 0.003 | 63.8 ± 0.7 | 0.289 ± 0.004 | 40.0 ± 0.3 | 1.073 ± 0.124 | 10.6 ± 0.3 | −1.987 ± 0.371* |
| E64D | 0.059 ± 0.005 | 93.0 ± 6.5 | 0.242 ± 0.024 | 57.7 ± 1.1 | 0.981 ± 0.030 | 34.5 ± 1.3 | −2.521 ± 0.129* |
| E64N | Nd | Nd | Nd | Nd | Nd | Nd | Nd |

mutation of adGSTD3-3, rate constants decreased for all mutants (Table 2). This is because the removal of the negative charge or size decrease of the side-chain at this position destabilized the transition state and thereby increased the activation energy for folding. In particular, the $\Delta\Delta G_{ref}$ value for E64D is greater than E64Q, suggesting that the functional group size is important for the Glu[64] position, which contributes to stabilizing the transition state. Previous investigations of the equivalent residue, Glu[66], in PtGSTU1-1 (plant Tau class GST) demonstrated that alanine replacement made the enzyme unstable at 50 °C, retaining only about 15 % of its activity compared with 95 % for the wild-type enzyme [37]. In contrast, the reactivation yield of E66A was 2-fold greater than the wild-type. The effect of the mutation at this equivalent residue in PtGSTU1-1 was less than found in adGSTD3-3, an insect Delta class GST. This result might be explained by data for Glu[64] in adGSTD4-4, an alternatively spliced product derived from the same gene as adGSTD3-3. Glu[64] is not only located at the dimeric interface of the enzyme, but has also been identified as a 'lock' residue in the Delta class specific 'lock-and-key clasp' motif, which is not found in plant Tau class GST [38]. The lock-and-key motif, including the Delta class specific lock-and-key clasp motif, is located at the intersubunit interface and plays a crucial role in the structural stability of dimeric GSTs [39,40]. These data therefore confirm a critical structural role for the functionally conserved Glu[64] residue for both overall protein stability and initial folding process.

Steady-state kinetic constants were obtained with various concentrations of GSH and CDNB substrate. Michaelis–Menten kinetic analysis was performed using non-linear regression (Table 3). All of the mutations showed significantly increased $K_m$ values for GSH. Individually, the mutants; E64Q, E64D and E64N had values 26-, 34- and 29-fold greater than wild-type. Conversely, no significant changes were found in the $K_m$ values for CDNB substrate when compared with the wild-type enzyme. The differences in $k_{cat}$ values with CDNB observed for E64D and E64N decreased approximately 1.5- and 25-fold respectively. The kinetic studies of soluble Glu[64] mutant enzymes demonstrated that replacement with a glutamine residue, a similar size and property functional group, preserved the catalytic activity, whereas replacement with the slightly smaller amino acids aspartate and asparagine reduced $k_{cat}$, especially the arparagine replacement, which nearly abolished enzyme activity. This suggests that the volume of the amino acid at this position affects packing of the active-site, which directly impacts upon enzyme catalysis. However, all the mutants showed a substantially lower affinity (greater $K_m$) towards GSH indicating that the Glu[64] position impacts upon the binding of GSH possibly through active-site rearrangement. Catalytic efficiency can be related to the difference in free-energy change for formation of transition states in the mutant and wild-type enzymes ($\Delta\Delta G$), as calculated from eqn (9) [41]:

$$\Delta\Delta G = -RT \times \ln\left(k_{cat}/K_m^{GSH}\right)_{mut} / \left(k_{cat}/K_m^{GSH}\right)_{wt} \quad (9)$$

These calculated values are 8.03 kJ/mol for E64Q, 9.94 kJ/mol for E64D and 16.33 kJ/mol for E64N at 25 °C, indicative of a decreased stabilization of the transition state for the Glu[64] mutations. Stabilization of the transition state may occur through a pre-organized active-site contributing to catalysis through multiple mechanisms: binding interaction with GSH, activation of GSH by thiol deprotonation or nucleophilic attack at the electrophilic centre ($\sigma$-bond formation) by the thiolate. Deficiency in the pre-organized environment (the changes that occur along the reaction pathway from reactants to the transition state) would decrease the rate of catalysis by incompletely providing a stabilization of the transition state [42]. Therefore, the effect on the rate-limiting step in the catalytic mechanism was examined. The pH dependence of $k_{cat}/K_m^{CDNB}$ reflects a kinetically relevant ionization of the GST–GSH complex. Therefore, an apparent p$K_a$ value of 6.36 was determined for the wild-type adGSTD3-3. To differentiate the influence of the functional group of Glu[64] on the GSH thiol ionization, the p$K_a$ values for Glu[64] mutants were measured by this kinetic approach (Table 3). An increased p$K_a$ for bound GSH of approx. 0.6 and 1 pH unit greater than that found for wild-type were observed for the E64Q and E64N mutants. It has been shown previously that a crucial function of the electron-sharing

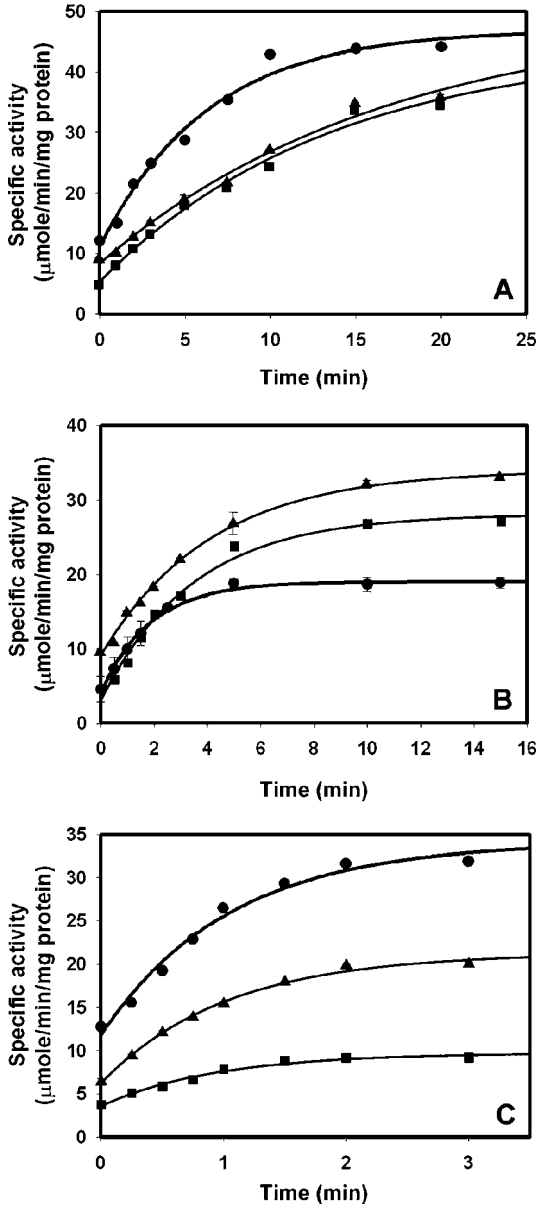


**Figure 6 Kinetics of reactivation of wild-type adGSTD3-3 (●), E64Q (■) and E64D (▲) during refolding at different temperatures: 18 °C (A), 25 °C (B) and 33 °C (C)**

Purified enzyme (20 $\mu$M), heterologously expressed at 18 °C, was first denatured in 4 M GdmCl for 30 min. This denaturant concentration was sufficient to completely unfold the proteins, as indicated by the loss of secondary structure shown by CD. Successive aliquots of unfolded enzyme were diluted (defining time 0) 1:40 into renaturation buffer at the different temperatures. The final GdmCl concentration was 0.1 M during the refolding. Appropriate aliquots from this incubation mixture were immediately assayed for catalytic activity at 25 °C.

network is to lower the p$K_a$ of the thiol group of the bound GSH [22]. Our results show that Glu$^{64}$ replacement with the polar amino acids glutamine and asparagine increased the p$K_a$ values by about 0.5–1.0 pH unit. This consequence appears to be due to the deletion of the negative charge, resulting in loss of ionic interaction within the electron-sharing network. This is supported by the replacement of the critical glutamate residue with the negatively charged aspartate, which has no affect on the ionization process. Therefore, an acidic amino acid in this position is essential to form an ionic interaction to fulfil the function of the electron-sharing network in the ionization process. However, the formation of a $\sigma$-complex intermediate in the enzyme-catalysed reaction was affected by the replacement with glutamine and aspartate. It is well established that the bimolecular nucleophilic substitution reactions proceed through a $\sigma$-complex intermediate [43]. Thus, the rate-limiting formation of a spontaneous $\sigma$-complex intermediate can be increased by replacement of chlorine in the CDNB molecule with the more electronegative fluorine. The ratio of the catalytic rate of GSH with FDNB and CDNB was comparable to the ratio of the second-order rate constants for a spontaneous uncatalysed reaction. That is, $k_{cat}^{FDNB}/k_{cat}^{CDNB} = 40$ is similar to $k_c^{FDNB}/k_c^{CDNB} = 47$, which indicates that the $\sigma$-complex formation is the rate-limiting step. Although the $k_{cat}^{FDNB}/k_{cat}^{CDNB}$ of all Glu$^{64}$ mutants reflected varying insensitivity to the nature of the leaving group, there were two mutants E64Q and E64D that exhibited significant differences in the catalytic efficiency ($k_{cat}/K_m$) (Table 4). For the E64N mutant, it appears that an alteration of the relative turn-over number is a consequence of changes in binding affinity towards different substrate leaving groups rather than a reflection of the rate of $\sigma$-complex formation. Differences in relative catalytic efficiency ($k_{cat}/K_m$) for the fluoride/chloride leaving group replacement may not strongly support the idea that the rate-determining step to $\sigma$-complex formation for E64Q and E64D was changed. Although it appears that transition state stability of the enzyme–intermediate complex, influenced by electron density and distribution in the $\sigma$-complex, was partially altered by these two amino acid replacements [43,44].

**Table 3 Steady-state kinetic constants and p$K_a$ values for the thiol group of GSH of wild-type and mutants of adGSTD3-3 for the CDNB conjugation reaction at pH 6.5 and 25 °C**

The enzyme activities were measured at various concentrations of CDNB and GSH in 0.1 M phosphate buffer pH 6.5. The p$K_a$ was obtained by using 0.1 M sodium acetate buffers (from pH 5.0 to 5.5) and 0.1 M potassium phosphate buffer (from pH 6.0 to 8.5).The reaction was monitored at 340 nm, $\varepsilon$ 9600 $M^{-1}cm^{-1}$. Statistics were performed using one-way ANOVA and Tukey–Kramer multiple comparisons test. Values significantly different from wild-type are shown by * $P < 0.001$. The wild-type values have been reported previously [25].

| Enzyme | $k_{cat}$ ($s^{-1}$) | $K_m^{GSH}$ (mM) | $K_m^{CDNB}$ (mM) | $k_{cat}/K_m^{GSH}$ ($s^{-1}$/mM) | $k_{cat}/K_m^{CDNB}$ ($s^{-1}$/mM) | p$K_a$ |
|---|---|---|---|---|---|---|
| Wild-type | 35.4 | 0.27 ± 0.05 | 0.14 ± 0.01 | 131 | 246 | 6.36 ± 0.11 |
| E64Q | 36.3 | 7.10 ± 0.28* | 0.43 ± 0.03 | 5.11 | 83.6 | 6.97 ± 0.14* |
| E64D | 21.6 | 9.12 ± 0.20* | 0.28 ± 0.01 | 2.37 | 75.8 | 6.42 ± 0.12 |
| E64N | 1.4 | 7.89 ± 0.19* | 0.33 ± 0.01 | 0.18 | 4.4 | 7.37 ± 0.07* |

**Table 4 Effect of fluoride/chloride leaving group substitution on the rate of catalysis**

The ratios of kinetic constants for the conjugation reaction catalyzed by adGSTD3-3 enzymes for GSH with CDNB or FDNB as co-substrates were calculated at pH 6.5. Statistics performed using one-way ANOVA and Tukey–Kramer multiple comparisons test. Values significantly different from wild-type are shown by * $P < 0.001$. The wild-type values have been reported previously [25].

| Enzyme | $k_{cat}^{FDNB}/k_{cat}^{CDNB}$ | $(k_{cat}/K_m)^{FDNB}/(k_{cat}/K_m)^{CDNB}$ |
|---|---|---|
| Wild-type | 2.40 ± 0.08 | 6.72 ± 0.34 |
| E64Q | 6.97 ± 0.24* | 14.36 ± 1.22* |
| E64D | 8.40 ± 0.08* | 10.31 ± 0.38* |
| E64N | 5.92 ± 0.05* | 6.58 ± 0.05 |

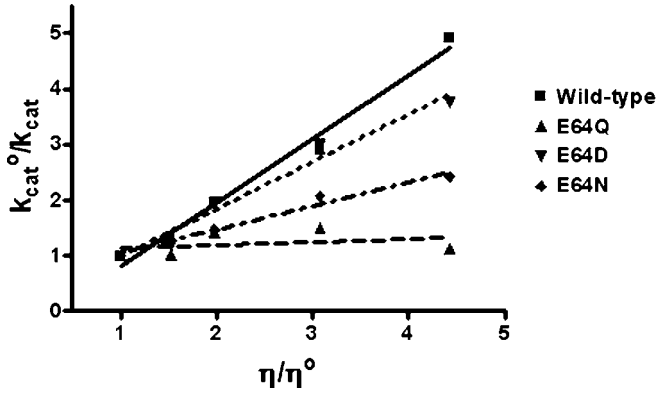


**Figure 7 Viscosity effect on kinetic parameters of wild-type adGSTD3-3 and mutant enzymes**

The effect of viscosity on kinetic constants was assayed by using 0.1 M potassium phosphate buffer, pH 6.5, with various glycerol concentrations. Dependence of the reciprocal of the relative turn-over number ($k_{cat}^{o}/k_{cat}$) on the relative viscosity ($\eta/\eta^{o}$) for CDNB as a co-substrate. The experiment was performed in triplicate and the lines were calculated by linear regression analysis. The slopes of the linear regression lines are $1.14 \pm 0.01$ for wild-type, $0.05 \pm 0.01$ for E64Q, $0.85 \pm 0.01$ for E64D and $0.42 \pm 0.02$ for E64N.

The effect of viscosity on kinetic parameters was examined to elucidate the rate-limiting step in the catalytic reaction. A decrease in the rate constant with increasing medium viscosity should reflect the weight of diffusion events on catalysis [45]. It would indicate that the rate-limiting step is related to diffusion-controlled motions of the protein or the dissociation of the product. A plot of the reciprocal of the relative catalytic constant ($k_{cat}^{o}/k_{cat}$) against the relative viscosity ($\eta/\eta^{o}$) should be linear. The slope should be equal to unity when the product release or structural transition is limited by a strictly diffusional barrier. If the slope approaches zero either the chemistry or another non-diffusion barrier is rate-limiting. For wild-type adGSTD3-3, a plot of the inverse relative rate constant ($k_{cat}^{o}/k_{cat}$) versus the relative viscosity ($\eta/\eta_{o}$) gives a linear dependence with a slope ($1.14 \pm 0.01$) very close to unity (Figure 7). In contrast the E64Q mutant enzyme yields plots that are fully viscosity independent, with a slope approaching zero ($0.05 \pm 0.01$). The other mutants, E64D and E64N, exhibited $k_{cat}$ values with different degrees of viscosity dependence compared with the wild-type enzyme. The viscosity experiment showed that the rate-limiting step catalysed by adGSTD3-3 is a non-physical step (Figure 7). However, structural alterations in the Glu[64] mutants decreased the viscosity effects on the enzyme to intermediate values ($0 < \text{slope} < 1$), especially for the replacement with the polar residues glutamine and asparagine. This indicates that the rate-limiting step is not strictly dependent on a diffusion barrier or other viscosity-dependent motions and that conformational changes of the engineered proteins contribute to the rate-limiting step [45]. This suggests that the structural flexibility of functionally important regions of the engineered enzymes have been altered. Previously, we have observed [22] that changing the residues in the electron-sharing network can influence the topology of the active-site, which affects both the catalytic mechanism as well as the structural maintenance of the enzyme. The results of the present study demonstrate that the functionally conserved Glu[64], which is now identified as being part of the electron-sharing network, impacts upon enzyme catalysis not only through its negative charge but also through structural effects.

In conclusion, the results of the present paper, as well as the high level of functional conservation of the residue at position 64 among all classes of GSTs supports the hypothesis that Glu[64] is part of a functionally conserved electron-sharing network. The present paper now extends the network identified previously to include three critical residues that form ionic bridge interactions. These are between a negatively charged/polar active site residue (glutamate, aspartate or glutamine), a positively charged GSH glutamyl $\alpha$-amino, a negatively charged GSH glutamyl $\alpha$-carboxylate, a positively charged active-site residue (primarily arginine) and a negatively charged active-site residue (glutamate or aspartate) stabilized by hydrogen-bonding networks with surrounding residues (serine, threonine and/or water mediated contact). Glu[64] in the electron-sharing network contributes to the function of this motif and the base-assisted deprotonation model which are essential for the GSH ionization process in the catalytic mechanism. However, this residue also appears to affect additional steps in the enzyme catalytic strategy including binding of GSH to the enzyme active site, nucleophilic attack by thiolate at the electrophilic centre and product formation. Therefore, the Glu[64] position also appears to impact upon catalysis through roles in both initial folding and structural maintenance.

This work was supported by the Thailand Research Fund. P.W. was supported by a Royal Golden Jubilee Scholarship and a scholarship from the Senior Research Fellowship of Professor Emeritus Sakol Panyim.

## REFERENCES

1 Sheehan, D., Meade, G., Foley, V. M. and Dowd, C. A. (2001) Structure, function and evolution of glutathione transferases: implications for classification of non-mammalian members of an ancient enzyme superfamily. Biochem. J. **360**, 1–16
2 Cho, S.-G., Lee, Y. H., Park, H.-S., Ryoo, K., Kang, K. W., Park, J., Eom, S.-J., Kim, M. J., Chang, T.-S., Choi, S.-Y. et al. (2001) Glutathione *S*-transferase Mu modulates the stress-activated signals by suppressing apoptosis signal-regulating kinase 1. J. Biol. Chem. **276**, 12749–12755
3 Gate, L., Majumdar, R. S., Lunk, A. and Tew, K. D. (2004) Increased myeloproliferation in glutathione *S*-transferase $\pi$ deficient mice is associated with a deregulation of JNK and janus kinase/STAT. J. Biol. Chem. **279**, 8608–8616
4 Ronai, Z. (2001) Coordinated regulation of stress kinases by GSTp. Chem. Biol. Interact. **133**, 285–286
5 Hayes, J. D. and Pulford, D. J. (1995) The glutathione S-transferase supergene family: regulation of GST and the contribution of the isoenzymes to cancer chemoprotection and drug resistance. CRC Crit. Rev. Biochem. Mol. Biol. **30**, 445–600
6 Mannervik, B. and Danielson, U. H. (1988) Glutathione transferases: structure and catalytic activity. CRC Crit. Rev. Biochem. **23**, 283–337
7 Armstrong, R. N. (1997) Structure, catalytic mechanism, and evolution of the glutathione transferases. Chem. Res. Toxicol. **10**, 2–18
8 Habig, W. H., Pabst, M. J. and Jakoby, W. B. (1974) Glutathione *S*-transferases. The first enzymatic step in mercapturic acid formation. J. Biol. Chem. **249**, 7130–7139
9 Ahmad, H., Wilson, D. E., Fritz, R. R., Singh, S. V., Medh, R. D., Nagle, G. T., Awasthi, Y. C. and Kurosky, A. (1990) Primary and secondary structural analyses of glutathione S-transferase $\pi$ from human placenta. Arch. Biochem. Biophys. **278**, 398–408
10 Board, P., Baker, R. T., Chelvanayagam, G. and Jermiin, L. S. (1997) Zeta, a novel class of glutathione transferases in a range of species from plants to humans. Biochem. J. **328**, 929–935
11 Mannervik, B., Ålin, P., Guthenberg, C., Jensson, H., Tahir, M. K., Warholm, M. and Jörnvall, H. (1985) Identification of three classes of cytosolic glutathione transferase common to several mammalian species: correlation between structural data and enzymatic properties. Proc. Natl. Acad. Sci. U.S.A. **82**, 7202–7206
12 Mannervik, B., Awasthi, Y. C., Board, P. G., Hayes, J. D., Di Ilio, C., Ketterer, B., Listowsky, I., Morgenstern, R., Muramatsu, M., Pearson, W. R. et al. (1992) Nomenclature for human glutathione transferases. Biochem. J. **282**, 305–306
13 Meyer, D. J., Coles, B., Pemble, S. E., Gilmore, K. S., Fraser, G. M. and Ketterer, B. (1991) Theta, a new class of glutathione transferases purified from rat and man. Biochem. J. **274**, 409–414
14 Motoyama, N. and Dauterman, W. C. (1978) Molecular weight, subunits, and multiple forms of glutathione S-transferase from the house fly. Insect Biochem. **8**, 337–348

15 Pemble, S. E. and Taylor, J. B. (1992) An evolutionary perspective on glutathione transferases inferred from class-Theta glutathione transferase cDNA sequences. Biochem. J. **287**, 957–963
16 Ding, Y., Ortelli, F., Rossiter, L. C., Hemingway, J. and Ranson, H. (2003) The *Anopheles gambiae* glutathione transferase supergene family: annotation, phylogeny and expression profiles. BMC Genomics **4**, 35–50
17 Wilce, M. C. J. and Parker, M. W. (1994) Structure and function of glutathione S-transferases. Biochim. Biophys. Acta **1205**, 1–18
18 Armstrong, R. N., Rife, C. and Wang, Z. (2001) Structure, mechanism and evolution of thiol transferases. Chem. Biol. Interact. **133**, 167–169
19 Caccuri, A. M., Ascenzi, P., Antonini, G., Parker, M. W., Oakley, A. J., Chiessi, E., Nuccetelli, M., Battistoni, A., Bellizia, A. and Ricci, G. (1996) Structural flexibility modulates the activity of human glutathione transferase P1-1. Influence of a poor co-substrate on dynamics and kinetics of human glutathione transferase. J. Biol. Chem. **271**, 16193–16198
20 Caccuri, A. M., Antonini, G., Nicotra, M., Battistoni, A., Lo Bello, M., Board, P. G., Parker, M. W. and Ricci, G. (1997) Catalytic mechanism and role of hydroxyl residues in the active site of theta class glutathione S-transferases. Investigation of Ser-9 and Tyr-113 in a glutathione S-transferase from the Australian sheep blowfly, *Lucilia cuprina*. J. Biol. Chem. **272**, 29681–29686
21 Gustafsson, A., Pettersson, P. L., Grehn, L., Jemth, P. and Mannervik, B. (2001) Role of the glutamyl $\alpha$-carboxylate of the substrate glutathione in the catalytic mechanism of human glutathione transferase A1-1. Biochemistry **40**, 15835–15845
22 Winayanuwattikun, P. and Ketterman, A. J. (2005) An electron-sharing network involved in the catalytic mechanism is functionally conserved in different glutathione transferase classes. J. Biol. Chem. **280**, 31776–31782
23 Caccuri, A. M., Antonini, G., Board, P. G., Parker, M. W., Nicotra, M., Lo Bello, M., Federici, G. and Ricci, G. (1999) Proton release on binding of glutathione to Alpha, Mu and Delta class glutathione transferases. Biochem. J. **344**, 419–425
24 Tan, K.-L., Chelvanayagam, G., Parker, M. W. and Board, P. G. (1996) Mutagenesis of the active site of the human Theta-class glutathione transferase GSTT2-2: catalysis with different substrates involves different residues. Biochem. J. **319**, 315–321
25 Winayanuwattikun, P. and Ketterman, A. J. (2004) Catalytic and structural contributions for glutathione binding residues in a delta class glutathione S-transferase. Biochem. J. **382**, 751–757
26 Jirajaroenrat, K., Pongjaroenkit, S., Krittanai, C., Prapanthadara, L. and Ketterman, A. J. (2001) Heterologous expression and characterization of alternatively spliced glutathione *S*-transferases from a single *Anopheles* gene. Insect Biochem. Mol. Biol. **31**, 867–875
27 Bradford, M. M. (1976) A rapid and sensitive method for the quantitation of microgram quantities of protein utilizing the principle of protein-dye binding. Anal. Biochem. **72**, 248–254
28 Caccuri, A. M., Ascenzi, P., Lo Bello, M., Federici, G., Battistoni, A., Mazzetti, P. and Ricci, G. (1994) Are the steady state kinetics of glutathione transferase always dependent on the deprotonation of the bound glutathione? New insights in the kinetic mechanism of GST P1-1. Biochem. Biophys. Res. Commun. **200**, 1428–1434
29 Wolf, A. V., Brown, M. G. and Prentiss, P. G. (1985) Handbook of Chemistry and Physics, CRC Press, Boca Raton
30 Kong, G. K. W., Polekhina, G., McKinstry, W. J., Parker, M. W., Dragani, B., Aceto, A., Paludi, D., Principe, D. R., Mannervik, B. and Stenberg, G. (2003) Contribution of glycine 146 to a conserved folding module affecting stability and refolding of human glutathione transferase P1-1. J. Biol. Chem. **278**, 1291–1302
31 Stenberg, G., Dragani, B., Cocco, R., Principe, D. R., Mannervik, B. and Aceto, A. (2001) A conserved 'hydrophobic staple motif' plays a crucial role in the refolding of human glutathione transferase P1-P1. Chem. Biol. Interact. **133**, 49–50
32 Jackson, S. E., el Masry, N. and Fersht, A. R. (1993) Structure of the hydrophobic core in the transition state for folding of chymotrypsin inhibitor 2: a critical test of the protein engineering method of analysis. Biochemistry **32**, 11270–11278
33 Widersten, M., Kolm, R. H., Björnestedt, R. and Mannervik, B. (1992) Contribution of five amino acid residues in the glutathione binding site to the function of human glutathione transferase P1-1. Biochem. J. **285**, 377–381
34 Dirr, H. W. and Wallace, L. A. (1999) Role of the C-terminal helix 9 in the stability and ligandin function of class a glutathione transferase A1-1. Biochemistry **38**, 15631–15640
35 Jones, M. N. (1979) In Biochemical Thermodynamics (Studies in Modern Thermodynamics). (Jones, M. N., ed.), pp. 75–115, Elsevier, Oxford
36 Haynie, D. T. (2001) Statistical thermodynamics. In Biological thermodynamics, pp. 185–222, Cambridge University Press, Cambridge
37 Zeng, Q.-Y. and Wang, X.-R. (2005) Catalytic properties of glutathione-binding residues in a $\tau$ class glutathione transferase (PtGSTU1) from *Pinus tabulaeformis*. FEBS Lett. **579**, 2657–2662
38 Wongsantichon, J. and Ketterman, A. J. (2006) An intersubunit lock-and-key 'clasp' motif in the dimer interface of delta class glutathione transferase. Biochem. J. **394**, 135–144
39 Sayed, Y., Wallace, L. A. and Dirr, H. W. (2000) The hydrophobic lock-and-key intersubunit motif of glutathione transferase A1-1: implications for catalysis, ligandin function and stability. FEBS Lett. **465**, 169–172
40 Stenberg, G., Abdalla, A.-M. and Mannervik, B. (2000) Tyrosine 50 at the subunit interface of dimeric human glutathione transferase P1-1 is a structural key residue for modulating protein stability and catalytic function. Biochem. Biophys. Res. Commun. **271**, 59–63
41 Dirr, H. W., Little, T., Kuhnert, D. C. and Sayed, Y. (2005) A conserved N-capping motif contributes significantly to the stabilisation and dynamics of the C-terminal region of class alpha glutathione transferases. J. Biol. Chem. **280**, 19480–19487
42 Garcia-Viloca, M., Gao, J., Karplus, M. and Truhlar, D. G. (2004) How enzymes work: analysis by modern rate theory and computer simulations. Science **303**, 186–195
43 Chen, W.-J., Graminski, G. F. and Armstrong, R. N. (1988) Dissection of the catalytic mechanism of isozyme 4–4 of glutathione S-transferase with alternative substrates. Biochemistry **27**, 647–654
44 Graminski, G. F., Zhang, P., Sesay, M. A., Ammon, H. L. and Armstrong, R. N. (1989) Formation of the 1-(*S*-glutathionyl)-2,4,6-trinitrocyclohexadienate anion at the active site of glutathione *S*-transferase: evidence for enzymic stabilization of $\sigma$-complex intermediates in nucleophilic aromatic substitution reactions. Biochemistry **28**, 6252–6258
45 Johnson, W. W., Liu, S., Ji, X., Gilliland, G. L. and Armstrong, R. N. (1993) Tyrosine 115 participates both in chemical and physical steps of the catalytic mechanism of a glutathione S-transferase. J. Biol. Chem. **268**, 11508–11511

Received 16 August 2006/19 October 2006; accepted 14 November 2006
Published as BJ Immediate Publication 14 November 2006, doi:10.1042/BJ20061253

BJ www.biochemj.org

BJ Structure

Biochem. J. (2007) **401**, 635–644 (Printed in Great Britain) doi:10.1042/BJ20060603

**Reprint 3** **635**

# Differences in the subunit interface residues of alternatively spliced glutathione transferases affects catalytic and structural functions

Juthamart PIROMJITPONG, Jantana WONGSANTICHON and Albert J. KETTERMAN[1]

Institute of Molecular Biology and Genetics, Mahidol University, Salaya Campus, Nakhon Pathom 73170, Thailand

GSTs (glutathione transferases) are multifunctional widespread enzymes. Currently there are 13 identified classes within this family. Previously most structural characterization has been reported for mammalian Alpha, Mu and Pi class GSTs. In the present study we characterize two enzymes from the insect-specific Delta class, adGSTD3-3 and adGSTD4-4. These two proteins are alternatively spliced products from the same gene and have very similar tertiary structures. Several major contributions to the dimer interface area can be separated into three regions: conserved electrostatic interactions in region 1, hydrophobic interactions in region 2 and an ionic network in region 3. The four amino acid side chains studied in region 1 interact with each other as a planar rectangle. These interactions are highly conserved among the GST classes, Delta, Sigma and Theta. The hydrophobic residues in region 2 are not only subunit interface residues but also active site residues. Overall these three regions provide important contributions to stabilization and folding of the protein. In addition, decreases in yield as well as catalytic activity changes, suggest that the mutations in these regions can disrupt the active site conformation which decreases binding affinity, alters kinetic constants and alters substrate specificity. Several of these residues have only a slight effect on the initial folding of each subunit but have more influence on the dimerization process as well as impacting upon appropriate active site conformation. The results also suggest that even splicing products from the same gene may have specific features in the subunit interface area that would preclude heterodimerization.

Key words: *Anopheles dirus*, glutathione transferase (GST), hydrophobic interaction, subunit interface.

## INTRODUCTION

GSTs (glutathione transferases; EC 2.5.1.18) are a supergene family of multifunctional enzymes which are widely distributed in nature and found in most aerobic eukaryotes and prokaryotes. The dimeric cytosolic GSTs catalyse reactions with a broad range of substrates and play an essential role in detoxification of endogenous and xenobiotic compounds [1,2]. The dimerization of the GSTs not only contributes to stabilization of the subunit tertiary structure, but also allows for the construction of a fully functional active site [3]. Although tertiary structures of all classes of GSTs are similar, dimerization is highly specific and is thought to occur only between subunits within the same class [4,5].

The structural features at the dimer interface of the GSTs suggest at least two major subunit interaction areas [6]. The first area is the predominantly hydrophobic interaction at the outer ends of the interface called a hydrophobic 'lock-and-key' (also referred to as a 'ball-and-socket') motif which is formed by the insertion of an aromatic residue from domain I of one subunit into a 'lock' of five residues of domain II in the other subunit [6–9]. The second major subunit interaction area is the symmetry axis interactions at the 2-fold axis of the protein which show highly conserved electrostatic interactions at one edge of the subunit interface and a variety of interactions along the interface depending on the GST class. The *Anopheles dirus* mosquito is an important malaria vector in South East Asia. From an *A. dirus* genomic library, a 7.5 kb fragment containing the adgst1AS1 gene (*A. dirus* alternatively spliced GST gene) was identified [10]. This gene contains six exons that encode four Delta class GSTs, adGSTD1-1, 2-2, 3-3 and 4-4, which possess 61–77 % amino acid identity compared among themselves. Previously these proteins had been named adGST1-1, 1-2, 1-3 and 1-4, according to insect GST nomenclature in use (that is, insect class 1-protein 1, 2, 3 and 4 respectively). However, to be in alignment with a proposed universal GST nomenclature, the proteins were renamed adGSTD1-1, adGSTD2-2, adGSTD3-3 and adGSTD4-4 respectively [11,12]. The subunit number remains the same, since subunits were enumerated as they were initially discovered, 'D' refers to GST Delta class and '4-4' refers to the homodimeric isoenzyme. These four GSTs share an untranslated exon 1 and a translated exon 2 coding for 45 amino acids at the N-terminus but vary between four different exon 3 sequences (exons 3A–3D). The arrangement of each exon is similar to the aggst1$\alpha$ gene from *A. gambiae,* the major malaria vector in Africa, with approx. 79 % nucleotide identity for the two genes [13]. In *A. dirus*, although four splice products are encoded from the same gene, the enzymes possess distinct enzyme kinetic properties for substrates, inhibitors, including insecticides, as well as physical properties such as stability [14,15]. Although two splice products, adgstD3-3 (PDB accession number: 1JLV) and adgstD4-4 (PDB accession number: 1JLW), have very similar tertiary structures when aligned, the amino acid identity is only 68 % [16].

When compared with human Alpha, Mu and Pi classes, the dimer interfaces of both Delta class isoenzymes are more extensively hydrophilic. Although lacking the previously identified hydrophobic 'lock-and-key' motif (a conserved motif in human Alpha, Mu and Pi classes), the Delta class does possess a 'Clasp' motif with a similar function [17]. In addition to this motif, there are nine amino acids making major contributions to the interactions within this interface area, which can be separated into three regions: conserved electrostatic interactions in region

Abbreviations used: ANS, 8-anilino-1-naphthalene sulfonate; CDNB, 1-chloro-2,4-dinitrobenzene; DCNB, 1,2-dichloro-4-nitrobenzene; EA, ethacrynic acid; GST, glutathione transferase; PNBC, p-nitrobenzyl chloride; PNPB, p-nitrophenethyl bromide.

[1] To whom correspondence should be addressed (email albertketterman@yahoo.com).

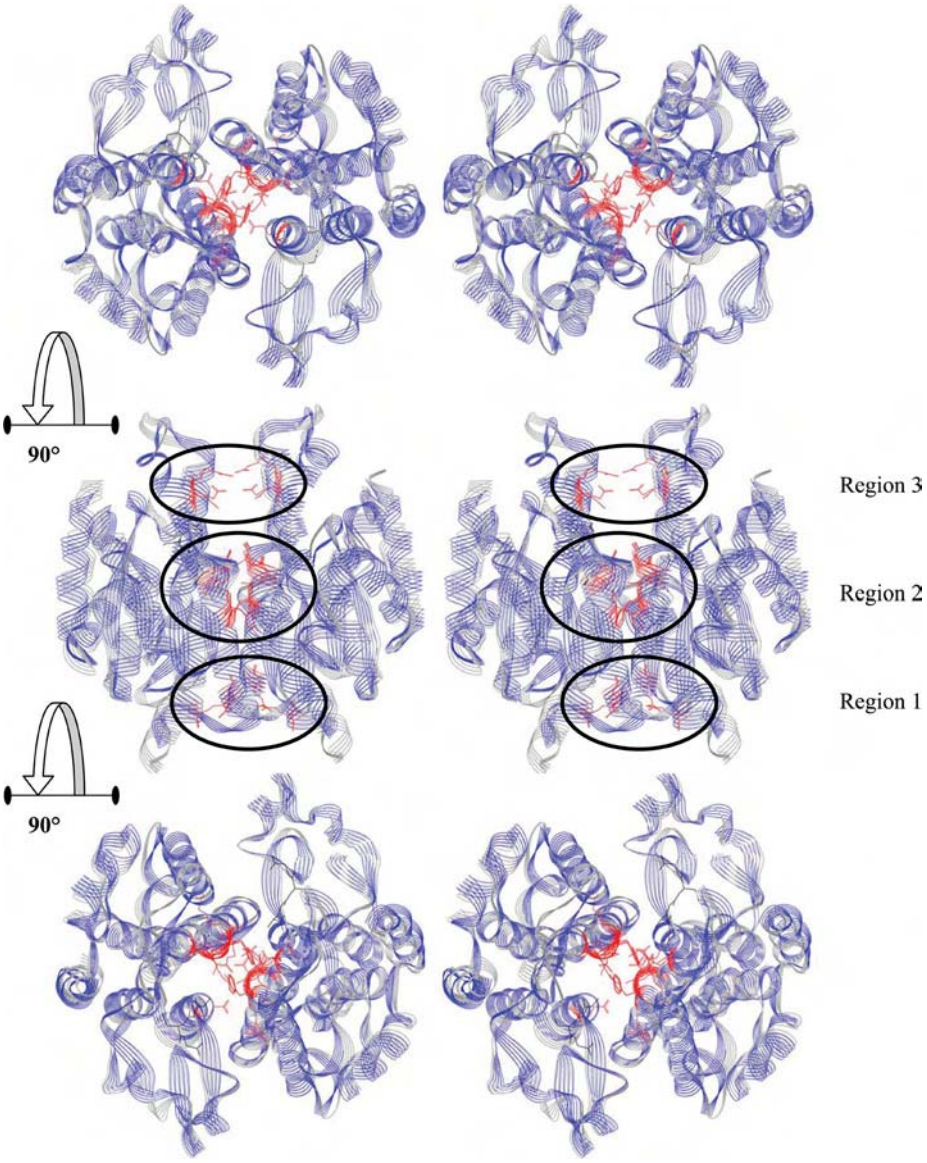


**Figure 1 The three regions of the interface characterized in the present study**

The two GST proteins are carbon backbone aligned with the adGSTD3-3 secondary structure wire ribbon shown in blue and the adGSTD4-4 secondary structure ribbon shown in grey. The GSH in the two active sites is shown as a black stick; the residues engineered in the present study are shown in red. The top panel is a stereo view looking at the 2-fold axis from the side opposite to the active sites. The middle panel shows the proteins rotated 90°, to show the position of the studied interface residues down the length of $\alpha$-helices 3 and 4. The bottom panel shows the proteins rotated a further 90° and looking down upon the 2-fold axis on to the active sites. The Figure was created using Accelrys DS ViewerPro 5.0.

1, hydrophobic interactions in region 2 and an ionic network in region 3 (Figure 1).

The conserved electrostatic interactions in region 1 of the subunit interface are formed by two amino acid residues from one subunit (a glutamate residue in $\alpha$-helix 3 and an arginine residue in $\alpha$-helix 4) interacting with the same two amino acids from the other subunit. These interactions are of interest because the four amino acid side chains interact with each other as a planar rectangle with distances of 3.83–4.26 Å (1Å = 0.1 nm). These interactions are highly conserved among the GST classes, Delta, Sigma and Theta, however at present there are no reports of these interactions for any of the three GST classes. In adGSTD4-4, each arginine residue not only interacts with both of the negatively charged Glu$^{75}$ residues in both subunits, but also forms cation–$\pi$ interactions with the aromatic ring of Tyr$^{89}$ and an ionic interaction with the carboxy group of Pro$^{90}$. In adGSTD3-3, the equivalent residues to Glu$^{75}$ and Arg$^{96}$ of adGSTD4-4 are Glu$^{74}$ and Arg$^{90}$. These residues also form the same planar rectangle arrangement within adGSTD3-3 and are stabilized in a similar manner by interactions with Tyr$^{83}$ and Pro$^{84}$ (Tyr$^{89}$ and Pro$^{90}$ in adGSTD4-4). Therefore as the motif appears to be highly conserved in both proteins it was only studied in adGSTD4-4. In addition, these interactions appear to be highly conserved among the insect GST classes. Therefore the aim of the present study was to determine whether the inter- and intra-subunit electrostatic interactions of these residues are important contributions that help to maintain tertiary and quaternary structures.

Region 2 at the subunit interface shows the most variation in amino acid residues at equivalent positions between the two isoenzymes, Tyr$^{98}$, Met$^{101}$ and Gly$^{102}$ of adGSTD3-3 and Phe$^{104}$,

Val[107] and Ala[108] of adGSTD4-4 respectively. These residues are of interest because they are not only subunit interface residues but also active site residues with several of them involved in both active sites of the dimeric enzyme. Therefore the amino acids at the equivalent positions of the two isoenzymes were studied by switching the amino acids of the two proteins; Y98F, M101V, G102A and Y98F/M101V/G102A of adGSTD3-3 and F104Y, V107M, A108G and F104Y/V107M/A108G of adGSTD4-4.

The last region is the hydrophilic area in region 3 of the subunit interface, Asp[110] of adGSTD3-3 and Glu[116] of adGSTD4-4. Not only are these subunit interface residues, but these two equivalent positions also are involved in the active site as part of the H-site (hydrophobic substrate-binding site). For adGSTD4-4, Glu[116] forms hydrogen bonds with Arg[134] in both inter- and intra-subunit interactions; however, these interactions do not appear in adGSTD3-3. For adGSTD3-3, there are hydrogen bonds only in the same subunit between Asp[110] and the highly conserved residue Glu[106]. To study the influence of the ionic network in region 3 of the subunit interface and whether it impacts upon the catalytic activity and stability of the enzymes, mutations at the equivalent positions of these two isoenzymes were generated, that is, D110A of adGSTD3-3 and E116A of adGSTD4-4.

## MATERIALS AND METHODS

### Site-directed mutagenesis and protein purification

The adGSTD3-3 and adGSTD4-4 plasmid DNA templates were prepared from previous constructs [14]. The construction of the mutants was based on the Stratagene QuikChange® site-directed mutagenesis kit using *pfu* DNA polymerase. The expression constructs of recombinant plasmid that were obtained were sequenced at least twice and transformed into *Escherichia coli* BL21DE3plysS. The soluble recombinant GSTs were purified by GSTrap affinity chromatography (Amersham Phamacia) as previously described [14]. After purification, proteins were homogeneous as judged by SDS/PAGE, and the protein concentration was determined using the Bradford protein reagent with bovine serum albumin as a standard [18].

### Catalytic activity and kinetic studies

Steady-state kinetics were studied at various concentrations of CDNB (1-chloro-2,4-dinitrobenzene) and GSH in 0.1 M phosphate buffer (pH 6.5). The reaction was monitored at 340 nm, $\varepsilon = 9600\ M^{-1} \cdot cm^{-1}$. Apparent kinetic parameters, $k_{cat}$, $K_m$ and $k_{cat}/K_m$ were determined by fitting the collected data to a Michaelis–Menten equation by non-linear regression analysis using GraphPad Prism version 4 (GraphPad software; www.graphpad.com) [19,20]. Specific activities of the enzymes were determined with five different substrates; CDNB, DCNB (1,2-dichloro-4-nitrobenzene), EA (ethacrynic acid), PNPB (p-nitrophenethyl bromide) and PNBC (p-nitrobenzyl chloride) as previously described [21]. Specific activities reported are the means ± S.D. from at least three independent experiments. One-way ANOVA with Dunnett's post test was performed using GraphPad InStat version 3.06 for Windows (GraphPad software; www.graphpad.com).

### Structural studies

Enzymes at 0.1 mg/ml final concentration were incubated at 45 °C. Inactivation time courses were determined by withdrawing suitable aliquots at different time points for an assay of remaining activity to calculate the half-life of the enzyme [22]. Data are the means ± S.D. from at least three independent experiments.

Spectroscopic properties of wild-type and mutant proteins were measured for evidence of conformational changes. Intrinsic fluorescence emission spectra were measured at an excitation wavelength of 295 nm and $\lambda_{max}$ and fluorescence intensity of emission spectra were analysed at a protein concentration of 0.2 mg/ml [23].

A refolding experiment was performed with enzymes first being denatured in 4 M guanidinium chloride in renaturation buffer [0.2 M phosphate, 1 mM EDTA and 5 mM dithiothreitol (pH 7.0)] at room temperature (25 °C) for 1 h and then rapidly diluted (defining time zero) 1:40 into renaturation buffer. Therefore the final guanidinium chloride concentration was 0.1 M during refolding. Recovered activity was monitored as a function of time by withdrawal of appropriate aliquots of renaturation mixture and immediately assaying for activity. Refolding rate constants were determined by non-linear regression analysis using a single exponential equation [23].

The ANS (8-anilino-1-naphthalenesulfonate) binding assay was monitored using a PerkinElmer Luminescence spectrometer LS50B. ANS [200 $\mu$M in 0.1 M sodium phosphate buffer (pH 6.5)] was added to a final concentration of 2 $\mu$M enzyme in a 400 $\mu$l reaction mixture [24]. The spectrum of ANS in phosphate buffer (pH 6.5) was subtracted from the spectrum of protein-binding ANS. A total of three scans each for blank and sample were recorded and averaged for each enzyme. Reported spectra are the means from at least three independent experiments. Enzyme activity measurements in the presence of ANS were assessed immediately after adding ANS by using the standard reaction assay.

## RESULTS AND DISCUSSION

The investigations of GST dimerization performed in mammalian GSTs indicated that the subunit interactions are a significant source of stabilization not only for the association of subunits but also for tertiary structures of the individual subunits [9,25,26]. In the present study, most mutations gave similar purification yields as the wild-type with the exception of the E75A and R96A mutants of adGSTD4-4, which had yields approx. 2 and 0.4 % of the wild-type respectively. As the proteins were expressed in similar amounts, it appears that the alteration of these residues disrupts the intra-subunit interaction between helix 3 and helix 4 which impacts upon the active site architecture thereby affecting binding to the affinity matrix.

Both adGSTD3-3 and adGSTD4-4 have two tryptophan residues in each subunit that are located in $\beta$-sheet 4 in domain I and $\alpha$-helix 7 in domain II. The tryptophan residue located in $\beta$-sheet 4 in domain I (Trp[63]) is in close proximity to the active site, with an involvement in sequestering the substrate glutathione, as well as being in the subunit interface. This makes it a sensitive fluorescence probe to monitor conformational changes at/near the active site. The normalized fluorescence spectra of adGSTD3-3 and adGSTD4-4 wild-type compared with the mutants were obtained to study the effect of mutations on the enzyme tertiary structure (Figure 2). The results showed that although every mutant had the same $\lambda_{max}$ as the wild-type, several mutants presented differences in the normalized intensities of fluorescence, implying that the mutations caused significant conformational changes in the environment of the tryptophan residues located near the subunit interface and the mutation site. The mutants also had different intensities from their wild-type especially R96A, with the intensity of fluorescence decreased by approx. 66 %. This finding suggests that there are significant conformational changes in the tryptophan residue neighbourhood that distinguish the final structure of the mutant from that of the wild-type. This decrease

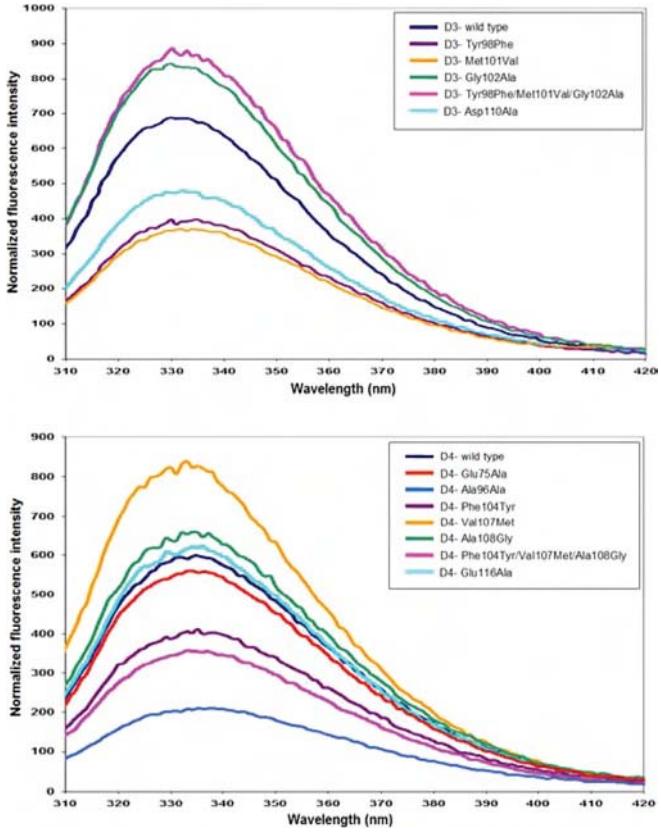


**Figure 2 Normalized intrinsic tryptophan residue fluorescence spectra of the adGSTD3-3 and adGSTD4-4 (wild-type) and the recombinant mutant GSTs**

The same colour represents the equivalent position. The data are means of three independent experiments.

demonstrates that movements have occurred in the tryptophan residues or in the surrounding fluorescence quenching groups.

The half-life of the enzymes corresponds to the time of incubation when there is 50 % remaining activity (Table 1). The conserved cation–$\pi$ interaction residue, Arg[96], and the conserved electrostatic interaction residue, Glu[75], have important roles in stabilizing enzyme structure as shown by a much decreased stability for R96A and E75A of approx. 15- and 7.4-fold respectively. For region 2, several mutants possessed similar stability as the wild-type enzymes. However, there were three mutants which had very different thermal stabilities. Two of the mutations were at an equivalent position, adGSTD3-3 Gly[102] and adGSTD4-4 Ala[108]. Replacement of a glycine residue by an alanine residue in adGSTD3-3 at this position caused decreases of about 8-fold in half-life, whereas a glycine residue substitution of adGSTD4-4 showed an increase in half-life of about 4.7-fold. The other mutant that showed stability changes was the V104M protein which decreased the half-life by approx. 3-fold. For region 3, the half-life of D110A of adGSTD3-3 was similar to the wild-type. However, the equivalent adGSTD4-4 mutation E116A disrupted the charge–charge network and showed a 64 % decreased stability for the enzyme. The results showed that the positively charged residue at the edge of the subunit interface of adGSTD4-4 participates in stabilizing the enzyme structure while the equivalent residue of adGSTD3-3 appeared to have only a minor contribution.

Three mutations in adGSTD4-4, E75A, R96A and V107M, did not recover activity after being unfolded by 4 M guanidinium chloride (Table 1). This implies that these residues play a critical role in the folding process of the enzymes. For the remaining mutants, the refolding rate constants were similar. The activity recovered illustrates the ability of the enzymes to recover their appropriate active site conformation for catalytic activity. After unfolding, the enzymes were able to recover activity ranging from 19 % to 94 %. To study the influence of mutations on protein folding and to assess whether the changes affected tertiary folding of each subunit or dimerization of the two subunits, intrinsic tryptophan residue fluorescence spectroscopy was performed. The fluorescence spectra of native, unfolded and refolded enzymes were monitored to compare the tertiary structure of the proteins in each state (Figures 3 and 4). The $\lambda_{max}$ values of the native (335 nm) and the unfolded form (355 nm) of the protein were observed for every enzyme. The data showed that the enzymes were refolded in a similar manner as the native form, as shown by similar $\lambda_{max}$ values, including the E75A, R96A and V107M mutants, although

**Table 1 Half-life, refolding rate constants, activity recovered (%) and the effect of ANS on CDNB specific activity of the adGSTD3-3 and adGSTD4-4 (wild-type) and the recombinant engineered GSTs**

The data are means ± S.D. for at least three independent experiments. One-way ANOVA with Dunnett's post test was performed to show statistical significance with $*P < 0.05$ and $\dagger P < 0.01$. D3 and D4 indicate adGSTD3-3 and adGSTD4-4 respectively. Inside parentheses the numbers indicate the subunit interface region: 1 is region 1, 2 is region 2 and 3 is region 3; and the same lowercase letter indicates an equivalent residue position for the two GST isoenzymes. nd, not detectable.

| Enzymes | Half-life (min) | Refolding rate constant ($min^{-1}$) | Activity recovered (%) | Inhibition by ANS (%) |
|---|---|---|---|---|
| D3-wild-type | 2.71 ± 0.35 | 0.87 ± 0.09 | 56.9 ± 0.23 | 24.6 ± 1.41 |
| D3-Y98F (2/a) | 3.12 ± 0.33 | 0.58 ± 0.05† | 66.1 ± 2.83* | 13.1 ± 0.54† |
| D3-M101V (2/b) | 2.77 ± 0.43 | 0.42 ± 0.05† | 40.5 ± 1.93† | 11.9 ± 0.80† |
| D3-G102A (2/c) | 0.34 ± 0.03† | 0.38 ± 0.07† | 94.4 ± 5.77† | 13.7 ± 2.66† |
| D3-Y98F/M101V/G102A (2/d) | 1.88 ± 0.01* | 0.31 ± 0.03† | 85.8 ± 4.39† | 18.4 ± 0.65† |
| D3-D110A (3/e) | 2.21 ± 0.24 | 0.58 ± 0.11† | 80.5 ± 3.48† | 23.4 ± 1.83 |
| D4-wild-type | 14.0 ± 1.70 | 0.59 ± 0.03 | 19.7 ± 0.70 | 18.4 ± 1.20 |
| D4-G75A(1) | 1.89 ± 0.13† | nd | 0.00 | 22.5 ± 0.82 |
| D4-R96A(1) | 0.91 ± 0.07† | nd | 0.00 | 18.8 ± 3.89 |
| D4-F104Y (2/a) | 17.1 ± 1.76* | 0.28 ± 0.02† | 23.5 ± 0.51 | 31.9 ± 1.96† |
| D4-V107M (2/b) | 4.76 ± 0.15† | nd | 0.00 | 25.4 ± 1.41† |
| D4-A108G (2/c) | 65.4 ± 1.45† | 0.32 ± 0.04† | 69.6 ± 7.55† | 32.8 ± 1.03† |
| D4-F104Y/V107M/A108G (2/d) | 16.7 ± 1.23 | 0.60 ± 0.10 | 25.0 ± 0.18 | 21.1 ± 1.83 |
| D4-E116A (3/e) | 5.16 ± 0.93† | 0.68 ± 0.11 | 9.93 ± 0.68* | 17.3 ± 2.05 |

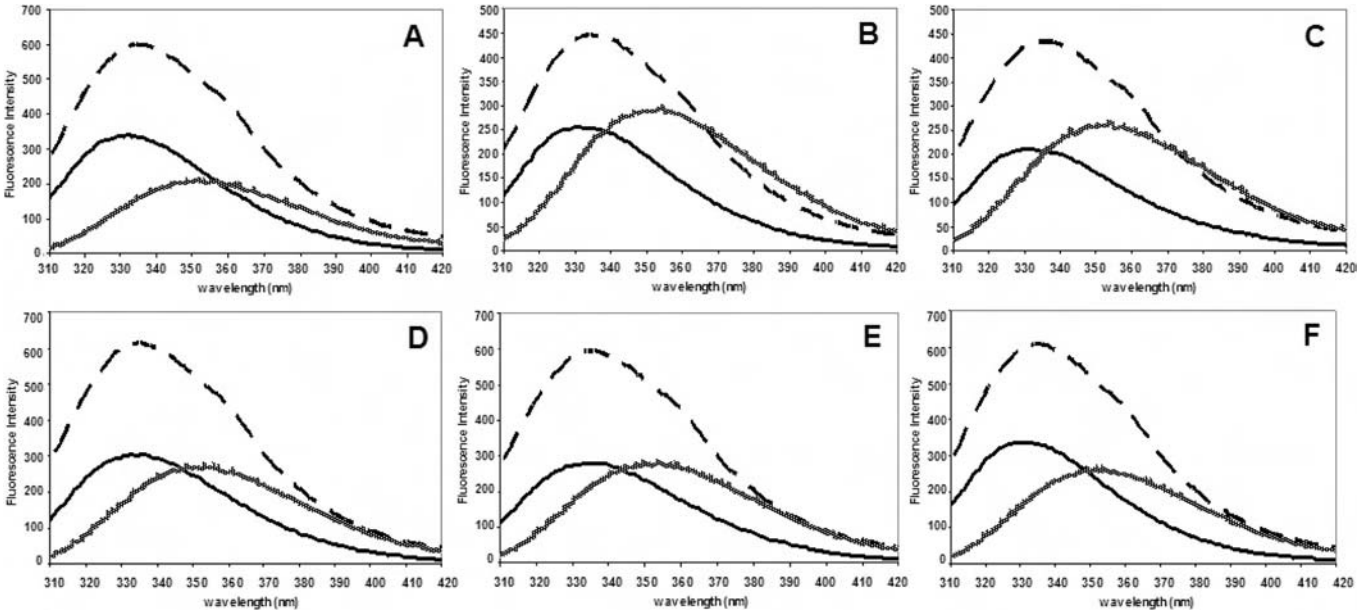


**Figure 3 Normalized intrinsic tryptophan residue fluorescence spectra compared with the native, refolded and unfolded forms of the adGSTD3-3 (wild-type) and the recombinant mutant GSTs**

(**A**) Wild-type, (**B**) Y98F, (**C**) M101V, (**D**) G102A, (**E**) Y98F/M101V/G102A and (**F**) D110A. The data are means for at least three independent experiments. Solid line, native form; dashed line, refolded form; and hashed line, unfolded form of the enzyme.

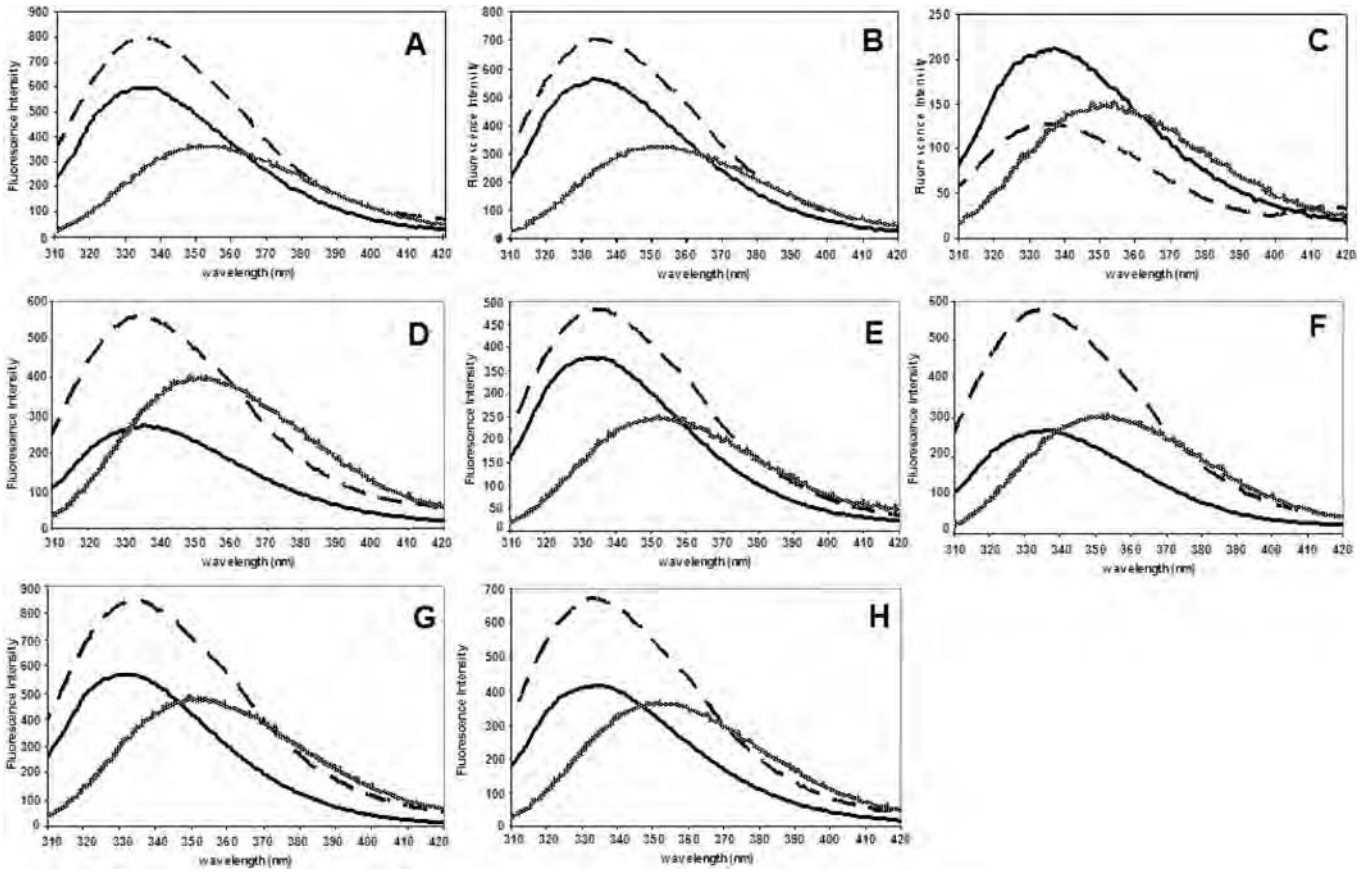


**Figure 4 Normalized intrinsic tryptophan residue fluorescence spectra compared with the native, refolded and unfolded forms of the adGSTD4-4 (wild-type) and the recombinant mutant GSTs**

(**A**) Wild-type, (**B**) G75A, (**C**) R96A, (**D**) F104Y, (**E**) V107M, (**F**) A108G, (**G**) F104Y/V107M/A108G and (**H**) E116A. The data are means for at least three independent experiments. Solid line, native form; dashed line, refolded form; and hashed line, unfolded form of the enzyme.

these enzymes could not recover catalytic activity. As shown by the similar patterns of the adGSTD3-3 mutant spectra, the mutations did not affect the tertiary folding of each subunit but influenced the dimerization process, which is necessary to achieve an appropriate active site conformation. Therefore both catalytic and structural data suggest that the single mutation of $Gly^{102}$ and the triple mutation had significant effects on the dimerization of the enzymes by increasing the activity recovered from 56.9 % for wild-type to approx. 94.4 % and 85.8 % for the two proteins respectively (Table 1). In both catalytic and structural experiments, the refolding data showed that loss of the conserved electrostatic interactions, E75A and R96A, and the hydrophobic residue, V107M, had a dramatic effect on the dimerization process, which is critical to formation of the complete active site pocket. The results for the $Arg^{96}$ position indicated that not only does this residue have a critical role in the dimerization process, but it is also important for the protein folding pathway of each monomeric subunit.

The anionic dye ANS has been shown to bind in the solvent-exposed cleft in the subunit interface of class Alpha and Pi enzymes [27–29]. Therefore ANS was utilized as a probe to monitor the appearance/disappearance of hydrophobic patches or surfaces on the proteins that were undergoing structural changes. When ANS was bound to the proteins the fluorescence was enhanced, accompanied by a blue shift in its emission maximum from 514 nm (free ANS in buffer) to 498 nm for adGSTD3-3 and 482 nm for wild-type adGSTD4-4, indicating that the polarity of the binding site had become more hydrophobic, with decreasing polarity the greater the blue shift.

When compared with the wild-type proteins, there was no change in the emission maximum wavelength of ANS bound to all mutants (Figure 5). For the ANS fluorescence intensity, which reflects the degree of solvent quenching of ANS bound to the protein, the adGSTD4-4 mutants showed variations in the amount of ANS bound, except E75A, which showed a similar intensity to the wild-type. However, there was no relative intensity change for the adGSTD3-3 mutants. The results showed that the residue substitutions of adGSTD4-4 with the adGSTD3-3 amino acids had a dramatic effect at the subunit interface, much more than for adGSTD3-3.

To study the impact of ANS on the enzyme conformation, the enzyme activity in the presence and absence of ANS was measured using the standard reaction assay. The results showed that for the mutants, ANS molecules can bind and alter the active site architecture in a manner similar to the wild-type (Table 1). It implied that differences in ANS spectra intensities in Figure 5 occurred only from an alteration of a hydrophobic patch at the subunit-binding site.

In general, the engineered enzyme reactions followed Michaelis–Menten kinetics as did the wild-type except for E75A, F104Y and E116A of adGSTD4-4 which showed positive co-operativity upon substrate binding. Positive co-operativity is shown by a sigmoidal velocity curve which reflects the substrate binding in the first active site, that then facilitates a second substrate molecule binding in the second active site by increasing the binding affinity of the vacant binding site [30]. For CDNB, two of the enzymes had significantly different Hill coefficients (shown by one-way ANOVA with Dunnett's post test) compared with wild-type enzyme [Hill coefficients for wild-type $1.08 \pm 0.08$ versus E75A $1.79 \pm 0.03$ ($P < 0.01$) and E116A $1.40 \pm 0.20$ ($P < 0.05$)]. For GSH only F104Y had a significantly different Hill coefficient (shown by one-way ANOVA with Dunnett's post test) compared with wild-type enzyme [Hill coefficients for wild-type $1.06 \pm 0.14$ versus F104Y $2.01 \pm 0.09$ ($P < 0.01$)]. These data show that two of the mutant enzymes, E75A and F104Y, had very strong positive co-operativity, with the Hill coefficients approaching the number of substrate-binding sites. In addition, comparison of the kinetic constants of the mutants with the wild-type values showed that the residue changes affected additional enzymatic properties (Table 2). These effects on the active site were also reflected in changes in substrate specificity with changes in the equivalent residue position showing different effects on the two isoforms (Table 3). For example, D110A activity was significantly decreased with CDNB and DCNB in adGSTD3-3 but E116A activity was significantly increased with CDNB and showed no significant activity with DCNB in adGSTD4-4. For another position, M101V in adGSTD3-3 equivalent to V107M in adGSTD4-4, both enzymes showed significant decreases in activity with CDNB. However, the adGSTD4-4 enzyme showed significant increases in activity with DCNB and EA, whereas the adGSTD3-3 enzyme showed a significant decrease with DCNB and no significant change with EA.

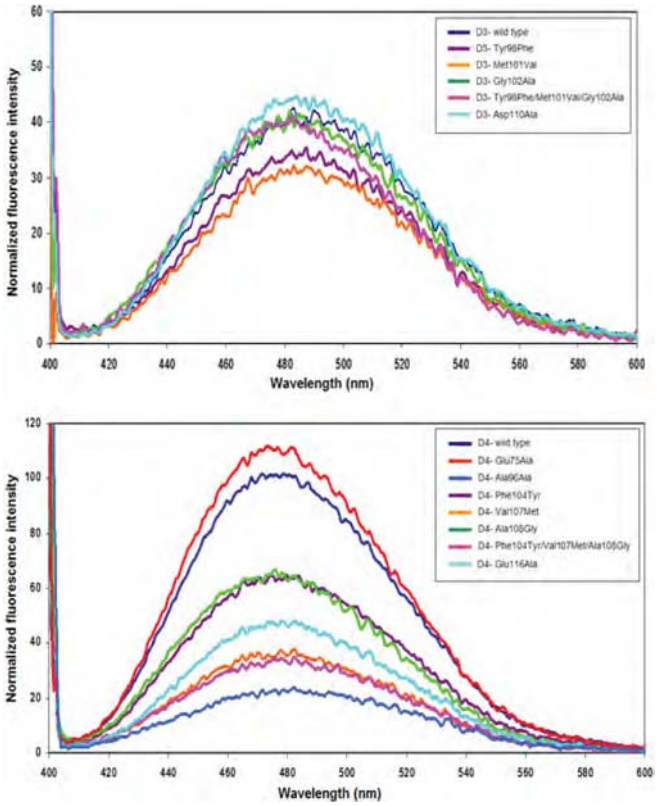


**Figure 5 ANS binding spectra of the adGSTD3-3 and adGSTD4-4 (wild-type) and the recombinant mutant GSTs**

The same colour represents the equivalent position. The spectra were measured immediately after addition of ANS. As ANS fluorescence is quenched by water, alteration of the fluorescence intensity of protein-bound ANS is highly dependent upon its accessibility to water. The data are means for at least three independent experiments.

The insect GST class Delta has a conserved planar rectangular electrostatic motif formed by four amino acid residues from different helices of both subunits ($Glu^{75}$ in $\alpha$-helix 3 and $Arg^{96}$ in $\alpha$-helix 4) (Figure 6). These interactions are highly conserved among GST classes Delta, Sigma and Theta. This is the first report of these interactions for any of these three classes. To study the function of this motif two mutants were generated, E75A and R96A, which break the conserved electrostatic interactions and ionic network at the dimer interface of adGSTD4-4. The results showed that the motif provides an important contribution

**Table 2 Yield of purification and kinetic parameters of the adGSTD3-3 and adGSTD4-4 (wild-type) and the recombinant engineered GSTs**

The data are means ± S.D. for at least three independent experiments. One-way ANOVA with Dunnett's post test was performed to show statistical significance with $*P < 0.05$ and $\dagger P < 0.01$. D3 and D4 indicate adGSTD3-3 and adGSTD4-4 respectively. Inside parentheses the numbers indicate the subunit interface region: 1 is region 1, 2 is region 2 and 3 is region 3; and the same lowercase letter indicates an equivalent residue position for the two GST isoenzymes.

| Enzymes | CDNB $k_{cat}$ ($s^{-1}$) | CDNB $K_m$ (mM) | CDNB $k_{cat}/K_m$ ($mM^{-1}•s^{-1}$) | GSH $K_m$ (mM) | GSH $k_{cat}/K_m$ ($mM^{-1}•s^{-1}$) | Purification yield (%) |
|---|---|---|---|---|---|---|
| D3-wild-type | 39.2 | 0.15 ± 0.01 | 258 | 0.29 ± 0.04 | 114 | 53.7 |
| D3-Y98F (2/a) | 24.9† | 0.12 ± 0.01 | 213 | 0.47 ± 0.05 | 53.1 | 49.2 |
| D3-M101V (2/b) | 26.0† | 0.72 ± 0.06† | 36.3 | 1.04 ± 0.06† | 25.0 | 60.0 |
| D3-G102A (2/c) | 23.5† | 0.37 ± 0.02† | 63.3 | 2.94 ± 0.38† | 7.99 | 47.6 |
| D3-Y98F/M101V/G102A (2/d) | 40.7 | 0.28 ± 0.03† | 147 | 1.12 ± 0.07† | 36.7 | 58.3 |
| D3-D110A (3/e) | 51.7† | 0.49 ± 0.07† | 106 | 0.54 ± 0.04 | 95.8 | 34.3 |
| D4-wild-type | 22.5 | 0.63 ± 0.09 | 35.7 | 0.67 ± 0.05 | 33.6 | 61.3 |
| D4-G75A (1) | 23.3 | 8.26 ± 2.63† | 2.82 | 0.54 ± 0.06 | 43 | 5.5 |
| D4-R96A (1) | 16.2† | 0.80 ± 0.06 | 22.0 | 1.08 ± 0.02 | 15.0 | 1.4 |
| D4-F104Y (2/a) | 15.5† | 0.52 ± 0.03 | 29.8 | 24.01 ± 2.94† | 0.65 | 42.2 |
| D4-V107M (2/b) | 13.7† | 1.6 ± 0.08 | 8.56 | 0.76 ± 0.11 | 18.0 | 60.0 |
| D4-A108G (2/c) | 26.8 | 0.87 ± 0.07 | 26.8 | 0.73 ± 0.12 | 36.7 | 59.2 |
| D4-F104Y/V107M/A108G (2/d) | 32.5† | 0.72 ± 0.04 | 45.2 | 0.25 ± 0.02 | 130 | 59.2 |
| D4- E116A (3/e) | 46.1† | 1.55 ± 0.01 | 29.7 | 1.24 ± 0.06 | 37.1 | 37.1 |

**Table 3 Specific activities of the adGSTD3-3 and adGSTD4-4 (wild-type) and the recombinant engineered GSTs**

The data are means ± S.D. for at least three independent experiments. One-way ANOVA with Dunnett's post test was performed to show statistical significance with $*P < 0.05$ and $\dagger P < 0.01$. The substrate concentrations used were 1 mM CDNB for adGSTD3 and 3 mM CDNB for adGSTD4, 1 mM DCNB, 0.1 mM PNBC, 0.1 mM PNPB and 0.2 mM EA. D3 and D4 indicate adGSTD3-3 and adGSTD4-4 respectively. Inside parentheses the numbers indicate the subunit interface region: 1 is region 1, 2 is region 2 and 3 is region 3; and the same lowercase letter indicates an equivalent residue position for the two GST isoenzymes. nd is not detectable.

| Enzymes | Specific Activity ($\mu$mol/min/mg) CDNB | DCNB | EA | PNPB | PNBC |
|---|---|---|---|---|---|
| D3-wild-type | 85.3 ± 3.23 | 0.25 ± 0.01 | 0.10 ± 0.05 | nd | 0.13 ± 0.01 |
| D3-Y98F (2/a) | 46.9 ± 6.38† | 0.23 ± 0.03 | 0.03 ± 0.01* | nd | 0.05 ± 0.00† |
| D3-M101V (2/b) | 41.1 ± 0.81† | 0.05 ± 0.01† | 0.08 ± 0.02 | nd | 0.09 ± 0.00† |
| D3-G102A (2/c) | 46.8 ± 0.25† | 0.08 ± 0.01† | nd | nd | 0.05 ± 0.00† |
| D3-Y98F/M101V/G102A (2/d) | 84.8 ± 5.47 | 0.21 ± 0.01* | 0.15 ± 0.01 | nd | 0.08 ± 0.00† |
| D3-D110A (3/e) | 71.6 ± 2.69† | 0.16 ± 0.01† | 0.01 ± 0.01† | 0.03 ± 0.01 | 0.07 ± 0.01† |
| D4-wild-type | 48.0 ± 1.98 | 0.03 ± 0.00 | 0.27 ± 0.00 | 0.06 ± 0.01 | 0.03 ± 0.01 |
| D4-E75A (1) | 36.6 ± 5.03† | 0.06 ± 0.01 | 0.12 ± 0.01 | 0.02 ± 0.01 | 0.06 ± 0.00 |
| D4-R96A (1) | 26.0 ± 0.13† | 0.27 ± 0.04† | 0.18 ± 0.01 | 0.23 ± 0.02 | nd |
| D4-F104Y (2/a) | 28.5 ± 2.24† | 0.06 ± 0.01 | 0.14 ± 0.01 | 0.05 ± 0.01 | 0.11 ± 0.05 |
| D4-V107M (2/b) | 22.0 ± 2.29† | 0.08 ± 0.004* | 2.06 ± 0.29† | 0.31 ± 0.08 | nd |
| D4-A108G (2/c) | 55.3 ± 2.07 | 0.06 ± 0.02 | 0.32 ± 0.01 | nd | 0.08 ± 0.02 |
| D4-F104Y/V107M/A108G (2/d) | 53.8 ± 1.43 | 0.05 ± 0.01 | 0.02 ± 0.00* | nd | 0.04 ± 0.01 |
| D4- E116A (3/e) | 56.3 ± 6.83* | 0.06 ± 0.01 | 0.01 ± 0.01* | 0.04 ± 0.01 | 0.04 ± 0.01 |

to the stabilization and folding of the protein. The mutants were expressed in both inclusion and soluble forms, with the R96A mutant mostly being expressed as an inclusion body. This evidence and the results from the refolding assay (Table 1; Figures 3 and 4) indicated that the folding process was altered by the mutations. In addition, decreases in yield as well as catalytic activity changes (Table 2), suggest that the mutations disrupt the active site conformation which decreases binding affinity, alters kinetic constants and substrate specificities.

Although both $Glu^{75}$ and $Arg^{96}$ are located in the same area, in the present study region 1 of the subunit interface, there is a conserved amino acid sequence around $Arg^{96}$ which forms a pocket around the arginine residue. $Arg^{96}$ is stabilized by several highly conserved residues in a cation–$\pi$ interaction with $Tyr^{89}$ and $Pro^{90}$, whereas $Glu^{75}$ does not have amino acids surrounding it, except $Arg^{96}$, as it is located within a hole in the subunit interface edge (Figure 6). Therefore substitution of an alanine residue for $Arg^{96}$ appears to have more impact on the tertiary and quaternary structure of the protein compared with $Glu^{75}$, as shown by decreases in the fluorescence intensities of both intrinsic tryptophan spectroscopy (Figure 2) and the ANS binding assay (Figure 5). This also suggests that there are significant conformational changes in amino acid side chains near the subunit interface and the mutation site. However, disappearance of the salt bridges with the loss of either $Glu^{75}$ or $Arg^{96}$ affected both initial protein folding, as shown in the refolding experiment, and the protein stability as shown by decreased half-life. Although $Arg^{96}$ is not located in the active site pocket, structural changes that occurred due to this mutation also affected the active site conformation, probably through packing effects (Tables 2 and 3).

Region 2 of the subunit interface, which shows the most variation in amino acid residues at the equivalent positions between adGSTD3-3 and adGSTD4-4, is of interest because the residues are not only in the interface but also in the active site,

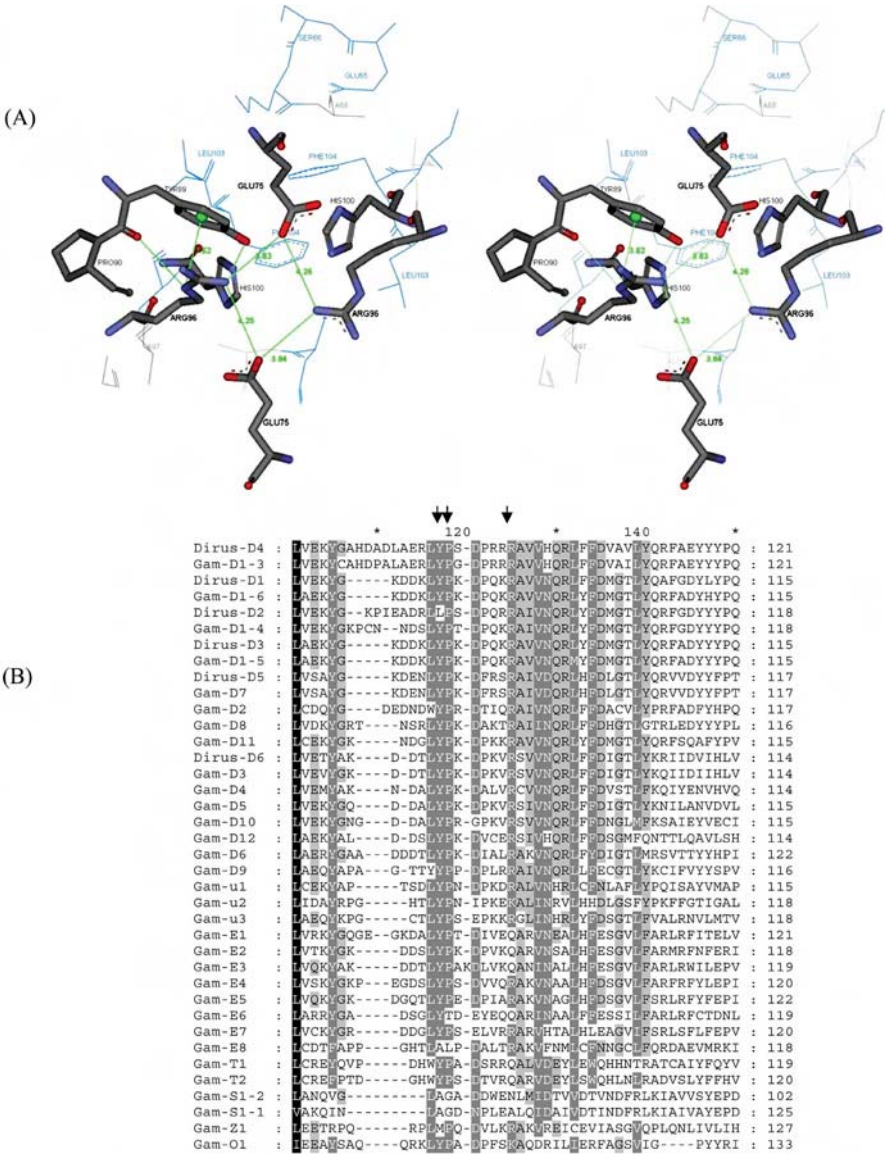


**Figure 6 Conserved electrostatic interaction in region 1 of the subunit interface**

(**A**) The planar rectangle electrostatic interaction of Glu$^{75}$ and Arg$^{96}$ from both subunits. Distances between the charged atoms are shown in Å. Also shown are the conserved anion–cation–$\pi$ interactions between Tyr$^{89}$, Pro$^{90}$ and Arg$^{96}$. (**B**) Amino acid alignment of insect GST classes. Dirus is *A. dirus* and Gam is *A. gambiae*. The arrows point to the highly conserved tyrosine, proline and arginine residues. D is Delta, u is unclassified, E is Epsilon, T is Theta, S is Sigma, Z is Zeta and O is Omega GST class. GenBank® accession numbers: adGSTD1 (AF273041), adGSTD2 (AF273038), adGSTD3 (AF273039), adGSTD4 (AF273040), adGSTD5 (AF251478), adGSTD6 (AY014406), agGSTD1-3 (Protein ID AAC79992), agGSTD1-4 (Protein ID AAC79994), agGSTD1-5 (Protein ID AAC79993), agGSTD1-6 (Protein ID AAC79995), agGSTD2 (Z71480), agGSTD3 (AF513638), agGSTD4 (AF513635), agGSTD5 (AF513634), agGSTD6 (AF513636), agGSTD7 (AF071161), agGSTD8 (AF316637), agGSTD9 (AY255857), agGSTD10 (AF515527), agGSTD11 (AF513637), agGSTD12 (AF316638), agGSTu1 (AF515521), agGSTu2 (AF515523), agGSTu3 (AF515524), agGSTE1 (AF316635), agGSTE2 (AF316636), agGSTE3 (AY070234), agGSTE4 (AY070254), agGSTE5 (AY070255), agGSTE6 (AY070256), agGSTE7 (AF491816), agGSTE8 (AY070257), agGSTT1 (AF515526), agGSTT2 (AF515525), agGSTS1-1 (L07880), agGSTS1-2 (AF513639), agGSTZ1 (AF515522), agGSTO1 (AY255856). agGSTD6 and agGSTD9 were suggested to be pseudogenes [33]. The Figure in (**A**) was created using Accelrys DS ViewerPro 5.0.

with several residues involved in both active sites of the dimer. The effects of the different hydrophobic amino acids at the equivalent positions of the two isoenzymes were studied by switching the equivalent amino acids with the amino acid from the other protein; that is, Y98F, M101V, G102A and Y98F/M101V/G102A for adGSTD3-3 and F104Y, V107M, A108G and F104Y/V107M/A108G for adGSTD4-4. The refolding experiments demonstrated that every enzyme could be refolded, although the activity recovered varied (Table 1). This indicates that the mutations have only a slight effect on the initial folding of each subunit but have more influence on the dimerization process through subunit interface conformation, as well as other structural aspects which impact upon appropriate active site conformation. When comparing the two isoforms adGSTD3-3 and adGSTD4-4, in terms of changes in catalytic activity, the mutations affected the proteins in different ways for the equivalent residues, as shown in Table 2. The crystal structures show that all selected equivalent positions are located in the active site pocket suggesting that the whole electrostatic field in the active site pocket was disturbed by the mutations, which thereby altered catalytic parameters of the enzymes. Moreover, these residues are also located at the interface of the two active

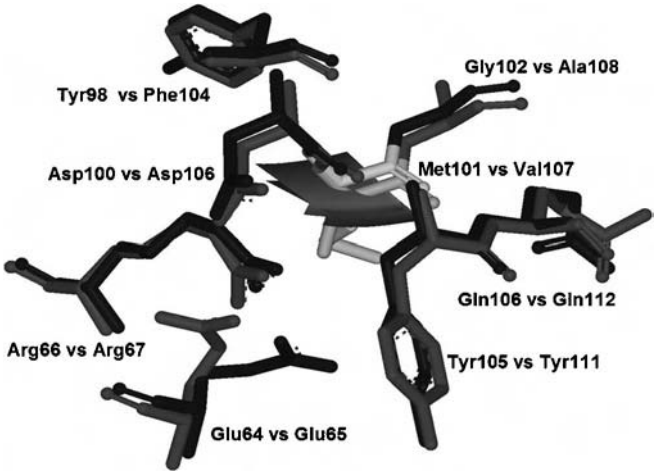


**Figure 7 In region 2 the amino acid milieu of adGSTD3-Met[101] and adGSTD4-Val[107]**

The dark grey represents adGSTD3-3 and medium grey is adGSTD4-4. The Figure was created using Accelrys DS ViewerPro 5.0.

site areas which provide different substrate-binding sites for GSH and the hydrophobic substrate. Therefore these positions would allow the residues to influence binding of both substrates as shown by the $K_m$ values.

The first sphere milieu of the equivalent positions, Met[101] of adGSTD3-3 and Val[107] of adGSTD4-4, consists of seven amino acids of which only two residues are different between the two isoforms, adGSTD3-3 Tyr[98] compared with adGSTD4-4 Phe[104] and adGSTD3-3 Gly[102] compared with adGSTD4-4 Ala[108] (Figure 7). However, the triple mutations which changed all three amino acids at these equivalent positions to the amino acid of the other isoform, showed that they had only a slight effect on the half-life. Steric interactions and van der Waals forces are important interactions for the stability of proteins [31,32]. The side chain size of the three amino acids at these equivalent positions had a major impact on subunit interface packing, with differences between the two splice forms, especially Met[101] and Gly[102] of adGSTD3-3 and Val[107] and Ala[108] of adGSTD4-4. Although the amino acids possess similar properties, the packing effects were great enough to alter the protein and enzyme properties.

From the conserved electrostatic interactions in region 1 to the hydrophobic area in region 2 of the subunit interface, every residue appears to contribute to either maintaining structure or subunit binding. The last area to be examined was the hydrophilic area in region 3 of the subunit interface, Asp[110] of adGSTD3-3 and Glu[116] of adGSTD4-4. Both mutations, D110A of adGSTD3-3 and G116A of adGSTD4-4, affected catalysis as shown by changes in both specific activity and kinetic constants. The equivalent residue in the human Alpha class A1-1 is Glu[104] whereas in the human Pi class GST it is a polar Ser[105]. In insects, the acidic residue appears to be conserved within the Delta class, however in the Epsilon class it is generally an aromatic amino acid and in the other insect classes, such as Sigma, Theta and Zeta, the residue is hydrophobic. This residue therefore appears to be conserved within a class and would contribute to class specific dimerization motifs. Additionally, in adGSTD4-4 the Glu[116] interacts with Arg[134] in a similar fashion to Glu[75] and Arg[96] in region 1 (Figure 8). That is, electrostatic interactions occur between the two residues within the same subunit as well as with the identical residues from the other subunit. So in adGSTD4-4 but not in adGSTD3-3 similar intra- and inter-subunit electrostatic interactions occur in both regions 1 and 3 of the subunit interface. In adGSTD3-3 the equivalent residue to Arg[134] is Asn[126] and so, because of the shorter side chains of the Asp[110] and the Asn[126], the distances preclude electrostatic interaction across the subunits.

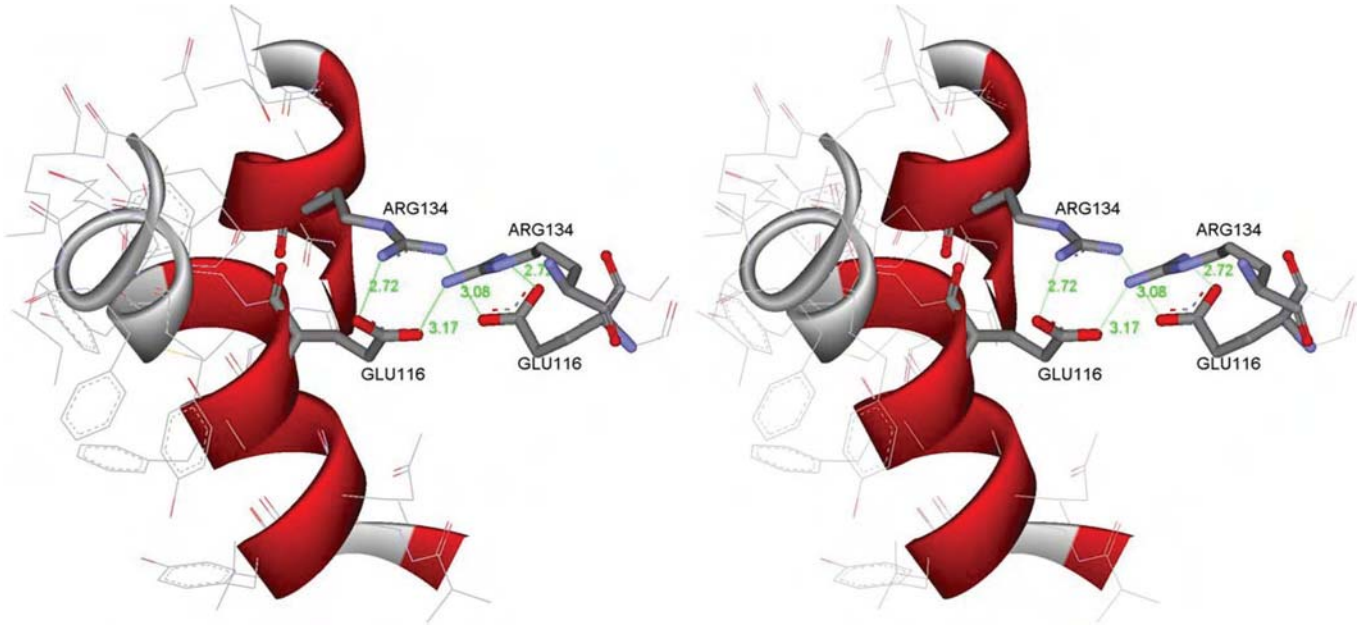


**Figure 8 The electrostatic interaction in region 3 of Glu[116] and Arg[134] in adGSTD4-4**

The two residues from each subunit are in proximity to interact electrostatically with each other as well as with the same residues from the other subunit. For the first subunit parts of $\alpha$-helices 4 and 5, containing Glu[116] and Arg[134] respectively, are shown. For clarity only Glu[116] and Arg[134] from the second subunit are shown. Distances between the charged atoms are shown in Å. The Figure was created using Accelrys DS ViewerPro 5.0.

In conclusion, the conserved electrostatic interactions between the charged residues from $\alpha$-helix 3 and $\alpha$-helix 4 show important roles for protein folding, stabilization and dimerization of the alternatively spliced enzymes. However, the subunit interface region with the most variation in amino acid residues at equivalent positions between adGSTD3-3 and adGSTD4-4 showed that although the mutations did not alter the overall protein folding, the enzyme properties were changed, especially the catalytic activity, thermal stability and subunit interface. Even highly conservative amino acid replacements changed the protein properties. The results suggest that even splicing products from the same gene may have specific features in the subunit interface area that would preclude heterodimerization.

This work was funded by the TRF (Thailand Research Fund). J. P. held a DPST (Development and Promotion of Science and Technology Talent) scholarship. J. W. was supported by a Royal Golden Jubilee scholarship.

## REFERENCES

1 Ketterer, B. (2001) A bird's eye view of the glutathione transferase field. Chem.-Biol. Interact. **138**, 27–42
2 Hayes, J. D., Flanagan, J. U. and Jowsey, I. R. (2005) Glutathione transferases. Annu. Rev. Pharmacol. Toxicol. **45**, 51–88
3 Luo, J.-K., Hornby, J. A. T., Wallace, L. A., Chen, J., Armstrong, R. N. and Dirr, H. W. (2002) Impact of domain interchange on conformational stability and equilibrium folding of chimeric class $\mu$ glutathione transferases. Protein Sci. **11**, 2208–2217
4 Hornby, J. A. T., Luo, J.-K., Stevens, J. M., Wallace, L. A., Kaplan, W., Armstrong, R. N. and Dirr, H. W. (2000) Equilibrium folding of dimeric class $\mu$ glutathione transferases involves a stable monomeric intermediate. Biochemistry **39**, 12336–12344
5 Luo, J.-K., Hornby, J. A. T., Armstrong, R. N. and Dirr, H. W. (2001) Equilibrium unfolding and enzyme kinetics of chimeric Mu class glutathione transferases. Chem.-Biol. Interact. **133**, 58–59
6 Sinning, I., Kleywegt, G. J., Cowan, S. W., Reinemer, P., Dirr, H. W., Huber, R., Gilliland, G. L., Armstrong, R. N., Ji, X., Board, P. G. et al. (1993) Structure determination and refinement of human Alpha class glutathione transferase A1-1, and a comparison with the Mu and Pi class enzymes. J. Mol. Biol. **232**, 192–212
7 Ji, X., Zhang, P., Armstrong, R. N. and Gilliland, G. L. (1992) The three-dimensional structure of a glutathione S-transferase from the Mu gene class: structural analysis of the binary complex of isoenzyme 3-3 and glutathione at 2.2 Å resolution. Biochemistry **31**, 10169–10184
8 Reinemer, P., Dirr, H. W., Ladenstein, R., Huber, R., Lo Bello, M., Federici, G. and Parker, M. W. (1992) Three-dimensional structure of class $\pi$ glutathione S-transferase from human placenta in complex with S-hexylglutathione at 2.8 Å resolution. J. Mol. Biol. **227**, 214–226
9 Hornby, J. A. T., Codreanu, S. G., Armstrong, R. N. and Dirr, H. W. (2002) Molecular recognition at the dimer interface of a class Mu glutathione transferase: role of a hydrophobic interaction motif in dimer stability and protein function. Biochemistry **41**, 14238–14247
10 Pongjaroenkit, S., Jirajaroenrat, K., Boonchauy, C., Chanama, U., Leetachewa, S., Prapanthadara, L. and Ketterman, A. J. (2001) Genomic organization and putative promotors of highly conserved glutathione S-transferases originating by alternative splicing in *Anopheles dirus*. Insect Biochem. Mol. Biol. **31**, 75–85
11 Chelvanayagam, G., Parker, M. W. and Board, P. G. (2001) Fly fishing for GSTs: a unified nomenclature for mammalian and insect glutathione transferases. Chem.-Biol. Interact. **133**, 256–260
12 Wongsantichon, J., Harnnoi, T. and Ketterman, A. J. (2003) A sensitive core region in the structure of glutathione S-transferases. Biochem. J. **373**, 759–765
13 Ranson, H., Collins, F. and Hemingway, J. (1998) The role of alternative mRNA splicing in generating heterogeneity within the *Anopheles gambiae* class I glutathione S-transferase family. Proc. Natl. Acad. Sci. U.S.A. **95**, 14284–14289
14 Jirajaroenrat, K., Pongjaroenkit, S., Krittanai, C., Prapanthadara, L. and Ketterman, A. J. (2001) Heterologous expression and characterization of alternatively spliced glutathione S-transferases from a single *Anopheles* gene. Insect Biochem. Mol. Biol. **31**, 867–875
15 Ketterman, A. J., Prommeenate, P., Boonchauy, C., Chanama, U., Leetachewa, S., Promtet, N. and Prapanthadara, L. (2001) Single amino acid changes outside the active site significantly affect activity of glutathione S-transferases. Insect Biochem. Mol. Biol. **31**, 65–74
16 Oakley, A. J., Harnnoi, T., Udomsinprasert, R., Jirajaroenrat, K., Ketterman, A. J. and Wilce, M. C. J. (2001) The crystal structures of glutathione S-transferases isozymes 1-3 and 1-4 from *Anopheles dirus* species B. Protein Sci. **10**, 2176–2185
17 Wongsantichon, J. and Ketterman, A. J. (2006) An intersubunit lock-and-key 'Clasp' motif in the dimer interface of Delta class glutathione transferase. Biochem. J. **394**, 135–144
18 Bradford, M. M. (1976) A rapid and sensitive method for the quantitation of microgram quantities of protein utilizing the principle of protein–dye binding. Anal. Biochem. **72**, 248–254
19 Prapanthadara, L., Koottathep, S., Promtet, N., Hemingway, J. and Ketterman, A. J. (1996) Purification and characterization of a major glutathione S-transferase from the mosquito *Anopheles dirus* (species B). Insect Biochem. Mol. Biol. **26**, 277–285
20 Udomsinprasert, R. and Ketterman, A. J. (2002) Expression and characterization of a novel class of glutathione S-transferase from *Anopheles dirus*. Insect Biochem. Mol. Biol. **32**, 425–433
21 Habig, W. H., Pabst, M. J. and Jakoby, W. B. (1974) Glutathione S-transferases: the first enzymatic step in mercapturic acid formation. J. Biol. Chem. **249**, 7130–7139
22 Vararattanavech, A. and Ketterman, A. (2003) Multiple roles of glutathione binding-site residues of glutathione S-transferase. Protein Pept. Lett. **10**, 441–448
23 Stenberg, G., Dragani, B., Cocco, R., Mannervik, B. and Aceto, A. (2000) A conserved 'hydrophobic staple motif' plays a crucial role in the refolding of human glutathione transferase P1-1. J. Biol. Chem. **275**, 10421–10428
24 Stevens, J. M., Hornby, J. A. T., Armstrong, R. N. and Dirr, H. W. (1998) Class Sigma glutathione transferase unfolds via a dimeric and a monomeric intermediate: impact of subunit interface on conformational stability in the superfamily. Biochemistry **37**, 15534–15541
25 Dirr, H. (2001) Folding and assembly of glutathione transferases. Chem.-Biol. Interact. **133**, 19–23
26 Sayed, Y., Wallace, L. A. and Dirr, H. W. (2000) The hydrophobic lock-and-key intersubunit motif of glutathione transferase A1-1: implications for catalysis, ligandin function and stability. FEBS Lett. **465**, 169–172
27 Sluis-Cremer, N., Naidoo, N. and Dirr, H. (1996) Class-Pi glutathione S-transferase is unable to regain its native conformation after oxidative inactivation by hydrogen peroxide. Eur. J. Biochem. **242**, 301–307
28 Sayed, Y., Hornby, J. A. T., Lopez, M. and Dirr, H. (2002) Thermodynamics of the ligandin function of human class Alpha glutathione transferase A1-1: energetics of organic anion ligand binding. Biochem. J. **363**, 341–346
29 Sluis-Cremer, N., Naidoo, N. N., Kaplan, K. H., Manoharan, T. H., Fahl, W. E. and Dirr, H. W. (1996) Determination of a binding site for a nonsubstrate ligand in mammalian cytosolic glutathione S-transferases by means of fluorescence-resonance energy transfer. Eur. J. Biochem. **241**, 484–488
30 Segel, I. H. (1993) Enzyme kinetics, Behavior and Analysis of Rapid Equilibrium and Steady State Enzyme Systems. John Wiley & Sons, New York
31 Otzen, D. E., Rheinnecker, M. and Fersht, A. R. (1995) Structural factors contributing to the hydrophobic effect: the partly exposed hydrophobic minicore in chymotrypsin inhibitor 2. Biochemistry **34**, 13051–13058
32 Xu, J., Baase, W. A., Baldwin, E. and Matthews, B. W. (1998) The response of T4 lysozyme to large-to-small substitutions within the core and its relation to the hydrophobic effect. Protein Sci. **7**, 158–177
33 Ding, Y., Ortelli, F., Rossiter, L. C., Hemingway, J. and Ranson, H. (2003) The *Anopheles gambiae* glutathione transferase supergene family: annotation, phylogeny and expression profiles. BMC Genomics **4**, 35–50

Received 24 April 2006/21 August 2006; accepted 29 August 2006
Published as BJ Immediate Publication 29 August 2006, doi:10.1042/BJ20060603

crystallization communications

Acta Crystallographica Section F
Structural Biology and Crystallization Communications
ISSN 1744-3091

# Crystallization and preliminary X-ray crystallographic analysis of a highly stable mutant V107A of glutathione transferase from *Anopheles dirus* in complex with glutathione

**Jantana Wongsantichon,[a] Jirundon Yuvaniyama[b] and Albert J. Ketterman[a]***

[a]Institute of Molecular Biology and Genetics, Mahidol University, Salaya Campus, Nakorn Pathom 73170, Thailand, and [b]Department of Biochemistry and Center for Excellence in Protein Structure and Function, Faculty of Science, Mahidol University, Rama 6 Road, Phayathai, Bangkok 10400, Thailand

Correspondence e-mail: frakt@mahidol.ac.th

Received 26 October 2005
Accepted 22 February 2006

An engineered mutant V107A of the dimeric glutathione transferase enzyme from *Anopheles dirus* (adgstD4-4) was cocrystallized with glutathione substrate using the hanging-drop vapour-diffusion method. The crystal diffracted to 2.47 Å resolution in space group $P3_221$ (unit-cell parameters $a = b = 49.4$, $c = 272.4$ Å). Although the crystal morphology differed from that previously obtained for the wild-type enzyme, the crystal packing was the same. At 318 K, the engineered mutant showed an enzyme stability that was increased by about 32-fold, while possessing a similar catalytic function to the wild type. Structural determination will provide valuable understanding of the role of Val107. This residue is in the dimeric interface and appears to contribute towards enhancing the physical properties of the entire protein.

## 1. Introduction

Glutathione transferases (GSTs; EC 2.5.1.18) are dimeric enzymes involved in phase II detoxication processes by conjugation of a thiol group from reduced glutathione ($\gamma$-glutamyl-cysteinyl-glyine; GSH) to an electrophilic centre of diverse xenobiotic compounds, producing less reactive and more polar substances in order to facilitate elimination from cells (Armstrong, 1991; Mannervik & Danielson, 1988). Cytosolic GSTs are generally found as multiple isoenzymes within organisms and with varying substrate selectivity (Hayes *et al.*, 2005; Hayes & Pulford, 1995). In the various GST dimeric structures, subunits are assembled by twofold symmetry, with subunit interactions that vary between the GST classes but generate a buried interface area of about 2700–3400 Å$^2$ (Dixon *et al.*, 2002). Therefore, homodimeric or heterodimeric GSTs are only formed by subunits from the same gene class and with comparable molecular recognition at the subunit interface.

The structural model of the wild-type GST adgstD4-4 from *Anopheles dirus* shows that Val107 is located in the subunit-interface region of the dimeric GST, forming part of an intersubunit lock-and-key 'clasp' motif (Oakley, Harnnoi *et al.*, 2001; Wongsantichon & Ketterman, 2006). The 'key' residue not only inserts into a hydrophobic pocket of the neighbouring subunit, but also itself acts as part of the 'lock' for the other subunit 'key'. In addition, the 'key' residues from both subunits hook around each other in an aromatic $\pi$–$\pi$ interaction through slightly offset aromatic ring stacking, generating a 'clasp' in the middle of the subunit interface. A special characteristic of the motif is to stabilize the GST dimeric structure in the middle region of the twofold axis. The motif was found to be highly conserved in many classes of insect GSTs, as shown by primary sequence alignments (Wongsantichon & Ketterman, 2006). The available crystal structures of insect-specific $\delta$-class GSTs such as *Lucilia* GST (Wilce *et al.*, 1994, 1995), adgstD3-3 (PDB code 1jlv; Oakley, Harnnoi *et al.*, 2001), adgstD4-4 (PDB code 1jlw; Oakley, Harnnoi *et al.*, 2001), adgstD5-5 (PDB code 1r5a; Udomsinprasert *et al.*, 2005), adgstD6-6 (PDB code 1v2a; Udomsinprasert *et al.*, 2005) and aggstD1-6 (PDB code 1pn9; Chen *et al.*, 2003) also reveal the highly conserved clasp-like motif (Wongsantichon & Ketterman, 2006). In the apo structure of adgstD4-4, the residue Val107 is also part of the wall of the active site. This residue's surface area is about 100–130 Å$^2$ and is only exposed to solvent in the active-site pocket. However, the residue is also part of the first-sphere interaction of

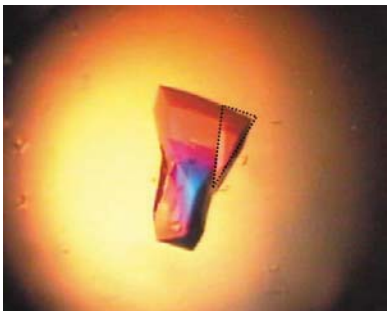

Leu103, which generates a small hydrophobic core interior to the active site and subunit interface (Wongsantichon *et al.*, 2003). In addition to this spatial motif, adgstD4-4 also possesses several other intersubunit interactions which contribute to interface formation, as previously discussed in Wongsantichon & Ketterman (2005). The Val107 residue has been studied by substitution with six different amino acids of various sizes and properties in order to elucidate its role in the dimeric enzyme (Wongsantichon & Ketterman, 2006). All engineered mutants were found to be catalytically active, demonstrating the presence of dimeric active forms, which suggests that the residue position is not critical for dimerization. Steady-state kinetics studies using GSH and CDNB as co-substrates show that substitutions by hydrophobic and uncharged residues at the Val107 position have no effect on the catalytic properties, whereas positively and negatively charged residues diminish the enzyme catalytic rate ($k_{cat}$) and weaken the binding affinity towards GSH substrate ($K_m$), with positive cooperativity observed upon binding. In this regard, charged residue replacements were considered to be unfavourable in the region. However, all engineered mutants appeared to enhance thermal stability as demonstrated by a heat-inactivation assay at 318 K, suggesting that the residue also plays a role in structural stabilization. Of the mutants, adgstD4-4 V107A shows the greatest half-life (390.2 $\pm$ 22.4 min), which is about 32 times that of the wild type (12.3 $\pm$ 0.9 min). There is no marked alteration in the secondary or tertiary structure of V107A as shown by far-UV circular dichroism and tryptophan intrinsic fluorescence, respectively. Nevertheless, conformational rearrangement at the quaternary structural level or subunit dimerization of the engineered enzyme was observed by fluorescence dye binding using 1-anilinonaphthalene-8-sulfonic acid (ANS), which is reported to bind in the hydrophobic cleft along the dimeric interface in GST class $\alpha$ (Sayed *et al.*, 2002). As shown by the above data, substitution of valine by alanine at position 107 in adgstD4-4 appears to be structurally important and alters the enzyme stability and subunit dimerization, while maintaining similar catalytic properties to the wild type. Therefore, structural determination of the mutant is of interest and would be useful in understanding the protein structure–function correlation, particularly for enzyme stability.

## 2. Material and methods

### 2.1. Construction and purification of V107A

A single point mutation of *A. dirus* glutathione transferase isoform 4 (adgstD4-4) was obtained by PCR-based site-directed mutagenesis, replacing valine with alanine at position 107 using the Stratagene Quick Change site-directed mutagenesis kit (Stratagene). The engineered enzyme was overexpressed by 0.1 m*M* IPTG (isopropyl 1-thio-$\beta$-D-galactopyranoside) induction at 298 K in *Escherichia coli* BL21(DE3) pLysS as soluble protein and was purified using GSTrap FF affinity chromatography (Amersham Pharmacia) as previously described (Wongtrakul *et al.*, 2003).

### 2.2. Crystallization and X-ray data collection

The purified protein was concentrated using an Amicon Ultra-15 centrifugal filter device (Millipore) with 10 kDa cutoff and filtered through an Ultrafree-MC 0.22 µm centrifugal filter unit (Millipore). Prior to crystallization, the protein concentration was adjusted to 9 mg ml$^{-1}$ in 50 m*M* Tris–HCl pH 7.5, 10 m*M* DTT in the presence of 10 m*M* GSH substrate. The hanging-drop vapour-diffusion method was used with a crystallization droplet comprising of 2 µl protein solution and 2 µl reservoir solution consisting of 0.1 *M* imidazole pH 7.0, 0.35 *M* ammonium acetate and 30%(*w*/*v*) polyethylene glycol (PEG) 4000. The volume of solution in the reservoir was 0.5 ml. Crystals appeared within one week at 295 K. A single prismatic crystal with dimensions 0.46 × 0.30 × 0.18 mm was obtained; it was dissected into a smaller piece of dimensions 0.28 × 0.08 × 0.07 mm and briefly soaked in a cryosolution consisting of 0.1 *M* imidazole pH 7.0, 0.368 *M* ammonium acetate, 32%(*w*/*v*) PEG 4000 and 10%(*v*/*v*) glycerol before being flash-frozen in a liquid-nitrogen stream at 110 K.

X-ray diffraction data were collected at the Center for Excellence in Protein Structure and Function, Faculty of Science, Mahidol University, Thailand. X-ray diffraction patterns were recorded on an R-AXIS IV$^{++}$ image-plate system (Rigaku/MSC) using Cu $K\alpha$ radiation from a Rigaku RU-H3R rotating-anode X-ray generator operating at 50 kV and 100 mA equipped with Osmic Confocal Maxflux multi-layer optics and a 0.3 mm collimator. The crystal was flash-frozen using an X-Stream 2000 low-temperature system (Rigaku/MSC). Data were processed and scaled using the *CrystalClear*/*d***TREK* program suite (Pflugrath, 1999).

## 3. Results and discussion

After initial screening, the crystallization conditions were optimized by varying the pH of the buffer from 4.6 to 7.5 and the concentration of ammonium acetate from 0.25 to 0.40 *M*. Two different crystal morphologies, fine rod-shaped and prism-shaped, were obtained from the screening in 0.1 *M* imidazole pH 7.0 within a week. A single prism-shaped crystal chosen for X-ray diffraction was obtained from conditions consisting of 32%(*w*/*v*) PEG 4000, 0.35 *M* ammonium acetate, 0.1 *M* imidazole pH 7.0 in the presence of 10 m*M* GSH. However, owing to its large dimensions of 0.46 × 0.30 × 0.18 mm, as shown in Fig. 1, a glass fibre was used to dissect the crystal to a smaller volume to facilitate freezing on a cryoloop. The crystal slice was briefly soaked in a cryosolution consisting of reservoir solution containing 10%(*v*/*v*) glycerol and approximately 5% higher concentrations of PEG 4000 and ammonium acetate. The crystal slice was flash-frozen in a liquid-nitrogen stream. Diffraction data were collected to an effective resolution of 2.47 Å using a 240 mm crystal-to-detector distance with an exposure time of 150 s and covering 0.25° oscillation per image (Fig. 2).

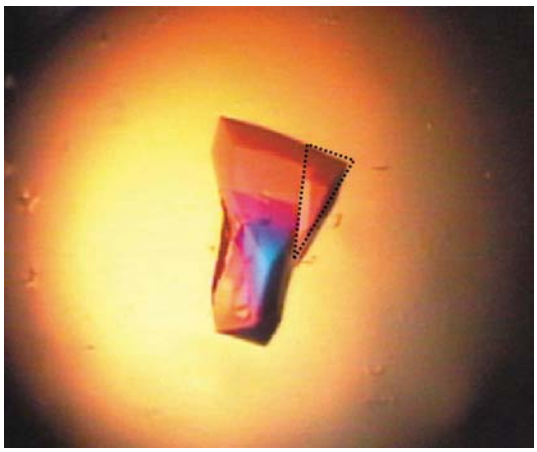

**Figure 1**
A prism-shaped crystal of adgstD4-V107A photographed under polarized light. The crystal size is 0.46 × 0.30 × 0.18 mm for the largest dimensions. The dotted triangle represents the crystal slice that was used for X-ray diffraction.

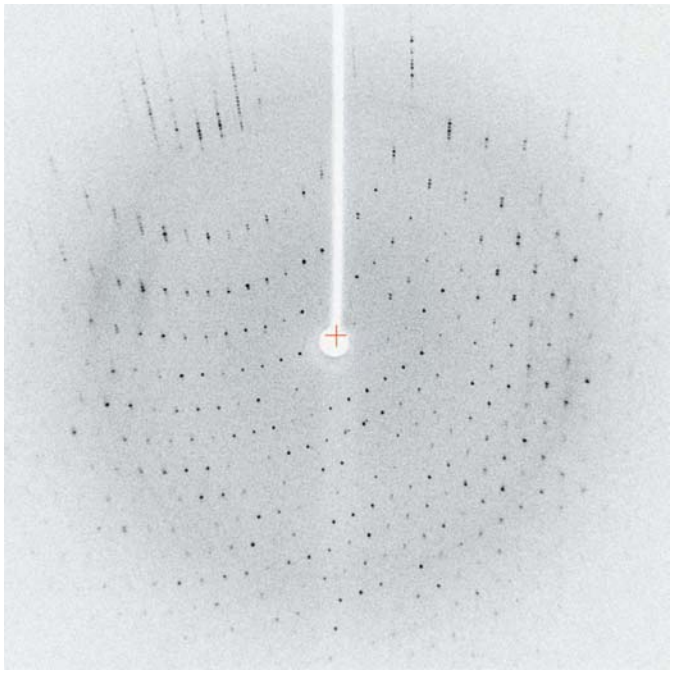

**Figure 2**
A 0.25° rotation photograph showing the X-ray diffraction pattern from the crystal slice.

The engineered mutant in this study can also be crystallized using the conditions previously reported for the wild-type enzyme (Oakley, Jirajaroenrat *et al.*, 2001), consisting of 30%(*w*/*v*) PEG 8000, 0.2 *M* sodium acetate and 0.1 *M* sodium cacodylate pH 6.5, generating fine rod-shaped crystals. In this regard, the present study demonstrates that different crystal morphologies can be derived from different crystallization conditions. However, preliminary X-ray crystallographic analysis shows that the diffraction patterns of a prism-shaped crystal from the engineered mutant and of a rod-shaped $P3_221$ crystal of the wild type (PDB code 1jlw) are isomorphous (Oakley, Jirajaroenrat *et al.*, 2001). Diffraction spots of the mutant were initially scaled and merged in space group *P*321 (as summarized in Table 1) even though they showed absences that could be characteristic of either of the trigonal space groups $P3_121$ or $P3_221$. This was to preserve all the data for subsequent verification of the correct space group by molecular-replacement calculations. The initial phases of the adgstD4-4 V107A structure were determined with *AMoRe* from the *CCP*4 program suite (Collaborative Computational Project, Number 4, 1994; Navaza, 1994) using chain *A* of the wild-type structure as a search model. Translation searches in the three space groups *P*321, $P3_121$ and $P3_221$ showed a good result for calculation in space group $P3_221$, which gave an amplitude correlation coefficient (CC) of 43.1% and an *R* factor of 48.1% for the best solution, compared with CC = 20.7%, *R* = 56.6% and CC = 23.1%, *R* = 55.0% for the other two space groups. Addition of the second molecule resulted in a CC of 72.3% on amplitude and 76.4% on intensity with an *R* factor of 35.8% after the fitting calculation. Examination of the best solution revealed good crystal packing and no clashes between symmetry-related molecules. This shows that the molecular packing is preserved, suggesting that the V107A mutation and the presence of GSH do not cause large structural deviation from the non-ligand-bound wild-type structure. This preliminary model of the engineered mutant is currently being refined and will be further studied to investigate the marked increase in structural stability.

**Table 1**
Data-collection statistics for adgstD4-4 V107A crystals in complex with GSH.

Values in parentheses correspond to the highest resolution shell.

| | |
|---|---|
| Space group | $P3_221$ |
| Unit-cell parameters | |
| *a*, *b* (Å) | 49.4 |
| *c* (Å) | 272.4 |
| $\alpha$, $\beta$ (°) | 90 |
| $\gamma$ (°) | 120 |
| Unit-cell volume (Å$^3$) | 575799 |
| Resolution limits (Å) | 42.78–2.47 (2.56–2.47) |
| No. of observed reflections | 65482 |
| No. of unique reflections | 14436 |
| Completeness (%) | 95.3 (80.0) |
| Multiplicity | 2.55 (1.5) |
| $R_{\rm merge}$† (%) | 10.2 (16.8) |
| $\langle I/\sigma(I)\rangle$ | 4.9 (2.2) |
| $V_{\rm M}$ (Å$^3$ Da$^{-1}$) | 1.9 |
| Solvent content (%) | 35.4 |
| No. of molecules per ASU | 2 |

† $R_{\rm merge} = \sum_{hkl}\sum_i |I_i(hkl) - \langle I(hkl)\rangle| / \sum_{hkl}\sum_i I_i(hkl)$, where $I_i$ is the intensity of the *i*th measurement of an equivalent reflection with indices *hkl*.

This work was supported by a grant from the Thailand Research Fund to AJK and a Royal Golden Jubilee scholarship to JW.

## References


Armstrong, R. N. (1991). *Chem. Res. Toxicol.* **4**, 131–140.
Chen, L., Hall, P. R., Zhou, X. E., Ranson, H., Hemingway, J. & Meehan, E. J. (2003). *Acta Cryst.* D**59**, 2211–2217.
Collaborative Computational Project, Number 4 (1994). *Acta Cryst.* D**50**, 760–763.
Dixon, D. P., Lapthorn, A. & Edwards, R. (2002). *Genome Biol.* **3**, 1–10.
Hayes, J. D., Flanagan, J. U. & Jowsey, I. R. (2005). *Annu. Rev. Pharmacol. Toxicol.* **45**, 51–88.
Hayes, J. D. & Pulford, D. J. (1995). *CRC Crit. Rev. Biochem. Mol. Biol.* **30**, 445–600.
Mannervik, B. & Danielson, U. H. (1988). *CRC Crit. Rev. Biochem.* **23**, 283–337.
Navaza, J. (1994). *Acta Cryst.* A**50**, 157–163.
Oakley, A. J., Harnnoi, T., Udomsinprasert, R., Jirajaroenrat, K., Ketterman, A. J. & Wilce, M. C. J. (2001). *Protein Sci.* **10**, 2176–2185.
Oakley, A. J., Jirajaroenrat, K., Harnnoi, T., Ketterman, A. J. & Wilce, M. C. J. (2001). *Acta Cryst.* D**57**, 870–872.
Pflugrath, J. W. (1999). *Acta Cryst.* D**55**, 1718–1725.
Sayed, Y., Hornby, J. A. T., Lopez, M. & Dirr, H. (2002). *Biochem. J.* **363**, 341–346.
Udomsinprasert, R., Pongjaroenkit, S., Wongsantichon, J., Oakley, A. J., Prapanthadara, L., Wilce, M. C. J. & Ketterman, A. J. (2005). *Biochem. J.* **388**, 763–771.
Wilce, M. C. J., Board, P. G., Feil, S. C. & Parker, M. W. (1995). *EMBO J.* **14**, 2133–2143.
Wilce, M. C. J., Feil, S. C., Board, P. G. & Parker, M. W. (1994). *J. Mol. Biol.* **236**, 1407–1409.
Wongsantichon, J., Harnnoi, T. & Ketterman, A. J. (2003). *Biochem. J.* **373**, 759–765.
Wongsantichon, J. & Ketterman, A. (2005). *Methods Enzymol.* **401**, 100–116.
Wongsantichon, J. & Ketterman, A. J. (2006). *Biochem. J.* **394**, 135–144.
Wongtrakul, J., Udomsinprasert, R. & Ketterman, A. (2003). *Insect Biochem. Mol. Biol.* **33**, 971–979.

Available online at www.sciencedirect.com
SCIENCE DIRECT
Food and Chemical Toxicology 44 (2006) 1348–1354
Reprint 5
Food and Chemical Toxicology
www.elsevier.com/locate/foodchemtox

# Effect of different Thai traditional processing of various hot chili peppers on urethane-induced somatic mutation and recombination in *Drosophila melanogaster*: Assessment of the role of glutathione transferase activity

P. Laohavechvanich [a,*], K. Kangsadalampai [a], N. Tirawanchai [b], A.J. Ketterman [c]

[a] *Institute of Nutrition, Mahidol University, Salaya, Phutthamonthon 4, Nakhon Pathom 73170, Thailand*
[b] *Department of Biochemistry, Medicine Faculty, Siriraj Hospital, Bangkok 10700, Thailand*
[c] *Institute of Molecular Biology and Genetics, Mahidol University, Nakhon Pathom 73170, Thailand*

Received 14 June 2005; accepted 23 February 2006

**Abstract**

Four different Thai traditional chili peppers, namely bird pepper (*Capsicum frutescens*), red chili spur peppers (*Capsicum annuum*), green bell peppers and sweet pepper (*C. annuum*) were investigated for their antimutagenic properties. Each chili was prepared in three formulations commonly used for chili food processing; raw paste (chili ground in water), pickled in vinegar or stir-fried in palm oil. Each sample was tested for its antimutagenic effect against urethane by using the somatic mutation and recombination of wing hair of *Drosophila melanogaster* as an indicator. Three-day-old larvae, *trans*-heterozygous for two genetic markers, multiple wing hairs *mwh* and orrigon (ORR; $flr^3$), were exposed to urethane alone or in combination with each chili formulation. The various processing methods for chilies differentially extracted the antimutagenic chili components. The specific chili as well as the method of processing influenced the observed antimutagenic properties against urethane. This suggested each chili contains a unique complex mixture of many antimutagens. Co-treatment and pre-treatment experiments showed that both direct and indirect protective mechanisms are involved in an 'activation' process to give antimutagenesis effects. An association between antigenotoxicity and glutathione transferase activity could not be established.


*Keywords:* Chili; Urethane; SMART; Glutathione transferase; Antimutagens

## 1. Introduction

Hot chili pepper is a common spice in Thai cuisine and it is widely consumed as a food additive throughout the world, particularly in South East Asia and Latin-American countries. The consumption of pepper (*Capsicum annuum*) has been traditional for thousands of years in some parts of the world with estimates of per capita dietary intake to be about 40 g/day (Gonzalez de Mejia et al., 1998). Peppers are an important source of β-carotene, which have antimutagenic and/or anticarcinogenic properties (Monsereenusorn et al., 1982). Initial work showed that rats fed diets containing 10% chili pepper developed liver tumors (Hoch-Ligeti, 1952). Contrastingly, extracts of certain spices or their isolated constituents could block the processes of experimental carcinogenesis and mutagenesis (Unnikrishnan and Kuttan, 1990). A recent study reported that green pepper juice had antimutagenic effects on the nitrosation process of methyl urea and sodium nitrite in a Drosophila spot test (Ramirez-Victoria et al., 2001). Although it is not clear whether the green pepper juice

*Abbreviations*: CYP, cytochrome; SMART, somatic mutation and recombination test.

* Corresponding author. Tel.: +66 2 800 2380x116; fax: +66 2 441 9344.
*E-mail address:* nuplh@mahidol.ac.th (P. Laohavechvanich).

0278-6915/$ - see front matter © 2006 Elsevier Ltd. All rights reserved.
doi:10.1016/j.fct.2006.02.013

had an inhibitory effect on the nitrosation process, or had an inhibitory effect on the mutagenic activity of the nitrosation product. Furthermore, El Hamss showed that bell peppers and black peppers possessed antimutagenic activity shown by somatic mutation and recombination assay using *Drosophila* at concentrations of bell pepper of 5% and 10% (w/v) and black peppers of 1% and 2% (w/v) (El Hamss et al., 2003).

In Asian cuisine, chilies are consumed in several different ways such as fresh chili, chili in vinegar or stir fried chili. These different methods of processing chili have never been tested to determine antimutagenicity effects. Four different Thai traditional chili peppers, namely bird pepper, red chili spur pepper, green bell pepper and sweet pepper were investigated for their antimutagenicity. Each chili was prepared to be a raw paste (chili ground in water), pickled in vinegar or stir-fried in palm oil. The solid and liquid extract (chili extract) of each sample were tested for their effect on the mutagenic activity of urethane using the somatic mutation and recombination test (SMART) of wing hair of *Drosophila melanogaster* as an indicator. The SMART assay is based on induced loss of heterozygosity, which may occur through various mechanisms, such as point mutation, deletions, certain types of chromosome aberrations as well as mitotic recombination and gene conversion (Graf et al., 1984). It is also well suited to determine the antimutagenic properties of single compounds or complex mixtures (Negishi et al., 1989; Graf et al., 1998). The high bioactivation (HB) strain of *D. melanogaster* used in this study is characterized by an increased cytochrome P450-dependent bioactivation capacity for promutagens and procarcinogens. We also examined whether the activity of the detoxication enzyme, glutathione transferase, changed with exposure to the chili samples in the presence and absence of urethane.

## 2. Material and methods

### 2.1. Chemical compounds and media

Ethyl carbamate (Urethane; CAS no. 51-79-6) purchased from Sigma, was dissolved in distilled water and mixed into the yeast–glucose–agar Drosophila medium which was slightly modified from the formula of (Robert, 1986). Reduced glutathione (GSH; CAS no.70-18-8), 1-chloro-2,4-dinitrobenzene (CAS no. 97-00-7) were purchased from Sigma Company. Bradford reagent (CAS no. 500-0006) was obtained from Bio-Rad Laboratories.

### 2.2. Chili preparation

This study used four types of chili. Three types of chilies were *C. annuum* L.; red chili spur pepper (hot pepper), green bell pepper and sweet pepper (non-hot chili). The fourth type was *Capsicum frutescens*, that is, bird chili pepper (hot pepper).

Chilies were purchased from the local market. Pedicles were removed and the chilies cleaned with tap water several times and soaked in sodium lauryl ether sulfate 7% (w/w) 20 min to remove adhering contaminants. Each chili was chopped into pieces and ground in an electrical blender and freeze dried. After freeze dry processing the chili were ground again in a blender.

Ground chili (0.5 g) was mixed with 4.5 ml water (1:9 w/w) or 5% distilled vinegar , and then added to the medium (corn flour 0.562, sugar 0.45 g, yeast 0.225 g, agar 0 .063 g). For the stir-fried chili in palm oil sample, ground chili (0.5 g) was stir-fried with palm oil 1.5 g (1:3 w/w) and mixed with medium.

Ground chili was suspended in water or vinegar (1:9 w/w) and then was further processed using a polytron homogenizer. The homogenate was filtered through Whatman paper No. 54 to obtain soluble fraction and residual fiber. The stir-fried chili in palm oil (1:3 w/w), after grinding, was extracted with 2 ml hexane and then filtered through cotton mesh and Whatman paper and dried under nitrogen gas. Chili extract (water extract, vinegar extract and oil extract) was diluted by adding the equivalent weight of chili extract to water (or vinegar) (1:1) and then mixed with medium.

### 2.3. D. melanogaster strains and crosses

Two strains of *D. melanogaster* were used. Virgin Females of *ORR/ORR;flr*$^3$*/In (3LR) TM3, ri p*$^p$ *sep l (3) 89Aa bx*$^{34e}$ *e Bd*$^s$, *Ser* were crossed with males of *mwh/mwh*. Both strains were obtained from the Institute of Toxicology, Swiss Federal Institute of Technology and University of Zurich.

### 2.4. Somatic mutation and recombination test (SMART assay)

The Virgin *ORR;flr3* females and *mwh* males were mated on the standard medium. Six days after mating, the 3-day-old larvae were transferred in equal batches to experimental medium (chili control), the experimental medium containing 20 mM urethane (test model), standard medium (negative control) and standard medium containing 20 mM urethane (positive control). The surviving adult flies were collected on days 7–10 after pupation. Only the insects bearing the marker *trans*-heterozygous (*mwh+/+flr*$^3$) indicated by round wings were stored in 70% ethanol. Subsequently, the wings were removed, mounted and scored by using a compound microscope for observation of the wing spots (Graf et al., 1984; Graf et al., 1989; Graf et al., 1994).

### 2.5. Co-treatment

Three day old larvae were transferred to a tube with *Drosophila* medium that contained one of the 3 different processed forms of each chili. Three different processed forms of each chili, urethane and each processed chili with urethane were used for chronic larval feeding. For negative controls, the larvae were transferred into medium prepared with distilled water, or 5% distilled vinegar, or palm oil.

### 2.6. Pre-treatment

The flies were mated on the experimental medium. Six days after mating, the 3-day-old larvae were transferred in equal batches to either experimental medium containing 20 mM urethane or the experimental medium without urethane as sample control. Negative and positive controls were conducted similarly to those in co-administration study. The surviving adult flies were collected on days 10–12 after pupation.

### 2.7. Data evaluation and statistical analysis

To obtain a statistical assessment of antimutagenicity, the frequencies of total spots per wing were compared in pairs (that is, urethane alone versus urethane plus each chili; urethane plus each chili versus urethane plus each chili) using the non-parametric Mann–Whitney *U*-test (Frei and Wurgler, 1995). Level of significance was set for $p < 0.05$. To allow a quantitative comparison, the percentage of inhibition was determined for each category of spot. The percentage of inhibition was also calculated as following $100(a - b)/a$ where $a$ is the frequency of spots induced by urethane alone and $b$ the frequency of spots induced by urethane in the presence of chili (Abraham, 1994).

### 2.8. Assay of glutathione transferase activity

All subsequent preparation procedures were carried out below 4 °C. Larvae were ground in 0.2 M phosphate buffer, pH 6.5 at the ratio of 0.5 g per 0.5 ml buffer with a glass rod. The homogenate was centrifuged at 15,000 g. for 10 min. The supernatant was diluted immediately (1:5) with 0.1 M phosphate buffer before assaying glutathione transferase activity. This assay is based on the reaction between 1 mM 1-chloro-2,4-dinitrobenzene and 10 mM glutathione in 0.1 M sodium phosphate buffer, pH 6.5 (Habig et al., 1974). Protein concentration was determined by the Bradford method (Bradford, 1976) using the Bio-Rad Laboratories (Hercules, CA, USA) protein reagent with bovine serum albumin as standard protein.

## 3. Result

The ground chili pastes (ground chili in water, in vinegar and in oil) as well as each chili extract were not toxic in 48 h larval feeding. The frequency of total spots per wing recorded in these sample controls was 0.00–0.15 (data not shown). In the negative control series (water, vinegar and oil) the frequency of spots was within the range of 0.12– 0.35 (Tables 1–6). The data given in Tables 1–6 demonstrate that the different processing were not equally effective in significantly reducing the mutagenicity of urethane. In the pre-treatment experiments, each of the chili showed a broad but differing range of effectiveness with bird pepper (3–95%), red chili spur pepper (17–82%), green bell pepper (8–31%) and sweet pepper (24–54%). In general the different processing, when effective, significantly reduced not only the total spot frequency but also the twin spot frequency. Single spots are produced either by mitotic recombination or by somatic mutation, deletion or other changes. Twin spots are produced exclusively by mitotic recombination occurring between the proximal marker *flr* and the centromere.

Hot chili pepper (bird pepper; *C. frutescens*) in oil extract reduced mutagenicity more than green bell pepper or sweet pepper (*C. annuum*) in both pre-treatment and co-treatment (Fig. 1). However, sweet pepper gave greater

Table 1
Inhibitory effect of ground chili in water on 20 mM urethane induced mutagenicity in pre-treatment

| Pre-treatment study of ground chili in water | Frequency of spots per wing (number of spots from 40 wings)* | | | | | | | | % Inhibition |
|---|---|---|---|---|---|---|---|---|---|
| | Small single spots (1–2 cells) | | Large single spots (>2 cells) | | Twin spots | | Total spots | | |
| Water control | 0.33 | (13) | 0.03 | (1) | 0.00 | (0) | 0.35 | (14) | |
| Urethane (URE) | 5.58 | (223)$^{a}$ | 1.85 | (74)$^{a}$ | 1.35 | (54)$^{a}$ | 8.78 | (351)$^{a}$ | |
| Bird pepper + URE | 3.73 | (149)$^{b}$ | 1.43 | (57)$^{a}$ | 1.15 | (46)$^{ab}$ | 6.30 | (252)$^{c}$ | 28 |
| Red chili spur pepper + URE | 3.98 | (159)$^{b}$ | 1.83 | (73)$^{a}$ | 1.33 | (53)$^{a}$ | 7.13 | (285)$^{b}$ | 19 |
| Green bell pepper + URE | 3.90 | (156)$^{b}$ | 1.55 | (62)$^{a}$ | 1.20 | (48)$^{a}$ | 6.65 | (266)$^{bc}$ | 24 |
| Sweet pepper + URE | 4.08 | (163)$^{b}$ | 1.63 | (65)$^{a}$ | 0.95 | (38)$^{b}$ | 6.65 | (266)$^{bc}$ | 24 |

* Within a column different superscripts are significantly different at $p < 0.05$.

Table 2
Inhibitory effect of ground chili in vinegar on 20 mM urethane induced mutagenicity in pre-treatment

| Pre-treatment study of ground chili in vinegar | Frequency of spots per wing (number of spots from 40 wings)* | | | | | | | | % Inhibition |
|---|---|---|---|---|---|---|---|---|---|
| | Small single spots (1–2 cells) | | Large single spots (>2 cells) | | Twin spots | | Total spots | | |
| Vinegar control | 0.18 | (7) | 0.00 | (0) | 0.00 | (0) | 0.18 | (7) | |
| Urethane (URE) | 5.00 | (200)$^{a}$ | 1.53 | (61)$^{a}$ | 1.13 | (45)$^{a}$ | 7.65 | (306)$^{a}$ | |
| Bird pepper + URE | 3.15 | (126)$^{bc}$ | 1.05 | (42)$^{b}$ | 0.50 | (20)$^{bc}$ | 4.70 | (188)$^{c}$ | 39 |
| Red chili spur pepper + URE | 3.00 | (120)$^{c}$ | 1.00 | (40)$^{b}$ | 0.50 | (20)$^{bc}$ | 4.50 | (180)$^{c}$ | 41 |
| Green bell pepper + URE | 3.48 | (139)$^{b}$ | 1.15 | (46)$^{b}$ | 0.63 | (25)$^{b}$ | 5.25 | (210)$^{b}$ | 31 |
| Sweet pepper + URE | 2.83 | (113)$^{c}$ | 0.63 | (25)$^{c}$ | 0.28 | (11)$^{c}$ | 3.73 | (149)$^{d}$ | 51 |

* Within a column different superscripts are significantly different at $p < 0.05$.

Table 3
Inhibitory effect of ground chili in oil on 20 mM urethane induced mutagenicity in pre-treatment

| Pre-treatment study of ground chili in oil | Frequency of spots per wing (number of spots from 40 wings)* | | | | | | | | % Inhibition |
|---|---|---|---|---|---|---|---|---|---|
| | Small single spots (1–2 cells) | | Large single spots (>2cells) | | Twin spots | | Total spots | | |
| Oil control | 0.10 | (4) | 0.02 | (1) | 0.00 | (0) | 0.12 | (5) | |
| Urethane (URE) | 4.88 | (195)$^{a}$ | 1.65 | (66)$^{a}$ | 1.18 | (47)$^{a}$ | 7.70 | (308)$^{a}$ | |
| Bird pepper + URE | 0.90 | (36)$^{d}$ | 0.23 | (9)$^{d}$ | 0.10 | (4)$^{c}$ | 1.23 | (49)$^{e}$ | 84 |
| Red chili spur pepper + URE | 2.98 | (119)$^{c}$ | 0.80 | (32)$^{b}$ | 0.43 | (17)$^{b}$ | 4.20 | (168)$^{c}$ | 45 |
| Green bell pepper + URE | 3.68 | (147)$^{b}$ | 1.60 | (64)$^{a}$ | 1.10 | (44)$^{a}$ | 6.38 | (255)$^{b}$ | 17 |
| Sweet pepper + URE | 2.68 | (107)$^{c}$ | 0.55 | (22)$^{b}$ | 0.33 | (13)$^{b}$ | 3.55 | (142)$^{d}$ | 54 |

* Within a column different superscripts are significantly different at $p < 0.05$.

Table 4
Inhibitory effect of water extract on 20 mM urethane induced mutagenicity in pre-treatment

| Pre-treatment study of water extract of each chili | Frequency of spots per wing (number of spots from 40 wings)* | | | | | | | | % Inhibition |
|---|---|---|---|---|---|---|---|---|---|
| | Small single spots (1–2 cells) | | Large single spots (>2 cells) | | Twin spots | | Total spots | | |
| Water control | 0.22 | (9) | 0.02 | (1) | 0.00 | (0) | 0.25 | (10) | |
| Urethane (URE) | 5.50 | (220)$^{a}$ | 2.13 | (85)$^{a}$ | 1.55 | (62)$^{a}$ | 9.18 | (367)$^{a}$ | |
| Bird pepper + URE | 2.55 | (102)$^{d}$ | 0.90 | (36)$^{d}$ | 0.78 | (31)$^{b}$ | 4.23 | (169)$^{d}$ | 54 |
| Red chili spur pepper + URE | 3.08 | (123)$^{c}$ | 1.28 | (51)$^{c}$ | 0.85 | (34)$^{b}$ | 5.20 | (208)$^{c}$ | 43 |
| Green bell pepper + URE | 4.48 | (179)$^{b}$ | 1.55 | (62)$^{b}$ | 0.93 | (37)$^{b}$ | 6.95 | (278)$^{b}$ | 24 |
| Sweet pepper + URE | 4.43 | (177)$^{b}$ | 1.50 | (60)$^{bc}$ | 1.03 | (41)$^{b}$ | 6.95 | (278)$^{b}$ | 24 |

* Within a column different superscripts are significantly different at $p < 0.05$.

Table 5
Inhibitory effect of vinegar extract on 20 mM urethane induced mutagenicity in pre-treatment

| Pre-treatment study of vinegar extract of each chili | Frequency of spots per wing (number of spots from 40 wings)* | | | | | | | | % Inhibition |
|---|---|---|---|---|---|---|---|---|---|
| | Small single spots (1–2 cells) | | Large single spots (>2 cells) | | Twin spots | | Total spots | | |
| Vinegar control | 0.22 | (9) | 0.00 | (0) | 0.00 | (0) | 0.22 | (9) | |
| Urethane (URE) | 6.15 | (246)$^{a}$ | 2.15 | (86)$^{a}$ | 1.35 | (54)$^{a}$ | 9.65 | (386)$^{a}$ | |
| Bird pepper + URE | 5.90 | (236)$^{a}$ | 2.10 | (84)$^{ab}$ | 1.35 | (54)$^{a}$ | 9.35 | (374)$^{ab}$ | 3 |
| Red chili spur pepper + URE | 4.78 | (191)$^{b}$ | 2.15 | (86)$^{ab}$ | 1.08 | (43)$^{ab}$ | 8.00 | (320)$^{c}$ | 17 |
| Green bell pepper + URE | 5.63 | (225)$^{a}$ | 1.98 | (79)$^{ab}$ | 1.28 | (51)$^{a}$ | 8.88 | (355)$^{b}$ | 8 |
| Sweet pepper + URE | 3.53 | (141)$^{c}$ | 1.73 | (69)$^{b}$ | 1.03 | (41)$^{b}$ | 6.28 | (251)$^{d}$ | 35 |

* Within a column different superscripts are significantly different at $p < 0.05$.

Table 6
Inhibitory effect of oil extract on 20 mM urethane induced mutagenicity in pre-treatment

| Pre-treatment study of oil extract of each chili | Frequency of spots per wing (number of spots from 40 wings)* | | | | | | | | % Inhibition |
|---|---|---|---|---|---|---|---|---|---|
| | Small single spots (1–2 cells) | | Large single spots (>2 cells) | | Twin spots | | Total spots | | |
| Oil control | 0.10 | (4) | 0.05 | (2) | 0.00 | (0) | 0.15 | (6) | |
| Urethane (URE) | 4.38 | (175)$^{a}$ | 1.68 | (67)$^{a}$ | 1.13 | (45)$^{a}$ | 7.18 | (287)$^{a}$ | |
| Bird pepper + URE | 0.30 | (12)$^{e}$ | 0.08 | (3)$^{d}$ | 0.00 | (0)$^{d}$ | 0.38 | (15)$^{e}$ | 95 |
| Red chili spur pepper + URE | 0.90 | (36)$^{d}$ | 0.28 | (11)$^{c}$ | 0.10 | (4)$^{c}$ | 1.28 | (51)$^{d}$ | 82 |
| Green bell pepper + URE | 3.58 | (143)$^{b}$ | 1.43 | (57)$^{a}$ | 0.75 | (30)$^{b}$ | 5.75 | (230)$^{b}$ | 20 |
| Sweet pepper + URE | 2.55 | (102)$^{c}$ | 0.68 | (27)$^{b}$ | 0.45 | (18)$^{b}$ | 3.68 | (147)$^{c}$ | 49 |

* Within a column different superscripts are significantly different at $p < 0.05$.

inhibition of mutagenicity than green bell pepper in all processing (Fig. 1c and d). In general, oil extracts of the chili showed greater antimutagenicity than the vinegar or water extracts in the co-treatment study (Fig. 1).

To determine whether glutathione transferase is involved in antimutagenicity of the chili two chili treatment groups showing the greatest effects were selected to assay glutathione transferase activity. No significant change in glutathione transferase activity was observed. This suggests that glutathione transferase is not involved in the antimutagenicity.

## 4. Discussion

This project was to compare the antimutagenic properties of various chili processed in several ways. The processing methods employed were chosen to mimic the processing used for chili in human diet. The antimutagenic properties were evaluated in the *Drosophila* wing spot test (SMART); using chili as a protective agent against genotoxic effects induced by urethane, which is a promutagen requiring metabolic activation. The results show the specific chili as well as the method of processing influence the observed antimutagenic properties against urethane. The genotoxicity of urethane and the reactive metabolites have been investigated in a variety of test systems or organisms, such as bacteria, yeast, mammalian cells, *Drosophila*, and rodents (Mirvish, 1996; Mirvish, 1968; Zimmerli and Schlatter, 1991; Giri, 1995; Ballering et al., 1996). The high bioactivation (HB) *D. melanogaster* strain used in the present study is highly sensitive to the genotoxic effects of urethane because of its high constitutive level of cytochrome P-450 activity (Frolich and Wurgler, 1990; Graf and van Schaik, 1992). Hence, it represents an extreme state of genetic

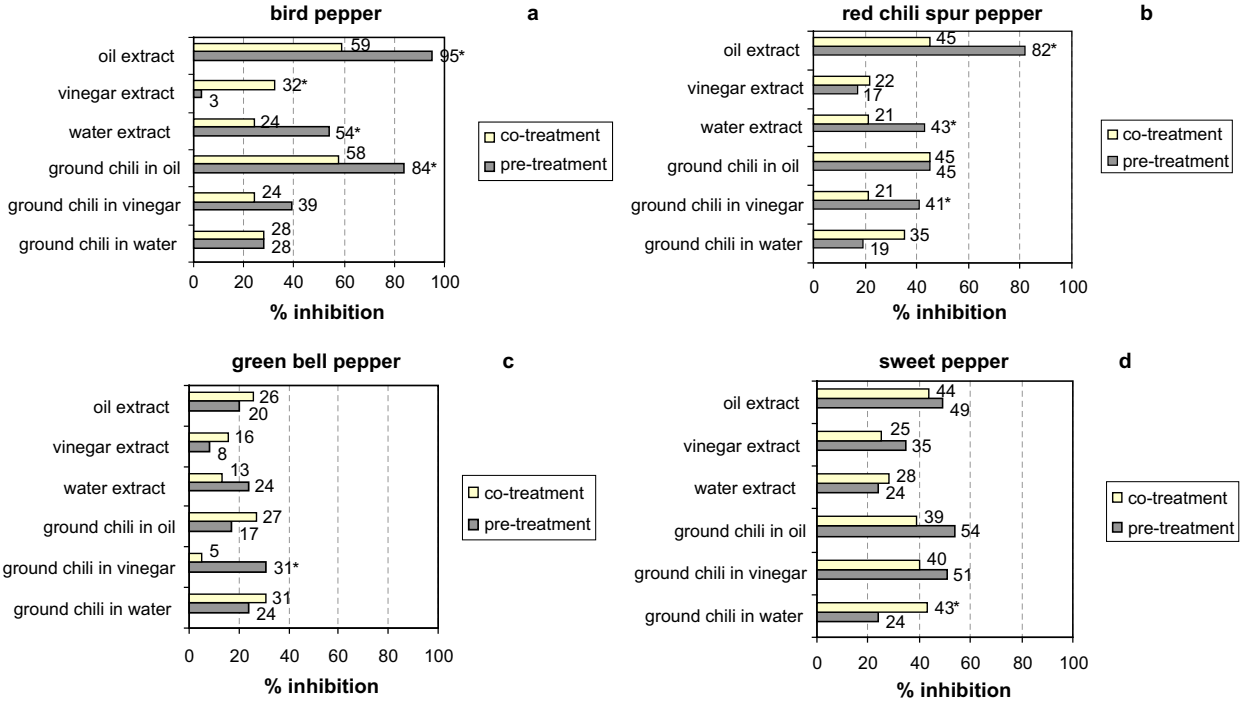


Fig. 1. Co-treatment and pre-treatment effects with four kinds of chili (bird pepper, red chili spur pepper, green bell pepper, and sweet pepper) on the mutagenicity of urethane in *D. melanogaster*. The experimental medium consisted of ground chili mixed with (1:9 w/w) water or 5% distilled vinegar and then added to the medium. For the stir-fried chili in palm oil sample, ground chili was stir-fried with palm oil (1:3 w/w) and mixed with medium. Chili extract (water, vinegar, oil) was the soluble fraction from extraction of the ground chili in water, in vinegar and in oil samples. Larvae of 72 h were exposed to experimental medium containing 20 mM urethane (co-treatment). For pre-treatment, the tester strain flies were mated on the experimental medium and then transferred in the experimental medium containing 20 mM urethane. The values beside the bars in the plots are percent inhibition of urethane mutagenicity. The significantly different ($p < 0.05$) values are indicated with an ∗. The inhibition of urethane mutagenicity by experimental medium which was calculated as follows: (genotoxin alone-genotoxin plus chili treatment/genotoxin alone) × 100.

susceptibility to urethane. The pathway of activation of urethane is thought to involve two steps, both catalyzed by the cytochrome P-450 CYP 2E1; these steps are desaturation or urethane to vinyl carbamate, followed by oxidation to vinyl carbamate epoxide (Guengerich et al., 1991). The metabolic activation of urethane to DNA binding metabolites also involves cytochrome P-450 dependent enzyme activities in *D. melanogaster*. Urethane is found in very small quantities in several fermented foods and beverages such as stone-fruit brandies, sherries and table wines (Schlatter and Lutz, 1990; Stoewsand et al., 1991). This has evoked interest in carrying out investigations to identify chili pepper that can inhibit the carcinogenic effects of urethane.

Although to different extents, the chilies studied reduced all types of mutations induced by urethane. The differences in antimutagenic effect suggest that the mixture of anti- mutagenic compounds varied among the tested chilies. Moreover, the extraction of the available antimutagenic compounds occurred with different efficiencies depending on the chili processing method employed. In addition the treatment condition, co- or pre-treatment, also impacted upon the chili antimutagenic affects. This suggests that some of the components either must undergo some sort of 'activation' or must induce or activate a biological pathway in vivo. This of course does not exclude the concept that some of these components may also react directly with the electrophilic mutagens. Thus the reduction in mutated cells produced by co-treatment and pre-treatment suggest that both direct and indirect protective mechanisms are involved in countering urethane-induced mutagenesis.

One of the possible antimutagenic components found in peppers are carotenoids. These compounds isolated from the fruits of red paprika (*C. annuum* L.) exhibit potent antitumor-promoting activity in vivo and in vitro (Maoka et al., 2001). Peppers are also important sources of carotenoids, mainly β-carotene followed by α-carotene and β-cryptoxanthin (Mejia et al., 1988). Extracts from bell pepper were found to give 87%, 79% and 73% inhibition on 1-nitropyrene; 1,6-dinitropyrene and 1,8-dinitropyrene mutagenicity, respectively (Gonzalez de Mejia et al., 1998). Antioxidants such as α- or β-carotene, xanthophylls and retinoid have been reported to inhibit some types of cancers (Hayatsu et al., 1988; Gross, 1991). These constituents also appear to inhibit a large number of mutagens in different test systems (Edenharder et al., 1998; Bianchi et al., 1996; Arriaga-Alba et al., 2000).

Capsaicin is the most pungent of the group of compounds called capsaicinoids that can be isolated from chili

peppers and also are sparingly soluble in water, but very soluble in fats. Hydrophobic compounds like capsaicin, analogs of capsaicin, and β-carotene would be found in chili extracts at higher concentrations in oil compared to a water extract. Green bell pepper showed the least inhibition of genotoxicity for all processed chili in both co-treatment and pre-treatment experiments. The hot chili peppers (bird pepper, red chili spur pepper) showed greater inhibition of genotoxicity. The capsaicin content is greater in the Thai peppers (50,000–100,000 Scoville unit) than the bell peppers (zero Scoville units) (Prapanoppasin and Sukprakan, personal communication). Capsaicin has been shown to inhibit the mutagenicity and/or tumorigenicity of vinyl carbamate, a metabolite of urethane activated by cytochrome P450 2E1 (Surh et al., 1995). This result agreed with previous reports that capsaicin inhibited rodent CYP2E1 activity in vitro (Surh et al., 1995) and dihydrocapsaicin, the saturated analogue of capsaicin, is a suicide or mechanism-based inhibitor of cytochrome P4502E1(CYP2E1) (Gannett et al., 1990).

In this study, we investigated the possible role of glutathione transferase in detoxication of urethane. The results suggested that glutathione transferase is not involved in antimutagenicity of chili. A similar effect was observed in male Swiss albino mice with aqueous extracts of spices (cinnamon, pepper, cumin, clove and cardamom) against the mutagenicity of urethane (Abraham et al., 1998). These extracts did not exert any significant effect on glutathione transferase activity. The chili may exert their antigenotoxic effect on urethane through inhibition of the cytochrome P-450 enzymes responsible for bio-activation of urethane. This has been reported previously where capsaicin pre-treatment gave a small but statistically significant inhibition of CYP1A2 activity which correlated with its antimutagenic activity against selected heterocyclic amine (Teel et al., 1997).

## 5. Conclusion

In conclusion, our study has shown that four types of chili, ground into a paste (with water, vinegar or oil) or equivalent extracts of each chili inhibit the genotoxic effects of urethane. Several commonly used food processing methods for chilies differentially extracted the antimutagenic chili components. This suggests each chili contains a unique complex mixture of many antimutagens. Co-treatment and pre-treatment experiments showed that both direct and indirect protective mechanisms are involved in an 'activation' process to give antimutagenesis effects. An association between antigenotoxicity and glutathione transferase activity could not be established.

## Acknowledgements

We are grateful to Jantana Wongsantichon for her technical support in the determination of glutathione transferase activity. This thesis was supported by the Faculty of Graduate Studies, Mahidol University in the academic year of 2005.

## References

Abraham, S.K., 1994. Antigenotoxicity of coffee in the Drosophila assay for somatic mutation and recombination. Mutagenesis 9, 383–386.

Abraham, S.K., Singh, S.P., Kesavan, P.C., 1998. In vivo antigenotoxic effects of dietary agents and beverages co-administered with urethane: assessment of the role of glutathione *S*-transferase activity. Mutat. Res. 413, 103–110.

Arriaga-Alba, M., Rivera-Sanchez, R., Parra-Cervantes, G., Barro-Moreno, F., Flores-Paz, R., Garcia-Jimenez, E., 2000. Antimutagenesis of beta-carotene to mutations induced by quinolone on *Salmonella typhimurium*. Arch. Med. Res. 31, 156–161.

Ballering, L.A., Nivard, M.J., Vogel, E.W., 1996. Characterization by two-endpoint comparisons of the genetic toxicity profiles of vinyl chloride and related etheno-adduct forming carcinogens in Drosophila. Carcinogenesis 17, 1083–1092.

Bianchi, L., Melli, R., Pizzala, R., Stivala, L.A., Rehak, L., Quarta, S., Vannini, V., 1996. Effects of beta-carotene and alpha-tocopherol on photogenotoxicity induced by 8-methoxypsoralen: the role of oxygen. Mutat. Res. 369, 183–194.

Bradford, M.M., 1976. A rapid and sensitive method for the quantitation of microgram quantities of protein utilizing the principle of protein-dye binding. Anal. Biochem. 72, 248–254.

Edenharder, R., Kerkhoff, G., Dunkelberg, H., 1998. Effects of beta-carotene, retinal, riboflavin, alpha-tocopherol and vitamins C and K1 on sister-chromatid exchanges induced by 3-amino-1-methyl-5H-pyrido[4,3-*b*]indole (Trp-P-2) and cyclophosphamide in human lymphocyte cultures. Food Chem. Toxicol. 36, 897–906.

El Hamss, R., Idaomar, M., Alonso-Moraga, A., Munoz Serrano, A., 2003. Antimutagenic properties of bell and black peppers. Food Chem. Toxicol. 41, 41–47.

Frei, H., Wurgler, F.E., 1995. Optimal experimental design and sample size for the statistical evaluation of ethyl carbamate (urethane) in mice. Food Chem. Toxicol. 29, 291–295.

Frolich, A., Wurgler, F.E., 1990. Genotoxicity of ethyl carbamate in the *Drosophila* wing-spot test: dependence on genotype-controlled metabolic capacity. Mutat. Res. 244, 201–208.

Gannett, P., Iversen, P., Iawson, T., 1990. The mechanism of inhibition of cytochrome P450IIE1 by dihydrocapsaicin. Bioorg. Chem. 18, 185–198.

Giri, A.K., 1995. Genetic toxicology of vinyl chloride—a review. Mutat. Res. 339, 1–14.

Gonzalez de Mejia, E., Quintanar-Hernandez, A., Loarca-Pina, G., 1998. Antimutagenic activity of carotenoids in green peppers against some nitroarenes. Mutat. Res. 416, 11–19.

Graf, U., Abraham, S.K., Judith, G., Wurgler, F.E., 1998. Antigenotoxicity studies in *Drosophila melanogaster*. Mutat. Res. 1998, 203–209.

Graf, U., Frei, H., Kagi, A., Katz, A.J., Wurgler, F.E., 1989. Thirty compounds tested in the Drosophila wing spot test. Mutat. Res. 222, 359–373.

Graf, U., Moraga, A.A., Castro, R., Diaz Carrillo, E., 1994. Genotoxicity testing of different types of beverages in the Drosophila wing somatic mutation and recombination test. Food Chem. Toxicol. 32, 423–430.

Graf, U., van Schaik, N., 1992. Improved high bioactivation cross for the wing somatic mutation and recombination test in *Drosophila melanogaster*. Mutat. Res. 271, 59–67.

Graf, U., Wurgler, F.E., Katz, A.J., Frei, H., Juon, H., Hall, C.B., Kale, P.G., 1984. Somatic mutation and recombination test in *Drosophila melanogaster*. Environ. Mutagen. 6, 153–188.

Gross, J., 1991. In: Gross, J. (Ed.), Pigments in Vegetables, Chlorophylls and Carotenoids, New York, pp. 75–79.

Guengerich, F., Kim, D., Iwasaki, M., 1991. Role of human P-450IIE1 in the oxidation of many low molecular weight cancer suspects. Chem. Res. Toxicol. 4, 168–179.

Habig, W.H., Pabst, M.J., Jakoby, W.B., 1974. Glutathione *S*-transferase. J. Biol. Chem. 249, 7130–7139.

Hayatsu, H., Arimoto, S., Negishi, T., 1988. Dietary inhibitors of mutagenesis and carcinogenesis. Mutat. Res. 202, 429–446.

Hoch-Ligeti, C., 1952. Naturally occurring dietary agents and their role in production of tumors. Tex. Rep. Biol. Med. 10, 996–1005.

Maoka, T., Mochida, K., Kozuka, M., Ito, Y., Fujiwara, Y., Hashimoto, K., Enjo, F., Ogata, M., Nobukuni, Y., Tokuda, H., Nishino, H., 2001. Cancer chemopreventive activity of carotenoids in the fruits of red paprika *Capsicum annuum* L. Cancer Lett. 172, 103–109.

Mejia, L., Hudson, E., Gonzalez de Mejia, E., Vazquez, F., 1988. Carotenoid content and vitamin A activity of some common cultivars of Mexican peppers (*Capsicum annuum*) as determined by HPLC. J. Food Sci. 53, 1448–1451.

Mirvish, S.S., 1968. The carcinogenic action and metabolism of urethane and *N*-hydroxyurethan. Adv. Cancer Res. 11, 1–42.

Mirvish, S.S., 1996. Inhibition by vitamins C and E of in vivo nitrosation and vitamin C occurrence in the stomach. Eur. J. Cancer Prev. 5 (Suppl. 1), 131–136.

Monsereenusorn, Y., Kongsamut, S., Pezalla, P.D., 1982. Capsaicin in: literature survey. CRC Crit. Rev. Toxicol. 10, 321–339.

Negishi, T., Arimoto, S., Nishizaki, C., Hayatsu, H., 1989. Inhibitory effect of chlorophyll on the genotoxicity of 3 amino-1-methyl-5*H*-pyrido[4,3-*b*] indole (Try-p-2). Carcinogenesis 10, 145–149.

Ramirez-Victoria, P., Guzman-Rincon, J., Espinosa-Aguirre, J.J., Murillo-Romero, S., 2001. Antimutagenic effect of one variety of green pepper (*Capsicum* spp.) and its possible interference with the nitrosation process. Mutat. Res. 496, 39–45.

Robert, D.B., 1986. Basic *Drosophila* care and techniques. In: Robert, D.B. (Ed.), Drosophila: A Practical Approach. IRL Press, Oxford, pp. 1–38.

Schlatter, J., Lutz, W.K., 1990. The carcinogenic potential of ethyl carbamate (urethane): risk assessment at human dietary exposure levels. Food Chem. Toxicol. 28, 205–211.

Stoewsand, G.S., Anderson, J.L., Munson, L., 1991. Inhibition by wine of tumorigenesis induced by ethyl carbamate (urethane) in mice. Food Chem. Toxicol. 29, 291–295.

Surh, Y.J., Lee, R.C., Park, K.K., Mayne, S.T., Liem, A., Miller, J.A., 1995. Chemoprotective effects of capsaicin and diallyl sulfide against mutagenesis or tumorigenesis by vinyl carbamate and *N*-nitrosodimethylamine. Carcinogenesis 16, 2467–2471.

Teel, R., Zhang, Z., Huynh, S., Hamilton, S., 1997. Effects of capsaicin on the metabolic activation of heterocyclic amines and on cytochrome P450 1A2 activity in hamster liver microsomes. Proc. Am. Assoc. Cancer Res. 38, 363.

Unnikrishnan, M., Kuttan, R., 1990. Tumor reducing and anticarcinogenic activity of selected spices. Cancer Lett. 51, 85–89.

Zimmerli, B., Schlatter, J., 1991. Ethyl carbamate: analytical methodology, occurrence, formation, biological activity and risk assessment. Mutat. Res. 259, 325–350.

RESEARCH ARTICLE
doi: 10.2306/scienceasia1513-1874.2006.32.159

*ScienceAsia* 32 (2006): 159-165

**Reprint 6**

# Characterization of *Anopheles dirus* Glutathione Transferase Epsilon 4

**Gulsiri Charoensilp[a], Ardcharaporn Vararattanavech[a], Posri Leelapat[b], La-aied Prapanthadara[b] and Albert J. Ketterman[a*]**

[a] Institute of Molecular Biology and Genetics, Mahidol University, Salaya Campus, Nakhon Pathom 73170, Thailand.
[b] Research Institute for Health Sciences, Chiang Mai University, P.O. Box 80, Chiang Mai 50202, Thailand.

* Corresponding author, E-mail: frakt@mahidol.ac.th

*Received 4 Nov 2005*
*Accepted 8 Feb 2006*

**ABSTRACT:** The coding sequences of a wild type glutathione transferase (GST) Epsilon 4 and three isoenzymes were obtained by RT-PCR from a Thai malaria mosquito, *Anopheles dirus*. After confirmation by sequencing, the RT-PCR products were subcloned into an expression vector and proteins were expressed, purified, and biochemically characterized to study the function of these enzymes and for comparison with two orthologs from *An. gambiae* (agGSTE4-4) and *Aedes aegypti* (aaGSTE4-4). The results showed that *An. dirus* GST Epsilon 4 (adGSTE4-4) shares more than 85% amino acid sequence similarity with agGSTE4-4 and aaGSTE4-4. However, adGSTE4-4 possesses a greater catalytic efficiency ($k_{cat}/K_m$) for 1-chloro-2,4-dinitrobenzene as well as greater activities for several other substrates compared with agGSTE4-4 and aaGSTE4-4. Moreover, adGSTE4-4 enzyme possesses peroxidase and DDT dehydrochlorinase activities while these activities were not observed for agGSTE4-4. In addition, adGSTE4-4 binds two pyrethroid insecticides (permethrin and l–cyhalothrin) with a relatively high affinity. We conclude that adGSTE4-4, unlike agGSTE4-4, can contribute to DDT resistance by DDT dehydrochlorinase activity as well as to pyrethroid resistance by sequestration and protection against oxidation from secondary pyrethroid metabolites via its peroxidase activity.

**KEYWORDS:** Glutathione transferase; Epsilon class; *Anopheles dirus*; DDT dehydrochlorinase; pyrethroid insecticide.

## INTRODUCTION

Glutathione transferases (GSTs: E.C. 2.5.1.18) are a diverse family of multifunctional enzymes that play roles in metabolism, transportation, xenobiotic compound detoxification, and cell mediation against oxidative stress[1]. They are found in almost all living organisms and catalyze a conjugation reaction by transferring the thiol group of reduced glutathione (GSH) to an electrophilic substrate, making the resultant products more water soluble and excretable. GSTs are composed of two subunits and each subunit consists of two domains containing a highly conserved glutathione binding site (or G site) and a hydrophobic substrate binding site (or H site). Currently, more than 40 GST genes have been detected and grouped into at least 13 different classes[1,2]. Generally, the intra-class GSTs have greater than 40% amino acid sequence identity whereas the inter-class GSTs have amino acid sequence identity less than 30%[3]. The insect GSTs are of particular interest because they have the potential to confer resistance to all major groups of insecticides. GST-based resistance has been detected by elevated levels of GST activity in strains of insects resistant to organophosphates[4], organochlorines[5], and pyrethroids[6]. The mechanisms that GSTs use to detoxify insecticides are direct metabolism of insecticides or the secondary products, prevention of the oxidative damage induced by insecticide and sequestration[7]. Recently, the complete genome of *Anopheles gambiae* (an African malaria mosquito) was obtained and GST genes in this species have been annotated into at least six different classes (namely Theta, Sigma, Zeta, Omega, Delta, and Epsilon). Two insect specific classes, Delta and Epsilon, encode two-thirds of the *An. gambiae* cytosolic GSTs[2]. Moreover, a cluster of eight insect-specific epsilon class GSTs (*gste1 - gste8*) have been identified and co-localized with a DDT resistance locus, *rtd1*, on polytene chromosome arm 3R division 33B[8]. In addition, a quantitative PCR assay showed five of the eight epsilon GSTs (namely *gste1, gste2, gste3, gste4*, and *gste7*) are expressed at significantly greater levels in the DDT resistant strain[2]. Earlier studies had shown that GSTE2-2 was very efficient at metabolizing DDT, GSTE1-1 possessed peroxidase activity whereas GSTE4-4 and GSTE8-8 had no detectable DDT dehydrochlorinase or peroxidase activities[9]. In our laboratory, we are interested in Epsilon class GSTs in

the malaria mosquito, *Anopheles dirus*. Malaria is a major public health problem in Thailand, resulting in 325 reported deaths and 37,335 cases in 2003[10]. Furthermore, a comparison between the genomes of *An. dirus* and *An. gambiae* showed that the two Anopheline species possess a similar pattern of GST isoenzymes, although the individual enzymes differ significantly at the functional level[11]. For example, when comparing the equivalent alternatively spliced GSTs from *An. dirus GST1AS1* and *An. gambiae GST1a*, the amino acid sequence identities for adGSTD1-1 versus agGSTD1-6, and adGSTD3-3 versus agGSTD1-5 are 93% and 92%, respectively[12], but the catalytic efficiencies toward 1-chloro-2,4-dinitrobenzene (CDNB) are 16.5-fold and 1.5-fold different, respectively[13,14]. Despite the high level of sequence identity between GST enzymes from *An. dirus* and *An. gambiae*, the enzymes display different kinetic properties and substrate specificities that may lead to differences at the functional level. The aim of this study was to obtain and characterize Epsilon GSTs from the Thai malaria vector, *An. dirus*. To be in alignment with a proposed universal GST nomenclature the enzyme reported here was named adGSTE4-4 (in insect GST nomenclature, "E" refers to the Epsilon class and "4-4" refers to the homodimeric isoenzyme[15,3]). Here we report the amino acid sequences of GST Epsilon 4 (adGSTE4-4) enzyme and three variant isoenzymes from *An. dirus,* and compare with the orthologous enzymes from *An. gambiae* and *Aedes aegypti*.

## Materials and Methods

### Mosquito Strain

An *Anopheles dirus* B colony established at the Department of Parasitology, Faculty of Medicine, Chiang Mai University, was used in this study. The colony was identified on the basis of its morphological and chromosomal characteristics[16].

### RT-PCR and cDNA Sequencing of *An. dirus gste4*

Total RNA was extracted from 0.1 g of fourth instar larvae of *An. dirus* using TRI reagent (SIGMA, USA), according to the manufacturer's instructions. Then mRNA was reverse transcribed into cDNA using ImProm-II™ Reverse Transcriptase (Promega, USA) and oligo(dT) primer (5'-CGGTCGACATATG$(dT)_{18}$-3') following the instructions from Promega. PCR used cDNA as a template, a 5' primer started at ATG codon based on *An. gambiae gste4* sequence (5'-ATGCCGA ACATCAAGCTGTAC-3'), a 3' oligo(dT) primer, and *Taq* DNA Polymerase (Promega, USA). PCR (consisted of 35 cycles of 94°C for 10 s, 55°C for 30 s, 72°C for 1 min) was performed in a Perkin–Elmer thermocycler (USA). Then RT-PCR product was directly sequenced in both directions using a Bigdye™ terminator cycle sequencing kit (Perkin Elmer, USA). Multiple alignments of nucleotide sequences and translated amino acid sequences were analyzed using the ClustalX program.

### 5'Rapid Amplification of cDNA Ends (RACE) of *An. dirus gste4*

To determine 5' amino acid sequence identity of *An. dirus gste*, 5' RACE was performed according to the 5' RACE System for Rapid Amplification of cDNA Ends, Version 2.0 instruction manual (GIBCO BRL, USA). Total RNA was extracted and reverse transcribed into cDNA as previously described using *adgste4* gene specific primer 1 (5'-ATTCGT CGCCGCATAGTAGGG-3') to obtain full-length *An. dirus gste4* coding sequence.

### Cloning, Expression and Purification of *An. dirus gste4*

Full-length coding region of *An. dirus gste4* was amplified by RT-PCR as described above using *Taq* DNA Polymerase, 3' primer containing *Bam*HI site (5'-GC**GGATCC**TCACTTTGCTTTAGCACGGTTC-3'), and two different 5' primers containing *Bam*HI site (5'-AAAC**CCATGG**ATCCATGCCGAA CATCAAGCTG-3') or *Nde*I site (5'-CG**CATATG**CCAAACATTAAGCTGTA CACGG-3'). These two RT-PCR products were subcloned into two different sites (*Bam*HI site or *Nde*I–*Bam*HI site) of the pET3a expression vector (Novagen, USA) to generate adGSTE4-4 enzymes with or without a T7tag on the N-terminus, respectively. Then recombinant plasmids were analyzed by restriction digestion, sequenced and transformed into *E. coli* BL21(DE3)pLysS. Proteins were expressed as previously described[17] and soluble target proteins were purified using cation exchange chromatography using a SP-XL column, followed by hydrophobic interaction chromatography using a HiTrap Phenyl Sepharose column (Amersham Biosciences, USA). The SP-XL column was equilibrated with 50 mM phosphate buffer pH 7 and lysate was applied to the column. The adGSTE4-4 enzymes did not bind to the SP-XL column, so flow-through was collected and NaCl added to a final concentration of 3 M before loading to a HiTrap Phenyl Sepharose column pre-equilibrated with 50 mM phosphate buffer, pH 7, containing 3 M NaCl. Protein was eluted with a linear gradient from 2 - 0.75 M NaCl in 50 mM phosphate buffer, pH 7, containing 10 mM dithiothreitol (DTT). The major activity of adGSTE4-4 enzymes were eluted in 50 mM phosphate buffer, pH 7, containing 1 or 0.75 M NaCl. Purified enzymes were concentrated and desalted by Hitrap desalting columns (Amersham Biosciences, USA) as previously described[18]. GSTs were observed to be homogenous by SDS-PAGE. The enzymes were stored in 50 mM phosphate buffer, pH 6.5, 10 mM DTT, 50% (v/v)

glycerol at -20°C. Protein concentrations were determined by Bio-Rad protein reagent (Bio-Rad) with bovine serum albumin as standard protein[19].

## Enzyme Characterization

Steady-state kinetics were performed by varying concentrations of 1-chloro-2,4-dinitrobenzene (CDNB) and glutathione (GSH) in 0.1 M phosphate buffer, pH 6.5, as previously described to obtain kinetic parameters, $k_{cat}$, $K_m$ and $k_{cat}/K_m$, of wild type adGSTE4-4 and variant enzymes [17]. Substrate specificity of the enzymes were determined as previously described with five different substrates; CDNB, 1,2-dichloro-4-nitrobenzene (DCNB), ethacrynic acid (EA), *p*-nitrophenethyl bromide (PNPB) and *p*-nitrobenzyl chloride (PNBC)[17]. A thermal stability assay was performed to determine half life of wild type and variant enzymes by incubating enzymes (1 mg/ml in 0.1 M potassium phosphate, pH 6.5, containing 5 mM DTT and 1 mM EDTA) at 45°C and enzyme aliquots were assayed for activity at different time-points as previously described[17]. Insecticide $K_i$ experiments for permethrin and λ-cyhalothrin (SUPELCO, USA) were performed by varying CDNB concentrations with 30 mM GSH in the presence and absence of the pyrethroid insecticides. The initial rate of reaction was used to construct a double reciprocal plot, 1/*V* versus 1/*S*, and the inhibition constant ($K_i$) was determined as previously described[20,13]. Peroxidase activities of wild type and variant enzymes were determined at 340 nm by coupling the reduction of cumene hydroperoxide (CHP) to the oxidation of NADPH by oxidized GSH with glutathione reductase as previously described[21]. DDT dehydrochlorinase activity was determined by conversion of DDT to 1,1-dichloro-2,2-bis-(*p*-chlorophenyl)ethane (DDE) detected by high-

```
                      *        20         *        40         *        60         *        80
adGSTE4-4 WT       : MPNIKLYTAKLSPPGRAVELTGKALGLEFDISPINLIAGDHLREEFRKLNPQHTIPLIDD-AGTIVYESHAIIVYLVTKY
:  79
adGSTE4-4 Pro14Leu : .............L.............................................-...................
:  79
adGSTE4-4 Glu44Lys : ..........................................K.................-...................
:  79
adGSTE4-4 Ile131Thr: ..........................................................-...................
:  79
agGSTE4-4          : ................S....A......L..V......QE..T.A................-N.....D....N.......
:  79
aaGSTE4-4          : .GK.Q.................A.....DL..H...........P..V...........V.ED.....D............
:  80
adGSTD3-3          : ---.DF.YLPG.A.C......AA.....L..KLT.....E...P..L......C..T.V.-N.FA....R..CT..AE..
:  76


                             *       100         *       120         *       140         *       160
adGSTE4-4 WT       : G--ADDSLYPSDAVTRSKVNAALHFDSGVLFARLRFYLEPILYYGSTETPQEKIDNLYRAYELLNATLVD--DYIVGSRL
: 155
adGSTE4-4 Pro14Leu : .--.....................................................................--........
: 155
adGSTE4-4 Glu44Lys : .--.....................................................................--........
: 155
adGSTE4-4 Ile131Thr: .--.....................................................T................--........
: 155
agGSTE4-4          : .KPEG.......V.Q.A.................F...........A...................D....--E....NE.
: 157
aaGSTE4-4          : A--K......K.IA..A.............................PD...D...YAC.......D....--E....N..
: 156
adGSTD3-3          : .--K..K...K.PQK.AV..QR.Y..M.T..Q.FAD.YY.Q..AKQPAN-A.NEKK.KD.VDF..-.F..GHK..A.DS.
: 152


                             *       180         *       200         *       220
adGSTE4-4 WT       : TLADLSCVASIASMHAIFPIDAGKYPKLLAWVERIAKLPYYAATNQAGAEELAQLYHAKLAENRAKAK : 223
adGSTE4-4 Pro14Leu : ..................................................................... : 223
adGSTE4-4 Glu44Lys : ..................................................................... : 223
adGSTE4-4 Ile131Thr: ..................................................................... : 223
agGSTE4-4          : ............................AG..K........E...R..........R...E...TN.. : 225
aaGSTE4-4          : ..............Y........A.....A......E.....KG...E......A..RD.......GK. : 224
adGSTD3-3          : ......V....S.YDVAG-FELA...H.A..Y..TR.EAPG..I....I..FRKY.EK---------- : 209
```

**Fig 1.** Amino acid sequence alignment of *An. dirus* GSTE4-4 wild type (adGSTE4-4 WT) and variants (Pro14Leu, Glu44Lys, and Ile131Thr), *An. gambiae* GSTE4-4 (agGSTE4-4), *Aedes aegypti* GSTE4-4 (aaGSTE4-4), and *An. dirus* GSTD3-3 (adGSTD3-3). Gaps introduced to maximize sequence similarity are shown by a horizontal dash while a dot represents the same amino acid. GenBank accession numbers for the sequences are: adGSTE4-4, DQ168030; agGSTE4-4, AY070254; aaGSTE4-4, AY819709; adGSTD3-3, AF273039.

**Table 1.** Substrate specificities, kinetic parameters, and half life of *Anopheles dirus* and *Anopheles gambiae* GSTE4-4 enzymes.

| | adGSTE4-4 WT | adGSTE4-4 T7WT | adGSTE4-4 Pro14Leu | adGSTE4-4 Glu44Lys | adGSTE4-4 Ile131Thr | agGSTE4-4 |
|---|---|---|---|---|---|---|
| **Substrate specificity** | | | | | | |
| CDNB (μmol/min/mg) | 79.95 ± 0.81 | 77.03 ± 1.11 | 1.43 ± 0.08 | 71.21 ± 3.72 | 53.56 ± 2.71 | 16.50 ± 1.02 |
| DCNB (μmol/min/mg) | 0.324 ± 0.011 | 0.462 ± 0.011 | 0.002 ± 0.000 | 0.381 ± 0.016 | 0.276 ± 0.021 | 0.070 ± 0.010 |
| PNPB (μmol/min/mg) | 0.113 ± 0.009 | 0.123 ± 0.011 | not detected | 0.099 ± 0.005 | 0.128 ± 0.007 | - |
| PNBC (μmol/min/mg) | 0.140 ± 0.006 | 0.133 ± 0.008 | not detected | 0.124 ± 0.004 | 0.134 ± 0.001 | - |
| EA (μmol/min/mg) | 0.034 ± 0.006 | 0.095 ± 0.007 | 0.007 ± 0.002 | 0.029 ± 0.005 | 0.007 ± 0.004 | - |
| CHP (nmol/min/mg) | 118.02 ± 6.19 | - | not detected | 74.90 ± 6.46 | not detected | not detected |
| DDTase activity (nmol of DDE/mg) | 2.56 ± 0.32 | - | - | - | - | not detected |
| **Kinetic parameters** | | | | | | |
| $V_{max}$ (μmol/min/mg) | 94.83 ± 5.06 | 87.55 ± 1.73 | 1.65 ± 0.04 | 83.17 ± 0.83 | 69.20 ± 1.05 | 16.30 ± 1.59 |
| $k_{cat}$ ($S^{-1}$) | 39.28 | 36.26 | 0.69 | 34.45 | 28.66 | 13.74 |
| $K_m$ for GSH (mM) | 4.53 ± 1.04 | 7.15 ± 0.18 | 11.26 ± 1.30 | 3.81 ± 0.15 | 5.12 ± 0.21 | 5.38 ± 0.79 |
| $k_{cat}/K_m$ for GSH ($S^{-1}.mM^{-1}$) | 8.7 | 5.1 | 0.06 | 9 | 5.6 | 2.5 |
| $K_m$ for CDNB (mM) | 0.076 ± 0.010 | 0.060 ± 0.006 | 0.144 ± 0.017 | 0.070 ± 0.010 | 0.040 ± 0.004 | 0.131 ± 0.026 |
| $k_{cat}/K_m$ for CDNB ($S^{-1}.mM^{-1}$) | 517 | 604 | 4.8 | 492 | 717 | 105 |
| $K_i$ for permethrin (μM) | 66.27 ± 2.75 | - | not inhibited | 53.28 ± 3.42 | 669.28 ± 27.42 | - |
| $K_i$ for λ-cyhalothrin (μM) | 115.43 ± 15.16 | - | not inhibited | 72.20 ± 1.66 | 433.79 ± 11.63 | - |
| **Half life at 45°C (min)** | 21.48 ± 0.40 | 18.93 ± 1.78 | 32.16 ± 2.53 | 13.93 ± 0.61 | 6.97 ± 0.85 | - |

The data are means ± standard deviation for at least three separate experiments. adGSTE4-4 T7WT indicates wild type GSTE4 containing the T7 tag on the N-terminus.
A dash indicates data not determined.
For substrate specificity, the concentrations used were: 1 mM CDNB (1-chloro-2,4-dinitrobenzene); 1 mM DCNB (1,2-dichloro-4-nitrobenzene); 0.1 mM PNPB (*p*-nitrophenethyl bromide); 0.1 mM PNBC (*p*-nitrobenzyl chloride); 0.2 mM EA (ethacrynic acid); and 1 mM CHP (cumene hydroperoxide). *An. gambiae* data are given for comparison[9].

performance liquid chromatography as described previously[13].

## Results

### Cloning, Expression and Purification of adGSTE4-4 Enzymes

The full-length coding sequence of *An. dirus gste4* contains 672 bp translated to give a polypeptide of 223 amino acids which is the same length as *Aedes aegypti gste4*[22] but two amino acids less than *An. gambiae gste4*[2]. A comparison of *An. dirus gste4* with *An. gambiae* and *Ae. aegypti* enzymes shows amino acid sequence identity/similarity for the enzymes of 81%/90% and 74%/85%, respectively (Fig. 1). In the 52 region *An. dirus gste4* had only two nucleotides differ from *An. gambiae gste4* although the same amino acids were still encoded. However, from 12 full-length sequenced clones of *An. dirus gste4*, three clones showed variations in amino acid sequences; the first (adGSTE4-4 Pro14Leu) had Pro14 changed to Leu, the second (adGSTE4-4 Glu44Lys) had Glu44 changed to Lys, and the third (adGSTE4-4 Ile131Thr) had Ile131 changed to Thr (Fig. 1). These variants and wild type *adgste4* were subcloned into the *Nde*I-*Bam*HI site of pET3a expression vector to generate enzymes without a fusion tag. Additionally a wild type *adgste4* sequence was subcloned into the *Bam*HI site of pET3a to generate adGSTE4-4 enzyme with a T7 tag on the N-terminus. This was to observe the effect of the T7 tag on enzyme properties and for comparison with *An. gambiae* GSTE4-4 enzyme which possessed a T7 tag[9]. Five adGSTE4-4 enzymes, wild type with or without T7 tag and three variants without T7 tag, were expressed as soluble proteins at high levels. These enzymes were purified by using cation exchange chromatography followed by hydrophobic interaction chromatography, which gave a 3-fold greater yield for wild type adGSTE4-4 enzyme without T7 tag when compared with purification by S-hexylglutathione affinity chromatography (data not shown).

### Substrate Specificity, Kinetic Properties, and Half Life Stability of adGSTE4-4 Enzymes

Six GST substrates were used to determine substrate specificity (Table 1). *An. dirus* adGSTE4-4 had 5-fold greater activities for CDNB and DCNB than the *An. gambiae* enzyme. Moreover, wild type adGSTE4-4 exhibited peroxidase and DDT dehydrochlorinase activities whereas these activities for *An. gambiae* agGSTE4-4 were undetectable. These results showed variation in substrate specificities among wild type adGSTE4-4 with or without T7tag, adGSTE4-4 variants, and the orthologous enzyme from *An. gambiae*. The kinetic property differences between these two enzymes may originate from either the 14 N-terminus amino acids (T7tag) of agGSTE4-4 or the 41 amino acids that are different between agGSTE4-4 and wild

type adGSTE4-4. However, the kinetic properties between wild type adGSTE4-4 with and without T7 tag were similar, which suggests the T7 tag had little effect on adGSTE4-4 kinetic properties, supporting the idea that the enzyme differences originate with the sequence differences.

When comparing wild type adGSTE4-4 with the variant enzymes, we observed that adGSTE4-4 Pro14Leu exhibited the lowest enzyme activities for all substrates tested including a dramatically decreased catalytic efficiency toward CDNB (107-fold). Thus Pro14 appeared to have a major impact on enzyme catalysis. In contrast, adGSTE4-4 Glu44Lys had similar kinetic properties to the wild type enzyme. Whereas adGSTE4-4 Ile131Thr had no detectable peroxidase activity and showed 5-fold lower activity for EA than the wild type.

The insecticide inhibition kinetics of permethrin and λ-cyhalothrin were shown to be a non-competitive inhibitor for two variants (adGSTE4-4 Glu44Lys, and adGSTE4-4 Ile131Thr). However, for wild type adGSTE4-4 permethrin and λ-cyhalothrin were found to be a non-competitive inhibitor and mixed inhibitor, respectively. A comparison of $K_i$ values for permethrin and λ-cyhalothrin illustrates differences between various *An. dirus* enzymes (Table 1), the most notable one being adGSTE4-4 Pro14Leu which showed no inhibition with either permethrin or λ-cyhalothrin.

The half lives of wild type adGSTE4-4 with and without T7 tag at 45°C were similar (Table 1). The half-life of adGSTE4-4 Pro14Leu increased 1.5-fold whereas those of adGSTE4-4 Glu44Lys and adGSTE4-4 Ile131Thr decreased 1.5- and 3-fold, respectively, when compared with the wild type enzyme. These residue changes therefore showed only small affects on the structural stability of the enzyme.

## Discussion

Despite the high degree of sequence identity between the two orthologous GSTE4-4 enzymes from *An. dirus* and *An. gambiae*, they displayed differences in kinetic properties and substrate specificity, especially for peroxidase and DDT dehydrochlorinase activities which were only observed for the *An. dirus* enzyme. In contrast to *An. gambiae* agGSTE2-2, agGSTE4-4 and agGSTE8-8 enzymes, which have undetectable peroxidase activities, *An. dirus* adGSTE4-4 possesses peroxidase activity comparable to the *Ae. aegypti* aaGSTE2-2 (0.11 mmol/min/mg), but 88.7-fold greater activity than agGSTE1-1 from the DDT resistant strain of *An. gambiae* (1.33 nmol/min/mg)[9,22]. This peroxidase activity has been shown to be protective against the damage caused by lipid peroxidation products induced by exposure to pyrethroid insecticides[23]. In contrast, several GSTs from the DDT resistant strain of *An. gambiae*, agGSTE1-1, agGSTE4-4, and agGSTE8-8, showed no detectable DDT dehydrochlorinase activity whereas, *An. dirus* adGSTE4-4 possessed DDT dehydrochlorinase activity (2.56 nmole of DDE/mg). However, this enzyme has 1000-fold lower DDT dehydrochlorinase activity than those of agGSTE2-2 and aaGSTE2-2 from the DDT resistant strains of *An. gambiae* (2.77 nmole of DDE/μg) and *Ae. aegypti* (4.16 nmole DDE/μg), respectively[9,22]. Previously it has been reported that GST enzymes protect against pyrethroid toxicity in insects by sequestering the insecticide[6]. In the pyrethroid inhibition study, *An. dirus* GSTE4-4 enzyme was affected by a non-competitive and mixed type inhibition by permethrin and λ-cyhalothrin, respectively, which demonstrates that both pyrethroids interacted with the enzyme although not in the active site. The $K_i$ value of adGSTE4-4 for permethrin indicates that it has similar permethrin binding affinity to *An. dirus* Delta class GSTs for which the $K_i$ values range from 9 – 53 mM[13].

Three variants of adGSTE4-4 enzymes (Pro14Leu, Glu44Lys, and Ile131Thr) were also obtained by RT-PCR. As no Epsilon GST structure is currently available we used the structure of adGSTD3-3[24] to model the variant residue positions (Fig. 2). Pro14Leu is near the critical active site serine residue involved in thiol deprotonation of GSH. The Pro14 residue is a highly conserved active-site residue in Delta, Epsilon, Theta, and several unclassified GSTs in insects[2,22,25], suggesting its importance for backbone orientation. As proline causes a kink in the peptide backbone, when changed to leucine it would therefore change the conformation of the active site pocket, impacting on substrate specificity as well as catalysis. In addition, the Pro14Leu variant enzyme was not inhibited by permethrin or λ-cyhalothrin. It appears that the Pro14Leu variant enzyme lost the pyrethroid binding site due to a change in the enzyme topology. The second variant enzyme, containing a Glu44Lys change had the same kinetic properties and permethrin binding affinity as wild type, but surprisingly had peroxidase activity slightly lower than the *An. dirus* wild type enzyme, which was similar to *Ae. aegypti* GSTE2-2. Glu44Lys had a 56.3-fold greater peroxidase activity than agGSTE1-1 from a resistant strain of *An. gambiae*[9,22]. Moreover, Glu44Lys variant enzyme had a 1.6-fold greater λ-cyhalothrin binding affinity when compared to the wild type adGSTE4-4. The Glu44 residue is a conserved negative charge residue in the Epsilon class GSTs[2]. It is difficult to interpret the contribution of the Glu44 residue to peroxidase activity and specificity as no Epsilon structure is currently available. However the model suggests Glu44 is in α helix 2 which is known to be involved in the active site through GSH binding but also influencing specificity

of the hydrophobic substrate as well[26]. In contrast, the third variant enzyme, Ile131Thr in α helix five, showed no peroxidase activity and had 10- and 3.7-fold lower binding affinities to permethrin and λ-cyhalothrin, respectively. The above data suggests one putative surface site of interaction for the pyrethroids is a hydrophobic groove consisting of four motifs from both domains 1 and 2. These four motifs include 1) residues 32-41 in the loop between β2 sheet and α helix, 2) the C-terminus of α4 and loop residues between and including the N-terminus of α5, 3) the C-terminus of α6 and 4) the C-terminus of α8. This area would be affected through structural adjustments brought about by the residue changes observed in this study.

In conclusion, the Epsilon 4 GST of *An. dirus* shares more than 85% amino acid sequence similarity with the two orthologs from *An. gambiae* and *Ae. aegypti*. However, adGSTE4-4 possesses greater catalytic efficiency ($k_{cat}/K_m$) for CDNB as well as greater activity for several other substrates. In contrast, the *An. dirus* adGSTE4-4 enzyme possesses peroxidase and DDT dehydrochlorinase activities while these activities were not observed for the *An. gambiae* enzyme. In addition, we have shown the *An. dirus* enzyme binds two pyrethroid insecticides (permethrin and λ–cyhalothrin) with relatively high affinity. From these results, we conclude that *An. dirus* GST Epsilon 4 enzyme can contribute to DDT resistance by DDT dehydrochlorinase activity and to pyrethroid insecticide resistance by sequestration as well as protect against oxidation from the secondary pyrethroid metabolites via its peroxidase activity.

## Acknowledgements

This project was funded by the Thailand Research Fund. G.C. and A.V. were funded by Royal Golden Jubilee Ph.D. scholarships.

## References

1. Hayes JD, Flanagan JU and Jowsey IR (2005) Glutathione transferases. *Annu Rev Pharmacol Toxicol* **45**, 51-88.
2. Ding Y, Ortelli F, Rossiter LC, Hemingway J and Ranson H (2003) The *Anopheles gambiae* glutathione transferase supergene family: annotation, phylogeny and expression profiles. *BMC Genomics* **4**, 35-50.
3. Chelvanayagam G, Parker MW and Board PG (2001) Fly fishing for GSTs: a unified nomenclature for mammalian and insect glutathione transferases. *Chem Biol Interact* **133**, 256-60.

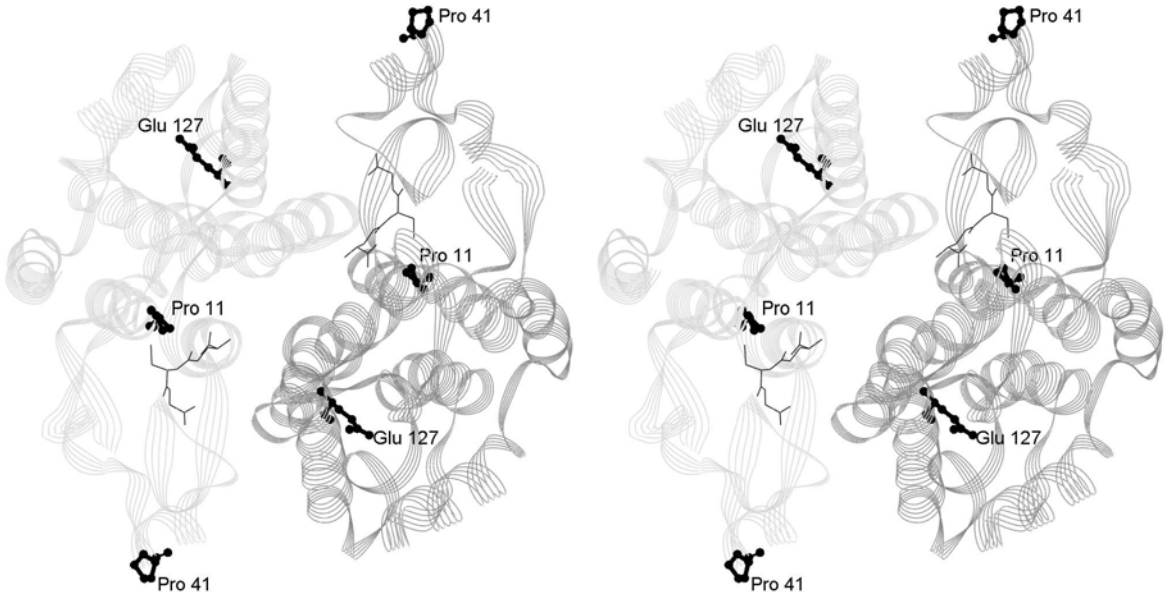


**Fig 2.** Stereo view of three amino acid residues in adGSTD3-3[24]. These three amino acids (Pro11, Pro41, and Glu127) are equivalent, as shown by amino acid alignment (Fig. 1), to the variant amino acid residues in adGSTE4-4: Pro14Leu, Glu44Lys, and Ile131Thr, respectively. This stereo view is looking at the two-fold axis on to the active sites. The three residues are shown as black ball-and-stick. GSH is shown in black stick in the active sites. The two subunits are shown in light gray and dark gray. The figure was generated using the program DS Viewer Pro.

4. Fournier D, Bride J-M, Poirié M, Bergé J-B and Plapp FW (1992) Insect glutathione S-transferases. Biochemical characteristics of the major forms from houseflies susceptible and resistant to insecticides. *J Biol Chem* **267**, 1840-5.
5. Grant DF and Hammock BD (1992) Genetic and molecular evidence for a *trans*-acting regulatory locus controlling glutathione S-transferase-2 expression in *Aedes aegypti*. *Mol Gen Genet* **234**, 169-76.
6. Kostaropoulos I, Papadopoulos AI, Metaxakis A, Boukouvala E and Papadopoulou-Mourkidou E (2001) Glutathione S-transferase in the defence against pyrethroids in insects. *Insect Biochem Molec Biol* **31**, 313-9.
7. Hemingway J, Hawkes NJ, McCarroll L and Ranson H (2004) The molecular basis of insecticide resistance in mosquitoes. *Insect Biochem Molec Biol* **34**, 653-65.
8. Ranson H, Jensen B, Wang X, Prapanthadara L, Hemingway J and Collins FH (2000) Genetic mapping of two loci affecting DDT resistance in the malaria vector *Anopheles gambiae*. *Insect Molecular Biology* **9**, 499-507.
9. Ortelli F, Rossiter LC, Vontas J, Ranson H and Hemingway J (2003) Heterologous expression of four glutathione transferase genes genetically linked to a major insecticide-resistance locus from the malaria vector *Anopheles gambiae*. *Biochem J* **373**, 957-63.
10. (2005) *http://w3.whosea.org/EN/Section10/Section21/Section340_4027 htm*
11. Prapanthadara L, Promtet N, Koottathep S, Somboon P and Ketterman AJ (2000) Isoenzymes of glutathione S-transferase from the mosquito Anopheles dirus species B: the purification, partial characterization and interaction with various insecticides. *Insect Biochem Molec Biol* **30**, 395-403.
12. Pongjaroenkit S, Jirajaroenrat K, Boonchauy C, Chanama U, Leetachewa S, Prapanthadara L and Ketterman AJ (2001) Genomic organization and putative promotors of highly conserved glutathione S-transferases originating by alternative splicing in *Anopheles dirus*. *Insect Biochem Molec Biol* **31**, 75-85.
13. Jirajaroenrat K, Pongjaroenkit S, Krittanai C, Prapanthadara L and Ketterman AJ (2001) Heterologous expression and characterization of alternatively spliced glutathione *S*-transferases from a single *Anopheles* gene. *Insect Biochem Molec Biol* **31**, 867-75.
14. Ranson H, Prapanthadara L and Hemingway J (1997) Cloning and characterization of two glutathione S-transferases from a DDT-resistant strain of *Anopheles gambiae*. *Biochem J* **324**, 97-102.
15. Mannervik B, Awasthi YC, Board PG, Hayes JD, Di Ilio C, Ketterer B, Listowsky I et al. (1992) Nomenclature for human glutathione transferases. *Biochem J* **282**, 305-6.
16. Baimai V (1989) Speciation and species complexes of the anopheles malaria vectors in Thailand.*The third conference on malaria research, Thailand*, 146-52.
17. Vararattanavech A and Ketterman A (2003) Multiple roles of glutathione binding-site residues of glutathione S-transferase. *Protein and Peptide Letters* **10**, 441-8.
18. Udomsinprasert R and Ketterman AJ (2002) Expression and characterization of a novel class of glutathione S-transferase from *Anopheles dirus*. *Insect Biochem Molec Biol* **32**, 425-433.
19. Bradford MM (1976) A rapid and sensitive method for the quantitation of microgram quantities of protein utilizing the principle of protein-dye binding. *Anal Biochem* **72**, 248-54.
20. Dixon M and Webb EC (1979) Enzyme inhibition and activation.**3**, 332-467.
21. Wendel A (1981) Glutathione peroxidase. *Methods Enzymol* **77**, 325-33.
22. Lumjuan N, McCarroll L, Prapanthadara L, Hemingway J and Ranson H (2005) Elevated activity of an epsilon class glutathione transferase confers DDT resistance in the dengue vector, *Aedes aegypti*. *Insect Biochem Molec Biol* **35**, 861-71.
23. Singh SP, Coronella JA, Beneš H, Cochrane BJ and Zimniak P (2001) Catalytic function of *Drosophila melanogaster* glutathione S-transferase DmGSTS1-1 (GST-2) in conjugation of lipid peroxidation end products. *Eur J Biochem* **268**, 2912-23.
24. Oakley AJ, Harnnoi T, Udomsinprasert R, Jirajaroenrat K, Ketterman AJ and Wilce MCJ (2001) The crystal structures of glutathione S-transferases isozymes 1–3 and 1–4 from *Anopheles dirus* species B. *Protein Science* **10**, 2176-85.
25. Sawicki R, Singh SP, Mondal AK, Beneš H and Zimniak P (2003) Cloning, expression and biochemical characterization of one Epsilon-class (GST-3) and ten Delta-class (GST-1) glutathione S-transferases from *Drosophila melanogaster*, and identification of additional nine members of the Epsilon class. *Biochem J* **370**, 661-9.
26. Ricci G, Caccuri AM, Lo Bello M, Rosato N, Mei G, Nicotra M, Chiessi E et al. (1996) Structural flexibility modulates the activity of human glutathione transferase P1-1. Role of helix 2 flexibility in the catalytic mechanism. *J Biol Chem* **271**, 16187-92.

Biochem. J. (2006) **394**, 135–144 (Printed in Great Britain) doi:10.1042/BJ20050915



# An intersubunit lock-and-key 'Clasp' motif in the dimer interface of Delta class glutathione transferase

Jantana WONGSANTICHON and Albert J. KETTERMAN[1]

Institute of Molecular Biology and Genetics, Mahidol University, Salaya Campus, 25/25 Phutthamonthol Road 4, Salaya, Nakhon Pathom 73170, Thailand

Structural investigations of a GST (glutathione transferase), adGSTD4-4, from the malaria vector *Anopheles dirus* show a novel lock-and-key 'Clasp' motif in the dimer interface of the Delta class enzyme. This motif also appears to be highly conserved across several insect GST classes, but differs from a previously reported mammalian lock-and-key motif. The aromatic 'key' residue not only inserts into a hydrophobic pocket, the 'lock', of the neighbouring subunit, but also acts as part of the 'lock' for the other subunit 'key'. The 'key' residues from both subunits show aromatic ring stacking with each other in a pi–pi interaction, generating a 'Clasp' in the middle of the subunit interface. Enzyme catalytic and structural characterizations revealed that single amino acid replacements in this 'Clasp' motif impacted on catalytic efficiencies, substrate selectivity and stability. Substitutions to the 'key' residue create strong positive co-operativity for glutathione binding, with a Hill coefficient approaching 2. The lock-and-key motif in general and especially the 'Clasp' motif with the pi–pi interaction appear to play a pivotal role in subunit communication between active sites, as well as in stabilizing the quaternary structure. Evidence of allosteric effects suggests an important role for this particular intersubunit architecture in regulating catalytic activity through conformational transitions of subunits. The observation of co-operativity in the mutants also implies that glutathione ligand binding and dimerization are linked. Quaternary structural changes of all mutants suggest that subunit assembly or dimerization basically manipulates subunit communication.

Key words: *Anopheles dirus*, aromatic ring stacking, glutathione transferase, lock-and-key, pi–pi interaction, subunit interface.

## INTRODUCTION

Glutathione transferases (GST; EC 2.5.1.18) are dimeric enzymes playing a major role in detoxication mechanisms by nucleophilic addition of GSH ($\gamma$-glutamyl-L-cysteinyl-glycine) to the electrophilic centre of diverse non-polar endogenous and xenobiotic compounds, rendering them less reactive and more water-soluble substances [1–4]. Cytosolic GSTs are ubiquitous enzymes found in all organisms to date. The nomenclature of this enzyme has now been categorized to contain at least 13 classes, including seven mammalian classes (Alpha, Mu, Pi, Sigma, Theta, Omega and Zeta) and six non-mammalian classes (Beta, Delta, Epsilon, Lambda, Phi and Tau) [4,5]. In addition, members in this enzyme superfamily are increasing due to the massive growth of genomic information, which also yields a number of novel unclassified GSTs [6], a so-called 'U' class.

In general, all GSTs adopt the same highly conserved tertiary structure [2]. A dimeric quaternary structure is thought to be essential for a fully functional active site, since the active site is formed by amino acid residues from both subunits. The dimeric structure also has been shown to be involved in stabilization of tertiary structures of individual subunits [7], as well as to provide a non-substrate ligand-binding site at the dimer interface [8,9]. Studies of equilibrium folding revealed that dimeric formation of GSTs such as Alpha [10], Pi [11] and Sj26GST [12] has significant impact on stabilization of subunit tertiary structure, whereas the dimerization of GSTs such as Sigma [13] and Mu [14] has less influence on subunit stability, due to the presence of stable monomeric intermediates in an unfolding/refolding pathway [15]. Therefore, although the overall tertiary structure is conserved, structural variations occur that generate diversity between the GST classes.

Structural observations of GSTs demonstrate two distinct types of intersubunit interactions [3]. The first is a 'ball-and-socket' or so-called 'lock-and-key' hydrophobic interaction, involving an aromatic 'key' residue from domain I of one subunit that inserts into several hydrophobic 'lock' residues of domain II in the other subunit. This interaction was reported to be specific to mammalian Alpha/Mu/Pi classes [16–19]. The second type of intersubunit interaction is more hydrophilic and lacks the 'lock-and-key' motif, as in Theta/Sigma classes [20,21]. The class-specific intersubunit interactions result in different interface topologies and contribute to interface specificity. Accordingly, only subunits with the same interfacing type appear to be compatible for dimerization.

In the present study, an available refined crystal structure of adGSTD4-4, an insect Delta class GST from the mosquito malaria vector *Anopheles dirus* [22], was investigated for intersubunit interactions along the dimer interface. The enzyme was previously reported as adGST1-4 and later renamed to be in concord with a universal GST nomenclature [23]. This Delta GST was also observed to possess a lock-and-key motif. However, this lock-and-key 'Clasp' motif is found in the centre of a 2-fold axis. Therefore the motif appears to be different from those reported in mammalian Alpha/Mu/Pi classes. A striking characteristic of this motif involving the 'key' residue is that it not only inserts into a hydrophobic pocket of the neighbouring subunit, but also itself acts as part of the 'lock' for the other subunit 'key'. In addition, the 'key' residues from both subunits 'hook around' each other in an aromatic pi–pi interaction, through slightly offset

Abbreviations used: ANS, 8-anilinonaphthalene-l-sulphonic acid; CDNB, 1-chloro-2,4-dinitrobenzene; CPK, Corey–Pauling–Koltun; DCNB, 1,2-dichloro-4-nitrobenzene; EA, ethacrynic acid; GST, glutathione transferase; PNBC, *p*-nitrobenzyl chloride; PNPB, *p*-nitrophenethyl bromide; TIM, triosephosphate isomerase.

[1] To whom correspondence should be addressed (email frakt@mahidol.ac.th).

aromatic ring stacking, generating a 'clasp' in the middle of the subunit interface. To examine the contribution of the lock-and-key 'Clasp' motif to Delta class structure and function, site-directed mutagenesis was performed to Phe-104 (the 'key' residue) and Val-107 (one of the 'lock' residues). Mutant recombinant enzymes were characterized for both enzymatic and structural properties by enzyme steady-state kinetics, substrate specificity, thermal stability, far-UV CD, tryptophan intrinsic fluorescence and fluorescent dye binding.

## EXPERIMENTAL

### Construction of mutants

A pET3a plasmid containing the full coding sequence of the *A. dirus* Delta class GST isoform 4, adGSTD4-4 (GenBank® accession number AF273040), was derived from a previous study [24]. PCR-based site-directed mutagenesis following the method of Stratagene Quik Change™ Site-Directed Mutagenesis kit (Stratagene, La Jolla, CA, U.S.A.) was used to introduce point mutations to the amino acid 104 or 107 of the wild-type enzyme. A clone with double mutations at both positions was also generated. The entire full-length regions encoding all mutant adGSTD4-4 were verified, using BigDye™ terminator cycle sequencing ready reaction kit version 3.1, at least twice to confirm the absence of undesirable mutations elsewhere. V107M mutagenic plasmid was kindly provided by J. Piromjitpong (Institute of Molecular Biology and Genetics, Mahidol University).

### Protein expression and purification

Wild-type adGSTD4-4 and mutants were expressed in *Escherichia coli* BL21(DE3)pLysS as previously described [24]. The temperature of 25 °C was used during protein expression under 0.1 mM isopropyl $\beta$-D-thiogalactoside induction. Cells were harvested by centrifugation at 5000 ***g*** for 10 min. The cell pellet was treated with lysozyme to a final concentration of 0.4 mg/ml and then incubated on ice for 20 min. Cell lysate was additionally disrupted by sonication, followed by cell debris separation by centrifugation at 10000 ***g*** for 20 min at 4 °C. The soluble recombinant GST proteins were purified from the supernatant by using GSTrap™ FF affinity chromatography (Amersham Biosciences), except for those incapable of binding to the GSH matrix. In these cases, cation-exchange chromatography by HiTrap™ SP XL (Amersham Biosciences) and hydrophobic-interaction chromatography by HiTrap™ phenyl-Sepharose HP (Amersham Biosciences) were employed. The details of cationic and hydrophobic chromatography have been previously reported [25]. Purified recombinant proteins were homogeneous as judged by SDS/PAGE.

### Enzyme characterization and protein assay

Enzyme activity conjugating GSH to the CDNB (1-chloro-2,4-dinitrobenzene) substrate was determined by monitoring the increase in absorbance ($A$) at 340 nm over time using a SpectraMax® 250 spectrophotometer following a previously described method [26]. The dependence of the initial rate on the substrate concentration was analysed according to the Michaelis–Menten equation (eqn 1), where $V$ is the initial rate of the reaction, $V_{max}$ is the maximum velocity, [$S$] is the concentration of substrate and $K_m$ is the substrate concentration that gives the rate of the reaction equal to one-half of $V_{max}$:

$$V/V_{max} = [S]/(K_m + [S]) \quad (1)$$

The values for the kinetic parameters ($K_m$ and $V_{max}$) were calculated by using GraphPad Prism® 4 software, version 4.01. The steady-state kinetics and substrate-specificity studies were performed as described previously [24]. Five different hydrophobic electrophilic compounds were used in a substrate-specificity study. The results shown are means ± S.D. for at least three independent experiments. Protein concentration was determined by the Bradford method [27] using the Bio-Rad Laboratories (Hercules, CA, U.S.A.) protein reagent with BSA as the standard protein.

With evidence of co-operativity upon GSH binding, demonstrated by a sigmoidal curve instead of a hyperbolic curve on a Michaelis–Menten plot, a Hill equation (eqn 2) was used to fit the experimental kinetic data on the plot. $K_{0.5}$ is the substrate concentration that gives the rate of reaction at one-half of $V_{max}$, similar to the $K_m$ value for non-co-operative binding ($h = 1$):

$$Y = V/V_{max} = [S]^h/(K_{0.5} + [S]^h) \quad (2)$$

$$\log[Y/(1-Y)] = h\log[S] - \log K_{0.5} \quad (3)$$

A sigmoidal Hill equation was transformed into a linear rate equation (eqn 3), where $Y$ is the fractional saturation, $h$ is the Hill coefficient and $K_{0.5}$ is an averaged binding constant at $Y = 0.5$. A Hill plot, a plot between $\log[Y/(1-Y)]$ and $\log[S]$, was employed to determine the degree of co-operativity by the slope of the plot which yields the Hill coefficient ($h$) [28].

### Thermal stability assay

Enzymes derived from the different engineered clones [each at a concentration of 0.1 and 1 mg/ml in 0.1 M phosphate buffer (pH 6.5) containing 5 mM dithiothreitol and 1 mM EDTA] were incubated at 45 °C. Enzymatic activity was measured as a function of time. An appropriate amount of incubated mixture (adjusted for the specific activity of each engineered enzyme) was taken to assay for residual GST activity at various time points ranging from 0 to 420 min. The log percentage of original activity was plotted versus preincubation time. Slopes from linear regression analysis using GraphPad Prism® 4 software were used for the half-life calculation [28], $t_{1/2} = -(0.693/2.3)/\text{Slope}$.

### CD

Far-UV CD measurements were carried out on a Jasco J715 spectropolarimeter. CD spectra of proteins at a concentration of 0.4 mg/ml in 0.1 M phosphate buffer (pH 6.5) with no additives were measured in a 0.2 cm path length quartz cell at room temperature (25 °C). Spectra were recorded from 190 to 260 nm with 1 nm steps, averaged over three scans at a scan rate of 50 nm/min and corrected by subtraction of solvent spectra under identical conditions.

### Fluorescence measurements

Both intrinsic and ANS (8-anilinonaphthalene-l-sulphonic acid) fluorescence emission spectra were carried out on a Jasco model FP-6300 spectrofluorimeter in a 0.5 cm path length quartz cell. Excitation and emission bandwidths were kept at 2.5 nm. Fluorescence spectra of 2 $\mu$M enzyme in 0.1 M phosphate buffer (pH 6.5) with no additives were recorded at room temperature. All measurements were averaged over three scans at a scanning speed of 500 nm/min and corrected by subtraction of the solvent spectra under identical conditions.

Intrinsic fluorescence measurements were performed at an excitation wavelength of 295 nm and the emission spectra were recorded from 300 to 500 nm, whereas ANS fluorescence

**Table 1 Steady-state kinetic constants of engineered GSTs compared with adGSTD4-4 (wild-type)**

The results shown are the means ± S.D. for at least three independent experiments.

| Enzyme | $V_{max}$ ($\mu$mol · min$^{-1}$ · mg$^{-1}$) | $k_{cat}$ (s$^{-1}$) | $K_m$ (mM) | | $k_{cat}/K_m$ (mM$^{-1}$ · s$^{-1}$) | |
|---|---|---|---|---|---|---|
| | | | GSH | CDNB | GSH | CDNB |
| Wild-type | 44.7 ± 2.3 | 18.60 | 0.59 ± 0.06 | 0.73 ± 0.07 | 31.53 | 25.49 |
| F104A | 23.3 ± 1.7 | 9.67 | 11.99 ± 0.20 | 2.27 ± 0.31 | 0.85 | 4.26 |
| F104L | 49.3 ± 1.8 | 20.59 | 3.55 ± 0.40 | 0.69 ± 0.15 | 6.32 | 29.85 |
| F104M | 42.1 ± 1.9 | 17.51 | 2.21 ± 0.11 | 0.82 ± 0.06 | 10.81 | 21.36 |
| F104Y | 42.7 ± 1.2 | 17.86 | 6.96 ± 0.31 | 0.57 ± 0.05 | 2.76 | 31.34 |
| F104W | 3.9 ± 0.3 | 1.63 | 15.26 ± 0.54 | 1.49 ± 0.12 | 0.13 | 1.09 |
| F104H | 1.8 ± 0.1 | 0.74 | 16.97 ± 1.54 | 0.79 ± 0.05 | 0.04 | 0.94 |
| F104Q | 9.5 ± 0.4 | 3.97 | 15.35 ± 1.21 | 1.32 ± 0.11 | 0.29 | 3.00 |
| F104E | 4.6 ± 0.3 | 1.91 | 16.54 ± 1.34 | 1.86 ± 0.14 | 0.12 | 1.03 |
| F104K | 0.17 ± 0.01 | 0.07 | 6.62 ± 0.14 | 0.85 ± 0.13 | 0.01 | 0.08 |
| F104A/V107A | 15.3 ± 0.6 | 6.34 | 10.06 ± 0.58 | 2.07 ± 0.18 | 0.63 | 3.06 |
| V107A | 50.6 ± 1.5 | 21.04 | 0.73 ± 0.13 | 0.56 ± 0.02 | 28.82 | 37.57 |
| V107L | 46.9 ± 1.7 | 19.53 | 0.40 ± 0.03 | 0.47 ± 0.05 | 48.83 | 41.56 |
| V107M | 49.9 ± 0.8 | 20.89 | 0.64 ± 0.10 | 0.79 ± 0.04 | 32.64 | 26.44 |
| V107N | 37.2 ± 2.2 | 15.49 | 0.45 ± 0.09 | 0.68 ± 0.09 | 34.43 | 22.78 |
| V107D | 13.5 ± 0.4 | 5.62 | 1.23 ± 0.16 | 0.51 ± 0.03 | 6.32 | 11.02 |
| V107K | 0.29 ± 0.01 | 0.12 | 8.88 ± 0.19 | 0.71 ± 0.05 | 0.02 | 0.17 |

measurements were at an excitation wavelength of 395 nm and the emission spectra were recorded from 400 to 600 nm. The final concentration of 200 $\mu$M ANS was homogeneously mixed with enzyme solutions prior to the measurements.

## RESULTS

### Protein expression and purification

All recombinant proteins were effectively expressed at comparable levels in *E. coli* as soluble protein with a size of approx. 25 kDa. Generally, adGSTD4-4 was easily purified in a single chromatographic step using an immobilized GSH affinity chromatography column. It was found that the affinity for this matrix was strongly reduced for many mutants. Therefore an alternative method of cation-exchange and hydrophobic-interaction chromatography was employed. Protein purities from both techniques proved to be equivalent. All mutants were successfully purified and subjected to both enzymatic and structural characterizations.

### Enzymatic properties

#### Enzyme kinetics

Steady-state kinetics was performed using CDNB as a co-substrate for GSH conjugation. Mutant recombinant enzymes with an amino acid substitution at Phe-104 possessed altered catalytic rates ($k_{cat}$) ranging from approximately wild-type to 266-fold less than wild-type activity (Table 1). Substitutions with bulky (F104W) or polar/charged residues (F104H, F104Q, F104E and F104K) are catalytically unfavourable at position 104, as shown by a decrease of 5- to 266-fold in $k_{cat}$. The binding affinity towards GSH ($K_m^{GSH}$) for all Phe-104 mutants was dramatically affected in the range of 4–29-fold less than the wild-type. These decreases in binding affinity were also accompanied by a change to positive co-operativity for GSH binding. For positive co-operativity, a sigmoidal curve was obtained from Michaelis–Menten plots instead of a hyperbolic curve. The degree of co-operativity as shown by the Hill coefficients illustrates that communication occurs between the active sites (Table 2). The sigmoidal-shaped curve for GSH binding signifies that the binding of one molecule of GSH in one active site increases the affinity of the protein for that substrate in the neighbouring active site of the other subunit, reflecting the role of the residue in communication between subunits to stabilize the GSH binding. In addition, the binding affinity towards CDNB substrate ($K_m^{CDNB}$) of the Phe-104 mutants varied slightly as well in the range of 1–3-fold, which most probably results from structural perturbation within the active-site pocket.

**Table 2 Hill coefficients (*h*) for the binding of GSH substrate**

The results shown are the means ± S.D. for at least three independent experiments. ANOVA with Dunnett multiple comparisons test was applied with wild-type enzyme as control.

| Enzyme | *h* |
|---|---|
| Wild-type | 1.02 ± 0.14 |
| F104A | 1.67 ± 0.09* |
| F104L | 1.44 ± 0.12* |
| F104M | 1.23 ± 0.08 |
| F104Y | 1.73 ± 0.08* |
| F104W | 1.33 ± 0.15* |
| F104H | 2.10 ± 0.05* |
| F104Q | 1.64 ± 0.11* |
| F104E | 1.99 ± 0.15* |
| F104K | 1.58 ± 0.05* |
| F104A/V107A | 0.99 ± 0.09 |
| V107A | 0.96 ± 0.07 |
| V107L | 0.99 ± 0.14 |
| V107M | 0.93 ± 0.09 |
| V107N | 0.99 ± 0.11 |
| V107D | 1.34 ± 0.13* |
| V107K | 1.44 ± 0.11* |

* Significantly different ($P < 0.01$).

Amino acid replacements at the position Val-107 demonstrated that a charged residue substitution would impact upon the catalytic efficiency of the enzyme by reducing $k_{cat}$ and increasing $K_m^{GSH}$, in addition to inducing positive co-operativity for GSH binding. In contrast, substitutions with polar, uncharged or non-polar amino acid residues with various sized side chains show little impact on catalytic properties. Kinetic constants of the double mutant F104A/V107A also demonstrated that the disruption at the Phe-104 position has a major influence on catalysis, as

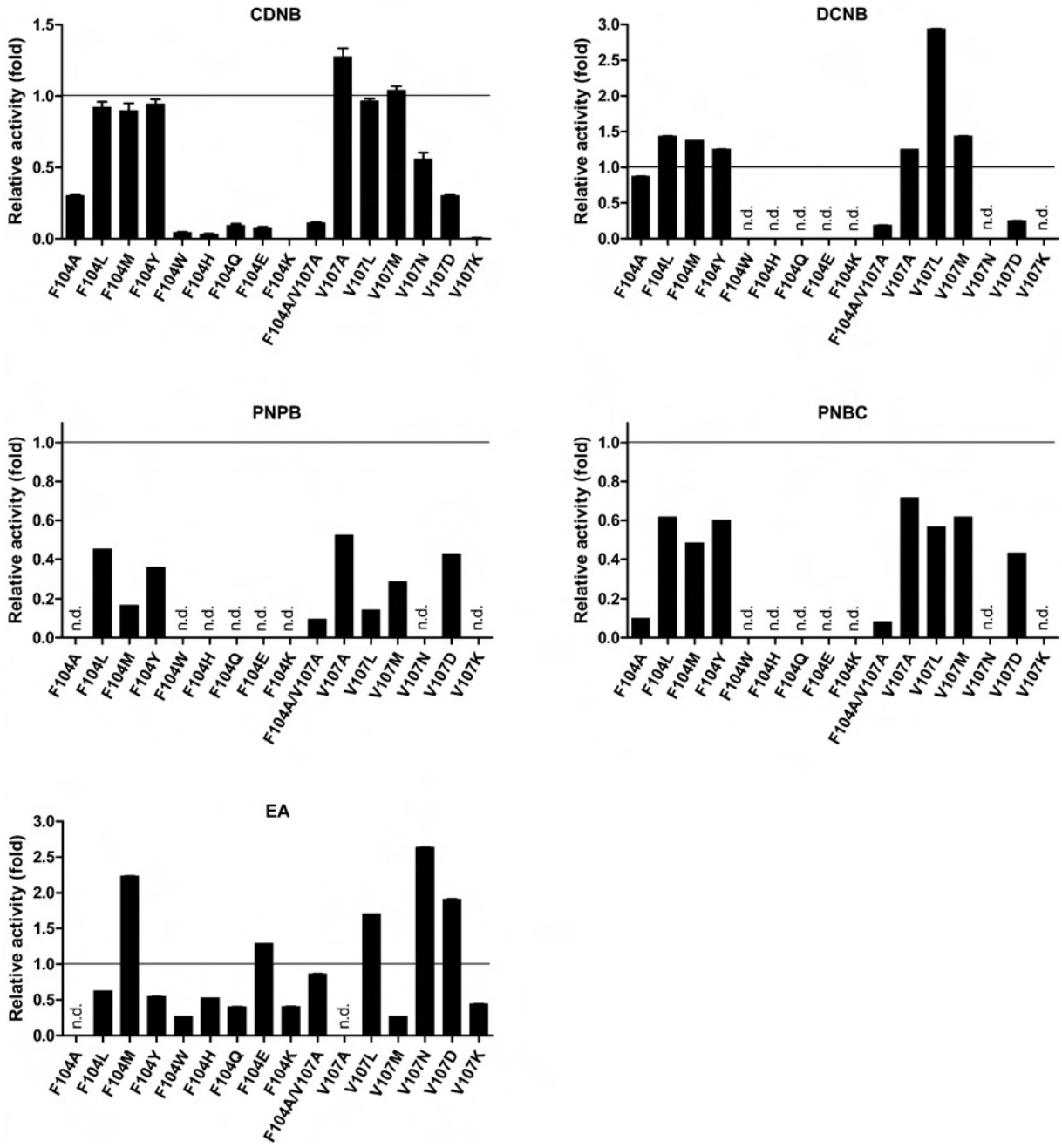


**Figure 1 Plots of the changes in substrate specificity for engineered GSTs relative to the wild-type enzyme**

The change in specific activity of each enzyme for each substrate is shown as fold change relative to the wild-type enzyme. The experiment was performed in triplicate and the results shown are means ± S.D.; n.d., no detectable activity.

shown by the kinetic properties of the single alanine mutations to either Phe-104 or Val-107. However, this double-mutation enzyme displayed a different characteristic from F104A by possessing non-co-operative binding for GSH substrate (Table 2). This demonstrates that the alanine substitution at Val-107 confers a different structural arrangement that affects the communication between subunits.

### Substrate specificity

Five different hydrophobic substrates were used to investigate the changes in substrate specificities of the mutant recombinant enzymes (Figure 1). Each engineered GST displayed a different pattern of substrate specificity. The engineered GSTs with low affinity towards GSH (high $K_m^{GSH}$) also appeared to possess low activity towards most hydrophobic substrates tested, including CDNB. In this regard, the decrease in activity appears to result from a major disturbance to the G-site (GSH-binding site). This disturbance produces active-site atom movements as well as electrostatic field rearrangement, causing substrate orientation to be in less suitable configurations resulting in catalytic changes. Interestingly, F104L, F104M and F104Y possess comparable activity and specificity with the wild-type enzyme towards CDNB, as shown by $k_{cat}$ and $(k_{cat}/K_m)^{CDNB}$. However, these

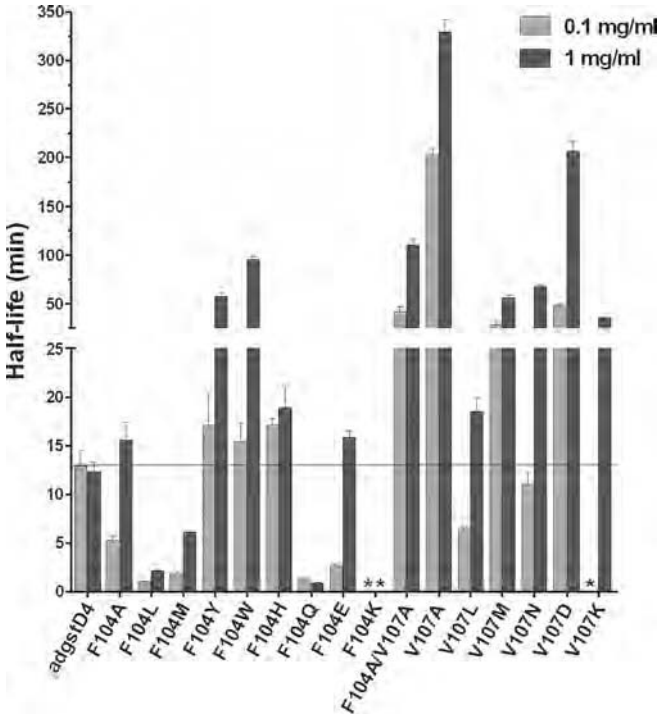


**Figure 2 Thermal stability of engineered GSTs compared with the wild-type adGSTD4-4**

Half-life determinations were from at least three independent experiments at 45 °C. Enzyme concentrations for heat inactivation are 0.1 and 1 mg/ml respectively. The bar graph represents mean ± S.D. (An asterisk indicates that enzyme activity was undetectable upon heat inactivation, which precluded half-life determination.)

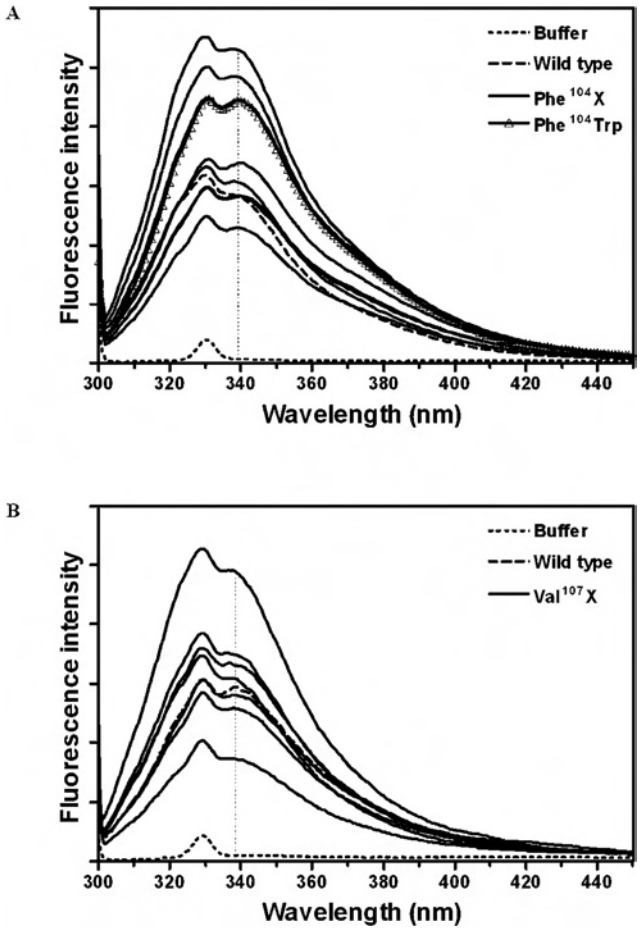


**Figure 3 Intrinsic fluorescence of engineered GSTs compared with wild-type adGSTD4-4**

F104X, F104W and V107X represent spectra of replacements of (**A**) Phe-104 with one of the amino acids in the present study, replacement of Phe-104 with Trp, and (**B**) replacements of Val-107 with one of the amino acids in the present study respectively. Fluorescence intensity was measured in arbitrary units. Additional lines illustrate variation between all the engineered GSTs.

enzymes displayed higher specific activity with DCNB (1,2-dichloro-4-nitrobenzene), lower specific activity with PNPB (*p*-nitrophenethyl bromide) and PNBC (*p*-nitrobenzyl chloride), but a variable activity with EA (ethacrynic acid) as the substrate. This evidence suggests that the replacement residues in the G-site Phe-104 position have significant consequences on the H-site (hydrophobic substrate-binding site) of the enzyme. Therefore diverse effects on the enzyme activities towards various substrates demonstrate that the different enzyme–substrate interactions that occur are affected in distinctly different ways.

The positively charged replacement V107K performed poorly with all hydrophobic substrates tested, whereas the other mutants showed variable activity towards the different substrates. The double mutant F104A/V107A had low specificity for most of the hydrophobic substrates tested. However, the enzyme demonstrated EA activity comparable with the wild-type, although no detectable EA activity was shown by either of the alanine single-mutation enzymes. Accordingly, the properties of F104A/V107A are not additive influences of F104A and V107A, but result from a particular rearrangement of the enzyme active site that occurs upon packing changes induced by the double mutation.

## Structural properties

### Enzyme stability

Thermal stability was monitored to demonstrate that amino acid substitutions at either Phe-104 or Val-107, residues involved in the lock-and-key 'Clasp' motif, have a role in structural stability of adGSTD4-4 (Figure 2). Most of the mutants showed a concentration-dependent thermal stability in which increasing concentration showed greater stability. The engineered enzymes appeared to undergo structural changes more rapidly at low concentrations compared with the wild-type, which displayed similar stability at both concentrations used. The results suggest that residue 104 is involved in regulating structural integrity of the enzyme, while substitutions to residue 107 appeared to enhance structural maintenance as shown by an increase in half-life.

### CD

CD was used to monitor for protein secondary-structure disruption. The ellipticity spectra measured for the Phe-104 mutants were similar to the spectrum of the wild-type enzyme, with ellipticity minima at 208 and 222 nm. This is characteristic of an $\alpha$-helix predominant structure and suggests no overall secondary-structure change (results not shown).

### Intrinsic fluorescence

Tryptophan intrinsic fluorescence (excitation at 295 nm) was used as a tertiary-structure probe. Each adGSTD4-4 subunit possesses two tryptophan residues located at positions 64 and 191. All mutants showed roughly the same emission maximum of 339 ± 2 nm (Figure 3). As expected, the F104W enzyme, with one additional tryptophan residue, also showed the same emission

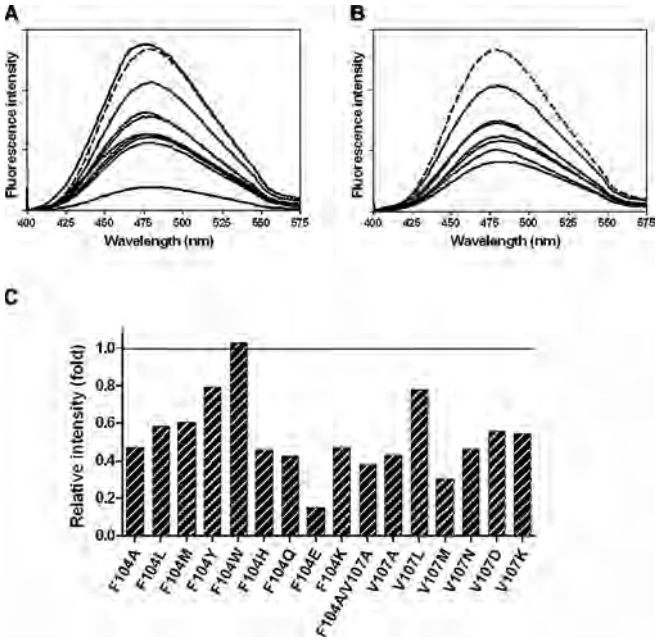


**Figure 4 Fluorescence spectrophotometry of ANS binding**

(**A**) Fluorescence spectra of Phe-104 mutants. (**B**) Fluorescence spectra of Val-107 mutants. (**C**) A bar graph representation of relative fluorescence intensity compared with the wild-type enzyme. Fluorescence intensity was measured in arbitrary units. Additional lines illustrate variation between all the engineered GSTs.

maximum (Figure 3A), demonstrating that residue 104 is buried in the interior core of the GST dimer interface. Although all substitutions in the present study had no impact on solvent exposure of the tryptophan residues, the variable fluorescent intensities from the different mutants indicate that differences occur in local quenching by the surrounding amino acids such as cysteine, histidine, glutamine and asparagine [29].

### Fluorescent dye binding

ANS (extrinsic fluorophore) binding was used as a quaternary structure probe. Upon binding, ANS fluorescence was significantly enhanced and its emission maximum wavelength shifted from 515 nm to approx. 479 nm. Most Phe-104 and Val-107 mutants showed a reduction of fluorescence intensity compared with wild-type (Figure 4). Only F104W slightly increased the fluorescent signal (Figure 4C). Both quenching and enhancement of the fluorescent signals demonstrate conformational changes in the non-substrate ligand-binding site for ANS.

## DISCUSSION

The lock-and-key 'Clasp' motif shows some similar characteristics to previously investigated lock-and-key motifs in the GST classes Alpha [30], Mu [31] and Pi [32], for example, stabilization of the dimeric structure through intersubunit interactions. However, the 'Clasp' motif is situated in a different location along the dimer interface and possesses a unique feature (Figure 5). Using the completed *Anopheles gambiae* genome project, an African mosquito malarial vector, members of the GST supergene family have been identified as insecticide-resistant-associated enzymes to enable the monitoring of resistance status of mosquitoes [33]. Putative GST genes were confirmed at the transcriptional level and 12 out of 28 putative genes were classified as insect-specific Delta class [6]. Primary sequences of *A. gambiae* GSTs were aligned with available *A. dirus* Delta class GSTs. Equivalent amino acid residues involved in the 'Clasp' motif of Anopheline GSTs are shown in Table 3, as well as residues of the Australian sheep blowfly (*Lucilia cuprina*) GST. The amino acid residues involved in the motif are shown to be highly conserved across several insect GST classes (Table 3). Available X-ray crystal structures of six Delta class GSTs show their structural conservation in the quaternary structure. Three-dimensional superimposition of equivalent residues in each of the Delta class enzymes shows conserved residues in similar environments (Figure 6). Several of the lock residues have been previously studied by alanine scanning in adGSTD3-3, which is an alternatively spliced product derived from the same gene as adGSTD4-4 [34]. The corresponding residue to adGSTD4-4 Glu-65 (Glu-64 in adGSTD3-3) was suggested to be involved in an initial folding step of the enzyme and this residue is highly conserved among GST classes. The corresponding residue to adGSTD4-4 Arg-67 (Arg-66 in adGSTD3-3) revealed a significant impact on the ionization process of GSH, as well as structural stabilization. However, the corresponding residue to adGSTD4-4 Val-107 (Met-101 in adGSTD3-3) showed no significant functional or structural effects. Leu-103 has previously been characterized in adGSTD4-4 and shown to be important for GSH binding, with evidence for positive co-operativity in some mutants, as well as being involved in structural

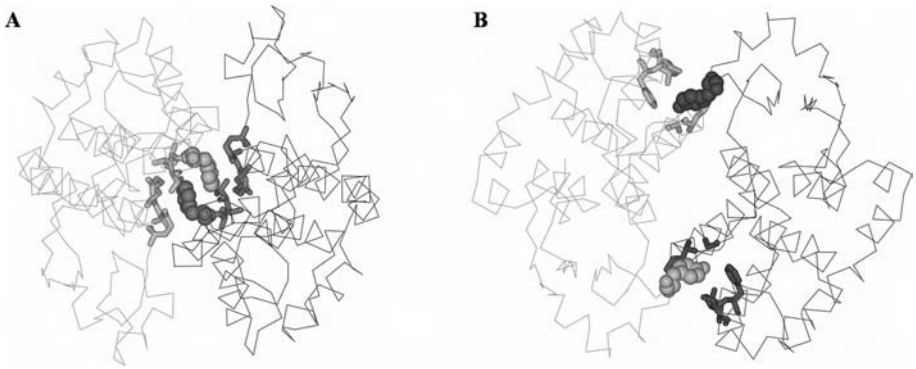


**Figure 5 Two types of intersubunit lock-and-key motifs found in different GST classes**

(**A**) Lock-and-key 'Clasp' motif in adGSTD4-4 (PDB id: 1JLW). (**B**) Lock-and-key motif in human GST class Pi, GSTP1-1 (PDB id: 1GSS). Subunits are distinguished by colouring in grey and dark grey, amino acid residues involved in the 'lock' are shown by stick representation, whereas the 'key' residues, Phe-104 in adGSTD4-4 or Tyr-50 in human GSTP1-1, are shown in CPK (Corey–Pauling–Koltun) space-filling mode.

**Table 3 Lock-and-key 'Clasp' residues in insect GST classes**

Numbering of residues is based on adGSTD4 sequence. * adGST, agGST and LcGST represent GSTs from *A. dirus*, *A. gambiae* and *L. cuprina* respectively. D is Delta, u is unclassified, E is Epsilon, T is Theta, S is Sigma, Z is Zeta and O is Omega GST class. GenBank® accession numbers: adGSTD1 (AF273041), adGSTD2 (AF273038), adGSTD3 (AF273039), adGSTD4 (AF273040), adGSTD5 (AF251478), adGSTD6 (AY014406), agGSTD1-3 (Protein ID AAC79992), agGSTD1-4 (Protein ID AAC79994), agGSTD1-5 (Protein ID AAC79993), agGSTD1-6 (Protein ID AAC79995), agGSTD2 (Z71480), agGSTD3 (AF513638), agGSTD4 (AF513635), agGSTD5 (AF513634), agGSTD6 (AF513636), agGSTD7 (AF071161), agGSTD8 (AF316637), agGSTD9 (AY255857), agGSTD10 (AF515527), agGSTD11 (AF513637), agGSTD12 (AF316638), agGSTu1 (AF515521), agGSTu2 (AF515523), agGSTu3 (AF515524), agGSTE1 (AF316635), agGSTE2 (AF316636), agGSTE3 (AY070234), agGSTE4 (AY070254), agGSTE5 (AY070255), agGSTE6 (AY070256), agGSTE7 (AF491816), agGSTE8 (AY070257), agGSTT1 (AF515526), agGSTT2 (AF515525), agGSTS1-1 (L07880), agGSTS1-2 (AF513639), agGSTZ1 (AF515522), agGSTO1 (AY255856) and LcGST (P42860). † 104a and 104b indicate that the residue at this position is from different subunits. ‡ agGSTD6 and agGSTD9 were suggested to be pseudogenes [6].

| | Key residue | | | Lock residue | | | |
|---|---|---|---|---|---|---|---|
| Enzyme* | 104a† | 65 | 67 | 68 | 103 | 104b† | 107 |
| adGSTD4 | F | E | R | A | L | F | V |
| adGSTD1 | F | E | R | A | L | F | M |
| adGSTD2 | Y | E | R | A | L | Y | M |
| adGSTD3 | Y | E | R | A | L | Y | M |
| adGSTD5 | H | E | R | V | L | H | L |
| adGSTD6 | F | E | Y | A | L | F | I |
| agGSTD1-3 | F | E | R | A | L | F | V |
| agGSTD1-4 | Y | E | R | A | L | Y | M |
| agGSTD1-5 | Y | E | R | A | M | Y | M |
| agGSTD1-6 | Y | E | R | A | L | Y | M |
| agGSTD2 | F | E | R | A | L | F | A |
| agGSTD3 | F | E | Y | A | L | F | I |
| agGSTD4 | F | E | C | A | L | F | V |
| agGSTD5 | F | E | Y | A | L | F | I |
| agGSTD6‡ | F | E | S | A | L | F | I |
| agGSTD7 | H | E | R | V | L | H | L |
| agGSTD8 | F | E | R | A | L | F | H |
| agGSTD9‡ | L | E | G | A | L | L | C |
| agGSTD10 | F | E | Y | A | L | F | N |
| agGSTD11 | Y | E | R | A | L | Y | M |
| agGSTD12 | F | E | Y | A | L | F | S |
| agGSTu1 | C | E | N | A | L | C | L |
| agGSTu2 | H | E | R | A | L | H | L |
| agGSTu3 | Y | E | K | A | L | Y | S |
| agGSTE1 | H | E | H | A | L | H | S |
| agGSTE2 | H | E | H | A | L | H | S |
| agGSTE3 | H | D | H | A | L | H | S |
| agGSTE4 | H | D | H | A | L | H | S |
| agGSTE5 | H | D | H | A | L | H | S |
| agGSTE7 | H | A | H | A | L | H | A |
| agGSTE6 | F | D | H | A | L | F | S |
| agGSTE8 | C | D | H | A | L | C | N |
| agGSTT1 | E | E | V | A | L | E | H |
| agGSTT2 | S | E | V | A | L | S | H |
| agGSTS1-1 | D | Q | L | A | V | D | N |
| agGSTS1-2 | D | Q | V | A | V | D | N |
| agGSTZ1 | E | E | V | S | C | E | A |
| agGSTO1 | E | E | L | V | I | E | A |
| LcGST | Y | E | R | A | L | Y | M |

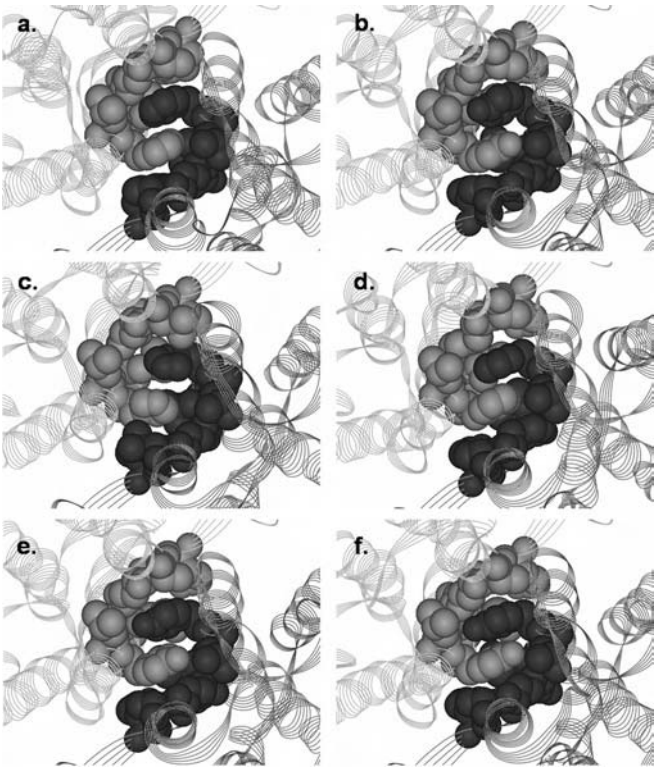


**Figure 6 Structural representations of highly conserved lock-and-key 'Clasp' motifs in various Delta class GSTs**

(**a**) *A. dirus* adGSTD4; (**b**) *A. dirus* adGSTD3; (**c**) *A. dirus* adGSTD5; (**d**) *A. dirus* adGSTD6; (**e**) *L. cuprina* LcGST; and (**f**) *A. gambiae* agGSTD1-6. Subunits are differentiated by grey and dark grey colours. Lock-and-key 'Clasp' residues are shown in CPK.

stabilization [35]. In an attempt to characterize the contribution of the lock-and-key 'Clasp' motif, the 'key' residue Phe-104 and the 'lock' residue Val-107 of adGSTD4-4 were investigated.

Enzymatic properties of the Phe-104 mutants demonstrated a major impact for this particular position on GSH binding affinity, as shown by increased $K_m^{GSH}$ values for all of the Phe-104 mutants. The altered side chains at position 104 in both subunits would impact on their interface interaction as well as causing a G-site topology change through rearrangement of 'lock' residues, several of which are in the G-site. Replacements with hydrophobic amino acids generated enzymes with varying catalytic rates. Reduced catalytic rates were observed for both F104A and F104W, indicating that not only hydrophobic packing in the region but also the size of the replaced residue is important for efficient subunit dimerization. Structural investigation reveals that the 'Clasp' motif resides within the interior core of the dimer interface that connects the G-site of one subunit to the other (Figure 7A). The communication between subunits through this Clasp motif was illustrated by catalytic co-operativity for GSH binding in all Phe-104 mutants, as shown by Hill coefficients (Table 2). In this regard, the $h$ value of $2.10 \pm 0.05$ upon GSH binding for F104H is likely to be statistically similar (95% confidence interval) to the maximum number of interacting sites of 2, which demonstrates extremely strong positive co-operativity or complete co-operativity between subunits. Therefore it is reasonable to state that the 'key' residue Phe-104 plays a pivotal role in the dimeric structure of adGSTD4-4 in modulation of GSH binding for both subunits.

The co-operativity event upon GSH binding has been previously reported for several GST studies. Interestingly, co-operativity from point mutations of a human GSTP1-1 at position Gly-41 [36], Cys-47 [37] and Lys-54 [38] was suggested to be a consequence of structural perturbation of helix $\alpha 2$, which in turn was transmitted to Tyr-50 and passed to the neighbouring subunit through the intersubunit lock-and-key motif, where Tyr-50 is the 'key' residue. Likewise, a single point mutation at His-38 located in helix $\alpha 2$ of adGSTD4-4 also revealed positive co-operativity for GSH binding [25]. In this case, three-dimensional

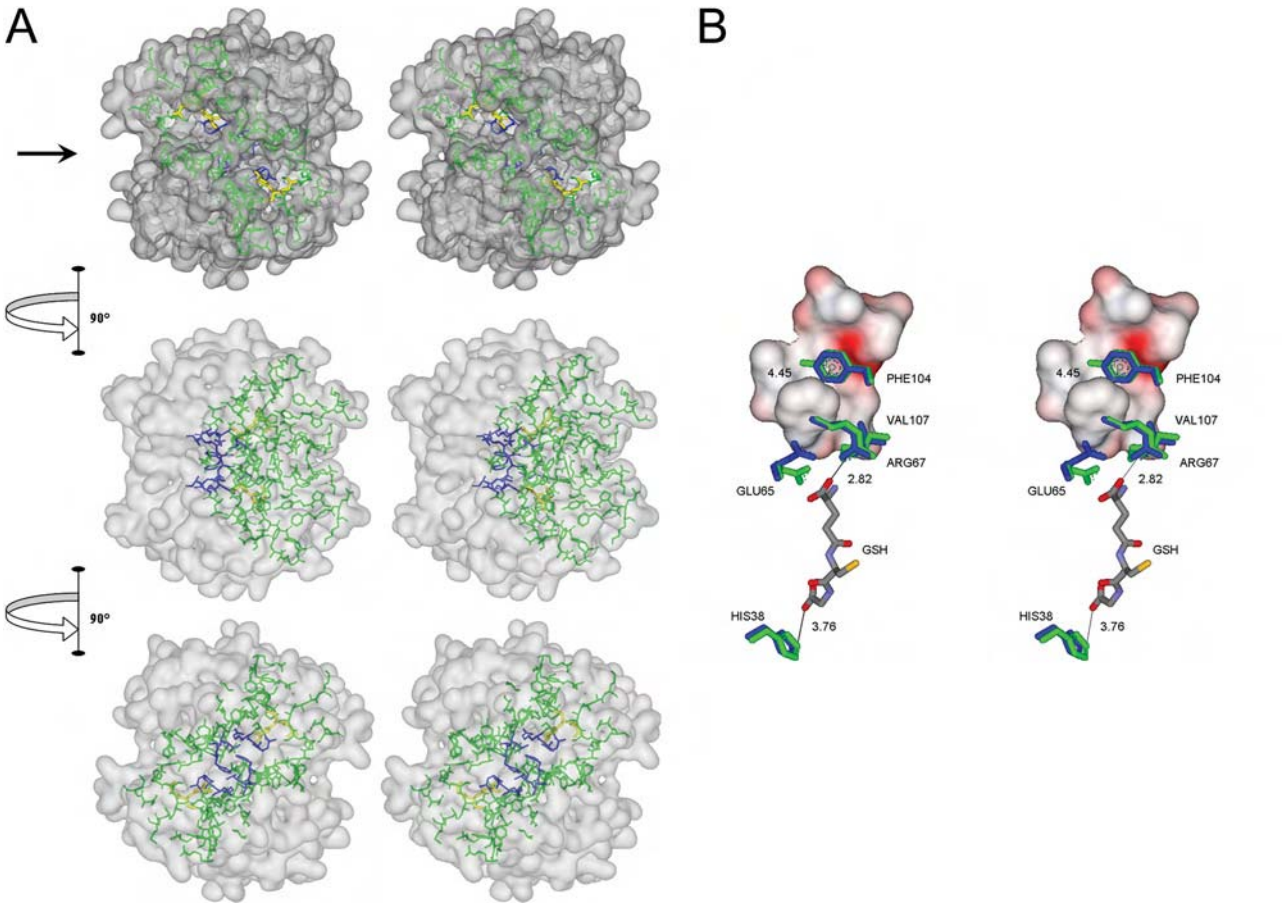


**Figure 7 Interactions of amino acids in the lock-and-key 'Clasp' motif of adGSTD4-4**

(**A**) Stereo view of the lock-and-key 'Clasp' motif connecting two active site pockets of adGSTD4-4. The surface of the dimeric enzyme is shown in grey, GSH in each active site in yellow, the active-site amino acids in green and the Clasp residues in blue. Five of the six Clasp amino acids are also active-site residues. The top panel is looking down on to the 2-fold axis at the two active sites, which are diagonal to each other. The arrow in the top panel points to the interface groove that runs across the protein. The middle panel shows the GST rotated 90° in the direction indicated and the bottom panel shows the GST rotated a further 90° in the same direction. (**B**) Stereo view showing communication of GSH binding from one active site to the other through residues involved in the Clasp motif. Crystal structure of adGSTD4-4 (PDB id: 1JLW) is superimposed on adGSTD3-3 (PDB id: 1JLV) by fitting 1616 backbone atoms, with an R.M.S.D. (root mean square deviation) of 0.82 Å (1 Å = 0.1 nm). Distances between centroids of aromatic 'key' residues are monitored from adGSTD4-4, whereas distances of GSH-interacting residues are monitored from the adGSTD3-3 enzyme complex. Amino acid labelling is for adGSTD4-4. Amino acid residues of adGSTD4-4 and adGSTD3-3 are coloured in blue and green respectively. The surface representation is of 'lock' residues from the subunit partner.

structure suggests that His-38 is a G-site residue in close contact with the glycine moiety of GSH. Therefore an alteration at His-38 may be transmitted to the lock-and-key 'Clasp' motif by the glutamyl moiety of GSH (Figure 7B). For subunit interface residues, co-operativity for GSH binding was evident in studies of Tyr-50 of human GSTP1-1 [32] as well as co-operativity for GSH conjugation of 4-hydroxynonenal through Arg-69 of murine GSTA4-4 [39] and Asp-101 of human GSTA1-1 [40]. As a whole, although the co-operativity mechanism upon substrate binding is unclear, the subunit communication is apparently triggered from one substrate binding site to the other neighbouring subunit through an existing subunit interface interaction that varies among the GST classes, and the Clasp motif seems to possess a major role in Delta class GSTs.

The Val-107 position exhibited the greatest influence on enzymatic properties when substituted with charged residues. This suggests that a hydrophobic amino acid is not necessary at this position, as shown by V107N. However, decreases in catalytic rates and affinity towards GSH with co-operativity on GSH binding of V107D and V107K suggest that these replacements might create additional electrostatic interactions to residues in close proximity, such as Glu-65 or Arg-67, that subsequently cause structural perturbation to the G-site. Particularly, the Val-107 position is of interest because almost all substitutions seemed to enhance structural stability of the enzyme, especially V107A. It is very unusual for mutants to be significantly more stable than the wild-type. The Clasp motif is composed of hydrophobic residues that can stabilize the structure through hydrophobic force as well as polar/charged residues that would maintain structural integrity by ionic interactions. The changes at the Val-107 position appear to contribute stabilizing forces between subunits and weaken conformational strain of the dimerization. V107A displayed appreciably improved stability while maintaining functionality.

There was no secondary or tertiary structural changes detected by CD or intrinsic fluorescence measurements of tryptophan. However, intensity differences of ANS binding indicate conformational alterations at the quaternary level. Blue shift of the fluorescence emission maximum of bound ANS indicates that the ANS-binding site in adGSTD4-4 is similar to hGSTA1-1 [30] and pGSTP1-1 [41] with an emission maximum of approx. 480 nm, but more hydrophobic than in squid GSTS1-1 [13], hGSTM1-1 [14] and rGSTM1-1 [31] which have emission

maxima in the range 490–500 nm. In hGSTA1-1, ANS binding was suggested to be at the cleft in the dimer interface binding one molecule per subunit in a native protein [42]. Assuming that ANS binding of adGSTD4-4 is also located along the subunit interface, the present study shows that the Clasp motif influenced ANS binding. Since ANS fluorescence is quenched by water, the reduction of fluorescence intensity of protein-bound ANS in mutants illustrates greater exposure of ANS to solvent. This suggests that amino acid substitution to either Phe-104 or Val-107 alters the binding-site topology/solvent exposure for ANS.

The aromatic stacking of the 'key' residues suggests aromatic residues to be important for enzyme stability, as shown by half-life data for F104Y, F104W and F104H, although these replacements are not always favourable for catalytic function. The presence of aromatic residues protruding from one subunit to the other was suggested to be advantageous for increasing interface affinity, hence gluing protein subunits together [43]. However, different aromatic residues employed in diverse Delta class GSTs would generate isoform-specific subunit interfaces. Therefore substitutions with 'key' residues from other Delta class GSTs such as in F104Y and F104H appear to induce conformation changes that impact upon catalytic function.

Phenylalanine residues interacting across a 2-fold axis also were shown at the dimer interface of the TIM (triosephosphate isomerase) enzyme family. The interface between TIM subunits is mainly composed of loops 1–3 from both monomers. At the tip of loop 2 in trypanosomal TIM, a phenylalanine residue (Phe-45) forms a hydrophobic contact across the dimer interface to the equivalent residue on the other subunit. In *Escherichia coli* TIM, the residue was replaced by a glutamate residue (Glu-46) [44]. The Glu-46 also interacts with its corresponding residue on the neighbouring subunit contributing extensive van der Waals contacts with its local environment, as a result inducing conformational changes to the remaining intersubunit contacts which are different from that observed in other TIMs [44]. This implies that intersubunit residue interactions of oligomeric enzymes are to stabilize quaternary structure or dimerization. With similar features to GSTs, all TIMs are active only in the dimeric form, although each monomer has its own active site [45]. In view of an important glycolytic function, TIMs are of major interest in recent years as a potential target for therapeutic drug design, principally by disturbing some of the intersubunit contacts of the protein. For example, disruption of subunit assembly through effects on pi–pi interactions of two aromatic clusters in the interface of trypanosomal TIM [46,47] and *Plasmodium falciparum* TIM [48,49] was investigated for anti-trypanosomal agents and antimalarial drug design.

We have shown that an intersubunit lock-and-key 'Clasp' motif of adGSTD4-4 demonstrates functional and structural significance of the amino acids that interact across the dimer interface. Although residues of this motif do not provide the only interaction between subunits of adGSTD4-4, it is noteworthy that the unique characteristic of aromatic stacking in the middle of the dimer interface in fact connects the two active sites, enabling them to work in a co-operative manner. Evidence of allosteric effects suggests an important role for this particular intersubunit architecture in regulating catalytic activity through conformational transitions of subunits. Quaternary structural changes of all mutants detected by ANS dye binding suggest that subunit assembly or dimerization basically manipulates subunit communication. The observation of co-operativity in the mutants also implies that GSH ligand binding and dimerization are linked, consistent with the ANS-indicated quaternary structural changes; consequently, GSTs are catalytically active only in their dimeric forms. Correlations between oligomerization and ligand binding have also been shown for many other enzymes, such as dimerization of pyrophosphatase subunits improving its ligand binding, and vice versa with active-site adjustments upon metal cofactor or substrate binding increasing the stability of the dimer [50].

In conclusion, for GSTs, the lock-and-key motif in general, and especially the 'Clasp' motif with the pi–pi interaction, appear to play a pivotal role in subunit communication between active sites as well as in stabilizing the quaternary structure. Continued elucidation of the mechanism of positive co-operativity between subunits of oligomeric proteins would provide useful information for protein engineering.

This work was funded by the Thailand Research Fund. J.W. was supported by a Royal Golden Jubilee scholarship.

## REFERENCES


1 Armstrong, R. N. (1991) Glutathione S-transferases: reaction mechanism, structure, and function. Chem. Res. Toxicol. **4**, 131–140
2 Wilce, M. C. J. and Parker, M. W. (1994) Structure and function of glutathione S-transferases. Biochim. Biophys. Acta **1205**, 1–18
3 Armstrong, R. N. (1997) Structure, catalytic mechanism, and evolution of the glutathione transferases. Chem. Res. Toxicol. **10**, 2–18
4 Hayes, J. D., Flanagan, J. U. and Jowsey, I. R. (2005) Glutathione transferases. Annu. Rev. Pharmacol. Toxicol. **45**, 51–88
5 Sheehan, D., Meade, G., Foley, V. M. and Dowd, C. A. (2001) Structure, function and evolution of glutathione transferases: implications for classification of non-mammalian members of an ancient enzyme superfamily. Biochem. J. **360**, 1–16
6 Ding, Y., Ortelli, F., Rossiter, L. C., Hemingway, J. and Ranson, H. (2003) The *Anopheles gambiae* glutathione transferase supergene family: annotation, phylogeny and expression profiles. BMC Genomics **4**, 35–50
7 Erhardt, J. and Dirr, H. (1995) Native dimer stabilizes the subunit tertiary structure of porcine class pi glutathione *S*-transferase. Eur. J. Biochem. **230**, 614–620
8 Le Trong, I., Strenkamp, R. E., Ibarra, C., Atkins, W. M. and Adman, E. T. (2002) 1.3-Å resolution structure of human glutathione S-transferase with S-hexyl glutathione bound reveals possible extended ligandin binding site. Proteins Struct. Funct. Genet. **48**, 618–627
9 Yassin, Z., Ortiz-Salmerón, E., García-Maroto, F., Barón, C. and García-Fuentes, L. (2004) Implications of the ligandin binding site on the binding of non-substrate ligands to *Schistosoma japonicum*-glutathione transferase. Biochim. Biophys. Acta **1698**, 227–237
10 Wallace, L. A., Sluis-Cremer, N. and Dirr, H. W. (1998) Equilibrium and kinetic unfolding properties of dimeric human glutathione transferase A1-1. Biochemistry **37**, 5320–5328
11 Dirr, H. W. and Reinemer, P. (1991) Equilibrium unfolding of class Pi glutathione *S*-transferase. Biochem. Biophys. Res. Commun. **180**, 294–300
12 Andújar-Sánchez, M., Clemente-Jiménez, J. M., Rodríguez-Vico, F., Las Heras-Vazquez, F. J., Jara-Pérez, V. and Cámara-Artigas, A. (2004) A monomer form of the glutathione S-transferase Y7F mutant from *Schistosoma japonicum* at acidic pH. Biochem. Biophys. Res. Commun. **314**, 6–10
13 Stevens, J. M., Hornby, J. A. T., Armstrong, R. N. and Dirr, H. W. (1998) Class sigma glutathione transferase unfolds via a dimeric and a monomeric intermediate: impact of subunit interface on conformational stability in the superfamily. Biochemistry **37**, 15534–15541
14 Hornby, J. A. T., Luo, J.-K., Stevens, J. M., Wallace, L. A., Kaplan, W., Armstrong, R. N. and Dirr, H. W. (2000) Equilibrium folding of dimeric class Mu glutathione transferases involves a stable monomeric intermediate. Biochemistry **39**, 12336–12344
15 Dirr, H. (2001) Folding and assembly of glutathione transferases. Chem. Biol. Interact. **133**, 19–23
16 Reinemer, P., Dirr, H. W., Ladenstein, R., Schäffer, J., Gallay, O. and Huber, R. (1991) The three-dimensional structure of class Pi glutathione S-transferase in complex with glutathione sulfonate at 2.3 Å resolution. EMBO J. **10**, 1997–2005
17 Ji, X., Zhang, P., Armstrong, R. N. and Gilliland, G. L. (1992) The three-dimensional structure of a glutathione S-transferase from the Mu gene class. Structural analysis of the binary complex of isoenzyme 3-3 and glutathione at 2.2-Å resolution. Biochemistry **31**, 10169–10184
18 Reinemer, P., Dirr, H. W., Ladenstein, R., Huber, R., Lo Bello, M., Federici, G. and Parker, M. W. (1992) Three-dimensional structure of class Pi glutathione S-transferase from human placenta in complex with S-hexylglutathione at 2.8 Å resolution. J. Mol. Biol. **227**, 214–226

19 Sinning, I., Kleywegt, G. J., Cowan, S. W., Reinemer, P., Dirr, H. W., Huber, R., Gilliland, G. L., Armstrong, R. N., Ji, X., Board, P. G. et al. (1993) Structure determination and refinement of human Alpha class glutathione transferase A1-1, and a comparison with the Mu and Pi class enzymes. J. Mol. Biol. **232**, 192–212
20 Ji, X., Von Rosenvinge, E. C., Johnson, W. W., Tomarev, S. I., Paitigorsky, J., Armstrong, R. N. and Gilliland, G. L. (1995) Three-dimensional structure, catalytic properties, and evolution of a sigma class glutathione transferase from squid, a progenitor of the lens S-crystallins of cephalopods. Biochemistry **34**, 5317–5328
21 Rossjohn, J., McKinstry, W. J., Oakley, A. J., Verger, D., Flanagan, J., Chelvanayagam, G., Tan, K.-L., Board, P. G. and Parker, M. W. (1998) Human theta class glutathione transferase: the crystal structure reveals a sulfate-binding pocket within a buried active site. Structure **6**, 309–322
22 Oakley, A. J., Harnnoi, T., Udomsinprasert, R., Jirajaroenrat, K., Ketterman, A. J. and Wilce, M. C. J. (2001) The crystal structures of glutathione S-transferases isozymes 1-3 and 1-4 from *Anopheles dirus* species B. Protein Sci. **10**, 2176–2185
23 Chelvanayagam, G., Parker, M. W. and Board, P. G. (2001) Fly fishing for GSTs: a unified nomenclature for mammalian and insect glutathione transferases. Chem. Biol. Interact. **133**, 256–260
24 Jirajaroenrat, K., Pongjaroenkit, S., Krittanai, C., Prapanthadara, L. and Ketterman, A. J. (2001) Heterologous expression and characterization of alternatively spliced glutathione S-transferases from a single *Anopheles* gene. Insect Biochem. Mol. Biol. **31**, 867–875
25 Vararattanavech, A. and Ketterman, A. (2003) Multiple roles of glutathione binding-site residues of glutathione S-transferase. Protein Pept. Lett. **10**, 441–448
26 Habig, W. H., Pabst, M. J. and Jakoby, W. B. (1974) Glutathione S-transferases. The first enzymatic step in mercapturic acid formation. J. Biol. Chem. **249**, 7130–7139
27 Bradford, M. M. (1976) A rapid and sensitive method for the quantitation of microgram quantities of protein utilizing the principle of protein-dye binding. Anal. Biochem. **72**, 248–254
28 Segel, I. H. (1993) Enzyme Kinetics. Behavior and Analysis of Rapid Equilibrium and Steady-State Enzyme Systems, John Wiley & Sons, New York
29 Gore, M. G. (2000) Spectrophotometry and Spectrofluorimetry, Oxford University Press, Oxford
30 Sayed, Y., Wallace, L. A. and Dirr, H. W. (2000) The hydrophobic lock-and-key intersubunit motif of glutathione transferase A1-1: implications for catalysis, ligandin function and stability. FEBS Lett. **465**, 169–172
31 Hornby, J. A. T., Codreanu, S. G., Armstrong, R. N. and Dirr, H. W. (2002) Molecular recognition at the dimer interface of a class Mu glutathione transferase: role of a hydrophobic interaction motif in dimer stability and protein function. Biochemistry **41**, 14238–14247
32 Stenberg, G., Abdalla, A.-M. and Mannervik, B. (2000) Tyrosine 50 at the subunit interface of dimeric human glutathione transferase P1-1 is a structural key residue for modulating protein stability and catalytic function. Biochem. Biophys. Res. Commun. **271**, 59–63
33 Ranson, H., Claudianos, C., Ortelli, F., Abgrall, C., Hemingway, J., Sharakhova, M. V., Unger, M., Collins, F. H. and Feyereisen, R. (2002) Evolution of supergene families associated with insecticide resistance. Science **298**, 179–181
34 Winayanuwattikun, P. and Ketterman, A. J. (2004) Catalytic and structural contributions for glutathione binding residues in a delta class glutathione S-transferase. Biochem. J. **382**, 751–757
35 Wongsantichon, J., Harnnoi, T. and Ketterman, A. J. (2003) A sensitive core region in the structure of glutathione S-transferases. Biochem. J. **373**, 759–765
36 Lo Bello, M., Nuccetelli, M., Chiessi, E., Lahm, A., Mazzetti, A. P., Parker, M. W., Tramontano, A., Federici, G. and Ricci, G. (1998) Mutations of Gly to Ala in human glutathione transferase P1-1 affect helix 2 (G-Site) and induce positive cooperativity in the binding of glutathione. J. Mol. Biol. **284**, 1717–1725
37 Ricci, G., Lo Bello, M., Caccuri, A. M., Pastore, A., Nuccetelli, M., Parker, M. W. and Federici, G. (1995) Site-directed mutagenesis of human glutathione transferase P1-1. Mutation of Cys-47 induces a positive cooperativity in glutathione transferase P1-1. J. Biol. Chem. **270**, 1243–1248
38 Lo Bello, M., Battistoni, A., Mazzetti, A. P., Board, P. G., Muramatsu, M., Federici, G. and Ricci, G. (1995) Site-directed mutatgenesis of human glutathione transferase P1-1: spectral, kinetic, and structural properties of Cys-47 and Lys-54 mutants. J. Biol. Chem. **270**, 1249–1253
39 Xiao, B., Singh, S. P., Nanduri, B., Awasthi, Y. C., Zimniak, P. and Ji, X. (1999) Crystal structure of a murine glutathione S-transferase in complex with a glutathione conjugate of 4-hydroxynon-2-enal in one subunit and glutathione in the other: evidence of signaling across the dimer interface. Biochemistry **38**, 11887–11894
40 Lien, S., Gustafsson, A., Andersson, A.-K. and Mannervik, B. (2001) Human glutathione transferase A1-1 demonstrates both half-of-the-sites and all-of-the-sites reactivity. J. Biol. Chem. **276**, 35599–35605
41 Bico, P., Erhardt, J., Kaplan, W. and Dirr, H. (1995) Porcine class Pi glutathione S-transferase: anionic ligand binding and conformational analysis. Biochim. Biophys. Acta **1247**, 225–230
42 Sayed, Y., Hornby, J. A. T., Lopez, M. and Dirr, H. (2002) Thermodynamics of the ligandin function of human class Alpha glutathione transferase A1-1: energetics of organic anion ligand binding. Biochem. J. **363**, 341–346
43 Jones, S. and Thornton, J. M. (1995) Protein-protein interactions: a review of protein dimer structure. Prog. Biophys. Mol. Biol. **63**, 31–65
44 Noble, M. E. M., Zeelen, J. Ph., Wierenga, R. K., Mainfroid, V., Goraj, K., Gohimont, A.-C. and Martial, J. A. (1993) Structure of triosephosphate isomerase from *Escherichia coli* determined at 2.6 Å resolution. Acta Crystallogr. Sect. D Biol. Crystallogr. **49**, 403–417
45 Waley, S. G. (1973) Refolding of triosephosphate isomerase. Biochem. J. **135**, 165–172
46 Téllez-Valencia, A., Olivares-Illana, V., Hernández-Santoyo, A., Pérez-Montfort, R., Costas, M., Rodríguez-Romero, A., López-Calahorra, F., de Gómez-Puyou, M. T. and Gómez-Puyou, A. (2004) Inactivation of triosephosphate isomerase from *Trypanosoma cruzi* by an agent that perturbs its dimer interface. J. Mol. Biol. **341**, 1355–1365
47 Espinoza-Fonseca, L. M. and Trujillo-Ferrara, J. G. (2005) Structural considerations for the rational design of selective anti-trypanosomal agents: the role of the aromatic clusters at the interface of triosephosphate isomerase dimer. Biochem. Biophys. Res. Commun. **328**, 922–928
48 Singh, S. K., Maithal, K., Balaram, H. and Balaram, P. (2001) Synthetic peptides as inactivators of multimeric enzymes: inhibition of *Plasmodium falciparum* triosephosphate isomerase by interface peptides. FEBS Lett. **501**, 19–23
49 Maithal, K., Ravindra, G., Nagaraj, G., Singh, S. K., Balaram, H. and Balaram, P. (2002) Subunit interface mutation disrupting an aromatic cluster in *Plasmodium falciparum* triosephosphate isomerase: effect on dimer stability. Protein Eng. **15**, 575–584
50 Salminen, A., Parfenyev, A. N., Salli, K., Efimova, I. S., Magretova, N. N., Goldman, A., Baykov, A. A. and Lahti, R. (2002) Modulation of dimer stability in yeast pyrophosphatase by mutations at the subunit interface and ligand binding to the active site. J. Biol. Chem. **277**, 15465–15471

Received 8 June 2005/7 September 2005; accepted 14 October 2005
Published as BJ Immediate Publication 14 October 2005, doi:10.1042/BJ20050915

Biochem. J. (2006) **393**, 89–95 (Printed in Great Britain) doi:10.1042/BJ20050555



# The structural roles of a conserved small hydrophobic core in the active site and an ionic bridge in domain I of Delta class glutathione S-transferase

Ardcharaporn VARARATTANAVECH*, Peerada PROMMEENATE† and Albert J. KETTERMAN*[1]

*Institute of Molecular Biology and Genetics, Mahidol University, Salaya campus, 25/25 Putthamonthol Road 4, Salaya, Nakhon Pathom, 73170 Thailand, and †BEC Unit, National Center for Genetic Engineering and Biotechnology, 83 Moo 8, Thakham, Bangkhuntien, Bangkok 10150, Thailand

GSTs (glutathione S-transferases; E.C.2.5.1.18) are a supergene family of dimeric multifunctional enzymes that have a major role in detoxification pathways. Using a GST from the mosquito *Anopheles dirus* (adGSTD4-4), we have characterized the enzymatic and physical properties of Leu-6, Thr-31, Leu-33, Ala-35, Glu-37, Lys-40 and Glu-42. These residues generate two motifs located in the N-terminal domain (domain I) that are functionally conserved across GST classes. The aim of this study was to understand the function of these two motifs. The first motif is a small hydrophobic core in the G-site (glutathione-binding site) wall, and the second motif contains an ionic bridge at the N-terminus of the $\alpha$2 helix and is also part of the G-site. The mutations in the small hydrophobic core appear to have structural effects, as shown by the thermal stability, refolding rate and intrinsic fluorescence differences. In the Delta class GST, interactions form an ionic bridge motif located at the beginning of the $\alpha$2 helix. The data suggest that electrostatic interactions in the $\alpha$2 helix are involved in $\alpha$-helix stabilization, and disruption of this ionic bridge interaction changes the movement of the $\alpha$2-helix region, thereby modulating the interaction of the enzyme with substrates. These results show that the small hydrophobic core and ionic bridge have a major impact on structural stabilization, as well as being required to maintain structural conformation of the enzyme. These structural effects are also transmitted to the active site to influence substrate binding and specificity. Therefore changes in the conformation of the G-site wall in the active site appear to be capable of exerting influences on the tertiary structural organization of the whole GST protein.

Key words: *Anopheles dirus*, Delta class glutathione S-transferase, mosquito, site-directed mutagenesis.

## INTRODUCTION

Cytosolic GSTs (glutathione transferases; E.C. 2.5.1.18) are a family of dimeric isoenzymes that catalyse the conjugation of glutathione (GSH) to a variety of organic compounds containing an electrophilic centre [1,2], many with carcinogenic and toxic properties [3–7]. This reaction plays an important part in cellular metabolism, transport and subsequent excretion of toxic organic compounds. Other functions of GSTs have been reported, including binding of bilirubin and carcinogens [8,9], isomerization of maleyl acetoacetate [10–12], regulation of the stress kinases [13] and modulation of the ryanodine receptor (a calcium ion channel; [14,15]). A membrane-bound microsomal GST has been well characterized, and seems to be structurally and genetically distinct from the cytosolic enzymes [16]. Despite low sequence homology among GST classes, all of these isoenzymes have very similar tertiary structures, topography of the active site and GSH-binding site [17–19].

The *Anopheles dirus* mosquito is an important malaria vector in South-East Asia. AdGSTD4-4 is one of four alternatively spliced products from 7.5 kb of the *adgst1*AS1 gene (*An. dirus* alternatively spliced GST gene), which has been identified from an *An. dirus* genomic library [20]. All four spliced products have 45 identical amino acids at the N-terminus, and were named adGST1-1, adGST1-2, adGST1-3 and adGST1-4, according to insect GST nomenclature that is in use [that is, GST-(insect class 1)-(protein 1, 2, 3 and 4) respectively]. However, to be in alignment with a proposed universal GST nomenclature, these were renamed adGSTD1-1, adGSTD2-2, adGSTD3-3 and adGSTD4-4 [21,22]. The subunit number remains the same, since subunits were enumerated as they were initially discovered; 'D' refers to GST Delta class and '4-4' refers to the homodimeric isoenzyme. Two available tertiary structures, for adGSTD3-3 and adGSTD4-4, have assisted studies on these proteins [23]. Moreover, GSTs are highly conserved across the insect GST Delta class at the N-terminus (e.g. in *An. dirus*, *An. gambiae*, *Lucilia cuprina*, *Musca domestica* and *Drosophila melanogaster*). Therefore, in the present study, characterization of the N-terminal residues in adGSTD4-4 can be used to understand their functions for all insect Delta class GSTs [21,24].

Many hydrophobic residues are found inside a folded protein contributing to tertiary structure as a hydrophobic core. In the G-site (GSH-binding site), there are several such residues (Leu-6, Leu-33 and Ile-52) surrounding the glycine moiety of GSH. In previous studies [25,26], Leu-33 and Ile-52 were shown to impact on structural aspects of the protein, such as folding and stability. In the present paper, we extend our previous studies on the small hydrophobic core in the G-site wall containing Leu-6, Thr-31, Leu-33 and Ile-52.

An induced-fit mechanism apparently conserved across all GST classes occurs through movement of the $\alpha$2 helix and its flanking regions to modulate G-site affinity for GSH; however, the relative contributions of residues to the flexibility in the $\alpha$2 helix have not been determined [27–30]. At the N-terminus of the $\alpha$2 helix, there is an ionic bridge interaction formed by Glu-37, Lys-40 and Glu-42. These residues are on the outside of the protein surface exposed to solvent. This ionic bridge interaction should impact upon movement of part of the active site, in addition to involvement in structural stabilization of the enzyme. Therefore the residues Glu-37, Lys-40 and Glu-42 were studied;

Abbreviations used: CDNB, 1-chloro-2,4-dinitrobenzene; DCNB, 1,2-dichloro-4-nitrobenzene; DTT, dithiothreitol; EA, ethacrynic acid; G-site, glutathione-binding site; GST, glutathione S-transferase; PNBC, *p*-nitrobenzyl chloride; PNPBr, *p*-nitrophenethyl bromide.

[1] To whom correspondence should be addressed (email frakt@mahidol.ac.th).

furthermore, Ala-35 was changed to arginine in an attempt to increase the ionic bridge interaction in the $\alpha$2-helix region.

## MATERIALS AND METHODS

### Site-directed mutagenesis

The mutants were generated using the QuikChange® site-directed mutagenesis protocol (Stratagene). The mutagenic primers used in these experiments were designed based on the sequence of the adGSTD4-4 wild-type gene (GenBank® accession number AF273040). The oligonucleotide primers, each complementary to opposite strands of the vector, were extended during temperature cycling by means of *Pfu* DNA polymerase, which replicates both plasmid strands with high fidelity. Each mutant was randomly screened by restriction digestion analysis. Mutant plasmids could be distinguished from template by digestion with restriction enzyme corresponding to the restriction recognition site introduced by the mutagenic primers. Then, full-length DNA sequencing in both directions was performed to confirm the engineered clone sequence.

### Protein expression and purification

After transformation of the mutant plasmids into *Escherichia coli* BL21(DE3)pLysS, protein expression was performed. All of the adGSTD4-4 clones were expressed in LB (Luria–Bertani) broth (containing 100 $\mu$g/ml ampicillin and 34 $\mu$g/ml chloramphenicol) and induced with 0.1 mM IPTG (isopropyl $\beta$-thiogalactoside) for 3 h at 37 °C. The pellets were collected and kept at − 20 °C until used. The expression levels of the protein were determined by SDS/PAGE. The cell pellets from 50 ml of culture were suspended by mixing with 4.8 ml of 50 mM Tris/HCl, pH 7.4, containing 1 mM EDTA, 200 $\mu$l of 100 mg/ml lysozyme and 3.6 $\mu$l of 1.4 M 2-mercaptoethanol. The suspension was incubated on ice for 20 min, then 50 $\mu$l of 1 M DTT (dithiothreitol) was added and the suspension was lysed at 900 lbf/in$^2$ (1 lbf/in$^2$ $\approx$ 6.9 kPa) in a French Press cell. The lysate was then centrifuged at 10000 ***g*** at 4 °C for 20 min. The supernatant containing the soluble form of the recombinant enzyme was separated from the pellet. The recombinant adGSTD4-4 mutants and the wild-type protein were purified by using either GSH-affinity chromatography or cation exchange followed by hydrophobic interaction chromatography, as described previously [25]. GSH-affinity chromatography was used according to manufacturer's instructions (Amersham Biosciences). A cation-exchange column (SP-XL) followed by hydrophobic interaction chromatography (phenyl-Sepharose column) was used for mutants that could not be purified on the GSH-affinity chromatography column. Briefly, cation-exchange chromatography employed an SP-XL column that was equilibrated with buffer A (20 mM phosphate buffer, pH 7.0, containing 10 mM DTT). After the lysate was applied to the column, the column was washed with buffer A. Then protein was eluted with a linear gradient from 80–500 mM NaCl in buffer A. The major amount of GST enzyme eluted in buffer A containing approx. 250 mM NaCl. The eluted GST fractions were pooled and loaded on to a phenyl-Sepharose column that was equilibrated with buffer A containing 2 M NaCl. Washing steps were performed by using stepwise decreases in salt concentration in buffer A. The GST enzyme was eluted from the phenyl-Sepharose column by using 20 % (v/v) ethylene glycol containing 10 mM DTT. The purified enzymes (in 50 mM potassium phosphate, pH 6.5) were stored in 50 % (v/v) glycerol at − 20 °C until used. Concentrations of the proteins were determined by Bio-Rad protein reagent (Bio-Rad) using BSA as the standard protein, and purity of the proteins was analysed by SDS/PAGE.

### Enzymatic characterization

The standard GST assay was performed in 0.1 M potassium phosphate buffer, pH 6.5, in the presence of 3 mM CDNB (1-chloro-2,4-dinitrobenzene) and 10 mM GSH [31]. The rate of conjugation between GSH and CDNB was monitored by measuring continuously the increase in absorbance at 340 nm for 1 min using a SpectraMax 250 apparatus at 25–27 °C. The molar absorption coefficient of 9.6 $mM^{-1} \cdot cm^{-1}$ was used to convert absorbance into moles [32].

The kinetic experiments were performed as described previously [31]. In brief, CDNB was chosen as the electrophilic substrate for determination of $V_{max}$, $K_m$, $k_{cat}$ and $k_{cat}/K_m$ values. The kinetic parameters were determined by varying the CDNB concentration (0.031–3.0 mM) while GSH was held constant at a saturating concentration, and by varying GSH concentrations (0.25–20 mM) at a saturating concentration of CDNB. The initial rate of the enzymatic reaction was measured spectrophotometrically as described for the GST activity assay determination. The steady-state kinetics followed Michaelis–Menten kinetics, except where stated. The maximal velocity ($V_{max}$) and the Michaelis constant ($K_m$) were determined by non-linear regression software analysis (GraphPad Prism 4). The turnover number (or catalytic-centre activity; $k_{cat}$) and catalytic efficiency ($k_{cat}/K_m$) were calculated on an active-site basis using the subunit molecular mass of each enzyme. The kinetic parameters are the means $\pm$ S.D. for at least three independent experiments.

The specific activities towards several GST substrates were determined as described previously [31]. All measurements were performed at 25–27 °C in 0.1 M potassium phosphate buffer at either pH 6.5 or 7.5. The GST activities were measured with GSH and five hydrophobic substrates: CDNB, DCNB (1,2-dichloro-4-nitrobenzene), EA (ethacrynic acid), PNPBr (*p*-nitrophenethyl bromide) and PNBC (*p*-nitrobenzyl chloride). Specific activities were calculated using the molar absorption coefficient for each substrate [32].

### Physical characterization

The enzymes at 0.1 mg/ml in 0.1 M phosphate buffer, pH 6.5, containing 1 mM EDTA and 5 mM DTT were incubated at 45 °C for various times, and the remaining activity was measured in the standard GST assay. Data were plotted as logarithms of the percentage of remaining activity against pre-incubation time. The half-life of the enzyme at 45 °C was calculated from the slope of the plot using the equation: slope $= k/2.3$, where $k = 0.693/t_{1/2}$.

Enzymes were completely unfolded by incubating 0.5 mg/ml enzymes in unfolding buffer [0.2 M phosphate buffer (pH 7.0)/1 mM EDTA/5 mM dithiothreitol] containing 4 M guanidinium chloride at room temperature ($\approx$25 °C) for 10 min. Unfolded enzymes were allowed to begin refolding by diluting 40-fold in 0.1 M phosphate buffer, pH 6.5, to a final guanidinium chloride concentration of 0.1 M. Appropriate aliquots from this incubation mixture were measured for reactivation by measuring GST activity as a function of time after dilution. GST activity versus time of refolding followed a non-linear regression single-exponential equation [33].

Intrinsic fluorescence of adGSTD4-4 was measured in a single-photon-counting spectrofluorimeter. Excitation was at 295 nm, and emission was scanned from 300–450 nm. Samples contained 0.1 mg/ml GST in 0.1 M potassium phosphate buffer, pH 6.5, and were prepared similarly for wild-type and mutant enzymes. The wavelength that gives the maximum fluorescence intensity ($\lambda_{max}$) and the fluorescence intensity at $\lambda_{max}$ were observed. The experimental data were corrected for both dilution and inner-filter effects, and normalized after background subtraction.

**Table 1 Steady-state kinetic constants using GSH and CDNB as GST substrates**

The rate of conjugation was monitored continuously by measuring the increase in absorbance at 340 nm for 1 min. The units of $V_{max}$, $k_{cat}$, $K_m$ and $k_{cat}/K_m$ are $\mu$mol · min$^{-1}$ · mg protein$^{-1}$, S$^{-1}$, mM and S$^{-1}$ · mM$^{-1}$ respectively.

| | | | CDNB | | GSH | |
|---|---|---|---|---|---|---|
| Enzyme | $V_{max}$ | $k_{cat}$ | $K_m$ | $k_{cat}/K_m$ | $K_m$ | $k_{cat}/K_m$ |
| Wild-type | 62.5 ± 1.24 | 26.1 | 0.50 ± 0.02 | 51.8 | 0.50 ± 0.10 | 52.1 |
| L33A | 23.5 ± 0.5† | 9.70 | 1.17 ± 0.05† | 8.30 | 8.20 ± 0.43† | 1.20 |
| L33Y | 0.32 ± 0.01† | 0.14 | 0.81 ± 0.12† | 0.17 | 1.10 ± 0.12§ | 0.13 |
| L33F | 1.55 ± 0.03† | 0.65 | 1.30 ± 0.06† | 0.50 | 2.42 ± 0.22† | 0.27 |
| L33I | 53.0 ± 1.71† | 22.2 | 0.73 ± 0.05§ | 30.3 | 0.42 ± 0.01 | 52.8 |
| L6A | 42.3 ± 1.64† | 17.7 | 1.49 ± 0.15† | 11.9 | 0.31 ± 0.01 | 57.1 |
| T31A | 23.3 ± 0.35† | 9.73 | 0.77 ± 0.05‡ | 12.6 | 11.4 ± 0.53*† | 0.85 |
| I52A | 0.630 ± 0.006† | 0.26 | 0.32 ± 0.02 | 0.81 | 7.04 ± 0.05*† | 0.04 |
| I52L | 43.8 ± 1.24† | 18.3 | 0.74 ± 0.02‡ | 24.8 | 0.30 ± 0.04 | 61.1 |
| E37A | 48.5 ± 1.45† | 20.4 | 0.54 ± 0.03 | 37.7 | 1.85 ± 0.09† | 11.0 |
| E37Q | 62.8 ± 0.92 | 26.3 | 0.58 ± 0.05 | 45.3 | 2.26 ± 0.04† | 11.6 |
| K40A | 51.3 ± 1.24† | 21.5 | 0.62 ± 0.04 | 34.6 | 1.14 ± 0.08§ | 18.8 |
| E42A | 63.4 ± 1.95 | 26.5 | 0.57 ± 0.05 | 46.4 | 0.63 ± 0.04 | 42.0 |
| A35R | 53.6 ± 1.18† | 22.4 | 0.52 ± 0.06 | 42.7 | 0.73 ± 0.05 | 30.7 |

* The mutants T31A and I52A showed positive co-operativity upon GSH binding, with Hill coefficients of 1.62 ± 0.09 and 1.49 ± 0.03 respectively.

ANOVA analysis revealed significant differences compared with the wild-type, where indicated: †$P < 0.001$; ‡$P < 0.01$; and §$P < 0.05$. The absence of a symbol indicates no significant difference compared with wild-type.

CD measurements in the far-UV region from 200–250 nm were performed with a spectropolarimeter. The enzymes at 0.2 mg/ml in 0.1 M phosphate buffer, pH 6.5, were measured at 25 °C. A cell of 1 cm path length and a 1 nm bandwidth were used. Spectra are the averages of ten scans after subtraction of the average of ten baseline scans.

## RESULTS AND DISCUSSION

### Protein expression and purification

In the present study we have characterized Leu-6, Thr-31, Leu-33, Ile-52, Ala-35, Glu-37, Lys-40 and Glu-42, located in domain I in the highly flexible loop region between the $\beta$2–$\alpha$2 or $\alpha$2–$\beta$3 loops. These residues were hypothesized to be involved in structural maintenance or stabilization of the proteins. The mutagenesis study was performed by individually changing each residue chosen to alanine and/or a conservative or non-conservative amino acid. In the present study, Leu-33 mutations generated for a previous report were included to extend that study with further experiments. An additional conservative amino acid replacement, L33I, was generated to confirm the function of Leu-33 in packing of the active site. In addition, Ala-35 was mutated to an arginine in an attempt to increase the ionic bridge interaction in the $\alpha$2-helix region. All 13 engineered enzymes could be expressed in soluble form at 37 °C in *E. coli* lysates. Two procedures were utilized for protein purifications: an affinity chromatography on immobilized GSH or sequential purification by ion-exchange chromatography (SP-XL) followed by phenyl-Sepharose chromatography. The latter procedure was used for the engineered enzymes that could not be purified by GSH-affinity chromatography, including L33A, L33F, L33Y and T31A. Purified enzymes gave a single band on SDS/PAGE, with a size of approx. 25 kDa, corresponding to the calculated molecular mass of the GST subunits.

### Enzymatic characterization

The kinetic constants for CDNB and GSH show that most of the residue positions only slightly affected enzyme catalysis (Table 1). All of these residues are located in the GSH-binding site, so it is interesting to note that Leu-6 changed the active-site conformation enough to significantly increase $K_m$ for the hydrophobic substrate CDNB (3-fold; ANOVA, $P < 0.001$) and decrease the $K_m$ for GSH (1.7-fold; ANOVA, $P < 0.05$). GSH steady-state kinetics of the T31A enzyme showed positive co-operativity, with a Hill coefficient of 1.62 ± 0.09 (the Hill coefficient for wild-type enzyme is 0.91 ± 0.02). Positive co-operativity indicates GSH binding in the first active site, then facilitates another GSH binding in the second active site by increasing binding affinity of the vacant binding site [34]. Thr-31 is located in the loop before the $\alpha$2 helix, and its side chain faces into the G-site in addition to being close to His-38, which interacts directly with GSH. The alanine mutation at Thr-31 must cause a packing rearrangement of the G-site, which increases the $K_m$ for GSH 23-fold, as well as generating intersubunit communication between the two active sites. One explanation is that the rearrangement would disturb His-38, which directly interacts with GSH. Mutations of His-38 were shown to have large effects on GSH binding affinity, as well as generating positive co-operativity [25]. The mutation of Ile-52 to alanine caused very large effects on catalysis, as exhibited by a decrease in $k_{cat}$ (1 % of wild-type activity) and affinity (14-fold increase in $K_m$), as well as positive co-operativity. The conservative change of Ile-52 to leucine showed smaller effects, including a slight increase in GSH affinity. Mutations of ionic-bridge residues showed only small effects on catalysis, although the GSH binding affinity was affected to a greater extent. Both Glu-37 and Lys-40, located in the middle of the $\beta$2–$\alpha$2 loop, appeared to impact more, suggesting a greater influence on $\alpha$2-helix movement during induced-fit conformational changes.

Although the residues studied are in or behind G-site residues, the substrate-specificity results show that these mutations yielded various changes in specificity for several hydrophobic substrates compared with wild-type GST (Table 2). As shown by the kinetic constants, these residues are not critical for enzyme catalysis or substrate binding; however, the mutations influence the enzymes' hydrophobic substrate interaction and catalysis. Compared with wild-type, the mutations at Leu-6, Thr-31 and Ile-52 resulted in decreases in specificity towards several substrates, especially

**Table 2 Substrate specificity changes of the engineered enzymes relative to the wild-type adGSTD4-4**

The substrates were used at the following concentrations: CDNB, 3 mM; DCNB, 1 mM; PNPBr, 0.1 mM; PNBC, 0.1 mM; and EA, 0.2 mM. The reactions were performed at a constant GSH concentration.

| | | Substrate specificity ($\mu$mol · min$^{-1}$ · mg protein$^{-1}$) | | | | |
|---|---|---|---|---|---|---|
| Enzyme | Substrate . . . | CDNB | DCNB | EA | PNPBr | PNBC |
| Wild-type | | 52.5 ± 0.52 | 0.035 ± 0.006 | 0.286 ± 0.062 | 0.074 ± 0.012 | 0.064 ± 0.002* |
| L33A | | 18.3 ± 0.3* | 0.031 ± 0.015 | 0.332 ± 0.061 | 0.019 ± 0.004* | 0.024 ± 0.004* |
| L33Y | | 0.253 ± 0.001* | < 0.0016* | 0.092 ± 0.006* | < 0.006* | < 0.007* |
| L33F | | 1.023 ± 0.018* | < 0.0016* | 0.059 ± 0.007* | < 0.006* | < 0.007* |
| L33I | | 45.4 ± 0.37* | 0.047 ± 0.002‡ | 0.247 ± 0.006 | 0.007 ± 0.001* | 0.044 ± 0.002* |
| L6A | | 28.0 ± 0.53* | 0.0053 ± 0.0003* | 0.380 ± 0.004 | 0.017 ± 0.002* | 0.031 ± 0.002* |
| T31A | | 17.5 ± 0.33* | 0.0059 ± 0.0006* | 0.186 ± 0.008† | < 0.002* | 0.039 ± 0.004* |
| I52A | | 0.511 ± 0.010* | < 0.001* | 0.307 ± 0.023 | < 0.004* | 0.011 ± 0.001* |
| I52L | | 35.4 ± 0.36* | 0.025 ± 0.001 | 0.373 ± 0.005 | 0.018 ± 0.001* | 0.036 ± 0.003* |
| E37A | | 39.1 ± 0.74* | 0.055 ± 0.005† | 0.135 ± 0.010* | < 0.008* | 0.122 ± 0.006* |
| E37Q | | 47.8 ± 0.22* | 0.053 ± 0.001† | 0.431 ± 0.026* | 0.033 ± 0.004* | 0.062 ± 0.002 |
| K40A | | 37.7 ± 0.16* | 0.037 ± 0.001 | 0.110 ± 0.004* | 0.038 ± 0.003* | 0.080 ± 0.002* |
| E42A | | 55.1 ± 0.40‡ | 0.059 ± 0.001* | 0.24 ± 0.02 | 0.016 ± 0.001* | 0.045 ± 0.002* |
| A35R | | 44.9 ± 0.56* | 0.056 ± 0.003* | 0.37 ± 0.04 | 0.020 ± 0.001* | 0.041 ± 0.002* |

ANOVA analysis revealed significant differences compared with the wild-type, where indicated: *$P < 0.001$; †$P < 0.01$; and ‡$P < 0.05$. The absence of a symbol indicates no significant difference compared with wild-type.

DCNB and PNPBr. The remaining mutations displayed major effects with regard to PNPBr, but specificities were comparable with that of wild-type for CDNB. However, changes in specificity for EA and PNBC as substrates were varied.

Both GSH- and hydrophobic-substrate-binding sites are located in different parts of the same active-site pocket. Therefore differences in the mutant enzymes appear to occur from changes in active-site conformation that disturb orientation of the substrates, as found in the wild-type enzyme. In addition, binding modes and orientations of the various substrates in the active site appear to be unique, as shown by dissimilar effects on specificity of the mutant enzymes.

## Physical characterization

The half-life at 45 °C of the mutant enzymes compared with adGSTD4-4 wild-type showed that the mutants decreased in stability, except for T31A, which displayed a slight increase (Table 3). L6A decreased enzyme stability approx. 9-fold, showing a major impact on structural maintenance. The mutation of ionic-bridge residues (Glu-37, Lys-40 and Glu-42) to alanine and the mutation of Ala-35 to arginine also resulted in decreases in enzyme stability, suggesting that the mutations cause a rearrangement of the $\alpha$2-helix, owing to disruption of the ionic bridge interaction. The replacement of positively charged Glu-37 with a similarly sized, polar glutamine residue decreased enzyme stability 2.3-fold, supporting the idea of charge distribution involvement in structural stabilization of the enzyme. However, the attempt to increase charge distribution with the A35R mutation decreased the half-life of the enzyme 1.7-fold. This suggests that residues in the $\beta$2–$\alpha$2-helix loop appear to affect helix dipole moment, which impacts upon structural stabilization of the enzyme.

AdGSTD4-4 became completely unfolded after incubation for 10 min in 4 M guanidinium chloride, as monitored by intrinsic fluorescence and CD spectroscopy. Refolding rates and percentages of recovered activities of wild-type and mutant enzymes were determined (Table 4). L6A showed a decreased refolding rate (2.5-fold compared with wild-type), suggesting the initial folding process was disturbed, which also slightly reduced the activity recovered as well as decreasing the enzyme stability, as described above. L33A showed an increased refolding rate of 1.6-fold and

**Table 3 Thermal stability of wild-type and engineered adGSTD4-4 mutants at 45 °C**

The remaining GST activity was measured after incubating the enzyme at various time points at 45 °C.

| Enzyme | Half-life ($t_{1/2}$) at 45 °C (min) |
|---|---|
| Wild-type | 15.3 ± 0.31 |
| L33A | 45.3 ± 1.56* |
| L33Y | 71.7 ± 1.71* |
| L33F | 212 ± 17.9* |
| L33I | 30.4 ± 1.5* |
| L6A | 1.73 ± 0.01* |
| T31A | 22.7 ± 1.77* |
| I52A | 9.58 ± 0.65* |
| I52L | 18.1 ± 1.33 |
| E37A | 1.73 ± 0.04* |
| E37Q | 6.54 ± 0.54* |
| K40A | 3.94 ± 0.20* |
| E42A | 8.44 ± 0.48* |
| A35R | 9.01 ± 0.54* |

ANOVA analysis revealed a significant difference compared with the wild-type enzyme, where indicated (*$P < 0.001$); the absence of an asterisk indicates no significant difference compared with wild-type (in these experiments, exclusively the I52L mutant).

3-fold greater stability than the wild-type enzyme, demonstrating that its final conformation is more stable. However, the mutants L33I and I52L showed only small effects on the refolding process. The ionic bridge mutations (Glu-37, Lys-40, Glu-42 and Ala-35) all decreased enzyme stability in the range 1.8- to 8.9-fold, although the refolding rates were altered differently. These data suggest that the changes in the refolding rates occur from differential 'flexing' of the engineered enzyme. An interesting observation for the E37A enzyme was that it possessed a slightly increased refolding rate of 1.3-fold, as well as a 1.8-fold increase in recovered activity, even though the enzyme had an 8.9-fold decreased stability (Table 3). This suggests that this residue position contributes to structural maintenance, but not to initial folding events. Therefore the ionic bridge motif appears to have a function in structural maintenance and modulation of $\alpha$2-helix movement, as well as a minor effect on folding.

**Table 4 Refolding rate constants and percentages of recovered activity from the reversible refolding experiment for the wild-type adGSTD4-4 enzyme and its engineered mutants**

The proteins were denatured initially with 4 M guanidinium chloride at room temperature for 10 min. Refolding rate constants ($k_{ref}$) were determined by non-linear regression analysis using a single-exponential equation (GraphPad Prism 4).

| | Refolding experiment | |
|---|---|---|
| Enzyme | Refolding rate constant ($min^{-1}$) | % recovery |
| Wild-type | 0.54 ± 0.02 | 20.7 ± 0.67 |
| L33A | 0.85 ± 0.05* | 18.6 ± 0.55 |
| L33Y | nd | nd |
| L33F | nd | nd |
| L33I | 0.53 ± 0.01 | 14.7 ± 0.76* |
| L6A | 0.22 ± 0.02* | 14.9 ± 0.77* |
| T31A | 0.41 ± 0.02* | 10.1 ± 0.41* |
| I52A | nd | nd |
| I52L | 0.67 ± 0.02* | 20.1 ± 0.61 |
| E37A | 0.69 ± 0.05* | 37.7 ± 1.49* |
| E37Q | 0.74 ± 0.03* | 14.0 ± 0.32* |
| K40A | 0.26 ± 0.02* | 14.2 ± 0.95* |
| E42A | 0.32 ± 0.02* | 31.5 ± 1.44* |
| A35R | 0.40 ± 0.01‡ | 29.6 ± 0.64† |

ANOVA analysis revealed significant differences compared with the wild-type, where indicated: *$P < 0.001$; †$P < 0.01$; and ‡$P < 0.05$. The absence of a symbol indicates no significant difference compared with the wild-type. nd, not determined (low activity precluded measurement).

**Table 5 The maximum emission wavelength ($\lambda_{max}$) and intrinsic fluorescence intensity at $\lambda_{max}$ of tryptophan fluorescence of adGSTD4-4 and the engineered enzymes**

The excitation wavelength ($\lambda_{ex}$) was set at 295 nm, and emission was scanned from 300–450 nm. Samples ($n = 3$) contained 0.1 mg/ml protein in 0.1 M potassium phosphate buffer, pH 6.5. The percentage intensities compared with wild-type enzyme were measured at fluorescence $\lambda_{max}$ averaged over three scans, corrected for dilution and inner-filter effects.

| | Intrinsic fluorescence ($\lambda_{ex}$ 295 nm) | |
|---|---|---|
| Enzyme | $\lambda_{max}$ (nm) | % intensity |
| Wild-type | 333 ± 0 | 100 |
| L33A | 334 ± 0 | 60.8* |
| L33Y | 334 ± 0 | 51.6* |
| L33F | 334 ± 0 | 47.9* |
| L33I | 333 ± 0 | 109.1 |
| L6A | 334 ± 0 | 138.6* |
| T31A | 334 ± 0 | 99.1 |
| I52A | 339 ± 0 | 98.8 |
| I52L | 333 ± 0 | 115.5* |
| E37A | 333 ± 0 | 66.8* |
| E37Q | 334 ± 0 | 107.7 |
| K40A | 334 ± 0 | 68.4* |
| E42A | 333 ± 0 | 75.5* |
| A35R | 334 ± 0 | 102.1 |

ANOVA analysis revealed a significant difference compared with the wild-type enzyme, where indicated (*$P < 0.001$); the absence of an asterisk indicates no significant difference compared with the wild-type.

The intrinsic fluorescence property of tryptophan in proteins is modulated by various interactions in the environment around the tryptophan residue. Therefore changes in $\lambda_{max}$ and the fluorescence intensity of the intrinsic fluorescence spectrum can suggest that changes have occurred in the local tertiary structure of the protein. There are two tryptophan residues present in adGSTD4-4 (Trp-64 and Trp-191). Trp-64 has the side chain exposed to solvent, located in the subunit interface at the base of the GSH-binding site, whereas Trp-191 is buried in the interior of domain II. Therefore this technique can be used to monitor active-site conformation indirectly. The same protein concentration of wild-type and mutant enzymes was used for comparison of the maximum emission wavelengths ($\lambda_{max}$) and fluorescence intensities (Table 5). The $\lambda_{max}$ of intrinsic tryptophan fluorescence for the mutants was approximately the same as that for the wild-type (333 ± 1 nm), except for I52A, which displayed a red-shifted spectrum with a $\lambda_{max}$ at 339 nm. Therefore I52A affected tertiary structure at the active site, causing a change in polarity in the tryptophan environment. In addition, there were differences in intensity of fluorescence between wild-type and several mutant proteins, indicating a limited conformational alteration in the active site of the final structure. The charged residue mutations (Glu-37, Lys-40 and Glu-42) displayed decreased fluorescence intensity. Located at the C-terminal end of the $\beta$4-sheet, Trp-64 is in proximity with the $\alpha$2-helix from which the ND2 side-chain nitrogen of Asn-47 extends 3.07 Å (1 Å = 0.1 nm) to have a cation–$\pi$ interaction with the aromatic ring of Trp-64. Disruption of the ionic bridge interaction would most likely increase flexibility of the $\alpha$2 helix, thereby disrupting this interaction and increasing solvent exposure of Trp-64, with a concomitant decrease in fluorescence. In addition, a rearrangement of the active-site topology appears to occur for the G-site-residue mutations Leu-6, Thr-31, Leu-33 and Ile-52, which affects orientation of Trp-64, as well as of its neighbouring residues, which also may contribute to changes in fluorescence.

CD spectroscopy was performed to determine whether secondary structure content of the proteins had changed. CD spectroscopy showed two 'troughs' at 210 and 222 nm, owing to the high helical content of the proteins. All the proteins had a similar far-UV CD spectrum (results not shown). This shows that, although some mutations affect active-site conformation, the overall secondary structure content of the enzymes has not been altered.

In the present paper, we have sought to understand the function of two features in domain I of adGSTD4-4 that have been found in all insect Delta class GSTs: a small hydrophobic core in the G-site and an ionic bridge at the N-terminus of the $\alpha$2-helix. The available structure of adGSTD4-4 shows that Leu-6, Thr-31, Leu-33 and Ile-52 form part of the wall in the GSH-binding site (Figure 1A). The mutation of Leu-6 leads to a structural perturbation in the G-site, resulting in altered substrate specificity, decreased stability, as well as modulation of the refolding of the enzyme. From a previous study [25], increasing hydrophobicity of the residue in the Leu-33 position increased enzyme stability 3- to 14-fold, although the mutants lost enzyme activity (0.9–62 % compared with wild type). In the present study, Leu-33 mutations altered intrinsic fluorescence intensity when compared with wild-type enzyme, suggesting changes in topology of the active site. The change in structural conformation and active-site topology of the Leu-33 mutations was confirmed by a trypsin proteolytic experiment: the mutation of Leu-33 to alanine increased the proteolytic rate almost 2-fold compared with the wild-type (results not shown).The conservative mutation of Leu-33 to isoleucine resulted in small effects on specificity and catalysis, the most notable of which was a 10-fold decrease for PNBr. L33I displayed only a 2-fold increase in half-life, with all other physical properties being similar to those of the wild-type. These data support the idea that the role of Leu-33 is to contribute to the small hydrophobic core for structural maintenance. Previously, Ile-52 had been characterized in adGSTD3-3 [26]. In the tertiary structures of adGSTD3-3 (PDB identification no. 1JLV) and adGSTD4-4 (PDB identification no. 1JLW), the location of Ile-52 is identical in both structures. A mutation of Ile-52 to alanine showed a decrease in enzyme stability of approx. 5.5-fold, a 24-fold increase

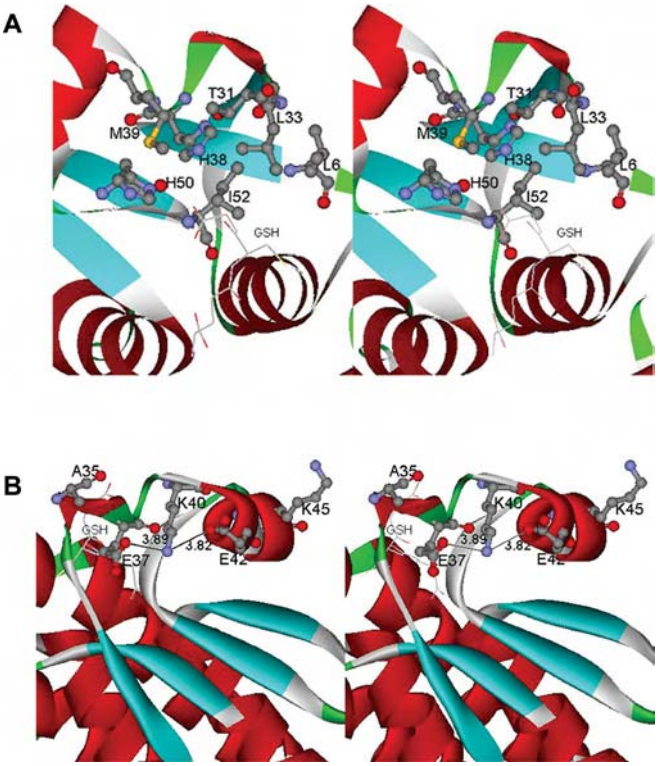


**Figure 1 Stereo views of domain I region characterized in this study**

(**A**) Stereo view of the active-site pocket of adGSTD4-4. Leu-6, Leu-33, Thr-31 and Ile-52 form part of the G-site wall. The hydrophobic residues Leu-6, Leu-33 and Ile-52 form a small hydrophobic cluster in the G-site. GSH in the active site is shown in stick form. (**B**) Stereo view of the charged residues located near the $\alpha$2 helix of adGSTD4-4. The ionic bridge motif formed by the charged residues (Glu-37, Lys-40 and Glu-42) is exposed to the solvent, located at the N-terminus of the $\alpha$2 helix. GSH in the active site is shown in stick form. Both parts of the Figure were created with Accelrys DS ViewerPro 5.0.

in the $K_m$ for GSH and a 2-fold decrease in $k_{cat}$ [26]. For adGSTD4-4, the I52A mutant showed different effects, with a 1.6-fold decrease in stability, a 14-fold increase in the $K_m$ for GSH and a 100-fold decrease in $k_{cat}$. The conservative replacement of Ile-52 with leucine showed smaller effects in enzyme properties, and the I52L mutant was very similar to the wild-type enzyme in terms of its physical properties. These data show that Ile-52 has roles in structural integrity and maintenance, as well as in the initial folding of the protein. Therefore it may be surmised that the small hydrophobic core formed by Leu-6, Leu-33 and Ile-52 at the G-site wall plays a critical role in packing and stabilization of the active site into an appropriate conformation, and this packing also impacts upon tertiary structure of the whole protein. A study of available crystal structures of other GST classes shows several hydrophobic residues clustered in the G-site wall in a similar fashion. For example, in the human GST isoenzyme hGSTP1-1 (PDB identification no. 11GS), these residues are Phe-8, Trp-38 and Leu-52, whereas in maize GST-I (PDB identification no. 1AXD) they are Phe-35, Ile-33 and Val-54. These residues are located in the G-site wall, and therefore are probably involved in packing of the active-site conformation as well.

Several studies show $\alpha$2 helices of Delta, Theta, Sigma and Pi GSTs to have high conformational flexibility and to display the highest temperature factors of the whole protein [29,35,36]. In insect Delta class GSTs, there is a unique ionic bridge motif exposed to solvent on the $\alpha$2 helix consisting of three charged residues: Glu-37, Lys-40 and Glu-42 (Figure 1B). The data suggest that this feature influences the flexibility of the $\alpha$2 helix and its flanking region in Delta class GSTs. In the present study, the alanine mutations of Glu-37, Lys-40 and Glu-42 in adGSTD4-4 showed structural effects in the domain I region, as shown by decreased thermal stability and changes in refolding rates and intrinsic fluorescence intensities. The apparent changes in $\alpha$2-helix movements resulting from mutations of the charged residues also appear to modulate interaction of the enzymes with substrates, as shown by changes in substrate specificity. The charged residues and ionic bridge motif in this region appear to play a role in maintenance of a stable conformation, as well as in influencing refolding of the enzymes. The attempt to increase the ionic-bridge interaction by constructing the A35R mutant did not result in any improvement in kinetic properties or enzyme stability, although it did appear to have some effects on substrate specificity. This may be because the side chain of arginine in A35R is not in the correct orientation for interacting with the other residues. In hGSTP1-1, there is an ion pair formed by Cys-47 and Lys-54 at the end of the $\alpha$2 helix. The disruption of the electrostatic interaction between Cys-47 and Lys-54 causes an increased mobility of the $\alpha$2 helix, local structural changes, lowered GSH-binding affinity and strong positive co-operativity towards GSH [37,38]. Therefore electrostatic interactions in the $\alpha$2 helix appear to be involved in $\alpha$-helix stabilization for GSTs in general. In cephalopod Sigma class GSTS1-1, charged residues at each end of the $\alpha$2 helix (Asp-37 and Lys-42 at the N- and C-termini of the $\alpha$2 helix respectively) have been described to interact with the helix dipole, and thereby stabilize the helix [39]. This feature is also found in adGSTD4-4 (residues Glu-37 and Lys-45), as well as in the blood fluke (*Schistosoma japonicum*) GST, Sj26GST, a GST of 26 kDa (PDB identification no. 1M9A; residues Glu-37 and Lys-44). These charged residues would appear therefore to interact with the helix dipole, and contribute to stabilizing the $\alpha$2 helix.

In the present study of adGSTD4-4, we examined the roles of conserved residues in the N-terminal domain (domain I) that are involved in a small hydrophobic core in the G-site wall and an ionic bridge motif in the N-terminus of the $\alpha$2 helix. The results have shown that both the small hydrophobic core and the ionic bridge motif can have a major impact on structural stabilization, as well as being required to maintain the structural conformation of the enzyme. The packing of the small hydrophobic core is important for structural integrity and, as part of the G-site wall, directly affects GSH binding. These packing effects in the active site appear not only to affect the G-site, but are transmitted through rearrangement of the active-site residues to the adjacent H-site, thereby impacting on specificity as well as catalysis.

This work was funded by the TRF (Thailand Research Fund). A.V. was supported by a Royal Golden Jubilee Ph.D. Research Scholarship.

## REFERENCES

1 Jakoby, W. B. and Habig, W. H. (1980) Glutathione transferases. In Enzymatic Basis of Detoxication, vol. 2 (Jakoby, W. B., ed.), pp. 63–94, Academic Press, New York
2 Hayes, J. D., Flanagan, J. U. and Jowsey, I. R. (2005) Glutathione transferases. Annu. Rev. Pharmacol. Toxicol. **45**, 51–88
3 Armstrong, R. N. (1997) Structure, catalytic mechanism, and evolution of the glutathione transferases. Chem. Res. Toxicol. **10**, 2–18
4 Mannervik, B., Funk, M., Frank, H. and Seidel, A. (1996) Glutathione S-transferase A1-1-catalysed conjugation of bay and fjord region diol epoxides of polycyclic aromatic hydrocarbons with glutathione. Carcinogenesis **17**, 1491–1498
5 Mannervik, B. and Danielson, U. H. (1988) Glutathione transferases – structure and catalytic activity. CRC Crit. Rev. Biochem. **23**, 283–337
6 Wilce, M. C. J. and Parker, M. W. (1994) Structure and function of glutathione S-transferases. Biochim. Biophys. Acta **1205**, 1–18

7 Ketterer, B. (2001) A bird's eye view of the glutathione transferase field. Chem. Biol. Interact. **138**, 27–42
8 Litwack, G., Ketterer, B. and Arias, I. M. (1971) Ligandin: a hepatic protein which binds steroids, bilirubin, carcinogens and a number of exogenous organic anions. Nature (London) **234**, 466–467
9 Hayes, J. D. and Pulford, D. J. (1995) The glutathione S-transferase supergene family: regulation of GST and the contribution of the isoenzymes to cancer chemoprotection and drug resistance. CRC Crit. Rev. Biochem. Mol. Biol. **30**, 445–600
10 Board, P., Baker, R. T., Chelvanayagam, G. and Jermiin, L. S. (1997) Zeta, a novel class of glutathione transferases in a range of species from plants to humans. Biochem. J. **328**, 929–935
11 Polekhina, G., Board, P. G., Blackburn, A. C. and Parker, M. W. (2001) Crystal structure of maleylacetoacetate isomerase/glutathione transferase zeta reveals the molecular basis for its remarkable catalytic promiscuity. Biochemistry **40**, 1567–1576
12 Board, P. G., Taylor, M. C., Coggan, M., Parker, M. W., Lantum, H. B. and Anders, M. W. (2003) Clarification of the role of key active site residues of glutathione transferase Zeta/maleylacetoacetate isomerase by a new spectrophotometric technique. Biochem. J. **374**, 731–737
13 Adler, V., Yin, Z., Fuchs, S. Y., Benezra, M., Rosario, L., Tew, K. D., Pincus, M. R., Sardana, M., Henderson, C. J., Wolf, C. R. et al. (1999) Regulation of JNK signaling by GSTp. EMBO J. **18**, 1321–1334
14 Dulhunty, A., Gage, P., Curtis, S., Chelvanayagam, G. and Board, P. (2001) The glutathione transferase structural family includes a nuclear chloride channel and a ryanodine receptor calcium release channel modulator. J. Biol. Chem. **276**, 3319–3323
15 Board, P. G., Coggan, M., Chelvanayagam, G., Easteal, S., Jermiin, L. S., Schulte, G. K., Danley, D. E., Hoth, L. R., Griffor, M. C., Kamath, A. V. et al. (2000) Identification, characterization, and crystal structure of the omega class glutathione transferases. J. Biol. Chem. **275**, 24798–24806
16 Jakobsson, P.-J., Morgenstern, R., Mancini, J., Ford-Hutchinson, A. and Persson, B. (1999) Common structural features of MAPEG – a widespread superfamily of membrane associated proteins with highly divergent functions in eicosanoid and glutathione metabolism. Protein Sci. **8**, 689–692
17 Dirr, H., Reinemer, P. and Huber, R. (1994) X-ray crystal structures of cytosolic glutathione S-transferases. Implications for protein architecture, substrate recognition and catalytic function. Eur. J. Biochem. **220**, 645–661
18 Wilce, M. C. J., Board, P. G., Feil, S. C. and Parker, M. W. (1995) Crystal structure of a theta-class glutathione transferase. EMBO J. **14**, 2133–2143
19 Rossjohn, J., McKinstry, W. J., Oakley, A. J., Verger, D., Flanagan, J., Chelvanayagam, G., Tan, K.-L., Board, P. G. and Parker, M. W. (1998) Human theta class glutathione transferase: the crystal structure reveals a sulfate-binding pocket within a buried active site. Structure **6**, 309–322
20 Pongjaroenkit, S., Jirajaroenrat, K., Boonchauy, C., Chanama, U., Leetachewa, S., Prapanthadara, L. and Ketterman, A. J. (2001) Genomic organization and putative promoters of highly conserved glutathione S-transferases originating by alternative splicing in *Anopheles dirus*. Insect Biochem. Mol. Biol. **31**, 75–85
21 Chelvanayagam, G., Parker, M. W. and Board, P. G. (2001) Fly fishing for GSTs: a unified nomenclature for mammalian and insect glutathione transferases. Chem. Biol. Interact. **133**, 256–260
22 Wongsantichon, J., Harnnoi, T. and Ketterman, A. J. (2003) A sensitive core region in the structure of glutathione S-transferases. Biochem. J. **373**, 759–765
23 Oakley, A. J., Harnnoi, T., Udomsinprasert, R., Jirajaroenrat, K., Ketterman, A. J. and Wilce, M. C. J. (2001) The crystal structures of glutathione S-transferases isozymes 1-3 and 1-4 from *Anopheles dirus* species B. Protein Sci. **10**, 2176–2185
24 Mannervik, B., Awasthi, Y. C., Board, P. G., Hayes, J. D., Di Ilio, C., Ketterer, B., Listowsky, I., Morgenstern, R., Muramatsu, M., Pearson, W. R. et al. (1992) Nomenclature for human glutathione transferases. Biochem. J. **282**, 305–306
25 Vararattanavech, A. and Ketterman, A. (2003) Multiple roles of glutathione binding-site residues of glutathione S-transferase. Protein Pept. Lett. **10**, 441–448
26 Winayanuwattikun, P. and Ketterman, A. J. (2004) Catalytic and structural contributions for glutathione binding residues in a delta class glutathione S-transferase. Biochem. J. **382**, 751–757
27 Ricci, G., Caccuri, A. M., Lo Bello, M., Rosato, N., Mei, G., Nicotra, M., Chiessi, E., Mazzetti, A. P. and Federici, G. (1996) Structural flexibility modulates the activity of human glutathione transferase P1-1. Role of helix 2 flexibility in the catalytic mechanism. J. Biol. Chem. **271**, 16187–16192
28 Stella, L., Caccuri, A. M., Rosato, N., Nicotra, M., Lo Bello, M., De Matteis, F., Mazzetti, A. P., Federici, G. and Ricci, G. (1998) Flexibility of helix 2 in the human glutathione transferase P1-1. Time-resolved fluorescence spectroscopy. J. Biol. Chem. **273**, 23267–23273
29 Stella, L., Nicotra, M., Ricci, G., Rosato, N. and Di Iorio, E. E. (1999) Molecular dynamics simulations of human glutathione transferase P1-1: analysis of the induced-fit mechanism by GSH binding. Proteins **37**, 1–9
30 Labrou, N. E., Mello, L. V. and Clonis, Y. D. (2001) Functional and structural roles of the glutathione-binding residues in maize (*Zea mays*) glutathione S-transferase I. Biochem. J. **358**, 101–110
31 Jirajaroenrat, K., Pongjaroenkit, S., Krittanai, C., Prapanthadara, L. and Ketterman, A. J. (2001) Heterologous expression and characterization of alternatively spliced glutathione S-transferases from a single *Anopheles* gene. Insect Biochem. Mol. Biol. **31**, 867–875
32 Habig, W. H., Pabst, M. J. and Jakoby, W. B. (1974) Glutathione S-transferases. The first enzymatic step in mercapturic acid formation. J. Biol. Chem. **249**, 7130–7139
33 Stenberg, G., Dragani, B., Cocco, R., Mannervik, B. and Aceto, A. (2000) A conserved "hydrophobic staple motif" plays a crucial role in the refolding of human glutathione transferase P1-1. J. Biol. Chem. **275**, 10421–10428
34 Segel, I. H. (1993) Enzyme kinetics. Behavior and analysis of rapid equilibrium and steady-state enzyme systems, John Wiley & Sons, Inc., New York.
35 Ji, X., Von Rosenvinge, E. C., Johnson, W. W., Tomarev, S. I., Paitigorsky, J., Armstrong, R. N. and Gilliland, G. L. (1995) Three-dimensional structure, catalytic properties, and evolution of a sigma class glutathione transferase from squid, a progenitor of the lens S-crystallins of cephalopods. Biochemistry **34**, 5317–5328
36 Oakley, A. J., Lo Bello, M., Ricci, G., Federici, G. and Parker, M. W. (1998) Evidence for an induced-fit mechanism operating in Pi class glutathione transferases. Biochemistry **37**, 9912–9917
37 Ricci, G., Lo Bello, M., Caccuri, A. M., Pastore, A., Nuccetelli, M., Parker, M. W. and Federici, G. (1995) Site-directed mutagenesis of human glutathione transferase P1-1. Mutation of Cys-47 induces a positive cooperativity in glutathione transferase P1–1. J. Biol. Chem. **270**, 1243–1248
38 Lo Bello, M., Battistoni, A., Mazzetti, A. P., Board, P. G., Muramatsu, M., Federici, G. and Ricci, G. (1995) Site-directed mutagenesis of human glutathione transferase P1-1. Spectral, kinetic, and structural properties of Cys-47 and Lys-54 mutants. J. Biol. Chem. **270**, 1249–1253
39 Stevens, J. M., Armstrong, R. N. and Dirr, H. W. (2000) Electrostatic interactions affecting the active site of class Sigma glutathione S-transferase. Biochem. J. **347**, 193–197


Received 5 April 2005/30 August 2005; accepted 12 September 2005
Published as BJ Immediate Publication 12 September 2005, doi:10.1042/BJ20050555

Available online at www.sciencedirect.com
SCIENCE DIRECT
Biochimica et Biophysica Acta 1754 (2005) 79 – 99
Reprint 9
BIOCHIMICA ET BIOPHYSICA ACTA
BBA
http://www.elsevier.com/locate/bba

Review

# Peptide inhibitors of protein kinases—discovery, characterisation and use

Marie A. Bogoyevitch [a,*], Renae K. Barr [a], Albert J. Ketterman [b]

[a] *Cell Signalling Laboratory, Biochemistry and Molecular Biology (M310), School of Biomedical, Biomolecular and Chemical Sciences, University of Western Australia, 35 Stirling Highway, Crawley, Western Australia 6009, Australia*
[b] *Institute of Molecular Biology and Genetics, Mahidol University, Salaya Campus, Nakorn Pathom 73170, Thailand*

Received 19 July 2005; received in revised form 26 July 2005; accepted 28 July 2005
Available online 8 September 2005

**Abstract**

Protein kinases are now the second largest group of drug targets, and most protein kinase inhibitors in clinical development are directed towards the ATP-binding site. However, these inhibitors must compete with high intracellular ATP concentrations and they must discriminate between the ATP-binding sites of all protein kinases as well the other proteins that also utilise ATP. It would therefore be beneficial to target sites on protein kinases other than the ATP-binding site. This review describes the discovery, characterisation and use of peptide inhibitors of protein kinases. In many cases, the development of these peptides has resulted from an understanding of the specific protein-binding partners for a particular protein kinase. In addition, novel peptide sequences have been discovered in library screening approaches and have provided new leads in the discovery and/or design of peptide inhibitors of protein kinases. These approaches are therefore providing exciting new opportunities in the development of ATP non-competitive inhibitors of protein kinases.


*Keywords:* Peptide inhibitor; Endogenous inhibitor; Pseudosubstrate; Library screening; Peptide design; Small molecule ATP non-competitive inhibitor

## 1. Introduction

Protein kinases comprise a large family of enzymes that catalyse the transfer of the terminal phosphoryl group of ATP to their specific protein substrates. When the sequences of protein kinases have been aligned, multiple conserved motifs have been identified [1]. This information has lead to the development of a standard nomenclature that defines critical subdomains or motifs within the protein kinase fold. These motifs have provided a powerful predictive tool in the identification of new protein kinases, and have revealed the presence of ~500 protein kinases within the human or mouse genomes [2,3].

It has been recognised for more than 50 years that protein phosphorylation regulates many aspects of cellular function such as metabolism, division, movement, survival and death. Thus, any disruption of normal phosphorylation can alter cell function and cause disease [4]. Protein kinases are now the second largest group of drug targets, coming after only the G-protein-coupled receptors [4]. To date, most protein kinase inhibitors in clinical development have been directed towards the ATP-binding site. However, one drawback with this current strategy is that these inhibitors must compete with high intracellular ATP concentrations. Furthermore, if they are to be specific, these inhibitors must discriminate between the ATP-binding sites of all protein kinases as well as >200 other human proteins that also utilise ATP (see review [5]).

For these reasons, it would be beneficial to target sites on protein kinases other than the ATP-binding site. However, protein–protein interaction interfaces have generally been considered as difficult targets for small molecule drug discovery. This is largely because the interactions appear to involve larger and frequently less well-defined contact areas when compared with classical drug targets such as enzyme active sites and ligand-binding sites on receptors. There have been some notable successes. For example, small molecule

*Abbreviations:* AKAP, A-Kinase Anchoring Protein; EGF-R, Epidermal Growth Factor-Receptor; GSK, Glycogen Synthase Kinase; $IC_{50}$, concentration of compound to achieve 50% inhibition; JIP, JNK Interacting Protein; JNK, c-Jun N-terminal Kinase; $K_i$, inhibition constant; MLCK, Myosin Light Chain Kinase; PKC, Protein Kinase C; PKI, Protein Kinase A Inhibitor; RACK, Receptor for Activated C-Kinase; SOCS, Suppressor of Cytokine Signalling; TI-JIP, truncated inhibitory region of JIP

* Corresponding author. Tel.: +61 8 6488 1348; fax: +61 8 6488 1148.
*E-mail address:* marieb@cyllene.uwa.edu.au (M.A. Bogoyevitch).

1570-9639/$ - see front matter © 2005 Elsevier B.V. All rights reserved.
doi:10.1016/j.bbapap.2005.07.025

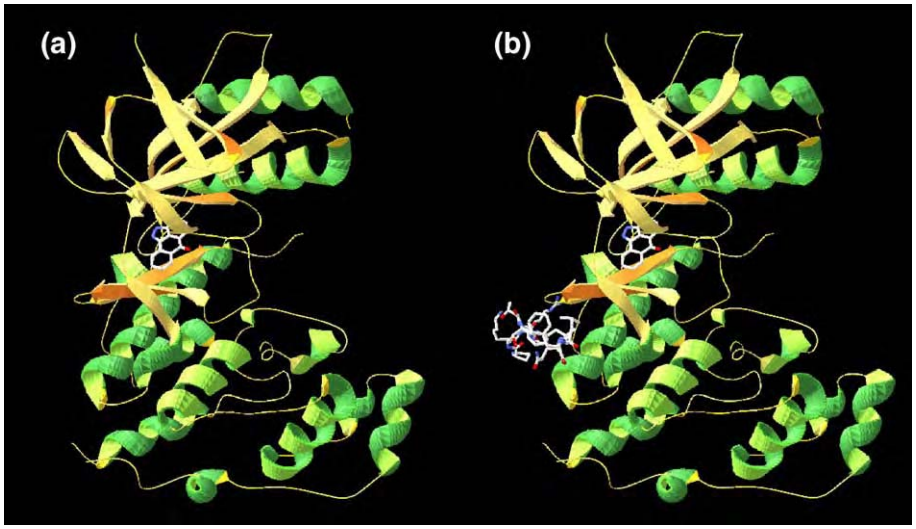


Fig. 1. Protein Kinase Interactions with ATP-competitive and ATP-noncompetitive inhibitors: c-Jun N-terminal Kinase. (a) In a recent example, structural analysis has shown that the ATP-binding site of the protein kinase c-Jun N-terminal Kinase (JNK) is occupied by an ATP-competitive inhibitor of JNKs, SP600125 [9]. (b) In this same study, the structure of the complex between JNK1 and the peptide inhibitor derived from the JNK pathway scaffold protein, JIP1, was solved. This shows the interaction of the JNK1 protein with the peptide inhibitor at a site remote from the ATP-binding pocket.

inhibitors of the interaction of p53 with its suppressor protein HDM2 have been designed, synthesised, tested in vitro and shown to have in vivo efficacy (see review [6]).

In this review, the discovery, characterisation and use of peptide inhibitors of protein kinases are considered. As will be shown, the development of many of these peptides has resulted from an understanding of the specific protein-binding partners for a particular protein kinase. In addition, novel peptide sequences as discovered in library screening approaches have provided new leads in the discovery and/or design of peptide inhibitors of protein kinases. Lastly, how information on peptide inhibitors can aid the development of new non-peptide small molecule inhibitors is considered alongside a number of examples of small molecule ATP-noncompetitive inhibitors of protein kinases. In combination, these approaches provide exciting new opportunities in the development of ATP non-competitive inhibitors of protein kinases.

## 2. Protein kinase inhibitors derived from biologically-relevant protein partners

The crystal structure of cAMP-dependent protein kinase [7] has provided insights into the organization of the catalytic core of serine/threonine kinases. Striking similarities have been

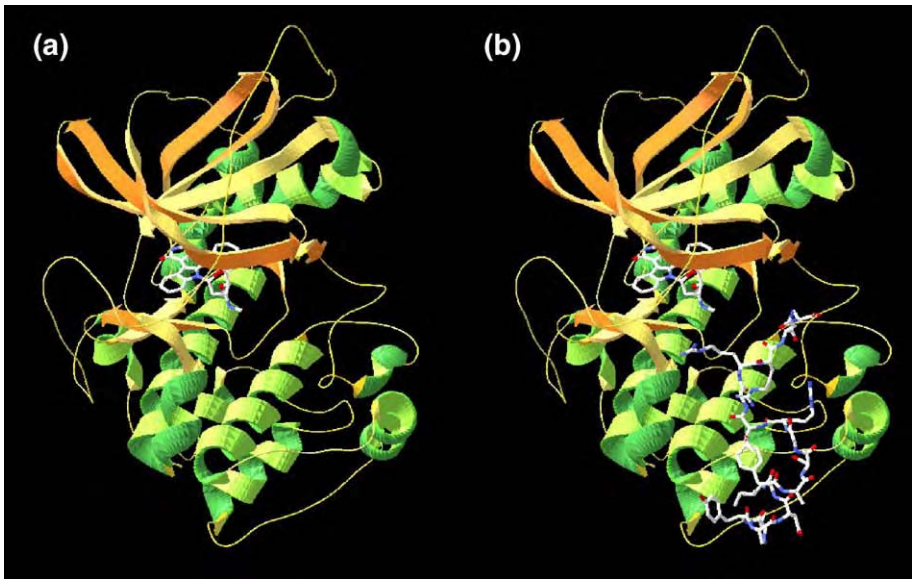


Fig. 2. Protein Kinase Interactions with ATP-competitive and ATP-noncompetitive inhibitors: cAMP-dependent Protein Kinase. (a) Structural analysis has shown that the ATP-binding site of cAMP-dependent protein kinase is occupied by an ATP-competitive inhibitor of protein kinases, staurosporine. (b) The structure of the complex between cAMP-dependent protein kinase and the peptide inhibitor derived from the Protein Kinase Inhibitor (PKI) protein. Again, this shows the interaction of cAMP-dependent protein kinase with the peptide inhibitor at a site remote from the ATP-binding pocket.

subsequently seen in other protein kinases, including tyrosine kinases, with at least 46 unique protein kinase structures now available [8]. From these structures, it is clear that a relatively small pocket of the protein kinase constitutes the ATP-binding region. This is highlighted in Fig. 1(a), where a recent example shows the ATP-binding site of the protein kinase c-Jun N-terminal Kinase (JNK) occupied by an ATP-competitive JNK inhibitor, SP600125 [9]. Similarly, a complex of cAMP-dependent protein kinase with the ATP-competitive inhibitor staurosporine is shown in Fig. 2(a). Thus there are extensive regions outside the ATP-binding site, but the question remains which, if any, of these regions act to regulate protein kinase activity? Furthermore, it is not obvious which regions might also be regulated by the binding of small peptides or other small molecules. In Figs. 1(b) and 2(b), peptide inhibitors of JNK and cAMP-dependent protein kinase are also shown. These structures highlight that the sites of interaction of these peptides can be remote from the ATP-binding site and that the sites of peptide inhibitor interaction may differ between protein kinases. In the following subsections, the development of peptide inhibitors using information derived from biologically-relevant protein partners for a number of kinases is presented.

### *2.1. Peptide kinase inhibitors derived from endogenous inhibitory proteins*

#### *2.1.1. Inhibitors of cAMP-dependent protein kinase derived from the specific inhibitory protein, Protein Kinase A Inhibitor (PKI)*

Studies published in the early 1970s characterising thermostable protein inhibitors of the cAMP-dependent protein kinase purified from crude tissue extracts [10–12] provided some of the first leads in the development of peptides as ATP non-competitive inhibitors of protein kinases. An 11-kDa inhibitory protein, known simply as Protein Kinase Inhibitor or PKI, was shown to interact specifically with the catalytic subunit of cAMP-dependent protein kinase, thus potently inhibiting kinase activity with an inhibition constant ($K_i$) of 2 nM [13]. Proteolytic digestion of PKI revealed a 20 amino acid inhibitory peptide corresponding to amino acids 11–30 [14,15]. This sequence is shown in Table 1, along with many other reported peptide inhibitor sequences that are discussed in this review. Interestingly, within this PKI-derived peptide, a short amino acid sequence resembled the optimal sequence phosphorylated by cAMP-dependent protein kinase. Thus, the peptide contained a pseudosubstrate sequence (R–R–X–S*, where S* represents the phosphoacceptor residue in the substrate that is a non-phosphorylated amino acid in the pseudosubstrate) [14]. Additional pseudosubstrate inhibitors are considered in Section 2.3 as this type of inhibition has now been observed for a number of other protein kinases.

The chemical synthesis of PKI-derived peptides has allowed further characterisation of inhibitory actions [14,15]. This revealed potent inhibition and high specificity towards cAMP-dependent protein kinase without inhibition of other protein kinases tested (phosphorylase kinase, skeletal muscle myosin light chain kinase, protein kinase C (PKC), casein kinase II or cGMP-dependent protein kinase) even when these peptides were included at millimolar concentrations in in vitro assays [14]. Further biochemical analyses of peptide sequences derived from PKI revealed the primary structural requirements for inhibition of cAMP-dependent protein kinase [16]. For example, residues 25–30 within PKI(11–30) were not essential for inhibition. Indeed, PKI(1–24) with a $K_i$ of 4.8 nM was ~150-fold more potent than PKI(11–30). Thus, the inhibitory effects of PKI(1–24) were comparable with the PKI protein [16], and showed that the inclusion of greater numbers of amino acids did not always maintain highest inhibitory activity. Furthermore, the critical nature of the two arginine residues within the pseudosubstrate site was confirmed when their individual substitution by glycine decreased inhibitory potency of the peptides by up to 500-fold [16]. Thus, a single amino acid change in this inhibitory peptide greatly reduced inhibition.

A 20mer peptide corresponding to PKI(5–24) (Table 1) has also been shown to inhibit cAMP-dependent protein kinase with potency comparable to full-length PKI and a $K_i$ of 2.3 nM [17]. Structural studies of PKI(5–22) revealed the secondary structure within this short sequence required for its high biological potency [18]. Amino acid substitutions further defined primary structural determinants essential for the inhibitory actions of the PKI-derived peptides [19] even prior to structural information on the peptide–protein kinase complex being available. Now that the structure of this complex has been solved [20], the amino acids making contact with the peptide have been identified and models developed on the mechanism of substrate binding and the phosphotransferase reaction. Fig. 2(b) shows the complex of cAMP-dependent protein kinase and PKI(12–24) together with the ATP-competitive inhibitor staurosporine and this highlights the spatial separation between the binding sites of the two different inhibitors. In summarising a range of studies, Walsh and Glass concluded that these PKI-based peptide inhibitors showed $K_i$ values in the range of 4 nM to 150 μM. Table 1 shows the sequence of the most potent 9mer inhibitor, PKI(14–22), with a $K_i$ of 36 nM [21]. This 9mer demonstrated that a minimal sequence could retain considerable affinity for inhibition of the cAMP-dependent protein kinase.

The studies on PKI or the PKI-derived peptides described thus far have emphasised the biochemical evaluation of structure–activity relationships in vitro. Studies addressing the intracellular roles of cAMP-dependent protein kinase have used various techniques for expression or delivery of PKI. An early study used a plasmid encoding PKI(1–31) to characterise the role of cAMP-dependent protein kinase in the transcriptional regulation of genes encoding collagenase, the chorionic gonadotrophin-alpha subunit, or enkephalin [22]. This plasmid-driven expression allowed continued production of the peptide intracellularly, chronic inhibition of cAMP-dependent protein kinase, and clear biological effects. Therefore, these results have demonstrated the value of this approach.

In contrast, the sensitivity of small peptides to proteolytic degradation could hamper their study in cells, particularly if longer-term inhibition is required. Thus, PKI(6–24) has been

Table 1
Peptide inhibitors of protein kinases

| Peptide name | Peptide sequence | Protein kinase inhibited | Source of inhibitor | References |
|---|---|---|---|---|
| PKI(11–30) | I–A–S–G–R–T–G–R–R–N–A–I–H–D–I–L–V–S–S–A | cAMP-dependent protein kinase | Inhibitory Protein-PKI | [14,15] |
| PKI(1–24) | T–D–V–E–T–T–Y–A–D–F–I–A–S–G–R–T–G–R–R–N–A–I–H–D–I–L–V–S–S–A | | Inhibitory Protein-PKI | [16] |
| PKI(5–24) | T–T–Y–A–D–F–I–A–S–G–R–T–G–R–R–N–A–I–H–D | | Inhibitory Protein-PKI | [17] |
| PKI(14–22) | G–R–T–G–R–R–N–A–I | | Inhibitory Protein-PKI | [21] |
| [Ala-5]Kemptide | L–R–R–A–A–L–G | | Synthetic substrate-Kemptide | [34,35] |
| Ht31 peptide | V–Q–G–N–T–D–E–A–Q–E–E–L–A–W–K–I–A–K–M–I–V–S–D–V–M–Q–Q | | Anchoring protein-AKAP | [120,123] |
| AKAP-*IS* | Q–I–E–Y–L–A–K–Q–I–V–D–N–A–I–Q–Q–A | | Anchoring protein-AKAP | [134] |
| AKB(RI), RI specific | F–E–E–L–A–W–K–I–A–K–M–I–W–S–D–V–F–Q–Q | | Anchoring protein-AKAP | [135] |
| n.d.[a] | Myr-R–K–R–T–L–R–R–L[b] | Protein Kinase C (PKC) | Synthetic peptide substrate modified by myristoylation | [40] |
| n.d.[a] | Myr- R–K–R–C–L–R–R–L[b] | | Synthetic peptide substrate modified by myristoylation and Cys substitution | [42] |
| n.d.[a] | R–F–A–R–K–G–A–L–R–Q–K–N–V–H–E–V–K–N | PKC-α/β/γ | PKC-α/β pseudosubstrate sequence (19–36) | [65] |
| n.d.[a] | R–F–A–R–K–G–A–L–R–Q–K–N–V | PKC-α/β/γ | PKC-α/β pseudosubstrate sequence (19–31) | [66] |
| myr-ψPKC | Myr-F–A–R–K–G–A–L–R–Q[b] | PKC-α/β/γ | PKC-α/β pseudosubstrate sequence (20–28) | [76] |
| myr-ψPKCζ | Myr-R–R–G–A–R–R–W–R–K[b] | PKC-ζ | PKC-ζ pseudosubstrate sequence (116–124) | [82] |
| βC2–4 | S–L–N–P–E–W–N–E–T | PKC-α/β/γ | PKC-β sequence (218–226) | [99] |
| δV1–1 | S–F–N–S–Y–E–L–G–S–L | PKC-δ | PKC-δ sequence (8–17) | [106] |
| "peptide 1" | K–G–D–Y–E–K–I–L–V–A–L–C–G–G–N | PKC | Annexin-1 (332–346) | [171] |
| MLC(11–19) | K–K–R–A–A–R–A–T–S | Myosin light chain kinase (MLCK) | C-terminal truncation of MLC phosphorylation site | [49] |
| n.d.[a] | A–K–K–L–S–K–D–R–M–K–K–Y–M–A–R–R–K–W–Q–K–T–G | | Myosin light chain kinase pseudosubstrate site (480–501) | [91] |
| n.d.[a] | K–R–R–F–K–K | | Variant on pseudosubstrate site that minimizes calmodulin inhibition | [91] |
| CaMKII(290–302) | L–K–K–F–N–A–R–R–K–L–K–G–A | Calmodulin-dependent protein kinase | Calmodulin-dependent protein kinase II pseudo-substrate/ Calmodulin-binding (290–309) | [95] |
| CaM peptide 1 | W–D–T–V–R–I–S–F | | Random Peptide Library Screening with Calmodulin | |
| CaM peptide 2 | W–P–S–L–Q–A–I–R | | | [154] |
| "Peptide 2" | V–E–L–D–P–E–F–E–P–R–A–R–E–R–T–Y–A–F–G–H | Akt1 | Substrate based | [45] |
| "Peptide 4" | V–E–L–D–P–E–F–E–P–R–A–R–E–R–A–Y–A–F–G–H | | Substrate based | [45] |
| Akt-in | A–V–T–D–H–P–D–R–L–W–A–W–E–K–F | | Peptide from Activator-TCL1 | [143] |
| KRX-014.H151 | Myr-G–G–Y–N–Q–N–H–Q–K–L–F–Q–L-amide[b] | | KinAce | [115] |
| n.d.[a] | R–K–Q–I–T–V–R | Phosphorylase kinase | Based on peptide substrate | [47] |
| "Peptide 3" | Y-c[Pen-Y–G–S–F–C]–K–K-amide[c] | c-Src | Substrate based | [51] |
| "Peptide 29" | Y-c[D-Pen-(3-Iodo-Y)–G–S–F–C]–K–R-amide[c] | | Substrate based | [51] |
| "Peptide 30" | Y-c[D-Pen-(3,5-diIodo-Y)–G–S–F–C]–K–R-amide[c] | | Substrate based | [51] |
| n.d.[a] | Myr-E–F–L–Y–G–V–F–F[b] | | Substrate and myristoylation | [53] |
| n.d.[a] | Myr-E–F–L–amide[b] | | Substrate and myristoylation | [53] |
| n.d.[a] | F–V–G–F–L–G–F–L–G | | Random Peptide Library Screening with kinase | [147] |
| C4 | T–Y–T–K–K–Q–V–L–R–M–A–H–L–V–L–K–V–L–T–F–D–L | Cyclin-dependent kinase 2 | Cyclin–cyclin-dependent kinase interface | [145] |
| "peptide 4" | K–L–I–L–F–L–L–L–L | ZAP70 | Oriented peptide library screen | [153] |
| TI-JIP | R–P–K–R–P–T–T–L–N–L–F | JNK | Based on JIP scaffold protein | [137] |

Table 1 (*continued*)

| Peptide name | Peptide sequence | Protein kinase inhibited | Source of inhibitor | References |
|---|---|---|---|---|
| KRX-147.D103 | Myr-G–N–L–L–N–F–L–R–R–K-amide[b] | c-Kit | KinAce | [115] |
| KRX-702.H105 | Myr-G–G–R–A–G–N–Q–Y–L-amide[b] | PDK1 | KinAce | [115] |
| KRX123.101 | Myr-G–I–V–T–Y–G–K–I-amide[b] | Lyn | KinAce | [114] |
| KRX-123.302 | Myr-G–L–V–T–(3,5-diIodo-Y)–k–K–I–K&-amide [b,d] | | KinAce | [114] |
| KRX-055.G106 | Myr-G–R–T–N–A–V–Nle-amide[b,f] | | KinAce | [115] |
| P1 | c[C–R–N–C–T–V–I–Q–F–S–C][e] | Casein Kinase 2 | Random Peptide Library | [155] |
| P15 | c[C–W–M–S–P–R–H–L–G–T–C][e] | | Screening with Substrate Peptide | |
| Tkip | W–L–V–F–F–V–I–F–Y–F–F–R | JAK2, EGF-R | Designed peptide | [33] |

A range of approaches has been used in the discovery and development of peptide inhibitors of protein kinases. This table summarises peptide sequences and their sources as described in this review. Further details on the characterisation of these peptide inhibitors including estimates of the affinities ($K_i$ or $IC_{50}$ values for inhibition) and their use in cellular studies is described in the text.

[a] n.d.=not defined. No name was specifically given to these peptides.

[b] In this sequence, myr=N-terminal myristoylation.

[c] In this sequence, the sequence contained within the designation c[ ] is cyclized by the formation of a disulphide bond between the side chain of the amino acid Penicillamine (Pen) and the side chain of Cysteine (C).

[d] In this sequence, k=D-stereoisomer of K, and K&=K-ε amino benzoyl.

[e] In this sequence, the sequence contained within the designation c[ ] is cyclized by the formation of a disulphide bond between the side chains of the of the 2 Cysteine (C) residues.

[f] In this sequence, Nle—norleucine.

modified to address this concern [23]. PKI(6–24), modified in two ways by the substitution of arginine in position 18 with its D-stereoisomeric form and blocking the side chain of the C-terminal aspartate with a cyclohexyl ester group, was active intracellularly for 4 to 6 h following its microinjection. This peptide prevented the changes in cell morphology and cytoskeleton following cAMP-dependent protein kinase activation [23]. Under the same conditions, the microinjection of non-modified PKI(6–24) was without effect [23]. Others have used microinjection of PKI-derived peptides in a wide range of studies. Examples include the evaluation of the role for cAMP-dependent protein kinase in mitosis and nuclear envelope breakdown [24], and more recently in the evaluation of cell cycle progression of one-cell stage mouse fertilised eggs [25]. PKI-derived peptides have also been added to permeabilised cells to evaluate cAMP-dependent protein kinase actions in renal tubule cells [26], $\beta_2$-adrenergic receptor desensitisation [27] and the $IP_3$-dependent release of $Ca^{2+}$ and relaxation of smooth muscle [28].

Intracerebroventricular injection of either PKI(6–22) or an N-terminal myristoylated form of PKI(14–22) has also significantly reversed the antinociception tolerance that followed low level morphine exposure [29]. In this example, the myristoylated PKI(14–22) was most effective, this being attributed to the lipophilic myristoyl moiety and smaller peptide size enhancing cellular permeability [29]. Similarly, the use of myristoylated PKI(14–22) has implicated cAMP-dependent protein kinase in insulin secretion by pancreatic beta-cells [30], as a mediator of ischemic preconditioning and isoprenaline-induced protection in the heart [31], and in the regulation of adenylyl cyclase and phosphodiesterase activity in smooth muscle [32]. Therefore, simple chemical modifications of the PKI-derived peptides have allowed a range of studies evaluating the biological functions of cAMP-dependent protein kinase.

#### *2.1.2. Endogenous inhibitory proteins as new leads in the development of protein kinase inhibitors*

Following the success of the approach to develop cAMP-dependent kinase inhibitors based on the endogenous inhibitory protein PKI, other protein kinase inhibitors could be developed using similar principles. To date, there are few reports of this approach to discover peptide inhibitors of protein kinases. However, as described in subsequent sections of this review, other proteins such as substrates, scaffolds or the protein kinases themselves have provided numerous leads in the development of peptide inhibitors of protein kinases. It is of interest that a peptide considered to mimic some of the actions of the Suppressors Of Cytokine Signalling (SOCS) protein family as inhibitors of Epidermal Growth Factor-Receptor (EGF-R) or JAK2 has been recently described [33]. However, a short 12mer peptide mimetic of SOCS-1, called Tkip (see Table 1), was designed to bind JAK2 and not found within the SOCS-1 sequence. Tkip is therefore considered further in Section 3.2 where approaches to the discovery of novel inhibitory peptide sequences are described in more detail.

### *2.2. Peptide inhibitors of protein kinases derived from substrates*

#### *2.2.1. Substrate-based inhibitors of cAMP-dependent protein kinase*

As described in Section 2.1.1, the inhibitory sequence within PKI has been attributed to a sequence resembling its substrate, i.e., a pseudosubstrate sequence. This relationship between substrate and inhibitor is further emphasised by the observation that the appropriate substitution of a single amino acid in PKI-derived peptides has produced effective substrates for cAMP-dependent protein kinase. Thus, the substitution of alanine at position 21 in PKI(4–22), with the phosphorylatable serine residue (sequence: E–T–T–Y–A–D–F–I–A–S–G–

R–T–G–R–R–N–S–I), has produced a kinase substrate more effective than the standard peptide substrate Kemptide (where the Kemptide sequence is L–R–R–A–S–L–G) [19]. In both sequences, the phosphorylated serine is denoted by the underline (i.e., S). It is therefore not surprising that some of the earliest attempts to develop inhibitors of cAMP-dependent protein kinase performed the reverse modifications. Thus, substituting the phosphorylatable serine in Kemptide with alanine produced an inhibitor, [Ala-5]-Kemptide (see Table 1) [34,35]. In addition, the irreversible inactivation of cAMP-dependent protein kinase has been achieved with peptide substrate analogs, some of which bind a highly reactive active site Cys residue [36,37] as well as other residues in the cAMP-dependent protein kinase active site [38].

### 2.2.2. Substrate-based peptide inhibitors of protein kinase C (PKC)

Other modifications of substrate peptides of protein kinases have also produced novel inhibitors. For example, as shown in Table 1, the major PKC phosphorylation site (Thr-654) of the EGF-R (i.e., T within the sequence context R–K–R–T–L–R–R–L) when added to an N-terminal myristoyl moiety produced an 8mer PKC inhibitory peptide rather than a substrate [39,40]. This myristoylated peptide entered cells more readily and inhibited PKC-mediated interleukin-2 and interleukin-2 receptor expression in Jurkat T cells [41]. When various substitutions of this peptide were then tested for their potency in PKC inhibition, myr-R–K–R–C–L–R–R–L was the most potent of the peptides evaluated [40]. However, its potency was decreased 10-fold in the presence of the reducing reagent dithiothreitol [40]. This sensitivity to dithiothreitol suggested a covalent interaction with a conserved active site Cys in PKC. Further studies confirmed an irreversible mechanism of inhibition following S-thiolation of PKC [42]. In addition, many studies as considered in Section 2.3 have evaluated the use of pseudosubstrate sequences as inhibitors of PKC.

Lee and colleagues have further generated peptide inhibitors specific for the α-PKC isoform based on the PKC-α consensus substrate sequence (sequence: R–R–K–G–*S*–Hyd–R, where Hyd = a hydrophobic amino acid, and the phosphorylated serine is underlined) [43]. Again, the phosphorylatable serine at position 5 in this sequence was replaced with an alanine, the residues considered essential (i.e., the two arginine residues and the hydrophobic residues), were retained whereas the other 3 positions were changed through the inclusion of each one of 720 carboxylic acid moieties within an (L)-2,3-diaminopropionic acid substitution. This resulted in a number of high affinity modified peptide inhibitors of PKC-α most notably with one inhibitor showing a $K_i$ of 0.8 nM. Interestingly this peptide also showed >350-fold preference for PKC-α over the closely-related conventional PKC isoforms, PKC-β and PKC-γ and even higher selectivity over the more distantly related PKCs (600-fold to 2730-fold). Thus, the substitutions in the original peptide sequence would appear to access a structurally distinct subsite unique to PKC-α. Further structural analysis of this complex will be of interest in the application of similar approaches to this family of kinases as well as the general approach to inhibitor design.

### 2.2.3. Substrate-based peptide inhibitors of Akt

Like cAMP-dependent kinase and PKC, the Akt family of kinases are serine/threonine kinases within the AGC group [2]. An optimal peptide substrate sequence (A–R–K–R–E–R–T–Y–S–F–G–H–H–A) discovered in an oriented peptide library screening approach has been shown to bind and inhibit Akt1 with a $K_i$ of 12 μM [44]. This has more recently been used in the development of small peptide inhibitors of Akt [45]. The most effective inhibitors showed $K_i$ values in the range of 0.1 μM. The sequence of one of these peptides is shown in Table 1, and this 100-fold improved inhibition was attributed to the addition of 9 amino acids from the FOXO3 transcription factor to the N-terminus of the original peptide and the substitution of threonine and serine residues by alanine [45]. When evaluating specificity by testing 8 other protein kinases, only Serum/Glucocorticoid-regulated Kinase SGK, which shares similar substrate preferences, was also inhibited [45].

Two approaches have been initially taken to deliver these Akt inhibitors to cells [45]. First, these peptide inhibitors were delivered to HeLa cells using the BioPORTER protein transfection reagent. This provided transient exposure to the peptide, and Glycogen Synthase Kinase (GSK)-3 phosphorylation was inhibited [45]. However, no phenotypic change in these cells was observed [45]. Thus, in a second approach, the peptide was synthesised as a fusion with a poly-arginine membrane-permeable sequence. Continuous incubation with this peptide provided a mechanism for sustained delivery. Significant inhibition of GSK3 phosphorylation was demonstrated, and growth of both HeLa and MiaPaCa cells was reduced as expected if growth inhibition required persistent Akt inhibition [45]. This has therefore demonstrated the importance of appropriate delivery mechanisms when determining the cellular efficacy of these peptide inhibitors.

### 2.2.4. Substrate-based peptide inhibitors of other serine/threonine kinases

In addition to the identification of peptide inhibitors of serine/threonine protein kinases based on their specific substrates as described in the preceding subsections, others have shown the ability of substrate-based peptides to inhibit protein kinase activities in vitro. Here, two additional inhibitors are considered, a minimal peptide inhibitor of phosphorylase kinase and a peptide inhibitor of smooth muscle myosin light chain kinase (MLCK).

Phosphorylase kinase is one of the key enzymes involved in glycogenolysis, catalysing the phosphorylation of phosphorylase *b* to its active form, phosphorylase *a*. Its reaction mechanism has been extensively studied, and specifically it has been of interest that other protein kinases cannot perform the function of phosphorylase kinase (see review [46]). In studying its catalytic mechanism, small peptide substrates have been identified and those poorly phosphorylated have been screened as potential competitive inhibitors [47]. Of those peptides screened, a threonine containing 7mer was studied